Parameters Influencing Seismic Structural Collapse with Emphasis on Vertical Accelerations and the Possible Related Risks for New and Existing Structures in the Central and Eastern United States

By:

Paul W. Spears

Thesis submitted to the Faculty of the Virginia Polytechnic Institute and State University in partial fulfillment of the requirements for the degree of

MASTER OF SCIENCE

In

CIVIL ENGINEERING

Approved:

Dr. Finley A. Charney

_____
Committee Chairman

Dr. Thomas M. Murray

_____
Committee Member

Dr. Raymond H. Plaut

_____
Committee Member

May 18, 2004
Blacksburg, Virginia

Keywords: Collapse, P-Delta Effects, Dynamic Instability, Vertical Accelerations, Nonlinear Analysis, Incremental Dynamic Analysis, Central and Eastern United States, Seismic Hazard, OpenSees

Parameters Influencing Seismic Structural Collapse with Emphasis on Vertical Accelerations and the Possible Related Risks for New and Existing Structures in the Central and Eastern United States

By:
Paul W. Spears
Committee Chairman: Dr. Finley A. Charney

(ABSTRACT)

This thesis presents the results of basically two separate studies. The first study involved identifying structural and earthquake parameters that influenced seismic structural collapse. The parameter study involved nonlinear dynamic analyses using single-degree-of-freedom (SDOF) bilinear models. Four parameters were associated with the SDOF models – the lateral stiffness, the post-yield stiffness ratio, the yield strength, and the stability ratio (P-Delta effects). Then, three parameters were associated with the ground motions – the records themselves, the lateral ground motion scales, and the vertical ground motion scales.

From the parameter study, it was found that the post-yield stiffness ratio augmented by P-Delta effects (r_p) in conjunction with the ductility demand was the best predictor of collapse. These two quantities include all four structural parameters and the seismic displacement demands. It was also discovered in the parameter study that vertical accelerations did not significantly influence lateral displacements unless a given combination of model and earthquake parameters was altered such that the model was on the verge of collapsing.

The second study involved Incremental Dynamic Analysis (IDA) using bilinear SDOF models representative of low rise buildings in both the Western United States (WUS) and the Central and Eastern United States (CEUS). Models were created that represented three, five, seven, and nine story buildings. Five sites from both the WUS and CEUS were used. Four different damage measures were used to assess the performance of the buildings. The IDA study was primarily interested in the response of

the structures between the earthquake intensities that have a 10 percent probability of occurring in 50 years (10/50) and 2 percent probability of occurring in 50 years (2/50).

The results showed that all structures could be in danger of severe damage and possible collapse, depending on which damage measure and which earthquake was used. It is important to note, though, that the aforementioned is based on a damage-based collapse rule. The damage-based rule results were highly variable.

Using an intensity-based collapse rule, proved to be more consistent. Due to the nature of the bilinear models, only those structures with negative r_p values ever collapsed using an intensity-based collapse rule. Most of the WUS models had positive r_p values and many of the CEUS models had negative r_p values. While many of the CEUS structures had negative r_p values, which made them prone to collapse, most of the CEUS structures analyzed did not collapse at the 2/50 intensity. The reason was that the periods of the CEUS models were much longer than the approximate periods that were required to determine the strengths. Consequently, the strength capacity of most of the CEUS models was much greater than the seismic strength demands. While many of the CEUS models did have sudden collapses due to the large negative r_p values, the collapses happened at intensities that were generally much higher than the 2/50 event.

In the IDA, it was also shown that vertical accelerations can significantly affect the ductility demands of a model with a negative r_p post-yield stiffness ratio as the earthquake intensity approaches the collapse intensity. Since IDA is concerned with establishing collapse limit states, it seems that the most accurate collapse assessments would include vertical accelerations.

Aknowledgements

Over the past two years, there have been many people and organizations who have assisted me in the pursuit of my Master's degree. I would like to take this opportunity to recognize them.

I would first like to thank my wife, Haley, for her patient endurance through this difficult time. I pray that she would be blessed beyond measure for her sacrificial love during the last two years. She has helped to keep me sane and has been an invaluable source of strength for me.

I also would also like to thank my committee. I would first like to thank my chairman and advisor, Dr. Finley Charney. I have learned more in the last year and a half from him than I would have ever dreamed possible. I was continually amazed at his depth and breadth of knowledge. I am grateful to have been molded by his tutelage. I would also like to thank my other committee members, Dr. Thomas Murray and Dr. Raymond Plaut. I am grateful for their insight and guidance on this thesis.

I would like to thank Mrs. Marion Via and the Charles E. Via, Jr. Department of Civil and Environmental Engineering for providing a significant portion of the funding for my research and education at Virginia Tech. It is a great honor and privilege to have been a Via Scholar. I would furthermore like to thank the Aspires Program for the rest of the funding for my research.

I would like to thank my parents, Wes Spears and Linda Spears, for helping mold me into the man I am today. Thank you for teaching me the value of humility, kindness, hard-work, faithfulness, and persistence. I want them both to know that I am very glad that they are my parents. Thanks also to my brother, Mark, whose confidence, humor, and ingenuity are always refreshing. I also would like to express appreciation to my in-laws, the Smiths, for being supportive and loving to me.

Finally, I would like to thank the rest of my family, friends, and fellow graduate students for help and encouragement along this journey.

Table of Conents

List of Figures

List of Tables

1.0 Introduction

1.1 – Motivation

Concern about damaging earthquakes in the Central and Eastern United States (CEUS) is growing, but many are still skeptical of the necessity for the concern. As ammunition, skeptics have the fact that a damaging earthquake has not occurred in the CEUS for over a century. However, based on historical and geological evidence, damaging earthquakes in the CEUS are both reasonable and probable (Frankel, et al. 1996). In the New Madrid area near Memphis, for example, an extremely damaging series of earthquakes occurred in the late nineteenth century.

The plausibility of damaging CEUS earthquakes in conjunction with the risks associated with their occurrence has resulted in increasingly more stringent seismic design provisions in the CEUS. In 1997, for example, the National Earthquake Hazards Reduction Program (NEHRP) significantly changed its provisions to provide a consistent level of seismic structural safety throughout the United States. It was desired that all structures should be designed to prevent collapse-related loss of life in the event of an earthquake that had a two percent probability of occurring in fifty years. It was found that pre-1997 CEUS buildings were designed for an earthquake intensity that was much lower than the two percent in fifty year event (Leyendecker, et al. 2000).

While US seismic design codes have become more stringent, particularly in the CEUS, there is really no way to be sure that the code provisions are adequate to prevent collapse for CEUS buildings unless a damaging earthquake were to occur. The adequacy of the seismic design codes in the Western United States (WUS) has developed as follows: an earthquake occurs, deficiencies in design codes are revealed, research is conducted to remedy the deficiencies, the seismic design codes are revised, and existing structures are retrofitted to eliminate the deficiencies. One might say that the seismic design codes are calibrated to the WUS conditions. So, WUS buildings are incrementally becoming increasingly earthquake resistant. In the CEUS, on the other hand, a similar process is not happening.

There have not been any earthquakes to validate seismic design practices in the CEUS. Consequently, there may be some deficiencies in the current seismic design

codes that would render CEUS buildings more collapse prone than similar buildings in the WUS. Of particular concern for CEUS structures are P-Delta effects. P-Delta effects are a potential issue because buildings in the CEUS are typically less stiff than those in the WUS. Moreover, buildings of similar size and material will generally weigh the same whether in the WUS or CEUS. As such, the stability ratios would be higher for CEUS structures. Also, it is very possible that vertical accelerations may exacerbate the P-Delta issue. A vertical earthquake pulse acting in conjunction with gravity may increase second order deflections if occurring in phase with increasing maximum displacements.

There is also the issue of the existing buildings in the CEUS. Although new buildings must conform to the newest seismic design codes, the existing buildings are not subject to the new design requirements. While some CEUS buildings may have been retrofitted to conform to the latest seismic design codes, it is highly likely that the majority have not been upgraded. Nonconforming CEUS buildings would likely have lower, more uncertain ductility capacities than newer CEUS buildings and in some situations may have lower hysteretic dissipation capabilities. It is also possible that CEUS buildings may experience higher amounts of strength and stiffness degradation than their WUS counterparts.

In sum, it is plausible that damaging earthquakes could happen in the CEUS. Furthermore, it is uncertain if CEUS buildings would survive a damaging earthquake. Thus, this study was prompted by concerns about the hazards and risks associated with the CEUS and the adequacy of past and present seismic designs to deal with those hazards and risks.

1.2 – Purpose and Objectives

There were two primary objectives of this study. The first was to identify structural and earthquake parameters that influence collapse. The second objective was to determine if CEUS buildings were more collapse prone than WUS buildings based on the parameter study.

The first objective of identifying structural and earthquake parameters that influence collapse was achieved in two ways. First, a comprehensive literature survey was conducted, which summarized and or identified the following:

- reasonable hazards and risks associated with the CEUS
- factors influencing dynamic structural collapse as determined by analytical and experimental studies and post earthquake reconnaissance reports
- various damage measures for determining structural damage and collapse
- previous considerations given to vertical accelerations
- realistic structural characteristics of CEUS steel and reinforced concrete (RC) buildings

Then, based on the literature survey, a parameter study was conducted, which incorporated the findings of the literature survey. Single-degree-of-freedom (SDOF) nonlinear analytical models were used in the parameter study. Both structural and earthquake parameters were varied.

After identifying structural and earthquake parameters that influenced collapse, representative models of CEUS and WUS buildings were constructed and analyzed. SDOF models were used for this portion of the study as well. The models were reasonable and within design limits, but were intentionally constructed to be near the limits states in the design codes. As such, many of them were on the verge of violating the seismic design codes. Incremental Dynamic Analysis (IDA) was used to determine the range of responses one might see in the CEUS and WUS structures.

To perform the analyses, OpenSees, an open source object oriented finite element program developed by the Pacific Earthquake Engineering Research Center (PEER) was used. This program was chosen for its versatility and speed. It was verified against SAP 2000 and proved to be much faster and just as accurate. It allowed many analyses with varying parameters to be run quickly with minimal human interaction.

A final note about this study is that it is meant to be a springboard for further research on CEUS seismic designs. As such, many of the findings are addressed in brief. Furthermore, many questions remain unanswered at the end of this study. The findings

do, however, provide a reasonable map for future earthquake engineering researchers who are examining the CEUS.

1.3 – Organization

Excluding this introductory chapter, this thesis has been organized into seven chapters. The second chapter contains the literature survey. In the second chapter, the groundwork for the parameter study as well as the IDA study is laid. The third chapter shows that OpenSees was a viable candidate for conducting the analyses in this study. After laying an informational groundwork and verifying OpenSees, the fourth and fifth chapters present the parameter study characteristics and the results. Chapter four describes the parameters and chapter five discusses the results of the parameter study. Based on the parameter study, models representative of the CEUS and WUS were constructed and subjected to a series of IDA's. Chapter six describes the characteristics of the models and damage measures used in the IDA's, and chapter seven describes the results of the IDA's. Finally, chapter eight provides conclusions and recommendations based on the parameter study and IDA study.

2.0 Background and Literature Survey

2.1 - Seismic Hazard and Risk in the Central and Eastern United States

Damaging earthquakes rarely happen in the Central and Eastern United States (CEUS). There has not been a significant earthquake in the CEUS since the late nineteenth century. This is not to say that the hazard is not present.

2.1.1 - CEUS Hazards

While infrequent, the CEUS has a history of damaging earthquakes. In 1811 and 1812 a series of three very damaging earthquakes with estimated moment magnitudes of M8.1, M7.8, and M8.0 occurred in the New Madrid Seismic Zone (Beavers 2002). Moreover, an earthquake of magnitude M7.3 occurred in Charleston, South Carolina, in 1886.

Not only have damaging earthquakes historically happened in the CEUS, but there is the potential for future damaging earthquakes. Moreover, researchers and scientists have confirmed that severe earthquakes in the CEUS would be felt over a much wider area. This would cause more widespread damage in the CEUS than a similar magnitude earthquake in the WUS.

2.1.2 - Code Changes Reflect Recognition of Hazards

In 1997, an overhauled version of the National Earthquake Hazards Reduction Program (NEHRP) work entitled "NEHRP Recommended Provisions for Seismic Regulations for New Buildings and Other Structures" (henceforth provisions), was completed (Leyendecker 2000). The provisions were a collaborative effort of the Building Seismic Safety Council (BSSC), the Federal Emergency Management Agency (FEMA), and the United States Geological Survey (USGS). The team of aforementioned participants working on the provisions was called the Seismic Design Procedure Group (SDPG). One of the more striking changes in the provisions was the decision to base

designs on a less probable earthquake event, one that has a 2 percent probability or less of occurring in 50 years (2/50 for brevity). A 2/50 earthquake has mean return interval of approximately 2500 years. The previous criterion was the 10 percent in 50 years (10/50 for brevity) event, which has approximately a 475 year mean return interval.

The rationale for the change was based on a desire to provide a "uniform margin against collapse" across the United States (Leyendecker 2000). The SDPG felt that well designed structures should have a seismic margin, or safety factor against collapse, of 1.5 built-in to the seismic designs of buildings. In other words, a building should be able to withstand 1.5 times the design earthquake with a low probability of collapse. On the West Coast, 1.5 times the design event, which was based on the 10/50 event, resulted in an earthquake that was approximately equal to the 2/50 event. While the 2/50 earthquake is quite rare, the SDPG thought it was not excessive to proportion structures to have a low probability of collapse if the 2/50 earthquake were to occur. In the Central and Eastern United States, the difference between the 10/50 event and the 2/50 event is much greater than in the west. Whereas the ratio is about 1.5 in the west, it can be as high as 5 in the east. Figures 2.1 and 2.2 show the differences between the 2/50 and 10/50 design events.

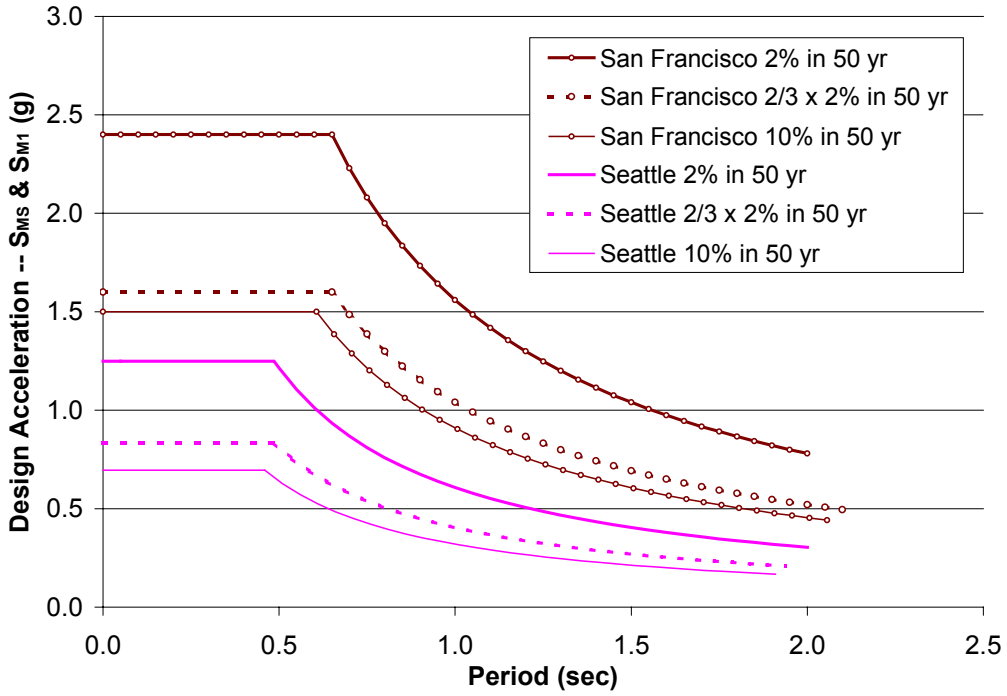

Figure 2.1 – Maximum Considered Spectral Response Accelerations for Selected WUS Cities

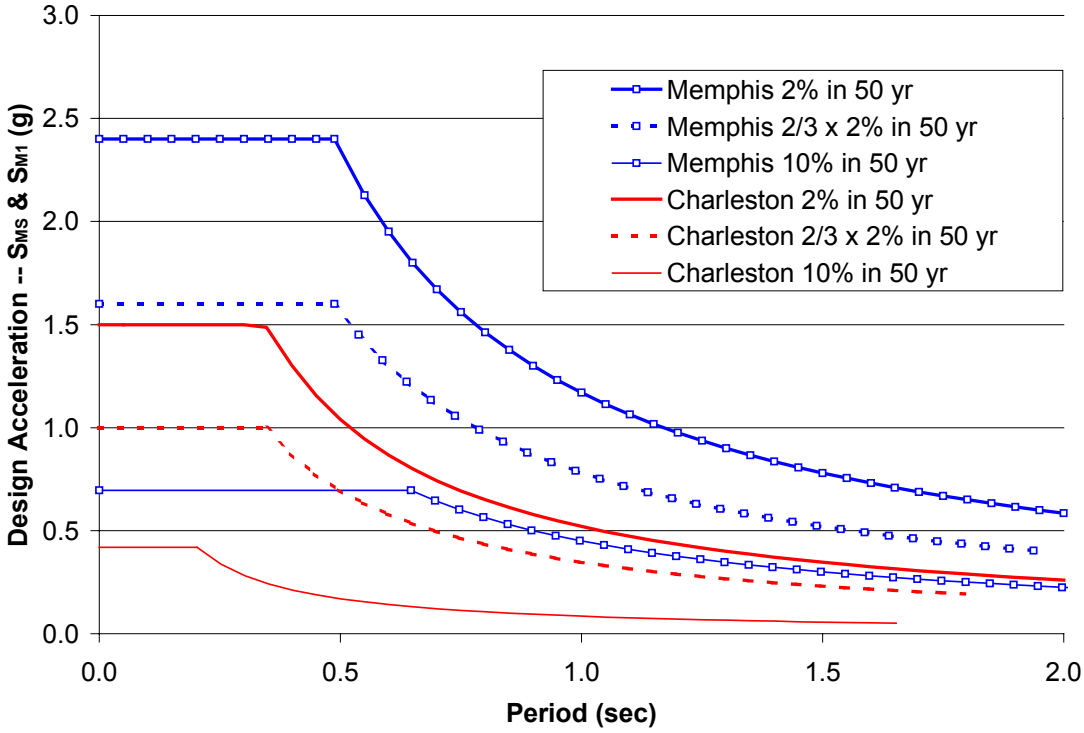

Figure 2.2 – Maximum Considered Spectral Response Accelerations for Selected CEUS Cities

Notice that 2/3rds of the 2/50 spectral response acceleration curves is approximately equal to the 10/50 design acceleration curves for the WUS cities in Figure 2.1. However, the 2/3rds of the 2/50 spectral response acceleration is much greater than the 10/50 spectral response acceleration for the CEUS cities shown in Figure 2.2.

So that structures throughout the US would have a uniform margin against collapse when subjected to the 2/50 event, the SPDG decided to change the design earthquake level to two thirds of the 2/50 event. Thus, all structures in the US should have a low probability of collapse in the 2/50 earthquake.

2.1.3 - CEUS Risk

Not only are there significant seismic hazards in the CEUS, there is considerable risk. As populations increase, so do the risks associated with seismic activity. Had the New Madrid Earthquakes of 1811 and 1812 happened today, they would have resulted in thousands of deaths and approximately $200 billion in damage (Beavers 2002). For

comparison's sake, the 1994 Northridge earthquake caused 57 deaths and $20 billion in damage.

Furthermore, a study by Hwang et al. (1997) indicated that a significant number of fire stations in Shelby County, Tennessee (Memphis and surrounding areas) would sustain heavy damage in magnitude 6.5 and 7.0 earthquakes. Hwang defines "heavy damage" as damage that is so extensive that repair is not feasible or major demolition is required. Specifically, Hwang reported that 53.5%, or 38 of 71 stations, would be heavily damaged in a 6.5 magnitude earthquake. Also, 94.4%, or 67 of 71 stations, would be heavily damaged in a 7.0 magnitude earthquake.

In summary, past earthquakes have shown that significant seismic hazard exists in the CEUS. Also, influential codification organizations have recently recognized this hazard by increasing the seismic design requirements. The hazards, coupled with the risks in the CEUS, warrant a fresh look at existing buildings in the CEUS as well as the current seismic building design requirements.

2.2 - Collapse and Related Literature

Collapse, as it relates to earthquakes, is not a simple subject. Uncertainties abound, as researchers have been unable to unanimously agree on even the definition of collapse. When a building is in rubble on the ground after an earthquake, it is clearly collapsed, whereas before the earthquake, it is not collapsed. Also, a building must be considered collapsed when it is damaged to an unusable degree. Much of the debate has revolved around how to quantify the intermediate stages between the uncollapsed and collapsed states. Matters have been complicated by the fact that there are a limited number of real case studies. In the last one hundred years, a relatively small number of buildings have collapsed in areas which have and enforce seismic design codes. As such, it is somewhat difficult to find studies on building collapses resulting from earthquakes. Further complicating factors in the collapse debate are the earthquakes themselves. Each new earthquake and its effects are ultimately unpredictable. New earthquakes do not have to conform to the predictive models of scientists and the design limits of engineers. This may be particularly true in the CEUS where the seismotectonic earthquake

generating process is still unknown. New earthquakes frequently challenge seismic design practice. Consequently, a major impetus for conducting new research on dynamic collapse and seismic damage is new earthquakes.

In the following sections, some of the lessons learned from past earthquakes, various experimental studies, and analytical studies will be summarized. Several sections are required to adequately address the findings of the collapse related research because there is a multitude of information and many varied viewpoints. The areas of emphasis are dynamic instability and P-Delta effects, the seismic performance of gravity load designed structures (gravity load design requirements are more substantial than lateral load design requirements), vertical acceleration effects, collapsed building investigations, and damage indices.

2.2.1 - Dynamic Instability and P-Delta Effects

Many researchers have conducted studies to identify factors that destabilize buildings subjected to earthquakes. One such destabilizing factor is the P-Delta effect. P-Delta effects reduce the effective lateral stiffness and strength of buildings and can become significant as the lateral displacements become large. The term "P-Delta", at least as far as this study is concerned, refers to an additional moment and subsequent displacement caused by the vertical or gravity loads (P) on a structure that has moved through an initial lateral displacement (Δ). P-Delta effects are considered to be second order effects because they are caused by initial displacements and result in secondary displacements. Figure 2.3 illustrates the moments caused by P-Delta effects.

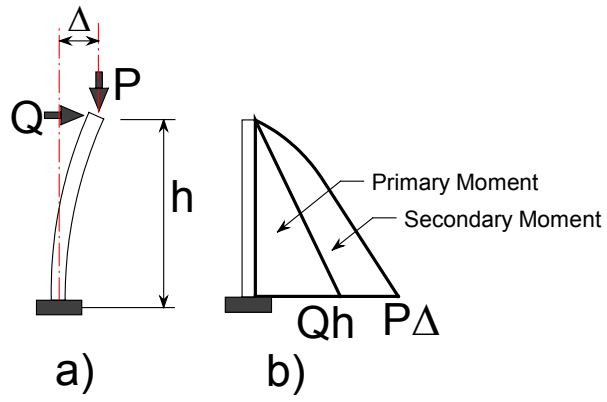

Figure 2.3 – P-Delta Effects and Related Moment Diagram

In Figure 2.3a, the lateral load (Q) causes a displacement (Δ), which in turn causes a moment in the structure that increases from zero at the top of the column to Q·h at the base of the column. The load, P, causes additional moment and displacement as it acts at a moment arm of Δ. It is important to note that Δ is not constant. P acts at a moment arm of Δ, which continues to increase until static equilibrium is reached. As with the lateral load, the moment due to P increases from zero to P·Δ at the base of the column. In Figure 2.3b, the moment diagram resulting from the loading of Figure 2.3a is shown. The total moment at the base of the column is the sum of the lateral force moment (Q·h) and the P-Delta moment (P·Δ). An important point to make about the moments at the base of Figure 2.3b is that the lateral force moments from a region with high seismic hazard will be much larger than those in a low seismic region. Furthermore, buildings will generally have similar gravity loads regardless of region and so will have similar P-Delta moments regardless of region assuming that such structures also have similar drifts. In other words, the P-Delta effects would be larger relative to the lateral force moments when comparing low seismic regions to high seismic regions. Macrae et al. (1993) made this point and observed that neglecting the P-Delta effects in a high seismic region may not be as hazardous as neglecting the P-Delta effects in a low seismic region.

P-Delta effects can be accounted for in analysis by reducing the lateral stiffness of a structure by a certain amount. The amount of stiffness reduction is called the geometric stiffness. Referring to figure 2.4, geometric stiffness is derived in the following manner.

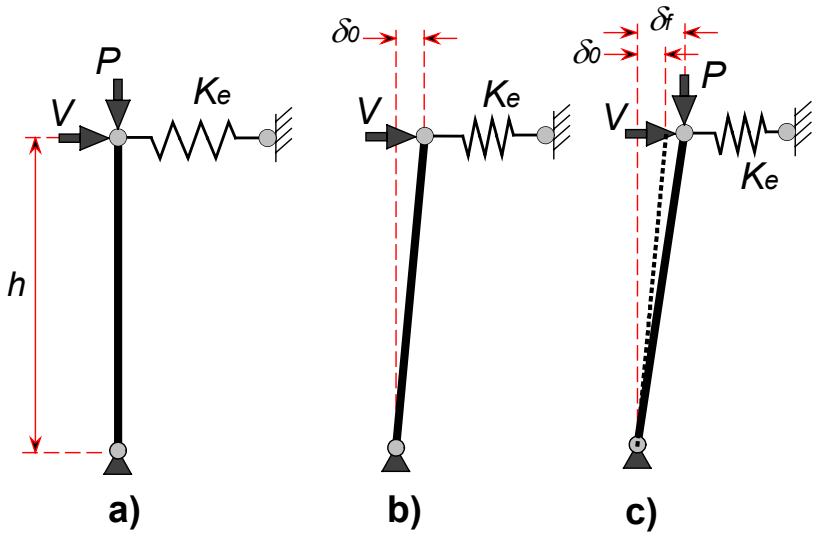

Figure 2.4 – Deriving Geometric Stiffness

Given the structure shown in figure 2.4a with an elastic stiffness, K_e, height, h, lateral load, V, and neglecting gravity load, P, equilibrium about the undeformed shape results in equation 2.1.

$$Vh - K_e \delta_0 h = 0 \qquad \textbf{(2.1)}$$

where

δ_0 = initial deformation resulting from V.

Solving equation 2.1 for δ_0,

$$\delta_0 = \frac{V}{K_e} \qquad \textbf{(2.2)}$$

The initial deformed shape resulting from equation 2.1 is shown in figure 2.4b. By considering Load, P, equilibrium about the deformed shape results in equation 2.3.

$$Vh + P\delta_f - K_e \delta_f h = 0 \qquad \textbf{(2.3)}$$

where

δ_f = total deformation resulting from P and V

Solving equation 2.3 for δ_f,

$$\delta_f = \frac{V}{K_e - \frac{P}{h}} \qquad \textbf{(2.4)}$$

Define the geometric stiffness, K_g as,

$$K_g = \frac{P}{h} \tag{2.5}$$

The sign convention of equation 2.5 is very important because a compressive force should always reduce the overall stiffness of a system. Thus, P should be negative when a member is in compression. Furthermore, when a member is in tension, the overall stiffness of a system should increase. So, P should be positive for a tensile force. Combining equation 2.5 and 2.4 results in,

$$\delta_f = \frac{V}{K_e + K_g} \tag{2.6}$$

The overall system stiffness is the sum of the elastic and geometric stiffness. From equation 2.4, the negative sign is incorporated in the K_g value of equation 2.6. Since K_g is negative due to a compressive force, the overall system stiffness is less than the initial elastic stiffness, K_e.

At this point, hopefully it is obvious that P-Delta effects reduce the lateral stiffness of structures by way of negative geometric stiffness. P-Delta effects also alter the force-deformation curve of a structure. MacRae (1994) provided a derivation of the P-Delta force-deformation alteration in an article he published dealing with P-Delta effects on single-degree-of-freedom structures. Figure 2.5 shows the alteration.

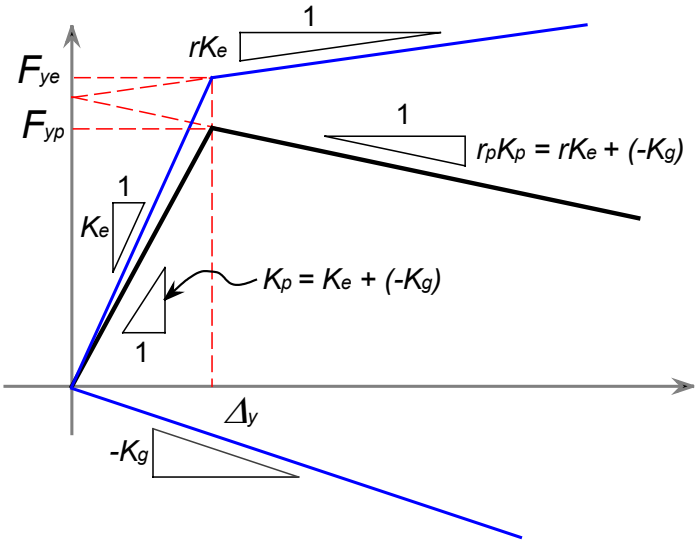

Figure 2.5 - Force Displacement Relationship Considering P-Delta Effects

In figure 2.5, the initial system parameters (without P-Delta effects) are denoted with the subscript "e." The initial stiffness of the system is K_e. For this case, the system is bilinear with a secondary stiffness that is the product of the initial stiffness (K_e) and a factor (r). The factor (r) is called the post-yield stiffness ratio. In Figure 2.5, the K_g term is shown as negative. This is because the P-Delta effects in buildings that are caused by gravity forces result in compressive forces in the columns. The altered characteristics of the system are denoted with the subscript "p." The altered stiffness and post-yield ratio values were derived as follows.

Change in Elastic Stiffness (K_e)

$$K_p = K_e - K_g$$

Define the stability ratio (θ) as

$$\theta = \frac{K_g}{K_e}, \tag{2.7}$$

In equation 2.7, K_g is a positive quantity. The destabilizing effect of K_g for compressive loads is handled by subtracting K_g and or θ in MacRae's derivation. Using the stability ratio as a positive quantity is consistent with the *NEHRP provisions*, but can become confusing in structures where the members are in tension, such as a cable structure. At any rate, P-Delta effects should reduce the elastic stiffness of a structure.

$$K_p = (1-\theta)K_e \tag{2.8}$$

Change in Yield Force (F_{ye})

$$F_{yp} = K_p \Delta_y \ , \ F_{ye} = K_e \Delta_y$$

$$F_{yp} = (1-\theta)K_e \Delta_y$$

$$F_{yp} = (1-\theta)F_{ye} \tag{2.9}$$

Change in Post-Yield Stiffness (r_pK_p) and Post-Yield Stiffness Ratio (r_p)

$$r_p K_p = rK_e - K_g$$

$$r_p K_p = rK_e - \theta K_e = (r-\theta)K_e$$

$r_p = (r-\theta)\frac{K_e}{K_p}$, from equation 2.8, r_p becomes

$$r_p = \frac{r-\theta}{1-\theta} \tag{2.10}$$

If the system shown in figure 2.5 is assumed to be infinitely ductile and one considers systems that have negative post-yield stiffnesses, then the collapse displacement, the point where zero force causes displacement, is denoted by Δ_c. The collapse displacement is path dependent in that a structure must follow the entire force deformation path from zero force to yield to Δ_c for collapse to occur. The value of Δ_c is given by the following equation.

$$\Delta_c = \left(1-\frac{1}{r_p}\right)\Delta_y$$

The corresponding ductility is

$$\mu_c = 1-\frac{1}{r_p} \tag{2.11}$$

In reality, no system is infinitely ductile and therefore the collapse displacement would not be a limiting value in systems with small negative post-yield stiffnesses. It could be a limiting value in systems with high negative post-yield stiffnesses, though.

The information provided up to this point has primarily explained why P-Delta effects occur and quantified the resulting changes to structural parameters. However, simply understanding the ways that P-Delta effects alter structural characteristics does not necessarily help predict the changes in seismic response due to the consideration of them. As such, many researchers have endeavored to determine the P-Delta sensitivity of various seismic loading situations and structural parameters.

MacRae (1994) and Macrae et al. (1993) explored P-Delta sensitivities using single-degree-of-freedom oscillators designed to represent bridge piers. In these studies, the researchers constructed 51 oscillators with varying r_p values and target ductilities. All of the models had damping ratios that were two percent of critical. In these studies, the authors made several discoveries. First, considering all factors, the post-yield stiffness ratio including P-Delta effects, r_p, had the greatest influence on strength demands. Their

analytical method involved specifying target ductilities and then modifying the strength of a model until the target ductility was achieved. The measure of strength used was a nondimensional value, which the researchers called the acceleration ratio (a_r). It is given by

$$a_r = \frac{a_{ye}}{a_e} = \frac{F_{ye}}{W}\frac{g}{a_e} \qquad \textbf{(2.12)}$$

where

F_{ye} = yield force

W = structure's weight

g = acceleration of gravity

a_e = elastic response acceleration determined from a response spectrum

Before discussing the usefulness of the acceleration ratio, it is worthwhile to further discuss the physical meaning of it. In terms of the NEHRP provisions, the acceleration ratio is most akin to the reciprocal of the R value. This is because the R value is the ratio of elastic force demand to yield force. Furthermore, the acceleration ratio can be expressed in the NEHRP provision's terms according to equation 2.13.

$$a_r = \frac{C_s}{S_a} \qquad \textbf{(2.13)}$$

where

C_s = Seismic Response Coefficient,

S_a = Elastic spectral acceleration as a percentage of gravity

Using the acceleration ratio, MacRae, Priestly, and Tao observed that the strength necessary to achieve the specified ductility demands increased sharply as the r_p value dropped below 0.1 and even became negative. It is important to note that there was some variation in the results due to period, but it does not compare with the influence of r_p. From the researchers' studies, limits were established to make sure that the ductility

requirements of a design, coupled with the r_p value, would result in a structure with adequate strength. The limits they established are presented in Table 2.1 below.

Table 2.1 – Average Acceleration Ratios for Oscillators with Periods Greater than 0.5 Seconds.

r_p	Ductility, μ			
	1	2	4	6
-0.25	1.000	0.568	0.456	--
-0.10	1.000	0.492	0.338	0.296
0.00	1.000	0.421	0.208	0.146
0.10	1.000	0.386	0.163	0.101
0.25	1.000	0.372	0.160	0.106
0.50	1.000	0.385	0.179	0.124
0.75	1.000	0.426	0.208	0.142
1.00	1.000	0.500	0.250	0.167

Notice in Table 2.1 that there is no acceleration value corresponding to a target ductility of 6 and an r_p of –0.25. This was because the yield strength required to reach a ductility of six was very large and most likely unreasonable. Also notice that when r_p is equal to one, the acceleration ratios are equal to the reciprocal of the ductility. This makes sense, because an r_p of one indicates an elastic structure, and so the ductility capacity as the researchers present it would be inversely proportional to the yield force, assuming that the equal displacement concept is valid.

To use table 2.1 in a design setting, three pieces of information are required. First, it is necessary to determine the structure's weight. Then, it is necessary to determine the structure's spectral acceleration value from a response spectrum, which requires some estimate of the building's period. Third, the acceleration ratio is determined using the required ductility capacity and a reasonably determined r_p value. The r_p value is based on the building weight, post-yield stiffness ratio, and an approximate elastic stiffness. With the aforementioned information, Table 2.1 would provide an acceleration ratio. The designer could then use the following equation to determine an estimate of the required yield strength:

$$F_{y-reqd} = (a_r S_a)W \qquad \textbf{(2.14)}$$

The designer would then have to check the yield strength to see if it violated the ductility demand limits, by conducting a nonlinear analysis of the system. If the ductility demands were not within a prescribed bound, then the strength would be increased until the ductility demand requirements were satisfied. Basically, the MacRae et al. (1993) research can be used to create preliminary models that can then be refined for final design.

Macrae et al. (1993) also found that energy input significantly influenced P-Delta effects, where energy was a measure of duration. To examine the effects of energy input, the researchers subjected each of the models to a particular earthquake twice successively. They found that oscillators with low to negative post-yield stiffness had significantly increased strength requirements when the energy input was increased. They also found that oscillators with negative post-yield stiffnesses tended to have permanent displacements, called residual displacements, at the end of a dynamic analysis. The researchers concluded that since energy input influences P-Delta effects, a proper P-Delta design methodology must not be based on static considerations alone.

In addition to the above observations, Macrae affirmed, as many others have, that the stability ratio was a good indicator of P-Delta sensitivity. They mention, though, that stability ratios would unlikely be greater than 0.1 and would typically be about 0.06 in real structures. It is important to note, however, that the researchers were studying bridge piers on the West Coast of the United States. Thus, their observation is may be untrue for Central and Eastern United States structures.

In other research, an analytical study of a ten story RC building by Shooshtari and Murat (1999) found that the inclusion of P-Delta effects could increase the lateral displacement by as much as 40%. The researchers also noted that P-Delta effects were most significant when large amounts of inelastic response occurred.

Gupta and Krawinkler (1999 and 2000a) showed the sensitivity of P-Delta effects in the modeling of multi-degree-of-freedom (MDOF) structures. In their work, they demonstrated the significant influence of panel zone modeling on the response of a structure. They also showed that the inclusion of other stiffness sources, such as nonstructural elements and interior gravity columns, can significantly reduce P-Delta effects. However, they admitted that strength and stiffness degradation, which was not

considered in their studies, could increase P-Delta effects. This was because degrading strength and stiffness has the ability to influence deformations. Furthermore, Gupta and Krawinkler noted that long, strong ground motions and pulses tend to accentuate P-Delta effects and increase residual displacements. They acknowledged that accounting for P-Delta effects is not a simple or straightforward procedure.

In MDOF moment resisting frame structures, P-Delta effects are essentially a story related issue. For a particular story, the stability ratio has been determined to be a good indicator of P-Delta sensitivity. It is given by:

$$\theta_i = \frac{P_i \Delta_i}{V_i h_i} \tag{2.15}$$

where

θ_i = the stability ratio of story i

P_i = the gravity loads in story i

Δ_i = the elastic story drift at story i associated with V_i

V_i = the total horizontal shear applied to story i

h_i = the height of story i

Gupta and Krawinkler, like MacRae, Priestly, and Tao, affirmed the stability ratio as a good indicator of second order displacement sensitivity, but emphasized that it was only an indicator and that the issue was too complicated to be characterized by only the stability ratio. Gupta and Krawinkler observed that the P-Delta effects were most severe in the lower stories of tall MDOF structures.

Gupta and Krawinkler claim that a good tool for determining P-Delta sensitivity is a pushover analysis. A pushover analysis involves developing a nonlinear analytical model with the applicable gravity loads and then applying small incremental lateral loads, or when necessary incremental imposed lateral displacements, until the structure collapses. At each load increment, the lateral displacement is recorded. The resulting plot of force versus displacement is the pushover curve. An example of a pushover curve is shown in figure 2.6.

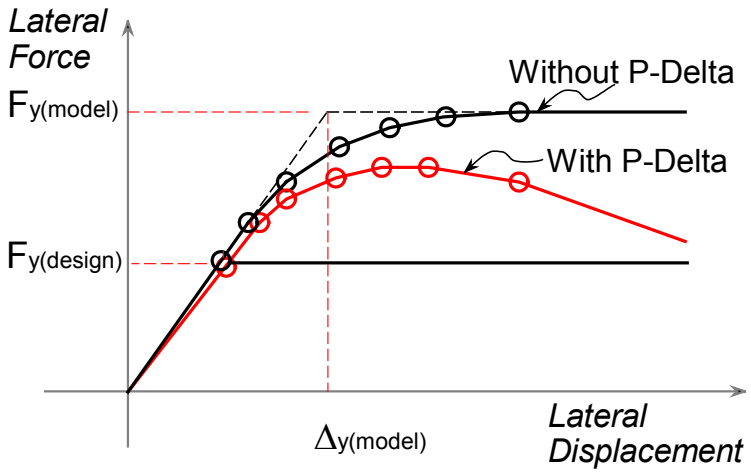

Figure 2.6 – Pushover Example

Notice that the pushover curve looks somewhat similar to figure 2.5. Further information on the usefulness of pushover curves is in Krawinkler and Seneviratna (1998).

In an earlier study, similar to that of Gupta and Krawinkler, Challa and Hall (1994) examined a twenty-story steel moment frame. They also observed P-Delta sensitivity in the lower stories of their analytical model. Moreover, they also observed residual displacements after subjecting their structure to pulse loading. Challa and Hall did not consider structural degradation in their research, but concluded that further studies should include degradation because of the large ductility demands and cyclic nature of the dynamic P-Delta issue.

In some of the aforementioned P-Delta studies, residual displacements were mentioned. Several researchers have argued that residual displacements are related to P-Delta effects and in fact should be considered separately to determine the post earthquake stability of a structure. MacRae and Kawashima (1997) and Kawashima and Macrae (1998) developed a residual displacement response spectrum to determine the amount of residual displacement that one might expect from a given ground motion. They standardized their response spectrum by dividing by the maximum residual displacement, which was generally equal to the maximum deformation minus the elastic deformation at that point. Given the standardization, MacRae and Kawashima's response spectrum ranged from zero for no residual displacements to one for maximum residual displacements. As with others studying P-Delta effects, the researchers found the post-yield stiffness ratio including P-Delta effects (r_p) to be most indicative of residual

displacement tendencies. By experimentation, they ruled out ground motion magnitude, site-to-epicenter distance, structural period, and soil conditions as strong indicators. MacRae and Kawashima found that residual displacements were approximately zero until the r_p value dropped below 0.1. Furthermore, they observed that the residual displacements quickly approached the maximum of 1.0 as the r_p values shifted from positive to negative.

Mehanny and Deierlein (2001) developed a method to determine the influence of damage and residual displacements on the instability of steel frames having composite floor systems. Their procedure was rather involved and had the following steps.

1. Perform a nonlinear analysis, record the spectral acceleration value, and calculate subsequent damage values.
2. Adjust the geometry (account for residual displacements) and structural characteristics (decrease strength and stiffness for damage)
3. Conduct a static buckling analysis of the adjusted structure by applying $\lambda_u P$ gravity loads until the structure becomes unstable, where P is the actual gravity load and λ_u is a factor to increase the original gravity load.
4. Repeat the first three steps of the procedure for a range of scaled ground motion values.

Mehanny and Deierlein defined the λ_u value as the stability index. It corresponded to a given level of spectral acceleration. Explicitly, it is defined as the ratio of ultimate vertical load at instability to unfactored gravity load. All structures should have stability index greater than one initially. This is because a stability index of one indicates that the unfactored gravity loads will cause the structure to collapse. To assess the effects of residual displacements on instability, Mehanny and Deierlein also calculated stability indices for structures where they only updated the geometry and did not account for damage. They found that about one third of the loss in frame stability was caused by residual displacements, and component damage accounted for about two thirds.

Other researchers have moved beyond trying to identify P-Delta sensitive characteristics and loading conditions toward the development of a more theoretically based dynamic instability criterion. Hjelmstad and Williamson (1998), for example, provide a good background on the theory behind dynamic instability and then propose

their own theoretical take on dynamic instability. In simple terms, Hjelmstad and Williamson defined dynamic stability as finite, predictable oscillations that do not grow beyond certain bounds. Dynamic instability occurs when oscillations grow exponentially without bound. The authors discussed the relevance of hysteretic shapes, vertical loads, damage accumulation, and residual displacements on the dynamic stability of structural systems.

In similar work, Araki and Hjelmstad (2000) endeavored to determine conditions where unbounded oscillations were most likely. They found that dynamic collapse was likely if both the sign of the minimum eigenvalue of the Hessian (a matrix of the second derivatives) of potential energy was negative and the loading direction coincided with the direction of collapse. They admitted that their dynamic instability criterion would require further refinement and perhaps simplification to be applicable to real structures and design situations. The researchers observed that P-Delta effects, the tangent stiffness, and the direction of unloading significantly influence the probability of dynamic collapse.

Williamson and Hjelmstad (2001) published further work in the field of dynamic instability, this time adding time varying axial loads to the mix. The researchers explored the issue by starting with the fact that vertical harmonic motion can cause lateral resonant motions. When the frequency of a vertical motion is equal to one or two times the lateral frequency of the structure, then the amplitude of the lateral oscillations is likely to grow unbounded for undamped systems. Williamson and Hjelmstad found that by increasing the amount of gravity load present on the structure, the envelope of unstable frequencies increases. The researchers also examined the effects of various constitutive models and found great variation in dynamic response. The variation did not lead to specific conclusions, but only emphasized the importance of the constitutive models to dynamic response.

Williamson and Rungamornrat (2002) conducted another related study examining the effects of adding white noise to harmonic vertical excitations. Included in the study was a critical review of various numerical integration methods. This was included because in some cases the harmonic excitations and white noise, in conjunction with complicated nonlinear models, created convergence and accuracy concerns. After

resolving the integration issue, they concluded that the white noise did not have a significant effect on the lateral vibration of the structure.

In yet further related research, Williamson (2003) specifically addressed the issue of damage on dynamic instability. Williamson incorporated the popular Park and Ang (1985) damage model into a hysteretic material for his research. The Park and Ang damage model, as Williamson used it, essentially had a term which accounts for damage due to maximum deformations and a term which accounts for damage due to fatigue or cyclic inelastic excursions. Moreover, the version of the Park and Ang index that Williamson used had factors, α and β, which adjusted the influence of the maximum displacement and fatigue terms, respectively. Williamson's version of the Park and Ang index is given by equation 2.16.

$$D_{PA} = \alpha \frac{x_{\max}}{x_{u,mon}} + \beta \frac{E_h}{F_y x_{u,mon}} \qquad \textbf{(2.16)}$$

where,

x_{max} = maximum cyclic displacement

$x_{u,mon}$ = ultimate displacement under monotonic loads

E_h = plastic dissipated energy

F_y = yield force

A more complete description of this damage model will be presented later. In his study, Williamson found that α and β values significantly affected the damage the structures incurred. In fact, he found that in some situations faster rates of damage actually reduced the deformation demands in the structures. It is important to note that Williamson's study was purely analytical and not tied to experimental results.

Most of the existing literature dealing with P-Delta effects and dynamic instability is analytical in nature, but there have been several experimental studies. Vian and Brunea (1999) subjected 15 small scale models to ground motions on a small shaking table. The models consisted of four square steel columns with a weight on top. The systems were restrained so that they would act as SDOF oscillators. KL/r values of 100, 150, and 200 were used.

From their research, Vian and Brunea concluded that the stability ratio (θ) had a significant impact on the P-Delta effects. Moreover, they concluded that the elastic spectral acceleration, ductility demand, and percent drift were all inversely proportional to θ. They found that models with stability ratios less than 0.1 were able to endure significantly higher ground motion accelerations, were more ductile, and accumulated higher drifts.

El-Attar et al. (1997) illustrated P-Delta effects experimentally when examining concrete structures designed only for gravity loads. Two experimental structures were used, a $1/6^{th}$ scale two story, one bay reinforced concrete frame, and a $1/8^{th}$ scale three story, three bay reinforced concrete frame. The authors observed that the moments at the mid-height of the columns were as much as 27% higher than those that should have been present due to the recorded accelerations at the top of the floor. The additional moments were caused by P-Delta effects.

In addition to the many articles trying to identify situations where P-Delta effects are significant, there have been several studies in which researchers have sought ways to include P-Delta effects in design. Bernal (1987) developed P-Delta amplification factors so that designers could simply account for P-Delta effects with elastic analyses. The amplification factors were dependent on the system ductility demand and stability coefficients. As both the ductility and stability coefficient increased, so did the amplification factor. The factors ranged from 1.014 for a structure with a ductility of one and a stability ratio of 0.025, to 3.423 for a structure with a ductility of six and a stability ratio of 0.2. Bernal developed the following P-Delta amplification (β) equation based on a regression analysis of his results:

$$\beta = 1.87(\mu - 1) \qquad \textbf{(2.17)}$$

where,

μ = the design ductility

Bernal noted that a weakness of his method was that the amplification factor did not provide a uniform margin of safety against collapse. He also noted that a limit should

be placed on the ductility to reduce residual displacements and increase post earthquake stability. As such, the maximum ductility used in Bernal's analyses is given by

$$\mu_m = \frac{1}{\lambda\theta} \tag{2.18}$$

where λ is the ratio between the ultimate gravity load and the gravity load present during the earthquake. It is given by

$$\lambda = \frac{P_u}{P_s} = \frac{(1.4D + 1.7L)}{\phi(D + 0.25L)}$$

where,

D = Dead Load

L = Live Load

ϕ = Resistance Factor (0.75 in Bernal's work)

Equation 2.18 was derived by considering two different levels of gravity load. An explanation of this follows and is graphically shown in figure 2.7.

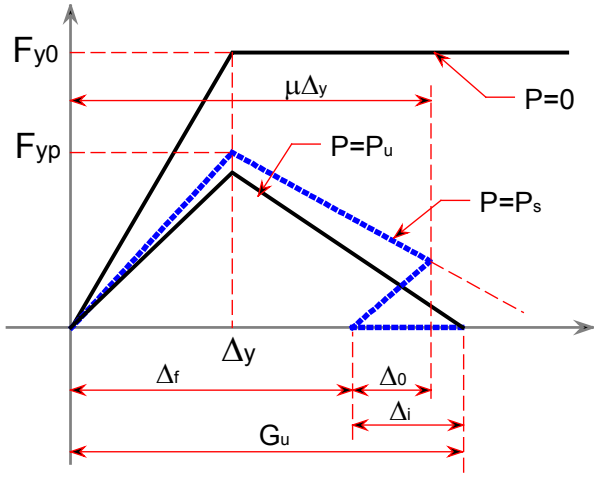

Figure 2.7 – Ductility Limitation based on Post Earthquake Stability

For a particular structure with a bilinear force deformation relationship, the shape of the curve is augmented by the level of gravity load on the system. This is shown in the three different curves in figure 2.5 ($P = 0$, $P = P_s$, $P = P_u$). As the gravity load increased from 0 to P_u, the effective stiffness and strength of the system decreased. When the

structure had zero gravity load, Bernal assumed that the system was elastic-perfectly-plastic as shown by the P = 0 curve. For a given amount of gravity load at the time of a seismic event (P_s), the structure would reach a maximum displacement of $\mu\Delta_y$ and would have a permanent deformation upon unloading of Δ_f. Similarly, if the same structure was, instead, subjected to the ultimate gravity load (P_u) and was pushed until collapse, the point in a path dependent sense where zero force would cause displacement, then the resulting collapse displacement would be G_u. Bernal defined the difference between G_u and Δ_f as Δ_i. He argued that one should limit the ductility so that if a structure with permanent deformation were subjected to the ultimate gravity load (P_u), then the sum of the resulting additional displacement (Δ_i) and the residual displacement (Δ_f) would be equal to or less than the collapse displacement (G_u). Equation 2.18 was derived from the following relationships, which correspond to figure 2.7.

$$\Delta_0 = \Delta_y \frac{(1-\mu\theta)}{(1-\theta)}$$

with the Δ_0 equation and the maximum displacement ($\mu\Delta_y$)

$$\Delta_f = \Delta_y \frac{(\mu-1)}{(1-\theta)} \qquad \textbf{(2.19)}$$

Then,

$$\Delta_i = (P_u - P_s)\frac{\Delta_f}{K_0 H(1-\theta_u)} \qquad \textbf{(2.20)}$$

where,

$$\theta_u = \frac{P_u}{K_0 H}$$

Using the fact that $G_u = \Delta_f + \Delta_i$, $\theta_u = \lambda\theta$, and equations 2.19 and 2.20.

$$G_u = \Delta_y \frac{(\mu-1)}{(1-\theta)}\left(1 + \frac{(P_u - P_s)}{K_0 H(1-\theta_u)}\right) \qquad \textbf{(2.21)}$$

which simplifies to

$$G_u = \Delta_y \frac{(\mu-1)}{(1-\lambda\theta)} \qquad \textbf{(2.22)}$$

Equation 2.22 is essentially derived from the dotted path shown in figure 2.7. G_u can also be derived solely from the curve where the gravity load equals P_u. The resulting G_u equation is

$$G_u = \frac{\Delta_y}{\lambda\theta} \tag{2.23}$$

By equating equations 2.22 and 2.23 and solving for ductility (μ), one ends up with equation 2.18. This long, tedious derivation is important because it is the basis for the stability limit used in the current NEHRP seismic provisions.

In Bernal's study, he assumed that the live load to dead load ratio was 0.4, and simplified the maximum ductility equation to

$$\mu_m = \frac{0.4}{\theta} \tag{2.24}$$

Charney and Harris (1988) argued for a refinement of Bernal's method. They contended that there should be an upper limit on the stability ratio, not on the ductility. The limit was given by

$$\theta = \frac{1}{\lambda C_d'} \tag{2.25}$$

where,

C_d' = the adjusted ductility demand.

C_d' is equal to C_d when seismic forces control design, and is calculated by the following equation when the actual capacity is greater than the seismic design capacity:

$$C_d' = C_d \frac{V_{xs}}{V_{xw}},$$

where,

V_{xs} = the seismic story shear

V_{xw} = the actual shear capacity

In the 2000 edition of the NEHRP Seismic Provisions, a modified version of the stability ratio given by equation 2.15 is used both as a limiting value and an altering value. The stability ratio is modified by dividing by the deflection amplification factor, C_d. The resulting equation is

$$\theta_i = \frac{P_i \Delta_i}{V_i h_i C_d} \qquad \textbf{(2.26)}$$

It is important to note that Δ_i is the total displacement including inelasticity. For a given story, i, if the stability ratio is less than 0.1, then P-Delta effects do not need to be considered. If the stability ratio is between 0.1 and θ_{max}, then the design story shears, V_i, must be increased. An acceptable method of altering the shears is to increase them by a factor, a_d. The equations for θ_{max} and a_d are given by the following equations:

$$\theta_{\max} = \frac{0.5}{\beta C_d} \le 0.25 \qquad \textbf{(2.27)}$$

where

β = the ratio of shear demand to shear capacity for the story in question. It may be taken as 1.0 conservatively.

$$a_d = \frac{\theta}{1-\theta} \qquad \textbf{(2.28)}$$

The quantity βC_d is essentially a modified ductility demand. It accounts for overstrength. Note that equations 2.18, 2.25, and 2.28 are very similar in their intent with slight modifications.

The resulting story shears including P-Delta effects are multiplied by $(1+a_d)$. This results in the following equation:

$$V_{iPD} = \frac{V_i}{1-\theta} \qquad \textbf{(2.29)}$$

Bernal (1992a, 1992b, 1998) also developed a method to check for dynamic instability with limited computations. The method involved reducing MDOF systems to SDOF systems and then statistically determining base shear coefficients to ensure stable response. An acceptable method to create equivalent SDOF systems is to conduct a

pushover analysis and fit a bilinear curve to the pushover curve. However, for the purposes of instability calculations, Bernal found that acceptable results could be obtained by only considering the initial elastic shape and collapse shape of the structure. The two necessary shapes were represented through stability ratios:

$$\theta_0 = \frac{3Ng\tau}{(2N+1)\omega_0^2 h} \tag{2.30}$$

where

θ_0 = elastic stability ratio (see equation 2.2-24)

N = number of stories

τ = the ratio of total weight assumed to be present during a ground motion to the weight used to calculate the natural period (usually between 1.1 and 1.2)

h = the total height of the building

ω_0 = the fundamental frequency

and

$$\theta_m = \frac{\Omega g\tau}{\omega_0^{\,2} h} \tag{2.31}$$

where

θ_m = collapse stability ratio

$$\Omega = \frac{\left(1 - \frac{G}{2h} - \frac{E}{h}\right)}{\frac{G}{h}\left(1 - \frac{2G}{3h} - \frac{E}{h}\right)} \tag{2.32}$$

Figure 2.8 defines the terms in equation 2.32.

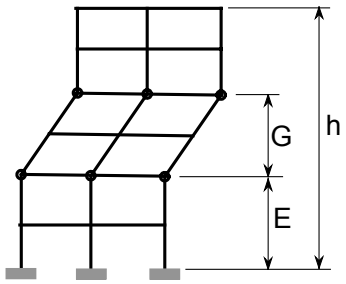

Figure 2.8 – Parameters that Define the Shape of an Arbitrary Mechanism

Bernal combined the two stability ratios into a single parameter for the SDOF idealization. The mixing of the two terms is adequate for determining instability, but does not provide an accurate force deformation plot. The resulting equivalent formulation of the stability ratio, fundamental frequency, and spectral acceleration is given by

$$\bar{\theta} = \frac{\theta_m}{Q}, \quad \bar{\omega}_0^2 = \omega_0^2 Q, \quad \bar{S}_{au} = S_{au} Q$$

where

$$Q = 1 - \theta_0 + \theta_m \tag{2.33}$$

Bernal then went on to statistically determine values of effective spectral acceleration that would lead to instability based on the effective SDOF parameters just described. For elastoplastic systems, the limiting spectral acceleration values are

$$\bar{S}_{ac} = \frac{5\bar{\theta}^{0.75}}{\bar{T}^{1.42}} PGV\sqrt{t_{0.9}} \le \frac{36\bar{\theta}^{0.75}}{\bar{T}^{1.86}} PGD \cdot t_{0.9}^{0.2} \tag{2.34}$$

For stiffness-degrading stystems, the limiting spectral acceleration values are

$$\bar{S}_{ac} = \frac{20\bar{\theta}^{0.85}}{\bar{T}^{1.35}} PGV \le \frac{54\bar{\theta}^{0.85}}{\bar{T}^{1.74}} PGD \tag{2.35}$$

where

$t_{0.9}$ = the duration in the central portion of the ground motion where 90% of the energy occurs.

$$\bar{T} = \frac{2\pi}{\bar{\omega}_0}$$

The margin of safety against collapse (I_c) was then calculated as

$$I_c = \frac{V_u}{V_c}, \tag{2.36}$$

where,

V_u = the ultimate base shear capacity

$V_c = \frac{M_t \bar{S}_{ac}}{Q}$ = the collapse base shear **(2.37)**

where M_t = total mass of the system

After deriving the above equations, Bernal compared his simplified SDOF method of determining instability to MDOF methods. In general, he found good agreement between the SDOF and MDOF methods. In this study, Bernal came to the conclusion that dynamic P-Delta amplification factors, which he developed in previous works, were inadequate to account for P-Delta effects. He further noted that P-Delta effects are a story wide issue.

In summary, P-Delta effects are very complicated. Researchers, in general, agree that the post-yield stiffness ratios, stability ratios, and ductility demands are the most important factors influencing P-Delta effects. Both analytical and experimental studies have confirmed these factors to be significant. As such, design methods have incorporated limits on stability ratios that incorporate ductility demands, post-yield stiffness ratios, and residual displacements. Other factors that influence P-Delta effects, but not to the degree of the aforementioned factors, are modeling choices and rates of damage accumulation.

2.2.2 - Gravity Load Designed (GLD) Structures

GLD structures are those that are primarily designed to withstand gravity loads. Such structures are designed for lateral loads, but lateral load demands are typically much less than the gravity load demands. Most of the low rise buildings constructed in the CEUS, at least those that are away from the coastline, would probably be considered GLD structures. Since a major emphasis of this work revolves around the CEUS, it is important to know how such structures would perform in an earthquake. In the literature, only reinforced concrete (RC) GLD structures have been specifically addressed, and so the rest of this section is devoted to them.

Beres et al. (1996) provide the most comprehensive description of GLD structures. After reviewing five decades of ACI codes and consulting practicing structural engineers, the authors came up with the following list of characteristics for RC GLD structures:

1) Longitudinal reinforcement in the columns of not more than 2%.
2) Lapped splices of column reinforcement at the maximum moment region just above the construction joint at the floor level.
3) Widely spaced column ties that provide little confinement to the concrete.
4) Little or no transverse reinforcement within the beam-to-column joint.
5) Discontinuous positive beam reinforcement with a short embedment length into the column.
6) Columns with bending moment capacity less than that of the beams.

All of the aforementioned RC GLD structure characteristics contribute to degradation of strength and stiffness and/or lower ductility capacity. Such structures would probably be considered ordinary moment frames. These characteristics are in contrast to special and intermediate moment frames for which the detailing requirements are more stringent so as to provide for more ductile behavior and smaller amounts of strength and stiffness loss.

Besides providing the above list, Beres, Pessiki, White, and Gergely conducted experiments on 34 RC interior and exterior beam-column joints in order to provide a better basis for joint design. In their findings, the researchers noted that higher axial loads increased the strength of the joints, but also accelerated strength degradation. Moreover, their findings seem to indicate that higher axial loads reduced the formation of diagonal cracking in the joints and so increased the joint shear capacity.

Further research on RC GLD structures was published in two articles by Kunnath et al. in1995 (a and b). In the first article the researchers evaluated current design practices. They examined three, six, and nine story RC buildings with story heights of twelve feet. They concluded that buildings would perform satisfactorily in moderate earthquakes, but may collapse if subjected to the MCE. The authors of this article

concluded that continuous longitudinal beam reinforcement through the joints increased joint performance more than comparable increases in both the joint shear strength and column confinement. In the second article by Kunnath, Hoffman, Reinhorn, and Mander, the researchers tested various improved RC beam-joints. The researchers found that when only the bottom reinforcing bars were continuous, the column and joint demands increased. This could lead to soft stories. By making the bottom bars continuous and adding joint hoop reinforcement, damage accumulation moved back into the beams. Furthermore, column confinement increased the capacity of the subassemblages tested. The researchers prepared cost estimates for the improved joint details and determined that the improvements would only increase structural costs by 8%-10% and would increase the overall cost of a building by only 1%-2%.

El-Attar et al. (1997) conducted another study of GLD RC buildings. In this study, two RC frames were constructed and tested on shake tables. As stated earlier, one frame was 1/6 scale, two stories, and one bay. The other frame was 1/8 scale, three stories, and three bays. The researchers concluded that moderate earthquakes tend to cause cracking of unconfined joints and pullout of discontinuous beam reinforcing which in turn reduces the stiffness of the frames. The increased flexibility increases the P-Delta effects. Furthermore, interior columns tended to fail before exterior ones due to higher axial loads. The increased axial loads increased the strength of the columns, but decreased the ductility.

Lee and Woo (2002) experimentally examined a three story, two bay RC frame designed for a low seismic hazard region in Korea. The study was conducted because many structures in Korea are medium to low rise structures that are not designed for moderate to major earthquakes. Lee and Woo concluded that such GLD structures were able to withstand design earthquakes and higher ground motions as a result of high overstrength, elongation of the fundamental period due to cycling, and increased damping ratios due to cycling. Also, Lee and Woo noted that joints designed according to Korean codes did not experience bond slippage, whereas joints designed according to ACI 318 did.

Similarly, Balendra et al. published a study dealing with structural design for low seismic hazard regions of Britain in 1999. The code in question for the study was BS

8110 (British Standards 1985). In this article, the researchers focused on overstrength, which is the amount of capacity above the design capacity that a structure has available before collapse. Factors contributing to overstrength are higher actual material strengths, non-structural component contributions, and increases in member size given stability and serviceability considerations. Pushover analyses of three, six, and ten story by three bay steel moment resisting frames revealed considerable overstrength in structures designed for low seismic areas in accordance with BS 8110. The overstrength factors decreased from 8 to 3.5 as the number of stories increased from three to ten. Moreover, the ductility factors were unaffected by height and were all around two. The researchers noted that overstrength decreases with increasing vertical load.

Quek et al. (2002) also published a paper on RC GLD buildings. This paper presents the experimental results of a study looking at frames subjected to horizontal and vertical excitations that were both in the high frequency range (40 Hz). The experiments were conducted on five half-scale models which had two stories and two bays. The authors found that the frames responded in the elastic range even up to a lateral base excitation of 1.2g. Unlike the horizontal accelerations, the vertical accelerations tended to amplify the deflection response moving up the structure. The authors noted that the vertical accelerations increase column and joint demands, which could be detrimental to GLD buildings.

Finally, Murty et al. (2003) examined exterior RC beam-column joints designed primarily for gravity loads. GLD RC joints typically have smaller volumes than those designed for high seismic zones. Consequently, it is difficult to keep joint shear stresses below limiting values and so the cores will crack before framing members reach their full capacities. Moreover, the smaller volumes require more reinforcing to make up for the inadequate shear capacity provided by the concrete in the joint. The smaller volumes are often unable to accommodate the amount of reinforcing required, further hindering the smaller joint's ability to be adequate. In the testing program, bond slippage of bottom bars occurred in every case. The slipping resulted in severe pinching of the hysteresis curves.

Literature specifically addressing steel GLD structures could not be found. However, there are many articles addressing steel component damage, which GLD steel

structures would most likely experience in a design earthquake. A later section deals with the issue of damage, however.

2.2.3 - Vertical Accelerations

In most seismic analyses, vertical accelerations are not specifically considered. This may or may not be acceptable considering the literature available on the subject. Before discussing the existing literature dealing with vertical accelerations, it is important to note that all of the vertical acceleration research has been conducted on WUS type structures. Thus, while the information available dealing with vertical accelerations may be useful for reference and guidance, it may not be directly applicable to CEUS structures.

Many studies have shown that vertical acceleration magnitudes can be as high or higher than the horizontal accelerations. Abrahamson and Litchiser (1989) showed that the ratio of vertical acceleration to horizontal acceleration (V/H) was dependent on the magnitude of the event and the distance from the site to the source. Bozorgnia et al. (1995) also noted that the V/H ratio was dependent on the site distance and earthquake magnitude. They also pointed out that the V/H acceleration response spectra ratio is dependent on the period of the structure in question. For short period structures, the ratio can be much greater than one, but for long period structures, the ratio is typically much less than one.

Bozorgnia et al. (1998) chronicled the vertical response of twelve structures in the 1994 Northridge earthquake. They also reinforced the idea that vertical ground motion is dependent on site-to-source distance and earthquake magnitude. At the time of Bozorgnia, Mahin, and Brady's work, it was apparently common practice to include vertical accelerations by applying additional gravity loads corresponding to $2/3^{rds}$ of the horizontal spectral acceleration. Similar methods for including vertical acceleration in design were presented in the FEMA 350 document (2000a) and the 1997 Unified Building Code. Bozorgnia, Mahin, and Brady found that many of the buildings examined in their study with shorter periods experienced vertical accelerations that exceeded the

lateral peak ground acceleration (PGA). They also found that structures closer to the epicenter experienced higher vertical accelerations than those far away.

Not only does site distance and period affect vertical accelerations, but soil conditions also affect them. Amirbekian and Bolt (1998) showed that the vertical acceleration component tends to be higher than the horizontal in alluvial basins.

There have also been many studies looking at the effects of vertical accelerations on structures. It is important to note that in the vertical acceleration studies, researchers have reached conflicting conclusions with regard to the impact that vertical accelerations have on structures.

Some have concluded that vertical accelerations do not significantly affect structural response. Maison and Kasai (1997), for example, analytically tested a thirteen story steel moment frame which was damaged in the Northridge earthquake and showed that the lateral displacement of the simulated structure was very similar with and without vertical accelerations included. Furthermore, the major emphasis of their research was to examine connection failures that occurred in the building during the earthquake. They noted that increased gravity loads actually reduced damage to the connections. They reasoned that this was because the gravity loads caused a compressive preloading of the bottom flanges of the beams. They further reasoned that perhaps the lack of gravity loads in buildings under construction during the Northridge earthquake explained why more of those buildings experienced connection damage. So, it would seem that real structures with gravity loads are less likely to be adversely affected by vertical accelerations.

Hjelmstad and Williamson (1998) and Williamson (2003) examined the dynamic stability of hysteretic single-degree-of-freedom inverted pendulum systems subjected to base excitation and noted that vertical accelerations increased lateral displacements in some situations if the vertical forcing frequency was twice the lateral frequency of the structure. The range of frequencies that caused dynamic instability was dependent on the axial load on the column. As the axial load in a structure approached the critical buckling load, the range of vertical frequencies that caused dynamic instability broadened. However, when modeling practical structures, Hjelmstad and Williamson noted that the axial loads in structures are relatively small. Consequently, they found that the vertical accelerations did not significantly increase lateral deflections of the structures they

studied. Jennings and Husid (1968) and Takizawa and Jennings (1980) have also shown that vertical accelerations have a negligible effect on the lateral response of structures.

For the most part, the design community has only superficially considered vertical accelerations. In the 2000 NEHRP provisions, vertical accelerations are indirectly included in the determination of the design lateral earthquake force for use in a load combination given by the following equation:

$$E = \rho Q_E + 0.2 S_{DS} D$$

where,

E = effect of horizontal and vertical earthquake-induced forces

S_{DS} = design spectral response acceleration at short periods

D = dead load

ρ = reliability factor (accounts for redundancy)

Q_E = effect of horizontal seismic forces

The factor $0.2S_{DS}D$ is meant to account for vertical accelerations. Furthermore, the commentary of the provisions state that, when using the equivalent lateral force method or the modal analysis method, the horizontal ground motion, vertical ground motion, and torsional effects are all accounted for in the distribution of the lateral loads. The commentary also states that the moments at the top of inverted pendulum structures, such as bridge piers, shall be increased to 0.5 times the moment at the base to account for vertical accelerations. While code officials deem vertical accelerations significant enough to account for them in some way, it would seem that they do not think that it is necessary to consider them explicitly.

While there are many studies indicating that vertical accelerations do not significantly affect structural response, there are also many which show that vertical accelerations do affect structural response. The studies showing vertical accelerations to be significant can be broadly categorized as involving component damage effects or lateral deflection effects.

First, there are many studies that indicate that vertical accelerations increase the damage to various structural components in a building. Anderson and Bertero (1973), for

example, analyzed a ten story steel moment frame subjected to horizontal and vertical ground motions from the San Fernando earthquake of 1971. From the study, they concluded that ductility requirements at critical regions would be inaccurate if vertical accelerations were not included. In the upper stories, for example, the ductility requirements were increased by fifty per cent by including vertical accelerations. Saadeghvaziri (1988) and Saadeghvaziri and Foutch (1991) examined the effects of vertical and horizontal accelerations on bridges. They noted that vertical accelerations cause severe fluctuations in the axial loads in bridge piers and that these fluctuations result in highly erratic hysteresis loops. Moreover, the vertical accelerations tend to increase the shear demand and reduce the shear capacity in bridge piers. The increased axial loads stiffened the columns, which in turn caused the columns to attract more force. At the same time, the increased axial load reduced the shear capacity of the piers. Also, the increased axial loads reduced the ductility of the columns. Saadeghvaziri and Foutch speculated that the severe damage to bridges in some earthquakes may be primarily caused by vertical accelerations. Hart et al. (1995) examined a six story special steel moment resisting frame subjected to both vertical and horizontal accelerations as part of the SAC Steel Project. Hart's research focused on the effects of tributary mass, both in the vertical and horizontal directions. The mass distribution causes a great deal of scatter in the axial forces in the columns. Hart noted that the effect of vertical accelerations was most pronounced in the interior columns, which are primarily designed to withstand axial loads. In some situations, Hart found that seismic axial forces could be twice the dead load. Higazy et al. (1996) examined reinforced concrete (RC) beam-column connections under vertical accelerations. They found that should vertical accelerations cause a RC connection to go into tension, then the shear capacity of the joint was reduced by eighteen to fifty percent. Also, the confinement in the joint core was rendered ineffective in the event of significant tension. Como et al. (2003) examined the likelihood that vertical accelerations would cause axial shortening in some columns and therefore increased rotations at beam ends.

A second category of vertical acceleration research has focused on its ability to contribute to lateral displacements. Iyengar and Shinozuka (1972) examined the effects of vertical accelerations on tall buildings. They modeled tall buildings as distributed

mass cantilevers. Iyengar and Shinozuka concluded that vertical accelerations considerably increased the tip deflection, base shear, and base moment for the cantilever models studied. Lin and Shin (1980) examined the effects of vertical accelerations on single degree of freedom inverted pendulum elastic structures. Lin and Shin noted that the vertical accelerations had the potential to amplify lateral response. Then, Shin and Lin (1982) performed a similar study involving single-degree-of-freedom-inverted pendulums except the systems were hysteretic rather than elastic. Shin and Lin examined systems with both 0.1 and 0.5 post-yield stiffness ratios. They found that for hysteretic models, the vertical accelerations had more of an effect on the lateral displacement than in the elastic models. Moreover, the lower post-yield stiffness ratio model was more influenced by vertical accelerations than the higher. Shin and Lin also noted that the vertical accelerations had a significant impact on the amount of residual deformations in their models. Ariaratnam and Leung (1990) analyzed a six story multiple degree of freedom building using random vibrations in both the vertical and horizontal directions. They concluded that both gravity loads and vertical inertial loads can increase the lateral displacement due to horizontal motion.

Of all of the studies conducted, it did not appear that any of them were specifically interested in determining types of structures and situations where vertical accelerations would be particularly damaging or contribute significantly to lateral deflection.

2.2.4 - Collapsed Building Investigations

Few articles are written specifically about collapsed buildings. Many are written generally about the extent of damage in an area subjected to an earthquake. There are also many articles that deal with the effects of dynamic loads on structural components. However, not many articles address specific collapses. Even so, the few articles addressing specific collapses do provide some insight. Belazougui (1989), for example, wrote about the destruction caused by the 1980 earthquake in El-Asnam, Algeria. Almost 80% of downtown El-Asnam buildings either collapsed or had to be torn down due to seismic damage. Belazougui cited negligence as a major reason for the collapses.

In many of the buildings, poor structural materials were used, the construction techniques and inspections were poor, and the buildings were not maintained upon completion. He also cited poor designs as a cause of collapse. In many of the collapsed buildings, a small one meter crawl space created a short story which resulted in very high shear stresses and subsequent failures in the reinforced concrete columns. The crawl space caused the collapse. Also, many buildings were highly irregular with varying mass, stiffness, and strength distributions throughout the buildings. Such structural proportioning increased torsion in the buildings. Many of the buildings had very heavy roofs which increased the P-Delta effects. In many of the concrete structures, reinforcing was not confined properly, which resulted in members with low ductility.

Another earthquake that was highly publicized for its destructiveness was the Mexico City earthquake of 1985. The epicenter of the earthquake was 250 miles from Mexico City and the magnitude of the earthquake was 8.1. It lasted for approximately three minutes. Even though the earthquake was very intense, it was relatively far away from Mexico City and one would think that it would not have affected Mexico City in such an adverse manner. However, Mexico City is built on very soft soil, an ancient lake bed, and so the seismic waves were greatly amplified. Many authors wrote about the damage in Mexico City (Ghosh and Corley 1986, Meli 1986, Osteraas and Krawinkler 1989).

Reinforced concrete structures fared far worse than steel structures. Ghosh and Corley (1986) addressed the performance of reinforced concrete buildings. They noted that column damage was more prevalent than beam damage in RC frames. Moreover, beam-column joints performed very badly. The major cause of the poor performance was lack of confinement. Meli (1986) also wrote on the performance of RC buildings in the 1985 Mexico City earthquake. He argued that the dominant modes of failure in such structures were shear or eccentric compression of columns which lead to strength degradation. He noted that hinges in the beam ends was less prevalent than in the columns. Also, he noted that many buildings had significant beam column joint damage.

While most of the damage sustained in Mexico City can be attributed to RC structures, some steel buildings were damaged and a few collapsed. Hanson (1986) noted that of the 350 buildings damaged in the earthquake, twelve were steel. Of those twelve,

ten were built before 1940. None of the steel buildings built after 1976 collapsed. Osteraas and Krawinkler (1989) examined the performance of three steel buildings during the earthquake. The first two buildings examined survived the earthquake relatively unscathed. The Torre Latinoamericana building was built in 1956 and is 44 stories high. This building was an example of a well designed steel building that performed well, too. The 77 Amsterdam Street building performed well also, but should not have. It is an eleven story building built around 1970. In this building, the connection strengths were as low as 50% of the beam capacity. There should have been many connection failures in the 77 Amsterdam Street building. The main reason the building performed well was because the frame was highly redundant. There were six moment resisting frames in the structure. Furthermore, the vertical welds connecting the beam webs to the columns provided a second line of defense once the beam flange to column welds had failed. The third building described by Osteraas and Krawinkler was a building in the Pino Suarez complex. There were five buildings in the complex, three were 21 stories and two were 14 stories. All three of the 21 story buildings suffered severe damage; one of them collapsed onto one of the 14 story buildings. Osteraas and Krawinkler believed that the most likely collapse scenario was as follows:

1) The exterior columns on the fourth floor buckled locally and lost all load carrying capacity
2) The vertical load was transferred both into lateral braces, which subsequently also buckled, and adjacent columns which, became overstressed
3) The buckled braces and overstressed columns allowed for increased lateral displacement, which made P-Delta effects significant
4) The structure eventually collapsed.

The major lesson learned from steel structures in the Mexico City earthquakes is that redundancy can be the difference between survival and collapse.

Structural performance in other earthquakes has also been explored. Soliman (1993) addressed the damage to RC structures in the Cairo earthquake of 1992. He specifically examined the damage to a school building in Nassar. Soliman cited poor

detailing as the main cause of collapse. There were large spaces between stirrups, and longitudinal reinforcing bars were distributed poorly. Repetto (1980) wrote about the influence of site characteristics on building damage during the Lima, Peru earthquake of 1974. In the article, he showed how the majority of seismic damage was focused in areas where the soil was mostly loose pebbles and rocks, called "cascajo." The soil type in this earthquake was the predominant factor causing damage.

Then, the Northridge, California earthquake that occurred in 1994 revealed a serious flaw in the prevailing steel moment connection designs of that time. Many steel moment frames experienced weld fractures that were not detrimental in most cases, but certainly could have been if the magnitude of the earthquake were greater.

Even though the number of case studies dealing with collapse is small, there are lessons to be learned from ones available. First, poor confinement in columns and joints was a major cause of damage and collapse in RC structures. Inadequate confinement may be an issue for structures located in the CEUS. Second, highly irregular buildings were more susceptible to collapse. It may be possible that irregular CEUS buildings would suffer the same fate in a moderate to severe earthquake. Third, highly redundant structures are much more likely to perform better in earthquakes than nonredundant ones. There are several types of buildings that are probably most at risk. First, braced frames are typically not very redundant, because only a small number of braces provide lateral stiffness. Second, moment frames with small numbers of moment connections are a redundancy risk, because such a building relies heavily on those connections to endure. Due to high labor costs, it is more likely today to find buildings with small numbers of large moment connections. In the past, one would be more likely to see large numbers of small moment connections.

2.2.5 - Damage Indices

It has already been said that collapse is difficult to quantify. As such, many researchers have endeavored to develop damage indices to illuminate a path between the initial and collapsed states. The main causes of damage in seismic events are maximum displacements and cyclic fatigue. Consequently the majority of damage indices that have

been developed are either maximum displacement based, fatigue based, or a combination of the two.

Before discussing the structurally based damage models, it is important to note that ground motion parameters can be a measure of earthquake destructiveness. Cosenza et al. (2000) have provided a comprehensive survey of these factors. Many have used PGA as a basic measure of earthquake damage potential, but Cosenza and his co-authors claim that peak ground velocity (PGV) is a better indicator because it is more directly connected to the energy demands. Moreover, they claim that PGV / PGA is arguably also a good measure of destructiveness. Another issue when considering earthquake destructiveness is duration. Duration unquestionably has an effect on damage, but it is debatable whether one should consider the whole duration of a ground motion or only a portion of it. If a portion is considered, the portion to consider is debatable. The portion of ground motion history to consider involves such concepts as bracketed duration. For the purposes of this study, it is enough to know that ground motion intensities and duration influence damage.

The simplest types of structurally based damage indices are those based on displacement. The maximum displacement at a particular location, for example, may be used as a damage measure. This does not universally translate into a damage index, and hence is usually normalized in some way. Some normalized measures of displacement are ductility, rotation ductility, curvature ductility, and interstory drift ratios. The rotation ductility and curvature ductility are primarily applicable on a local level to point hinge types of elements. Banon et al. (1981) presented formulations of the rotation ductility (μ_θ) and curvature ductility (μ_ϕ):

$$\mu_\theta = \frac{\theta_{\max}}{\theta_y} = 1 + \frac{\theta_0}{\theta_y} \qquad \textbf{(2.38)}$$

where

θ_y is assumed to be $\dfrac{M_y L}{6EI}$

where E and I are the modulus of elasticity and moment of inertia of the member in question

θ_0 = the residual rotation

$\mu_\phi = \frac{\phi_{\max}}{\phi_y} = 1 + \frac{\phi_0}{\phi_y}$, with a bilinear moment curvature relationship,

and

$$\mu_\phi = 1 + \frac{M_{\max} - M_y}{pM_y} \qquad \textbf{(2.38)}$$

where

ϕ_0 = the residual curvature (see figure 2.9 for definition)

ϕ_y = the yield curvature (see figure 2.9 for definition)

M_y = the yield moment

M_{max} = the maximum moment observed in the structure

p = the post-yield stiffness ratio (can not be zero)

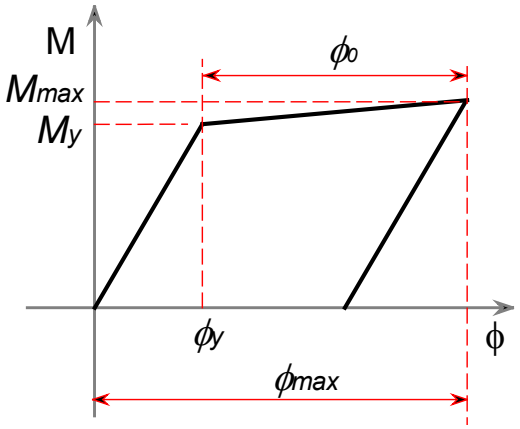

Figure 2.9 – Curvature Definitions

A limitation of the rotation ductility and curvature ductility is that they are not useful for determining the overall damage in an element, or global damage, in a structure. A quasi-global damage index is the interstory drift ratio (IDR). It is not entirely global, because it does not include the damage of all elements, just those from a particular story. The IDR is fairly popular and easy to calculate. It is merely the relative displacement of a story (displacement of level *i* – displacement of level *i*-1) divided by that story's height.

Another type of damage index that is based on displacement was presented by Lybas and Sozen (1977) and is called the Damage Ratio (DR). It is given by the following equation:

$$DR = \frac{K_0}{K_r} \tag{2.40}$$

where,

K_0 = the initial tangent stiffness

K_r = the secant stiffness at maximum displacement

It is thought that this type of damage index is more accurate than those based solely on displacement, rotation, or curvature, because it also indirectly measures strength degradation. Banon and Veneziano (1982) proposed a modified version of this damage measure for RC members because it is difficult to accurately determine the post cracking stiffness of RC members due to shear and slippage deformations. Banon and Veneziano's damage index was called the flexural damage ratio (FDR) and did not include shear deformations. It is given by the following equation:

$$FDR = \frac{K_f}{K_r}, \tag{2.41}$$

where

K_f = the initial flexural stiffness of the member neglecting shear deformations

$K_f = \frac{24EI}{L^3}$, for antisymmetric bending

where *E, I,* and *L* are the modulus of elasticity, moment of inertia, and length of the members in question, respectively.

All of the indices presented thus far do not account for cyclic fatigue, which can be a significant source of damage. As such, other researchers have focused on developing fatigue based damage indices. Banon et al. (1981) presented a cyclic version of the rotation ductility, called the normalized cumulative rotation. It is given by

$$NCR = \frac{\sum|\theta_0|}{\theta_y} \tag{2.42}$$

where

θ_0 is the maximum residual rotation achieved in a half cycle.

They also proposed a damage index based on dissipated energy that was normalized by the energy at yield. Bannon, Biggs, and Irvine called this index the normalized dissipated energy. It is given by the following equation:

$$E_n(t) = \frac{\int_0^t M(\tau)\theta(t)d\tau}{\frac{M_y\theta_y}{2}} \quad \textbf{(2.43)}$$

where,

t = the elapsed time since the beginning of loading

$\theta(t)$ = rotation increment as a function of time

Krawinkler (1987) also developed a fatigue based damage index. He argued that proper strength design could eliminate brittle failures in steel structures. However, inelastic cyclic effects can occur regardless of strength. The cycling will cause damage, which eventually leads to fatigue failure. As such, Krawinkler developed a damage index based on low cycle fatigue. It is given by the following equation:

$$D = \sum_{i=1}^{N_f} \frac{1}{N_{fi}} = C\sum_{i=1}^{N} (\Delta\delta_{pi})^c \quad \textbf{(2.44)}$$

where,

$N_{fi} = C^{-1}(\Delta\delta_p)^{-c}$,

N_f = number of cycles to failure

C and c are structural performance parameters.

$\Delta\delta_p$ = plastic deformation quantity in a particular cycle (strain, angle of distortion, rotation, deflection)

This model is fairly simple to understand and use. However, a drawback of it is that the structural performance parameters are based on random quantities, like weld consistency. It is further complicated by the fact that the response of a system must be divided into as many closed cycles as possible. To facilitate the division into closed cycles, a procedure called the rain-flow method is useful, but it is not straightforward. The reader is referred to Krawinkler (1987) for more information in the implementation of the low cycle fatigue damage index.

In an earlier work, Krawinkler (1983) developed the damage index just described probabilistically. The motivation for doing so came from the fact that member strengths and stiffnesses are random, thus making damage probabilistic.

Another cyclic based damage index is the linear damage cumulative law, or plastic fatigue damage functional, which was put forth by Cosenza et al. (1993). The basis of this index is that all structural members will have fatigue failures under a given number of inelastic displacement cycles. The damage measure is given by the following equation:

$$D_F = \sum_{i=1}^{n} \left(\frac{\mu_i - 1}{\mu_{u,mon} - 1} \right)^b \qquad \textbf{(2.45)}$$

where,

b is between 1.5 and 6 (typically = 1.8)

μ_i = the ductility demand in inelastic cycle, i.

$\mu_{u,mon}$ = the ductility at collapse under monotonic loading

n = the number of inelastic cycles.

When the above damage measure reaches one, the item in question has failed.

Still other damage indices are based on a combination of both maximum displacements and cyclic degradation. While more complicated to compute, these typically are the most realistic and accurate measures of damage. One of the most widely used damage indices was developed by Park and Ang (1985). This index was briefly presented earlier. The original formulation of this index was given by two equations.

Equation 2.46 is a less complicated approximate formulation of the index and equation 2.47 is more complicated, but ideally more accurate:

$$D = \frac{\delta_M}{\delta_u} + \frac{\beta}{Q_y \delta_y} \int dE \qquad \textbf{(2.46)}$$

or

$$D = \frac{\delta_M}{\delta_u} + \beta \int \left(\frac{\delta}{\delta_u} \right)^{\alpha} \frac{dE}{E_c(\delta)} \qquad \textbf{(2.47)}$$

where

δ_M = maximum deformation under earthquake

δ_u = ultimate deformation under monotonic loading

Q_y = calculated yield strength

$E_c(\delta)$ = hysteretic energy per loading cycle at deformation δ

dE = incremental absorbed energy

α, β are non-negative empirical parameters.

In equation 2.46, the first term is basically the maximum ductility demand, a measure of displacement. The second term in equation 2.46 is the cyclic term and is normalized by the yield energy. Park and Ang correlated their damage index with 141 monotonic tests and 262 cyclic tests using RC specimens. They obtained similar results with both equations. Due to its simplicity, Park and Ang advocated the usage of equation 2.46 over equation 2.47. They experimentally determined β values that range from –0.3 to +1.2. The average β value was 0.15. Cosenza et al. (1993) reproduced the Park and Ang damage index in their work and presented it in an arguably less complex form. Their interpretation of the Park and Ang index is as follows:

$$D_{PA} = \frac{x_{\max}}{x_{u,mon}} + \beta \frac{E_h}{F_y x_{u,mon}}$$

where

x_{max} and $x_{u,mon}$ = the maximum cyclic displacement and ultimate displacement under monotonic loads respectively

E_h = the plastic dissipated energy

F_y = the yield force

Banon and Veneziano (1982) developed a ductility and energy based damage index by combining the FDR and normalized dissipated energy indices presented above. They defined D_1 as the FDR value and D_2 as the E_n value. They developed their damage index with a desire that there should be a maximum damage that member could sustain given one type of damage, either D_1 or D_2. The authors argued that allowable combinations of D_1 and D_2, those that do not cause collapse, would be less than the maximum individual values. This is much like the column axial force-bending moment interaction diagrams of RC columns. To develop the combined index, Banon and Veneziano started by plotting D_1 versus D_2. The researchers then shifted the values such that arcs centered at the origin represented equal rings of damage accumulation. Figure 2.10 illustrates the shifting of the values and the equal rings of damage accumulation. Two new damage parameters were derived so that the damage accumulation would be the same where a particular ring crossed each axis. The new parameters were defined as $D_1^* = D_1 - 1$ and $D_2^* = 1.1 D_2^{0.38}$. Since the damage to a structure is delineated with radial lines projecting out from the origin, the resulting damage index essentially is the vector sum of the D_1^* and D_2^* values. The equation for the Banon and Veneziano damage index is given by

$$D_{BV} = \sqrt{(D_1^*)^2 + (D_2^*)^2} \qquad \textbf{(2.48)}$$

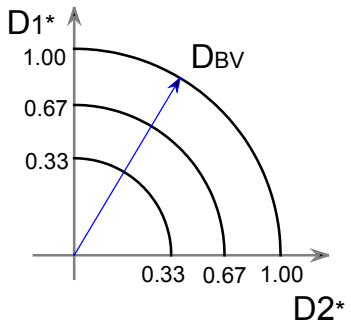

Figure 2.10 – Banon and Veneziano Damage Index Characteristics

An interesting point to make about the Banon and Veneziano damage index and the Park and Ang index is that they produce similar results for typical values of β.

A shortcoming of both the Park and Ang and the Banon and Veneziano indices is that neither of them accounts for loading history in the ductility term. Kumar and Usami (1996) observed that the inelastic displacements for a given cycle that were higher than any before caused much more damage than all the displacements before that point. In other words, it was more damaging to subject a structural member to increasing cyclic inelastic displacements, than subject the member to a maximum constant cyclic inelastic set of displacements. The damage index proposed by Kumar and Usami is very similar to that of Park and Ang, except it accounts for maximum relative displacements in the ductility term. The Kumar and Usami index is shown below.

$$D_{KU} = (1-\beta)D_{1KU} + \beta D_{2KU}, \tag{2.49}$$

where,

$$D_{1KU} = \sum_{j=1}^{N_1}\left(\frac{\delta_{\max,j} - \delta_y}{\delta_u - \delta_y}\right)^c \tag{2.50}$$

$$D_{2KU} = \sum_{i=1}^{N}\left[\frac{E_i}{H_y(\delta_u - \delta_y)}\right]^c \tag{2.51}$$

where,

β and c are constants (between 0.1-0.2 and 1-2 respectively)

N_1 = number of half cycles producing $\delta_{max,\,j}$ for the first time

N = total number of half cycles

E_i = energy dissipated in the i^{th} half cycle (a half cycle is the interval between two zero load points)

Mehanney (2001) developed a similar damage index to account for loading history on damage accumulation. His formulation divided a response history into positive and negative cycles as well as primary and follower half cycles. The positive and negative designation is somewhat arbitrary, but essentially just refers to

displacements to one side or the other from the initial position of the structure. Then, a primary half cycle (PHC) is defined as any cycle whose amplitude exceeds that of all the previous cycles. All other half cycles that are less than the primary cycles are defined as follower half cycles (FHC). Figure 2.11 graphically shows the distinction between positive, negative, primary, and follower cycles.

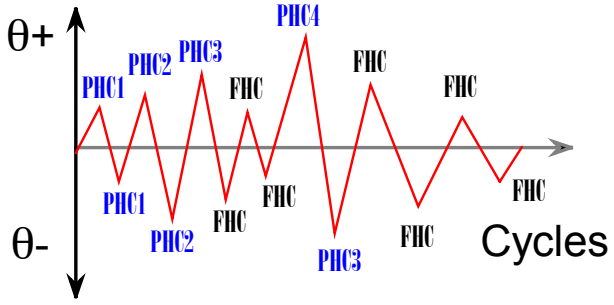

Figure 2.11 – Definition of PHC's and FHC's and Load Sequence Effects

In Figure 2.11, there are four positive primary half cycles and three negative primary half cycles. The rest of the cycles are follower half cycles. The equation for the damage index is given by:

$$D_{\theta}^{+} = \frac{\left(\theta_p^{+}\big|_{currentPHC}\right)^{\alpha} + \left(\sum_{i=1}^{n^{+}}\left(\theta_p^{+}\big|_{FHC,i}\right)\right)^{\beta}}{\left(\theta_{pu}^{+}\right)^{\alpha} + \left(\sum_{i=1}^{n^{+}}\left(\theta_p^{+}\big|_{FHC,i}\right)\right)^{\beta}} \qquad \textbf{(2.52)}$$

The above damage index is calculated for the positive half cycles and a similar index is calculated for the negative half cycles. The positive and negative values are then combined to form the following damage index:

$$D_0 = \sqrt{(D_{\theta}^{+})^{\gamma} + (D_{\theta}^{-})^{\gamma}} \qquad \textbf{(2.53)}$$

where

γ is a calibration factor.

The appropriate values of α, β, and γ are presented in table 2.2.

Table 2.2 Appropriate Values for α, β, and γ:

Parameter	RC Columns	Steel/Composite Beams	Composite Joints
α	1.00	1.00	0.75
β	1.50	1.50	3.00
γ	6.00	6.00	5.00

Collapse occurs when $D_0 \geq 1.0$.

While it would be interesting to try to incorporate all of the damage indices just discussed into the current study, it is not reasonably feasible. As such, only three of those described will be used. The three chosen are ductility demand, Park and Ang, and Kumar and Usami. These three were chosen to get a range of different indices but also because they are fairly easy to implement.

2.3 - Incremental Dynamic Analysis

Incremental dynamic analysis (IDA) is a procedure for tracing the performance of a nonlinear structural model subjected to multiple accelerograms over a range of ground motion intensities. The concepts of IDA are not new, but the terminology is new and computing power today makes it feasible. It is gaining popularity because it fits nicely with the procedures and objectives of Performance Based Earthquake Engineering (PBEE). The main premise of PBEE is that different structures built in various locations should have variable design criteria and that the design criteria be probabilistic. The FEMA 350 (2000) document is one of the initial attempts to bring probabilistic seismic design from academia to industry. The FEMA 350 authors define two basic performance levels for structures, collapse prevention and immediate occupancy. The use of a building, the amount of people that will use a building at any one time, and seismicity are some of the factors that influence the performance objectives. The FEMA 350 document advocates the IDA method as a way to determine the vulnerability of a structure. The FEMA 350 authors define vulnerability as " the capacity of the structure to resist greater damage than that defining a performance level." It is important to note, however, that the FEMA 350 document describes the IDA procedure in an appendix and allows it to only be used subserviently to the simplified procedures in the main body of the text.

Consequently, IDA is still in the beginning stages and will require further development and industry training before acceptance will be widespread.

Nonetheless, IDA fits nicely into the PBEE framework, because it allows one to see a range of building responses when subjected to various earthquakes and intensities. The general IDA procedure has been around for quite some time, but is only now becoming practical as personal computers are becoming powerful enough to conduct many analyses in a short amount of time. As Vamvatsikos (2002a) has mentioned, Bertero toyed with the concept as early as 1977. It was not until the SAC Joint Venture that significant work took place to develop IDA concepts and procedures more fully. To date, Vamvatikos has produced the most significant body of literature related to the subject.

Having said all of this, it is now pertinent to explicitly describe the IDA procedure. Generally speaking, an IDA involves constructing a nonlinear analytical model and then subjecting it to many earthquake records scaled to many different intensity measures (IM). The earthquake intensity may be measured a variety of ways, but is typically measured by the peak ground acceleration (PGA), peak ground velocity (PGV), or spectral acceleration. Any measure of earthquake intensity that may be monotonically scaled can be used.

From each analysis, a particular maximum response value is retained, which is called the damage measure (DM). There are many valid DMs that can be used, such as maximum displacement, base shear, ductility demand, or a damage index. Typically, it is beneficial to consider several DMs in an IDA because each DM provides a different perspective on the amount and type of damage a structure has sustained.

The IM values and corresponding DM values are then plotted. The result is a graphical representation of the effects of increasing ground motion intensities on response quantities. An example of an IDA curve is presented in Figure 2.12. The IDA curve was created from a model that will be described in chapter six. For now, it is enough to know that it is the Boston 7 story model with a post-yield stiffness ratio of 0.05 and a stability ratio of 0.125. The model has been subjected to the Northridge earthquake (EQ 9). The details of this earthquake are also described in chapter six of this work.

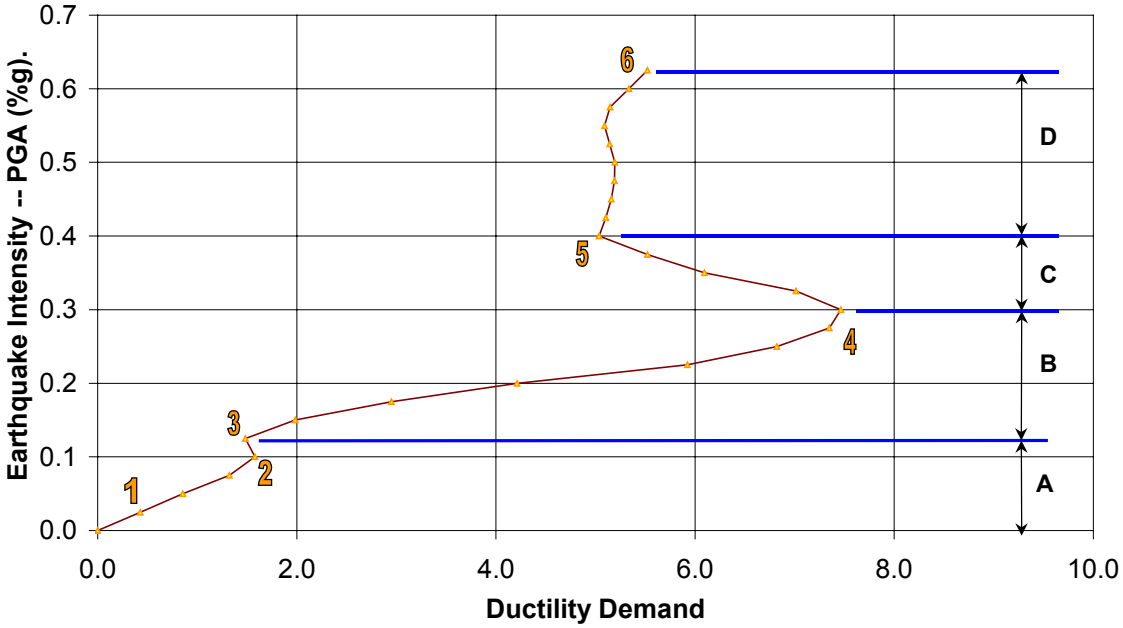

Figure 2.12 – Example IDA Curve

An interesting aspect of IDA curves, which can be seen in Figure 2.12, is the concept of resurrection (Vamvatsikos 2002a). Resurrection in an IDA curve is where there is a shift from increasing damage with increasing intensity to decreasing damage for increasing intensity. This is somewhat counterintuitive because it essentially means that a structure will sustain less damage if the earthquake is more severe. Resurrection is less puzzling when viewed at the response history level.

Each point in Figure 2.12 corresponds to a maximum ductility demand value from a nonlinear response history of the model in question. The ground motion scale was increased for each response history. A selected few of the response histories used to create the IDA plot of Figure 2.12 are shown in Figures 2.13, 2.14, 2.15, and 2.16. Each figure corresponds to a region, A through D, in figure 2.12.

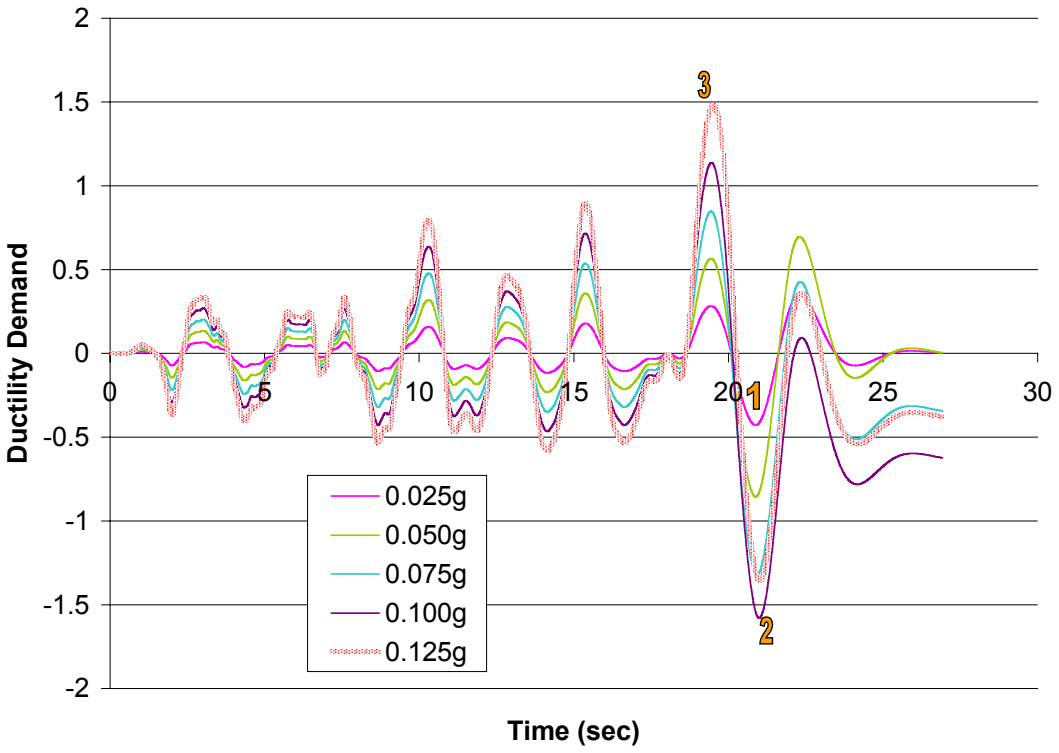

Figure 2.13 – Response Histories Corresponding to Region A (EQ9bost7R0.05ST0.125)

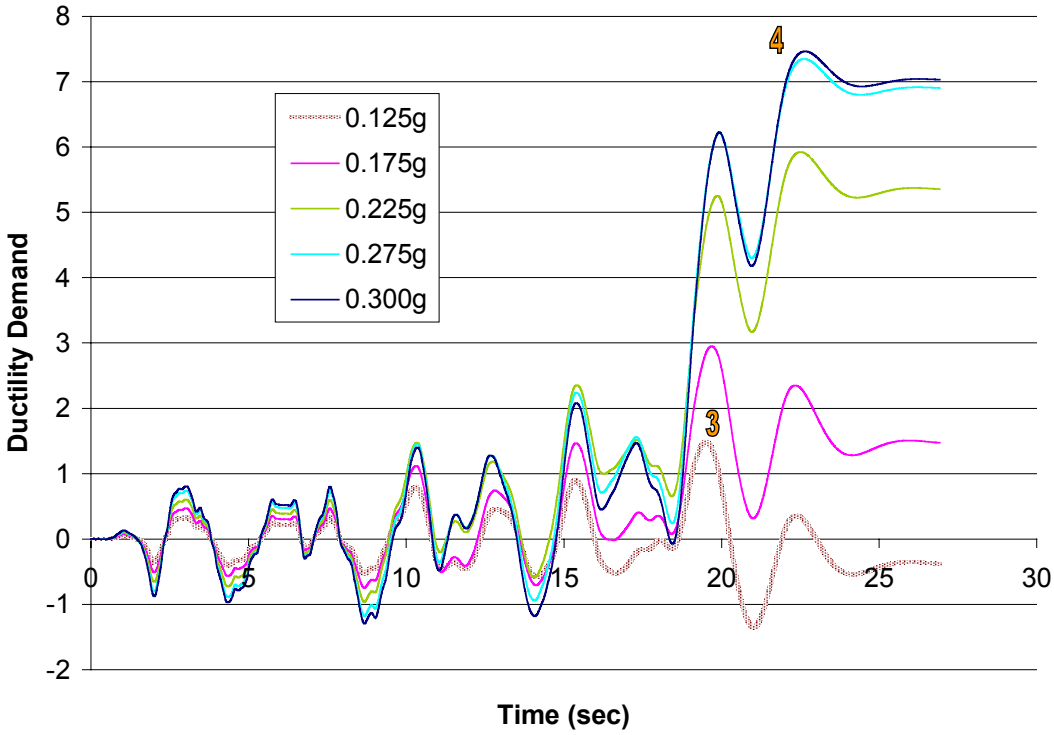

Figure 2.14 – Response Histories Corresponding to Region B (EQ9bost7R0.05ST0.125)

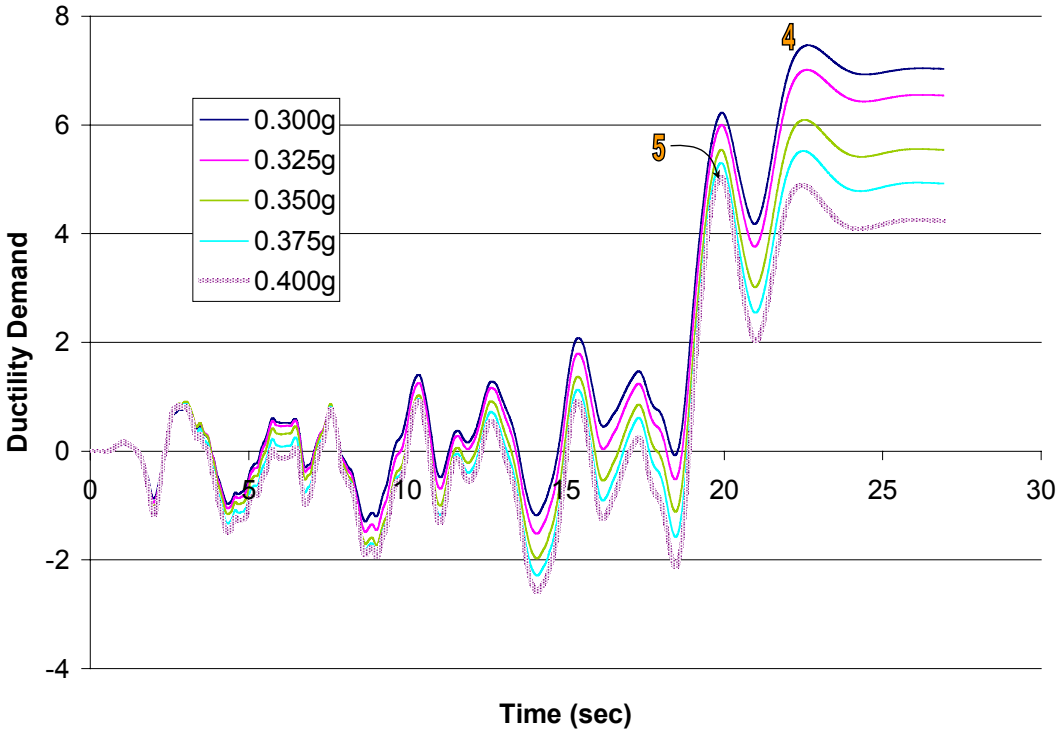

Figure 2.15 – Response Histories Corresponding to Region C (EQ9bost7R0.05ST0.125)

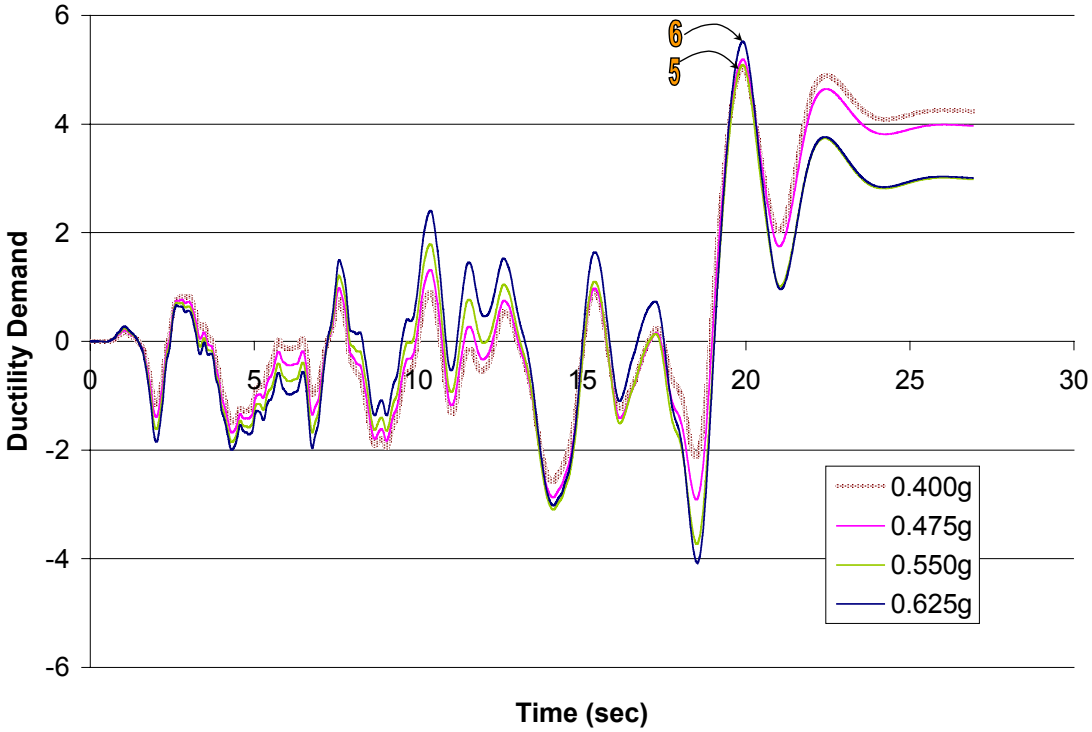

Figure 2.16 – Response Histories Corresponding to Region D (EQ9bost7R0.05ST0.125)

The resurrection occurrences in figures 2.12 occur because of permanent deformations, as can be seen by the residual displacements in figures 2.13 through 2.16. The weaving nature of the IDA curve of figure 2.12, and the variety of responses shown in figures 2.13 through 2.16, illustrate the uncertainty and randomness involved in IDA studies. Such uncertainty is why many earthquakes are required in a given IDA study. More earthquakes provide a higher level of confidence in the conclusions from the IDA study. The most ideal situation occurs when all of the IDA curves follow a similar path. In such a case, one would be confident that the structure in question would behave predictably in future earthquakes, as evidenced by the predicable behavior when subjected to a variety of past earthquakes. Inevitably though, there are differences between the IDA responses of various earthquakes. These differences in response, or DM, are called dispersion. IDA dispersion is illustrated in figure 2.17

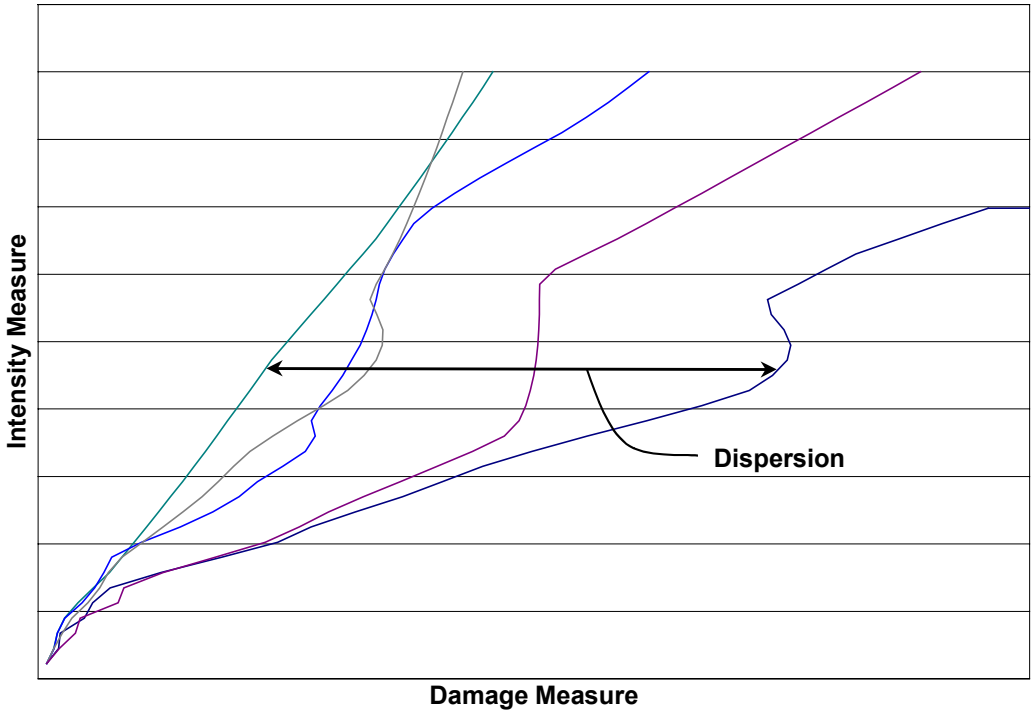

Figure 2.17 – IDA Dispersion

A major thrust of IDA research is focused on reducing the amount of dispersion in IDA analysis (Vamvatikos 2002a). Dispersion represents unpredictability in a design. Reduction of dispersion is essential for IDA to gain acceptance among design engineers.

Another complicating factor of IDA is the determination of limit-states. There are two ideas in circulation about how limit-states should be determined when conducting an IDA. The first method is based on the damage measure and the second method is based on the intensity measure. Figure 2.19 shows an implementation of each limit-state determination method as applied to the IDA plot of Figure 2.12.

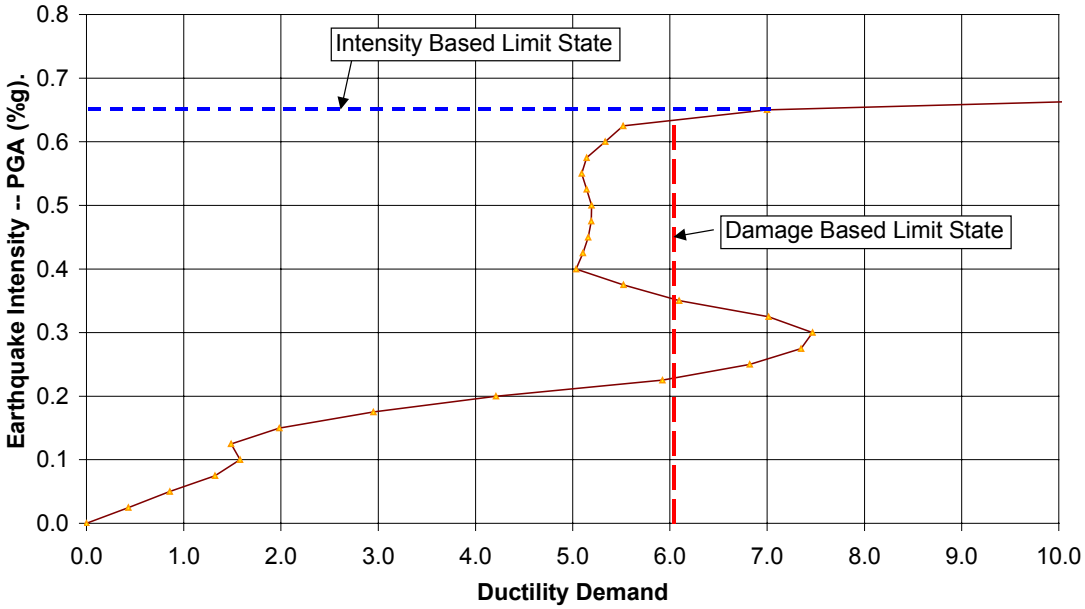

Figure 2.18 – Defining Collapse using IDA

The damage-based limit-state method sets a limit on the damage measure. In figure 2.18, the limit was set at a ductility demand of six. Notice that there are three points on the IDA that correspond to this limit. In a design situation, the lowest point where the IDA curve crosses the DM limit line would determine the limiting intensity.

The other method of specifying limit states is based on intensity. The limit of a structure's capacity is reached according to this method if small increases in intensity result in large increases in damage. In other words, the limit-state has been determined when the slope of the IDA curve drops below a specified value. FEMA 350 (2000a) advocates this method.

Each limit-state methodology has advantages and disadvantages. Damage-based limit-states, for example, are simple to determine and are meaningful in the context of current limit-state methods. An example of a current limit-state method that is easily implemented is the interstory drift ratio (IDR). Typical limits on IDR are around two

percent of the story height. It is easy from an IDA plot to determine the first point where the IDR exceeds two percent. However, damage-based limit states are typically not very good predictors of collapse. Intensity limit-state methods, on the other hand, while being slightly more difficult to determine, are more useful for determining collapse limit states (Vamvatsikos 2002a). The collapse limit-state is the intensity just before the damage would diverge toward infinity.

3.0 OpenSees Description and Verification

OpenSees is a relatively new finite element analysis program. It was developed at the University of California at Berkeley for use by the Network for Earthquake Engineering Simulation (NEES). It is an object oriented C++ program that uses the TCL scripting language as the interface. The developers of OpenSees refer to the software as a "framework" because it contains C++ components that alone are unusable. OpenSees is the framework through which a finite element analysis may be constructed. It is the analyst's responsibility to use the TCL scripting language to glue the C++ components together to create an analysis. The TCL scripting language provides much versatility to the analyst and that versatility is part of the reason that OpenSees was used in this study. The TCL scripting language made it possible to automate the variation of both structural and earthquake parameters in the analyses. Furthermore, OpenSees proved to be very fast compared to SAP 2000 for solving the SDOF models in this study. OpenSees would complete a nonlinear response history analysis in approximately 10 seconds whereas the same models took about 5 minutes to solve in SAP 2000.

While OpenSees is fast and versatile, it was necessary to verify that the results obtained from it match those of a trusted program. SAP 2000 version 8 was the benchmark program used for the verification. SAP 2000 has been used commercially and academically in many situations and has been carefully verified. Also, the SAP 2000 version 8 software package was chosen because it has the ability to include vertical accelerations as well as perform large displacement analysis.

The models used in the verification process were single degree of freedom inverted pendulum oscillators like the ones used in this study. The specific details of the models are fully described in chapter four. After many trials, the various structural and analytical parameters in each of the programs were set such that the two programs yielded essentially the same results. In regard to the process of obtaining similar results, several observations ought to be made.

3.1 - Member Section Properties

Slight differences in member section properties tended to influence the responses between SAP and OpenSees. First, shear deformations in the beam and column elements made a difference. The *elasticBeamColumn* and *nonlinearBeamColumn* elements in OpenSees do not include shear deformations, whereas the frame element in SAP 2000 does. In order to get the displacement responses of SAP and OpenSees to match, the effective shear areas of the frame elements in SAP had to be set so that shear deflections would be neglected. Also, it was essential to make sure that the elements were effectively rigid so that the lateral stiffness of the systems was dependent only on the rotational springs. In SAP, multipliers were applied to the section properties of the frame elements to make them effectively rigid. In OpenSees, values for cross sectional area and moment of inertia were set to the multiplied values that were used in SAP. Once all cross sectional properties were similar between SAP and OpenSees, the results were essentially identical.

3.2 - Dampers

The dampers used in each of the programs had to be equilibrated as well. Dampers constructed in SAP are NLink elements. The NLink elements enforce various types of relationships or links between nodes. The NLink element dampers in SAP conform to the Maxwell model of damping, which is shown in Figure 3.1.

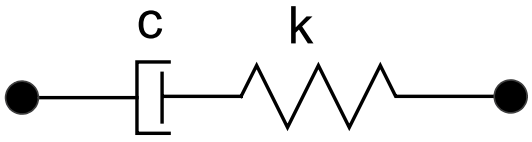

Figure 3.1– Maxwell Model of Damping

An NLink damper element has both a stiffness component and a damping component. In Figure 3.1, the stiffness portion of the NLink damper is designated with a "*k*" and the damping portion of the link damper is designated with a "*c*." The two components act in series. The force in the element is given by the following equation:

$$f = kd_k = c\dot{d}_c^{c\exp} \quad \textbf{(3.1)}$$

where

k = the stiffness of the spring portion of the damper

c = the damping coefficient

$cexp$ = the exponent applied to the velocity which determines the amount of nonlinearity in the damper.

d_k = the elastic deformation in the stiffness part of the element

$\dot{d}_c$ = the deformational velocity in the damping part of the element

To get the SAP link damper to act solely like a damper, the stiffness must be set high enough that there is virtually no deformation in the spring portion of the damper. However, if the stiffness is set too high, then numerical error is introduced. The SAP2000 Analysis Reference manual (Computers and Structures Inc., 2002) proposes the following equation to ensure that the stiffness of the damper (k_{damp}) is in an adequate range:

$$k_{damp} = \left(\frac{c}{dt}\right)^2 \quad \textbf{(3.2)}$$

where

c = damping value

dt = time step of the analysis

3.3 - Gravity Load Application

The gravity load application methodology was initially another source of discrepancy between SAP and OpenSees. In the OpenSees models, the loads were applied in two stages. This was because the vertical load had to be applied slowly using a linear method, starting with zero load at time zero to the full vertical load at ten seconds. The linear application method was necessary so that bouncing did not occur in the beam.

Bouncing happened when a load was applied instantaneously to a member. It was much like dropping a weight on the end of a diving board. A diving board will bounce unless a load is applied gradually. The vertical loads were applied at the center of a model's beam. Once the linear gravity loads had been applied, the ground motion accelerations were applied. With regard to the SAP models, it was originally assumed that the gravity point loads used for static analysis would not cause bouncing when the vertical ground motion was also included as a load. This was because no time series was associated with the static loads and so it was assumed that they would not behave dynamically. To determine if bouncing was occurring, the moment-rotation relationship was examined. The gravity load applied to the system, by nature, was supposed to result in a constant moment in the rotational springs where the beam was supported. From preliminary plots of the rotational spring's moment versus rotation relationship, it seemed that bouncing was not occurring. However, the resulting response histories were vastly different than those produced from OpenSees. Closer examination of the SAP rotational spring's moment versus rotation relationship revealed that there were harmonic fluctuations in the moment-rotation relationship prior to the application of the ground motion. While the oscillations in spring moment and rotation were small compared to the rotations and moments induced by the ground motion, they did affect the occurrences of certain yield events, which greatly influenced the lateral displacement histories of the models. Thus, the gravity loads in SAP had to be associated with in a linear (ramp) time series, similar to OpenSees, and then the ground motions were applied. Once these differences were resolved, the displacement responses from SAP and OpenSees were the same.

3.4 - Handling P-Delta Effects

A further difference between SAP and OpenSees occurred in the handling of P-Delta effects. To include vertical accelerations in the analyses, it was necessary for the analysis software to update the geometric stiffness matrix at each time step. The geometric stiffness must be updated because vertical accelerations continuously change the vertical loads on a system. Thus, the geometric stiffness must also always change. Most structural software packages do not continuously update the geometric stiffness.

Instead, a geometric stiffness matrix is calculated at the beginning of the analysis and is used for the duration of the analysis. In SAP 2000 version 8, there are two options for including P-Delta effects. The first option, the fast non-updating method, has been included in previous versions. The second option, the updating method, is new to the program and is implemented through a large displacement analysis option. OpenSees, on the other hand, has been developed so that the geometric stiffness is updated at each time step if P-Delta effects are included. In OpenSees, this is the only option for P-Delta analysis.

3.5 - Verification Plots

Once all of the aforementioned issues were properly handled, SAP and OpenSees produced very similar results. To prove this, similar structures were constructed in both SAP and OpenSees and then the response histories were compared. The period of the respective structures was 1.86 seconds. The yield strength of the models was provided by rotational springs at the joints of the models. The yield moments of the springs was 377 kip-in, which corresponded to a lateral yield force equal to 14 percent of the structure's weight. Post-yield stiffness ratios of 0.0 and 0.1 were used. A gravity load of 100 kips was used to create a destabilizing geometric stiffness. The vertical acceleration further introduced geometric stiffness. Damping was assumed to be five per cent of critical for the models. The models were subjected to the accelerograms from both the Northridge and Imperial Valley earthquakes. Table 3.1 provides more information about the earthquakes used in the comparative analysis.

Table 3.1 – Earthquakes Used to Compare SAP 2000 and OpenSees.

Earthquake	Station	Directions	PGA hor. & vert. (%g)
Imperial Valley 1979/10/15 23:19	5054 Bonds Corner	230, Up	0.775, 0.425
Northridge 1994/1/17 12:31	N. Hollywood, Coldwater Canyon	270, Up	0.271, 0.289

The ground motions shown in Table 3.1 were chosen somewhat arbitrarily just to have variety in the responses. The ground motion records were obtained from the Pacific Earthquake Engineering Research (PEER) Center website. They were scaled so that they

at least did not cause the models to collapse. Consequently, the Imperial Valley lateral acceleration record was scaled to 25 per cent of the original value and the Northridge lateral acceleration record was scaled to 50 per cent of its original value. Figures 3.2 through 3.5 show the response histories of SDOF structures subjected to the Northridge and Imperial Valley ground motions.

Figures 3.2 through 3.5 are organized into groups of three figures. In each group of three figures, designated by a trailing "a" through "c," the difference between the response histories is the method of analysis. For "a" figures, the analysis is geometrically linear, but materially nonlinear. Thus, for "a" figures P-Delta effects are not considered. Then, the "b" figures are both geometrically and materially nonlinear. However, the geometric stiffness of the SAP 2000 "b" models is never updated from the beginning of the analyses. Consequently, the SAP 2000 "b" models are not accounting for the P-Delta effects caused by vertical accelerations. Thus, there is a discrepancy between OpenSees and SAP in the "b" figures because OpenSees updates the geometric stiffness for each time step. In the "c" figures, the large displacement option of analysis has been used to solve the SAP models, causing OpenSees and SAP match once again.

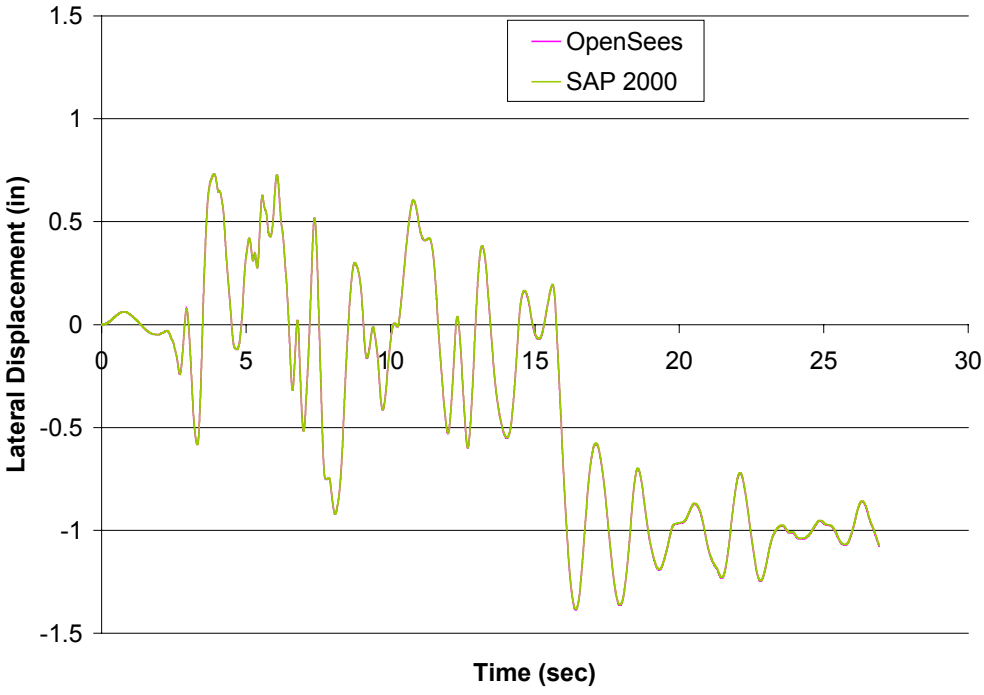

Figure 3.2a – Response Histories of SDOF Models Which Have Post-Yield Stiffness Ratios of 0.0, Neglect Geometric Stiffness, and were Subjected to the Imperial Valley Ground Motion.

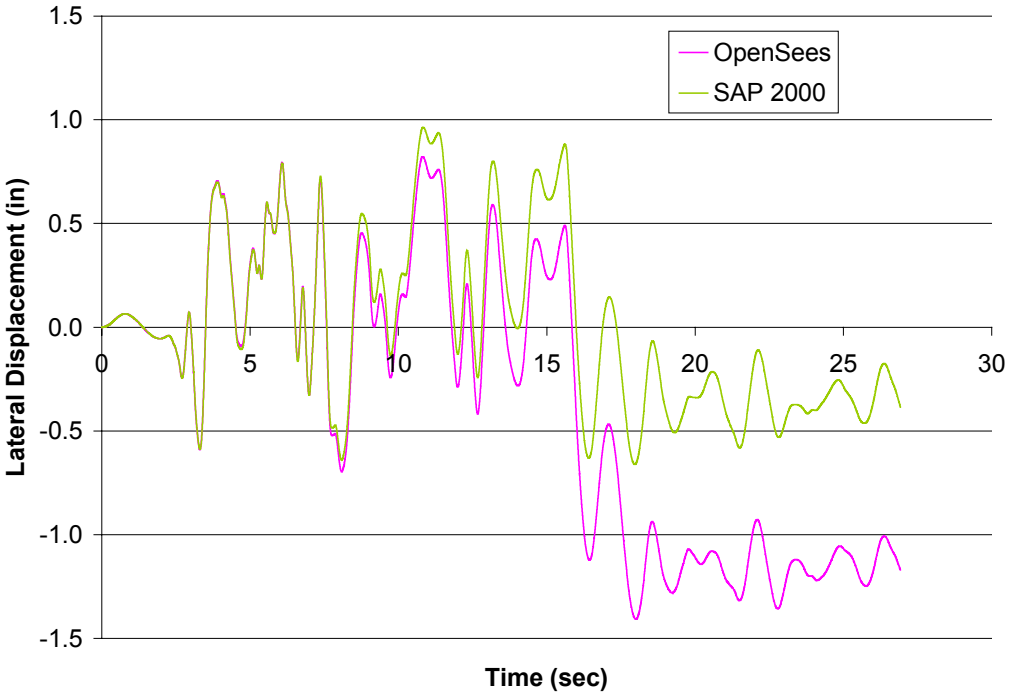

Figure 3.2b – Response Histories of SDOF Models Which Have Post-Yield Stiffness Ratios of 0.0, Include Geometric Stiffness, and were Subjected to the Imperial Valley Ground Motion.

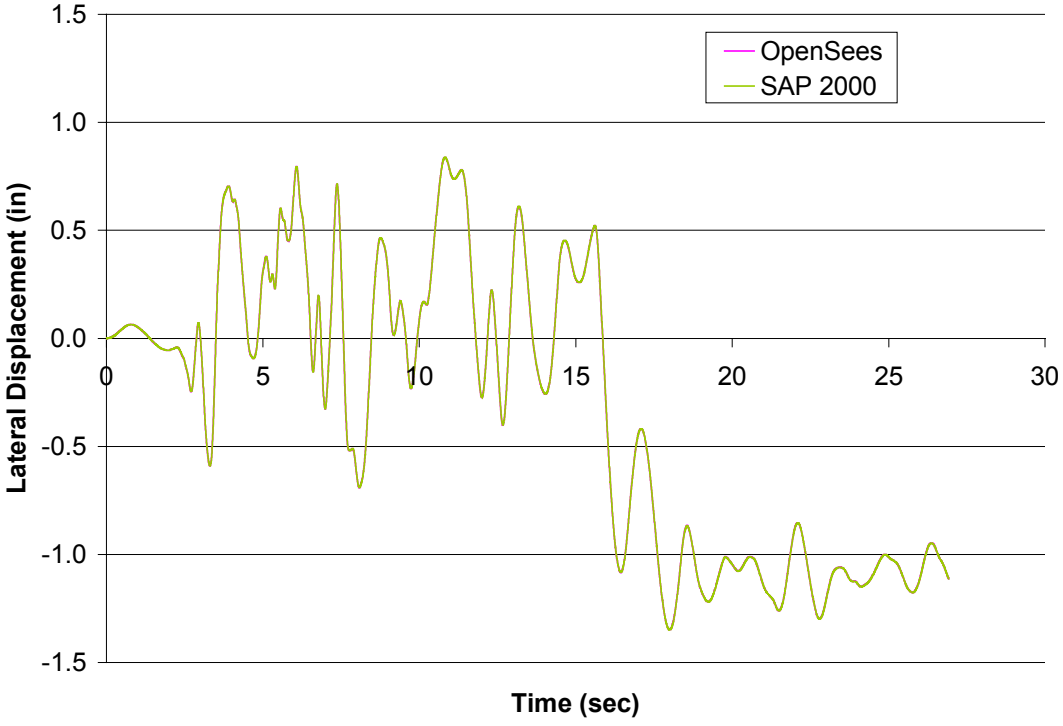

Figure 3.2c – Response Histories of SDOF Models Which Have Post-Yield Stiffness Ratios of 0.0, Include Geometric Stiffness, Use Large Displacement Analysis, and were Subjected to the Imperial Valley Ground Motion.

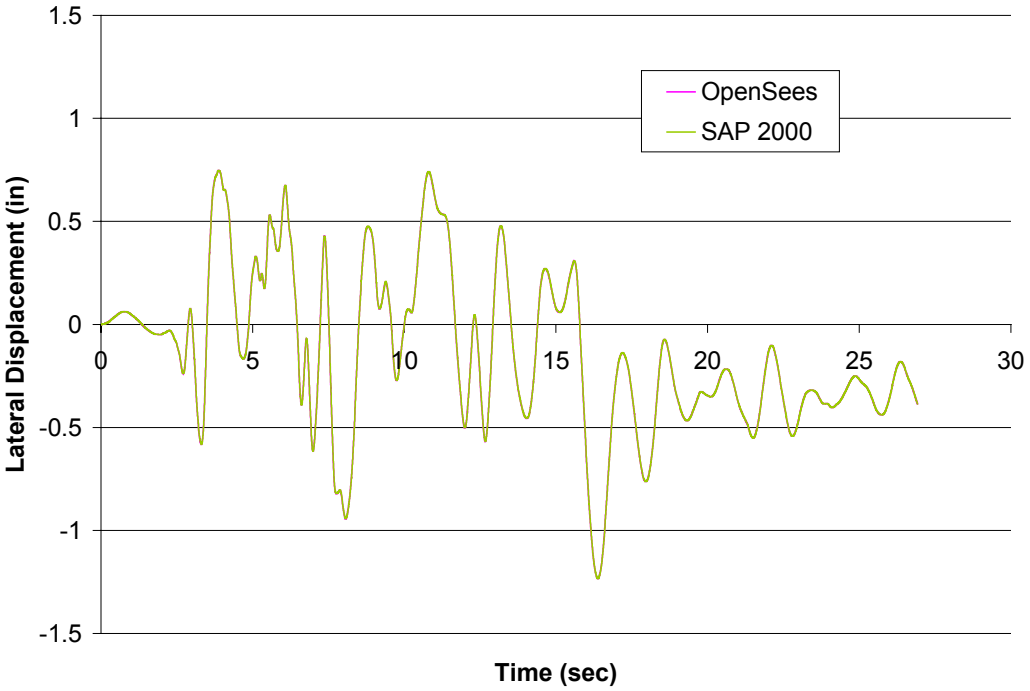

Figure 3.3a – Response Histories of SDOF Models Which Have Post-Yield Stiffness Ratios of 0.1, Neglect Geometric Stiffness, and were Subjected to the Imperial Valley Ground Motion.

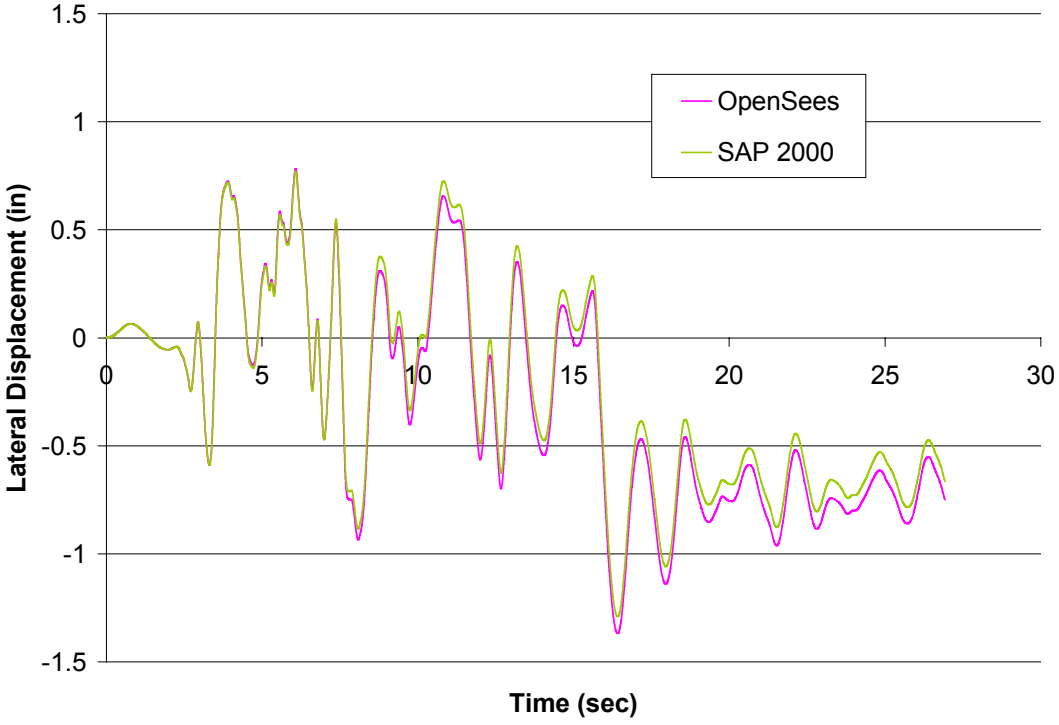

Figure 3.3b – Response Histories of SDOF Models Which Have Post-Yield Stiffness Ratios of 0.1, Include Geometric Stiffness, and were Subjected to the Imperial Valley Ground Motion.

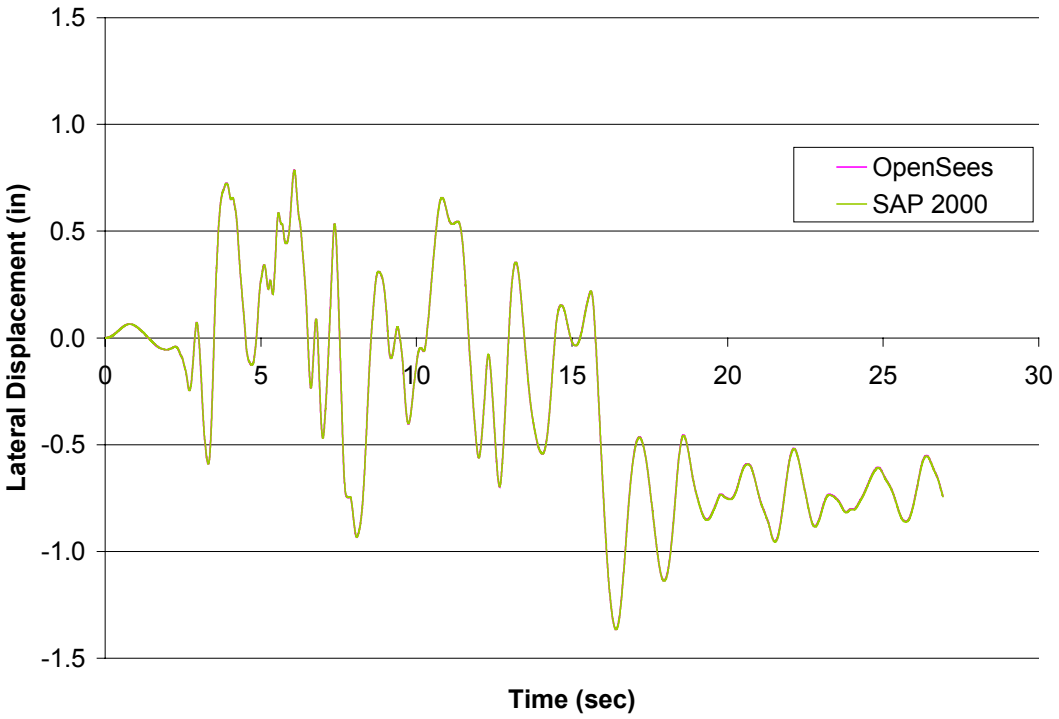

Figure 3.3c – Response Histories of SDOF Models Which Have Post-Yield Stiffness Ratios of 0.1, Include Geometric Stiffness, Use Large Displacement Analysis, and were Subjected to the Imperial Valley Ground Motion.

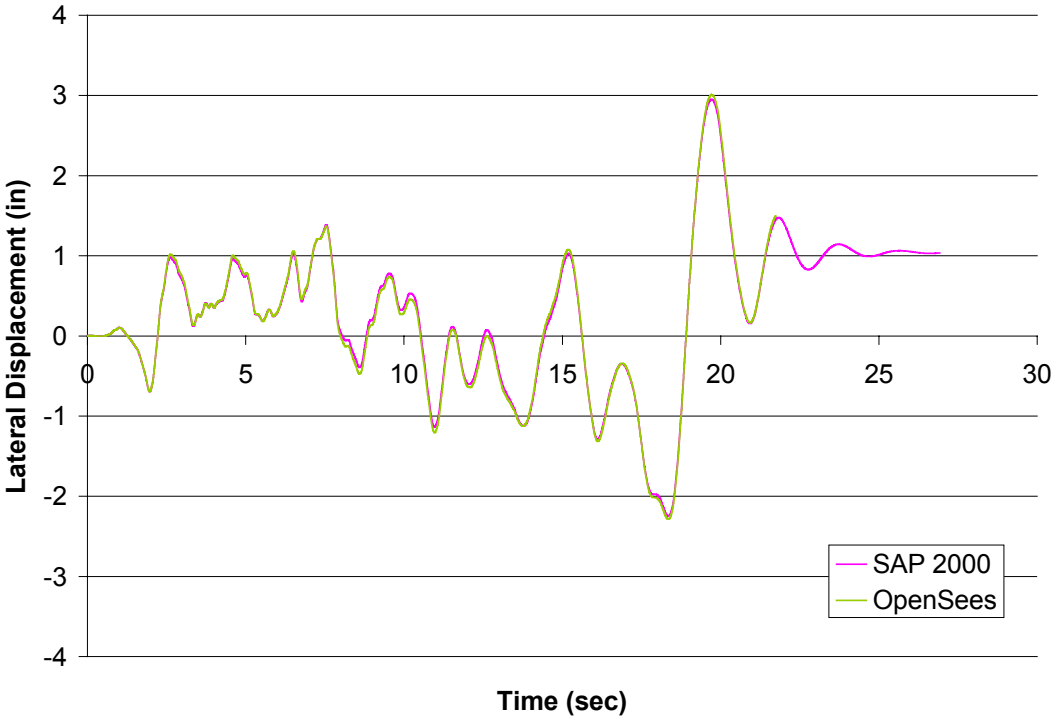

Figure 3.4a – Response Histories of SDOF Models Which Have Post-Yield Stiffness Ratios of 0.0, Neglect Geometric Stiffness, and were Subjected to the Northridge Ground Motion.

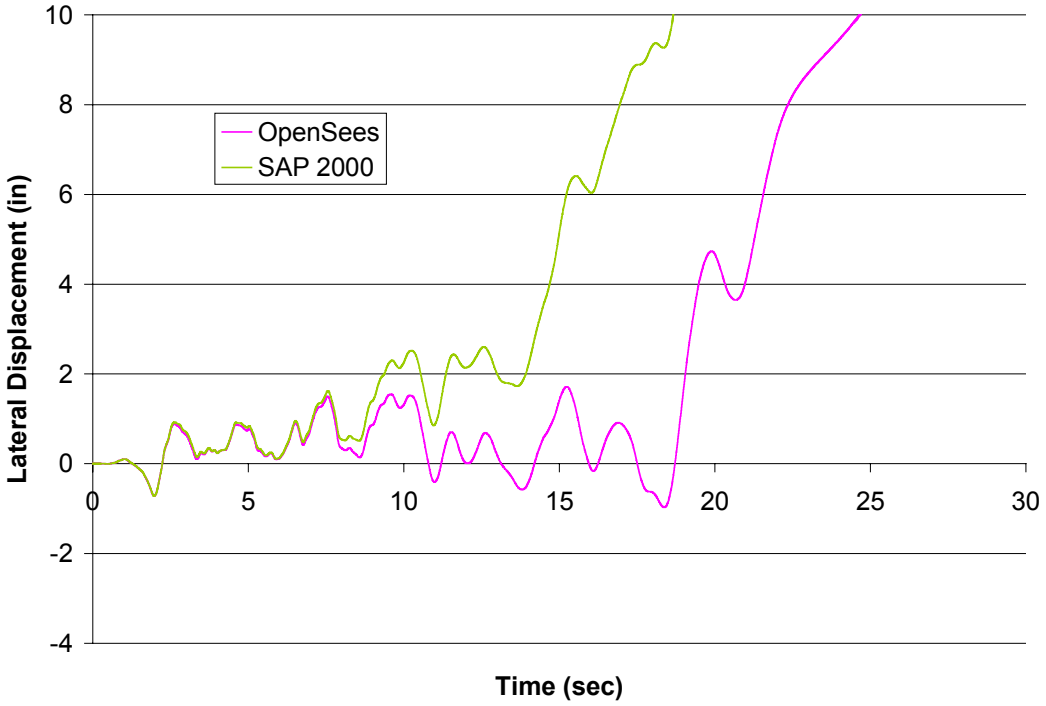

Figure 3.4b – Response Histories of SDOF Models Which Have Post-Yield Stiffness Ratios of 0.0, Include Geometric Stiffness, and were Subjected to the Northridge Ground Motion.

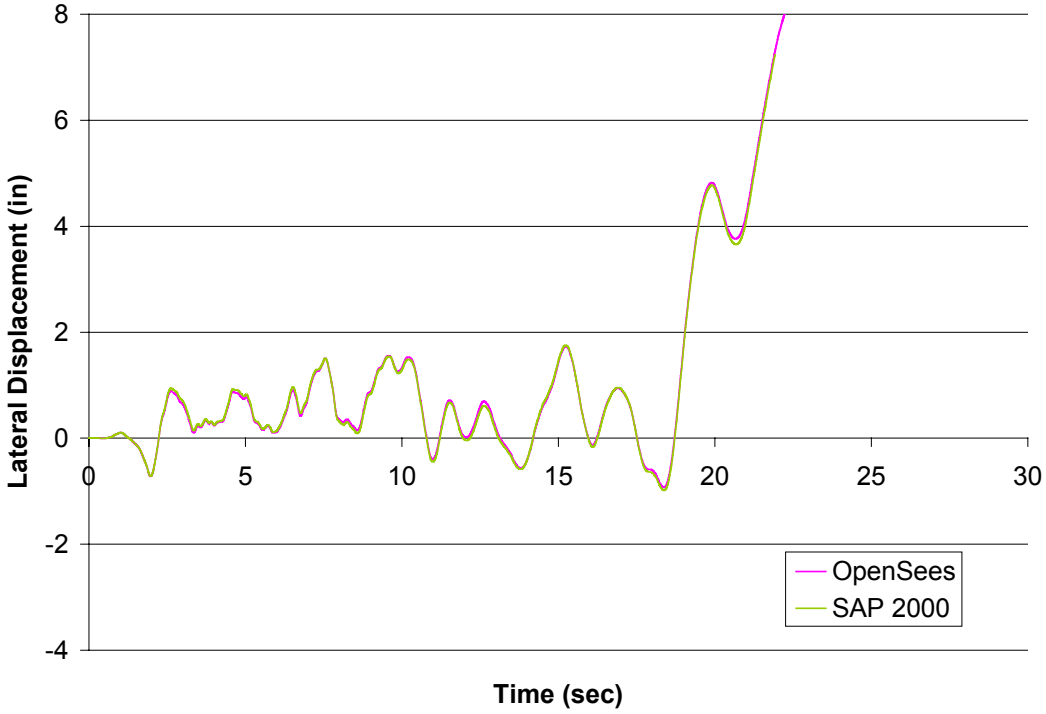

Figure 3.4c – Response Histories of SDOF Models Which Have Post-Yield Stiffness Ratios of 0.0, Include Geometric Stiffness, Use Large Displacement Analysis, and were Subjected to the Northridge Ground Motion.

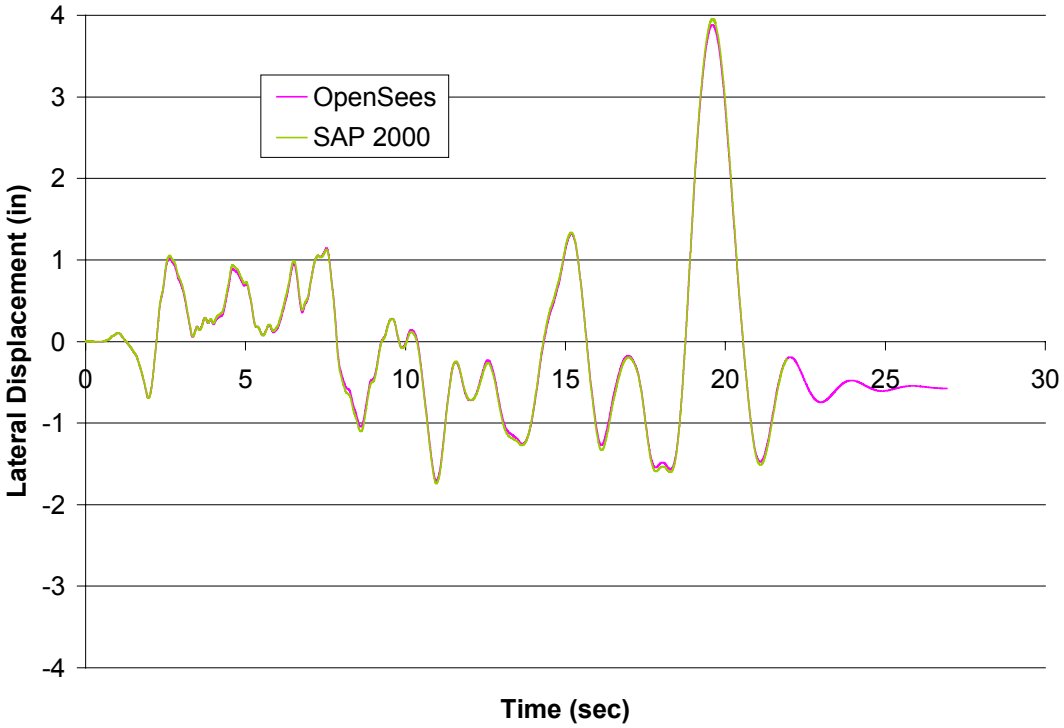

Figure 3.5a – Response Histories of SDOF Models Which Have Post-Yield Stiffness Ratios of 0.1, Neglect Geometric Stiffness, and were Subjected to the Northridge Ground Motion.

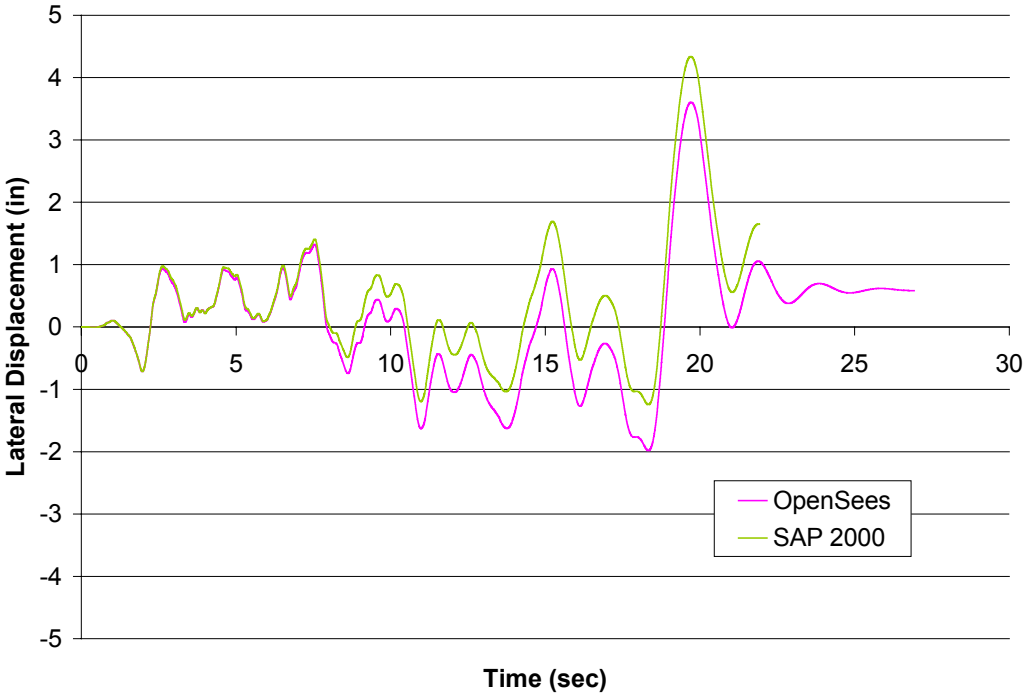

Figure 3.5b – Response Histories of SDOF Models Which Have Post-Yield Stiffness Ratios of 0.1, Include Geometric Stiffness, and were Subjected to the Northridge Ground Motion.

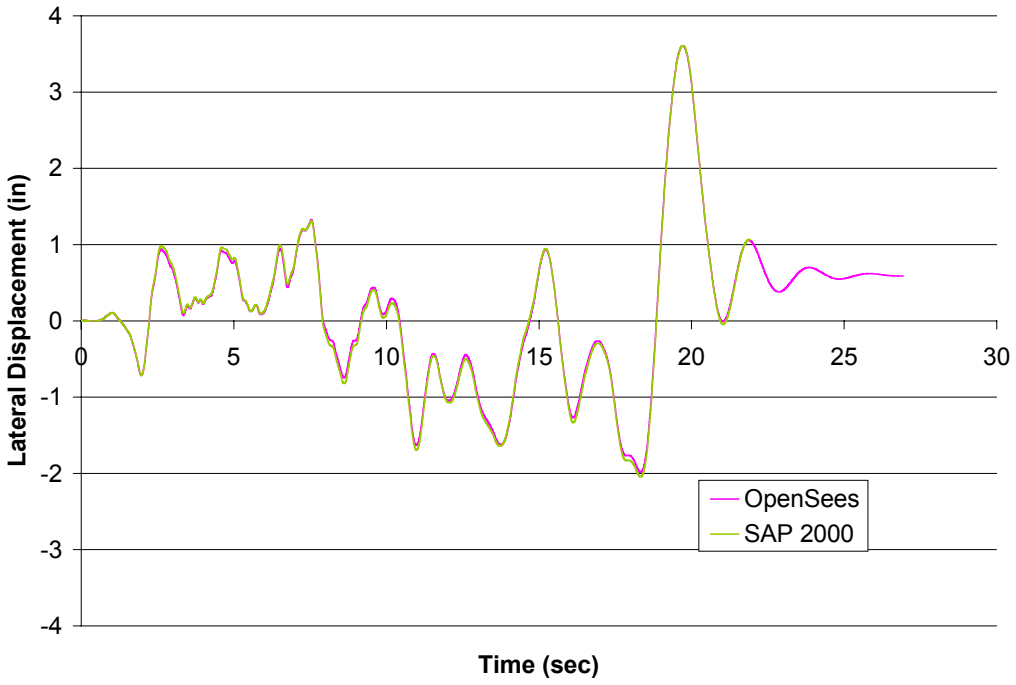

Figure 3.5c – Response Histories of SDOF Models Which Have Post-Yield Stiffness Ratios of 0.1, Include Geometric Stiffness, Use Large Displacement Analysis, and were Subjected to the Northridge Ground Motion.

Figures 3.2 through 3.5 illustrate the fact that SAP's large displacement analysis and OpenSees' P-Delta analysis are equivalent. The figures further illustrate that SAP's fast nonlinear analysis option, which does not update the geometric stiffness, does not match the results of OpenSees. For nonlinear analyses that did not consider P-Delta effects, both SAP and OpenSees produced the same results.

It is worth noting that the response histories of the "a" and "c" analyses in Figures 3.2 through 3.5 do not match exactly. This can most likely be explained if one were to examine the methods of both integration and convergence iteration. The two programs may have slightly different integration and iteration implementations, which could result in slightly different results. The discrepancy is not significant, as the above figures show that the models match, given the large displacements and erratic behavior of the models.

4.0 Parameter Study Model Descriptions

Before describing the details of the models used in this study, it is first important to justify the types of structures that were examined. The models used in this study were single-degree-of-freedom bilinear structures. Some might argue that such structures are too simplistic and that they do not capture the true behavior of buildings in earthquakes. This is true to an extent, but there are two very good reasons why the SDOF models used in this study were acceptable.

First, many researchers have developed methods to condense MDOF structures down to SDOF structures [Chopra et al. (2003), Mwafy and Elnashai (2001), Vamvatsikos and Cornell (2002b), Shibata and Sozen (1976), Krawinkler and Seneviratna (1998), Seneviratna and Krawinkler (1997), Saiidi and Sozen (1979)]. In short, it is possible and reasonable to represent MDOF structures as SDOF approximations given certain adjustment factors, but the justification is beyond the scope of this work.

Second, the SDOF models were adequate because they provided a foundation for further work in the area of collapse. One can not randomly choose parameters for an MDOF structure with the hope that it will prove to be sensitive to vertical accelerations or that it will tend to collapse at loads lower than those it is designed to withstand. Thus, it was necessary to start with simpler models where the changes in parameters could be more easily monitored.

4.1 - Model Descriptions

The models used in this study were essentially simple single-degree-of-freedom inverted pendulum structures. They were constructed as portal frames, but acted similar to inverted pendulums. Figure 4.1 illustrates the form and function of the models used in this study and their relation to inverted pendulums.

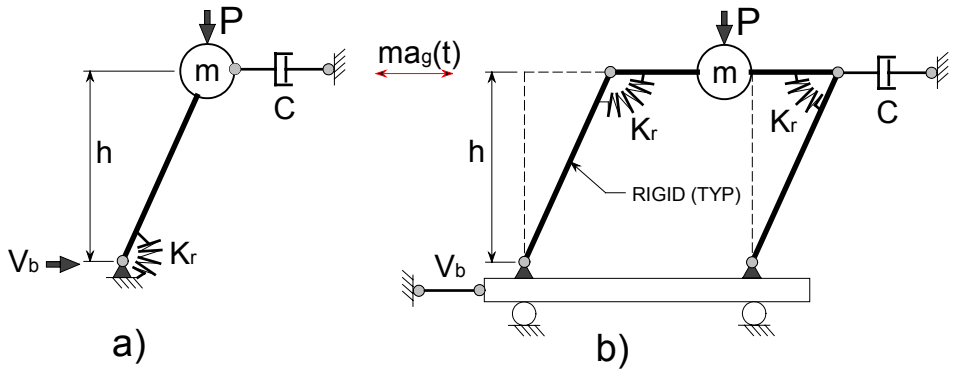

Figure 4.1 – a) Inverted Pendulm and b) Similar Portal Frame Structure

In figure 4.1, the similarities between the two systems are emphasized by the use of similar naming conventions between the two figures. The structures used in this study resemble those in Figure 4.1b. Each frame was composed of two rigid columns and a rigid beam, pinned at the ends. Furthermore, the frame structures were attached to a rigid horizontal member that acted like a sort of cart upon which the frames rode. The cart was tethered to a fixed location by a stiff truss member. The stiff tethering truss member kept the cart from moving while at the same time provided the base shear of the system throughout the analyses. The cart system was used because it simplified obtaining the base shear.

Damping was introduced into the structural system through a truss member defined with damping characteristics rather than stiffness. It is denoted in Figure 4.1b as the dashpot. OpenSees allows a user to define a viscous material for elements so that they may act as dampers. For an OpenSees element acting like a damper, the damping force (F_D) is proportional to the velocity and is defined by the following equation:

$$F_D = C\dot{u} \qquad \textbf{(4.1)}$$

where

F_D = the damping force

$\dot{u}$ = the velocity

C = the damping coefficient

The damping coefficient was calculated according to the approximate formula

$$C \approx 2\xi\sqrt{Km} \qquad \textbf{(4.2)}$$

where

ξ = the damping ratio as a percentage of critical damping

K = the lateral stiffness of the model

m = the mass of the model

Equation 4.2 will provide acceptable results when the damping ratio is less than about twenty percent. This is because equation 4.2 is an approximate relationship. Equation 4.2 neglects terms that are insignificant. Neglecting those terms is acceptable for damping ratios less than about twenty percent. Since the damping ratio used for all models in this study was five percent, the approximate formula was adequate.

The length of the dampers was also an important consideration. Since the structures were essentially inverted pendulums having arc shaped paths of motion, lateral displacements also meant that vertical displacements would occur. While the vertical displacements were very small in relation to the lateral displacements, they could be significant if the dampers were relatively short. It is important to note that the issue with damper lengths only applied because of the large displacements in the analyses. In general, small displacements will not cause significant error in damping forces. The problem is exemplified in Figure 4.2.

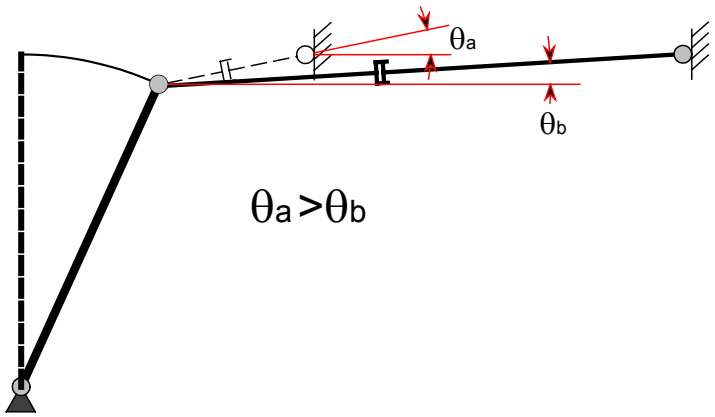

Figure 4.2 – Importance of Damper Length.

Notice in Figure 4.2 that θ_a, which corresponds to a shorter damper, is larger than θ_b, which corresponds to a longer damper. The length of the dampers introduced error because the damping force in the truss elements only acted axially. As the member rotated away from horizontal, the damping force was no longer acting completely horizontally. A component of it was acting horizontally, but another component was acting vertically. As the length of the dampers increased, the vertical force component decreased and the lateral force component increased. The damping lengths were chosen so that any amount of reasonable lateral displacement caused negligible changes in the damping force.

Furthermore, it is worth mentioning that it was preferable to use a specific damping device rather than Rayleigh proportional damping. This was because the structural response characteristics of a specific damper do not depend on model properties once the damping coefficient is calculated, whereas Rayleigh proportional damping depends on the mass and stiffness matrices of a system. This dependency becomes a problem in complicated models that include rigid members, rigid endzones, or ghost frames. While the entire structural system of such complicated models has a finite stiffness and thus finite damping, the rigid members, rigid endzones, and fictitious members can produce erroneous stiffness based damping during yield events when the Rayleigh proportional method is used.

In the models used in this study, a single mass was attached to a node at the center of the rigid beam as shown in Figure 4.1b. At that location, mass was specified for both the lateral and the vertical directions. Since vertical accelerations were included, it was necessary to include vertical mass. For P-Delta Analysis, a gravity load was applied to the same node where the mass was assigned.

The lateral stiffness of the models was provided by bilinear rotational springs in the upper corners of the model. The rotational springs were constructed in OpenSees from zero length elements with a bilinear material attached to them. The zero length elements were attached to two nodes having the same coordinates and slaved translational degrees of freedom. In Figure 4.1b, the rotational springs are designated as K_r. Not only did the rotational springs determine the stiffness of the models, but they also defined the

yield strength of the models, as well as the post-yield stiffness ratios. The bilinear behavior was achieved using a *steel01* material to the zerolength elements in OpenSees. Once the method for constructing the models was determined, the parameters were chosen.

4.2 - Parameter Determination

Seven parameters were identified and varied individually to study their influences on collapse. The first four parameters were related to the structural model and are shown in Figure 4.3. The other three are related to ground motions and are described in Section 4.2.8.

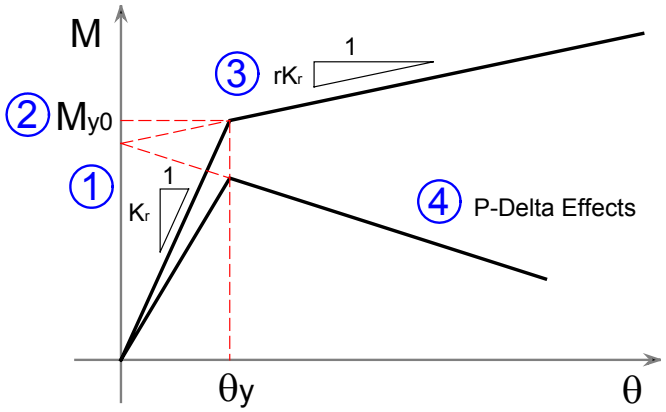

Figure 4.3 – OpenSees Model Parameters

The curves shown in Figure 4.3 represent the force deformation relationship of a rotational spring used in this study. The horizontal axis plots rotation, and the vertical axis plots moment. The parameters in numerical order from the above figure are rotational stiffness, yield moment, post-yield stiffness ratio, and P-Delta effects.
The ranges of the first two parameters, stiffness and yield strength, were determined according to the Equivalent Lateral Force (ELF) method as prescribed by the 2000 NEHRP Provisions. The ELF method was used because it allowed for a relatively quick determination of structural parameters without having to perform many calculations.

4.2.1 - Period Determination (Stiffness Parameter)

One of the first pieces of information required for an ELF design is a building's fundamental period. The period is used to determine the Seismic Response Coefficient, C_s. To determine a building's period, the mass and stiffness of that building is required. The mass is fairly easy to determine with a few simple calculations, but it is difficult to determine a building's stiffness without performing a fairly rigorous analysis. The NEHRP Provisions recognize this and thus present two equations for approximately determining a building's period. It is important to note that the approximate period equations are used to determine the C_s values and that the actual periods are not dictated by the approximate formulas. The equations are detailed in Section 5.4.2 of the Provisions and are presented as equations 4.3 and 4.4 below:

$$T_a = C_r h_n^x \quad \textbf{(4.3)}$$

where,

T_a = the approximate fundamental period

C_r and x = parameters dependent on structural type, determined from Table 5.4.2.1 of the NEHRP Provisions

Reinforced concrete moment frames -- $C_r = 0.028$, x = 0.8

Steel moment frames -- $C_r = 0.016$, x = 0.9

h_n = height (ft) above the base to the highest level of the structure

or,

$$T_a = 0.1N \quad \textbf{(4.4)}$$

where,

N = number of stories.

Equation 4.3 was developed from data collected from instrumented buildings in high seismic regions. Equation 4.4 is an approximation for "low to moderate height frames." Interestingly, the two formulas yield very different results for even low-rise

buildings. For example, a four-story reinforced concrete (RC) moment frame with twelve ft story heights would have a period of 0.62 seconds according to equation 2.3 and a period of 0.4 seconds according to equation 2.4. If the buildings have the same mass, the building with a 0.4 second period will be 2.4 times stiffer than the building with a 0.62 second period. For this research, equation 4.3 was used since it is based on measured data.

The 2000 NEHRP Provisions further specify that the approximate period determined from equation 4.3 may be modified by C_u factors, which are found in Table 5.4.2 of the Provisions, which account for the conservatism in the approximate equations and seismic hazard. The modification factors allow the designer to use a longer approximate period, which reduces the seismic demand and therefore the C_s values. As an example, consider once again a four story RC building with an approximate period of 0.62 seconds. If that building were built in a high seismic zone where the S_{D1} was greater than or equal to 0.3 g, then the modification factor would be 1.4, making the actual period 0.868 seconds. On the other hand, if the same building were going to be built in a moderate to low seismic region where the S_{D1} value was less than or equal to 0.15, the modification factor increases to 1.6, making the actual period 0.992. The difference in C_u values between high and low seismic hazard regions is based on the fact that seismic demands are lower in lower seismic hazard regions and therefore will result in buildings that are less strong and stiff compared to high seismic regions. If one assumes that the buildings have similar masses and that the modification factors are consistent with real buildings, then the increase in stiffness in high seismic hazard buildings with respect to low seismic hazard buildings would be 37 percent.

Due to the high variability inherent in the initial period determination, and consequently stiffness determination, the stiffnesses used for the parameter study cover a range of building heights, but at the same time are not explicitly representative of specific heights, hazard regions, or material composition. Recall that the approximate period, and consequently lateral stiffness, are dependent on height, seismic hazard region, and material composition. To illustrate the representative nature of the stiffness range, consider the first period used in the study, 0.705 seconds. This period is the average of the reinforced concrete and steel approximate periods as determined from equation 4.3

for a three story building with twelve foot story heights, modified by a factor of 1.6 due to low to moderate seismicity. Table 4.1 below describes other structures that also have approximate periods in the range of 0.705 seconds.

Table 4.1 – Structures with Periods of Approximately 0.7 Seconds Calculated Using the Approximate Formulas Presented in the 2000 NEHRP Provisions

Story Heights (ft)	Stories	S_{D1} (sec)	Equation	Period
12	4	> 0.3	RC 5.4.2.1-1	0.73
12	3	> 0.3	Steel 5.4.2.1-1	0.689
Irrelevant	5	> 0.3	5.4.2.1-2	0.7
11	4	0.2	RC 5.4.2.1-1	0.723
11	3	0.2	Steel 5.4.2.1-1	0.689
10	3	< 0.1	Steel 5.4.2.1-1	0.723
10	4	0.15	RC 5.4.2.1-1	0.708

Table 4.1 clearly shows that there are many combinations of story heights, number of stories, seismic hazards, and material types that result in buildings with fundamental periods around 0.705 seconds. Thus, the 0.705 second period used in this study could arguably apply to structures in the range of three to five stories in various seismic hazard regions, made of either reinforced concrete or steel and having story heights ranging between ten and twelve feet.

To reduce the number of parameters in the period calculation, it was assumed that the modification factor for all structures would be 1.6, the story heights would be 12 feet, and the average of the steel and concrete equations would be used. Thus, the period determination was condensed to one parameter, the number of stories. Table 4.2 lists the average periods determined by the aforementioned procedure and the actual periods used in the parameter studies calculated from structural properties.

Table 4.2 – Approximate and Actual Periods Used in the Parameter Study

Floor ht (ft) = 12			Factor = 1.6	
	Approximate Period			**Actual**
Floors	Steel	RC	Average	**Period**
3	0.788	0.644	0.716	0.705
4	0.991	0.834	0.913	0.903
5	1.185	1.020	1.103	1.093
6	1.371	1.202	1.287	1.278
7	1.551	1.381	1.466	1.459
8	1.726	1.557	1.642	1.635
9	1.897	1.731	1.814	1.808

The discrepancy between the approximate and actual periods results from round-off error when calculating the rotational stiffnesses. The discrepancy is not significant because of the great amount of variabilty when determining the fundamental period as discussed earlier.

4.2.2 - Removing Mass as a Parameter

Once the fundamental periods were determined, the next task was to determine the mass of the structures. Clearly, the mass of a four story building will be less than that of a seven story building of the same plan. Consequently, mass becomes another parameter. However, mass can be removed as a parameter much the same way that it is removed from the dynamic system of equations used to create an elastic response spectrum. Consider the equation of motion given by equation 4.5:

$$m\ddot{u}(t) + C\dot{u}(t) + Ku(t) = -m\ddot{u}_g(t) \qquad \textbf{(4.5)}$$

where

m = mass of the oscillator

C = damping coefficient (see equation 4.2)

K = stiffness of oscillator

$u(t)$ = displacement of the system as a function of time

$\ddot{u}_g(t)$ = acceleration of the ground as a function of time

By dividing the entire system by mass and substituting equation 4.2 for *C*, the equation of motion becomes,

$$\ddot{u}(t) + 2\xi\omega\,\dot{u}(t) + \omega^2 u(t) = -\ddot{u}_g(t) \qquad \textbf{(4.6)}$$

Thus, the response of an SDOF structure subjected to a given ground motion can be determined if one knows the damping ratio and the fundamental frequency of the system. The same procedure of removing the mass from the equation of motion was used in this study. By dividing all of the affected parameters by mass, the mass was eliminated as a parameter.

4.2.3 - The Equivalent Lateral Force Method and Massless Parameters

In the ELF method described in the NEHRP Provisions, the yield force and lateral stiffness are dependent on mass. First, the yield force is dependent on mass in that the equation used to calculate the design base shear, or yield strength, of a structure is dependent on the weight. The equation for calculating the base shear is given by equation 4.7:

$$V = C_s W = C_s mg \qquad \textbf{(4.7)}$$

where

V = the base shear (and yield strength)

C_s = the seismic response coefficient

W = the weight, or mass times gravity

If the mass in equation 4.7 is assumed to be a unit mass, the base shear effectively becomes independent of mass and results in the following:

$$V = C_s g \qquad \textbf{(4.8)}$$

To use equation 4.8, the seismic response coefficient must be determined. An important point to make about the seismic response coefficient is that it is essentially a ratio. It determines the yield strength of a building based on a percentage of the weight. So, it makes sense to speak of the C_s value in terms of percentage. The seismic response coefficient (C_s) is determined in accordance with section 5.4.1.1 of the NEHRP Provisions, which states,

$$C_s = \frac{S_{D1}}{T(R/I)} < \frac{S_{DS}}{R/I} \qquad \textbf{(4.9)}$$

where,

S_{DS}, S_{D1} = the design spectral response acceleration in the short period range and at one second, respectively.

R = the response modification coefficient (from table 5.2.2 of the Provisions)

I = the Importance factor (assumed to be 1 for these studies)

T = the period of the structure.

The components of the C_s equation are determined from seismic hazard, ductility, importance, and fundamental period. All of the ingredients in the seismic response coefficient are obtained from tables, graphs, and maps except the period, which can be determined according to the approximate methods described earlier. In this way, C_s is independent of mass. It is important to note that there is also a lower bound to the C_s values, given by

$$C_{s(\min)} = 0.044 S_{DS} I \qquad \textbf{(4.10)}$$

Next, the lateral stiffness of the models was made independent of mass. The lateral stiffness of an SDOF system is determined according to the following equation:

$$K_e = \varpi^2 m \qquad \textbf{(4.11)}$$

where

K_e = the initial lateral stiffness of the SDOF system (kips / in.)

m = the mass of the SDOF system

ω = the frequency of the SDOF system = $\frac{2\pi}{T}$

As for the base shear, if the mass is assumed to be a unit mass, the stiffness of models can be determined independent of mass. The resulting equation for lateral stiffness is given by equation 4.12:

$$K_e = \frac{4\pi^2}{T^2} \quad \textbf{(4.12)}$$

For the parameter study, equations 4.8 and 4.12 were used to determine the yield strengths and stiffnesses of the models.

4.2.4 - Rational Range for Stiffness and Yield Strength Parameters

Having derived equations to determine the lateral stiffness and yield force independent of mass, it was then necessary to determine rational ranges to use for the parameter study. The stiffness determination was simple because the only real input in equation 4.12 was the approximate period determined earlier. A rational range for the yield forces was more difficult to determine. This was because the yield force, as given in equations 4.8 and 4.9, was dependent on the fundamental period, the response modification coefficient (ductility), and the design spectral response accelerations. The design spectral response accelerations were dependent on geographic location and site characteristics. Thus, the yield force was dependent on five parameters. To better understand the yield force dependencies, it is prudent to further discuss how to determine C_s.

4.2.4.1 - Determining the Seismic Response Coefficient

4.2.4.1.1 - Framing System

A first step in determining the seismic response coefficient is to choose a framing system. In table 5.2.2 of the NEHRP Provisions, many structural systems are listed with various corresponding factors used in design. In this study, the structures considered were Special, Intermediate, and Ordinary moment frames. The primary difference between each of the moment frames is the amount of detailing required, which translates to ductility and toughness. Ordinary moment frames have the lowest amount of detailing requirements and Special moment frames have the highest detailing requirements. Ideally, more strict detailing requirements results in structures that can resist higher inelastic ductility demands. Thus, they can be designed to yield. In other words, they can be designed for a lower base shear. To account for a structure's ability to deform inelastically, the C_s value has the seismic response modification factor (R) in the denominator, which corresponds to the type of framing system and can be found in Table 5.2.2 of the Provisions,

The response modification factor concept has been developed according to the philosophy that structures cannot reasonably be designed to remain elastic when subjected to strong ground shaking, but will undergo approximately the same amount of displacement as an elastic structure. This concept is known as the "Equal Displacement" concept. This concept is further illustrated by Figure 4.4.

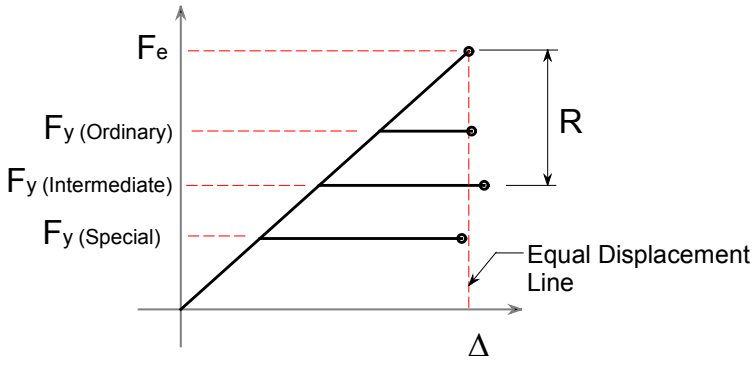

Figure 4.4 – Equal Displacement Theory

The force displacement relationship shown in Figure 4.4 plots the behavior of four different structures. First, an elastic structure would displace a certain amount, Δ, when subjected to a ground motion and would have a base shear of F_e. Then, the other three force deformation relationships shown in Figure 4.4 would correspond to structures that could allow inelastic deformation. Inelastic deformation is allowed because in regions of high seismicity, it may be extremely uneconomical to design a structure for F_e, but feasible to design the structure for F_y. It is important to note, though, that lower yield strengths demand higher inelastic displacement capacities because the ductility demands will be higher. Displacement capacity is primarily determined by detailing requirements. Thus, the lower the yield strength, the stricter the detailing requirements.

Another important point to bring up about Figure 4.4 is that each of the force deformation relationships shown has approximately the same ultimate displacement. Research has shown that a structure with given period will displace about the same amount for any given yield strength assuming infinite ductility capacity. This is the equal displacement concept. Thus, if the inelastic displacement capacity, or ductility, of a structural system is known beforehand, then one can determine the allowable decrease in the yield force. In the NEHRP Provisions, R values are used to characterize a structure's inelastic displacement capacity. Thus, special moment frames (R = 8) have higher R values than intermediate moment frames (R = 5.5 or 5), which have higher R values than ordinary moment frames (R = 3.5 or 3). Two R values are associated with the intermediate and ordinary moment frames because the first applies to steel moment frames and the second applies to reinforced concrete moment frames. Figure 4.4 illustrates the relationship between special, intermediate, and ordinary moment frames. Typically special moment frames are used in high seismic regions because the base shear demands necessitate a large amount of inelastic displacement, whereas ordinary moment frames are acceptable in low seismic regions because the base shear demands are low and so a structure will ideally not have a great deal of inelastic displacement.

4.2.4.1.2 - Spectral Accelerations

The next pieces of information required to calculate C_s are the design short period spectral acceleration (S_{DS}) and design one-second spectral acceleration (S_{D1}) values. The design spectral acceleration values were determined according to the procedure described in section 4.1.2 of the NEHRP Provisions. The equations for calculating the design spectral acceleration values are presented below.

$$S_{DS} = \frac{2}{3} F_a S_s \quad \textbf{(4.13)}$$

$$S_{D1} = \frac{2}{3} F_v S_1 \quad \textbf{(4.14)}$$

where,

F_a and F_v are site coefficients defined in tables 4.1.2.4a and b of the Provisions, respectively.

S_s and S_1 are the mapped spectral accelerations of the maximum considered ground motion at short periods and one second, respectively.

The design spectral acceleration values basically are the maximum ground accelerations that a structure should be designed to withstand. The S_s and S_1 values correspond to the "maximum considered earthquake" that has a 2 per cent probability of occurring in 50 years. The S_s and S_1 values can be obtained from seismic hazard maps included with the NEHRP Provisions or on the USGS web site. The S_S and S_1 values are reduced by 2/3 because of inherent overstrength in buildings and adequate performance of structures in past earthquakes. The values are then increased or decreased by the factors F_a and F_v, which account for site conditions. The ground motions at a site class E (soft soil) location, for example, will potentially be amplified, becoming more severe. The design spectral acceleration values for very soft soils are increased by a factor between 1.2 and 3.5 depending on the S_S and S_1 values.

4.2.4.1.3 - Importance Factor and Fundamental Period

The remaining pieces of information required to calculate the seismic response coefficient are the importance factor and the fundamental period. The importance factor for the parameter study was assumed to be 1.0 for all cases. Thus, the buildings were treated as ordinary non-essential buildings. The periods were determined according to the procedure described previously.

4.2.4.2 - Determining a Range for the Yield Force

There can be significant variance in the base shear calculation due to location, site conditions, building period, and framing type. As such, various permutations of the values required to calculate the seismic response coefficient were examined to determine a rational range for the yield forces used in the parameter study. Figures 4.5 through 4.8 show plots of the resulting permutations.

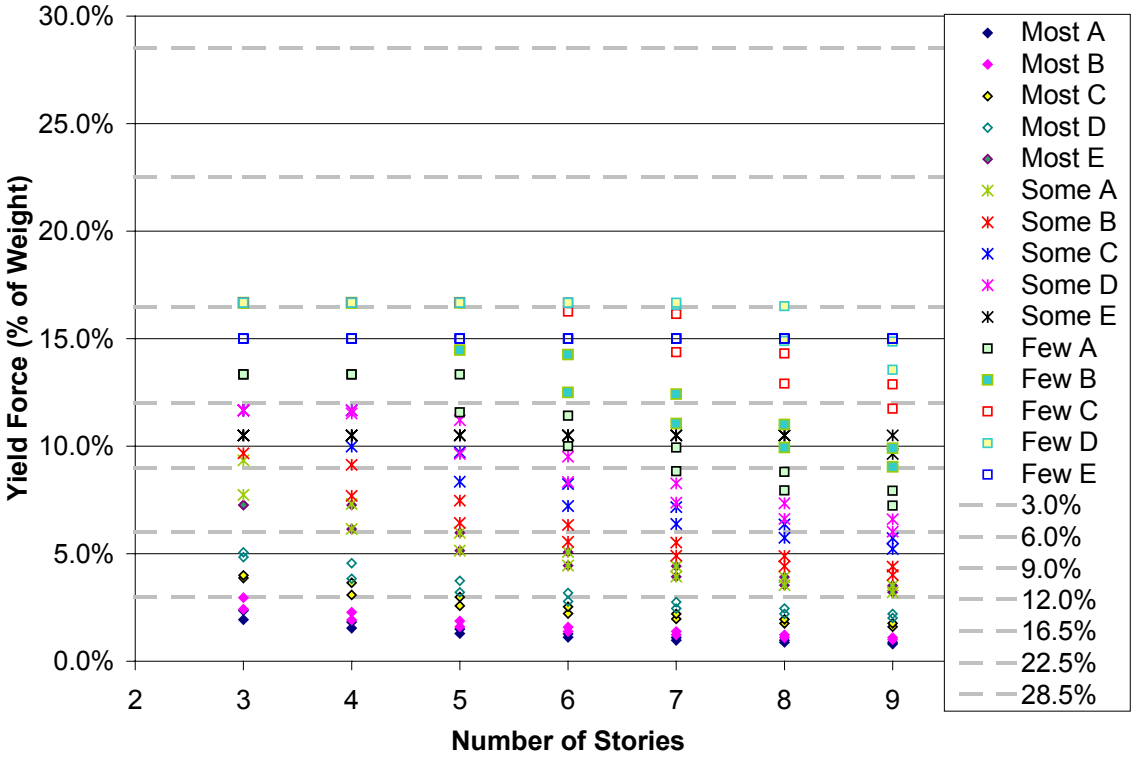

Figure 4.5 – WUS Special Moment Frames (R = 8)

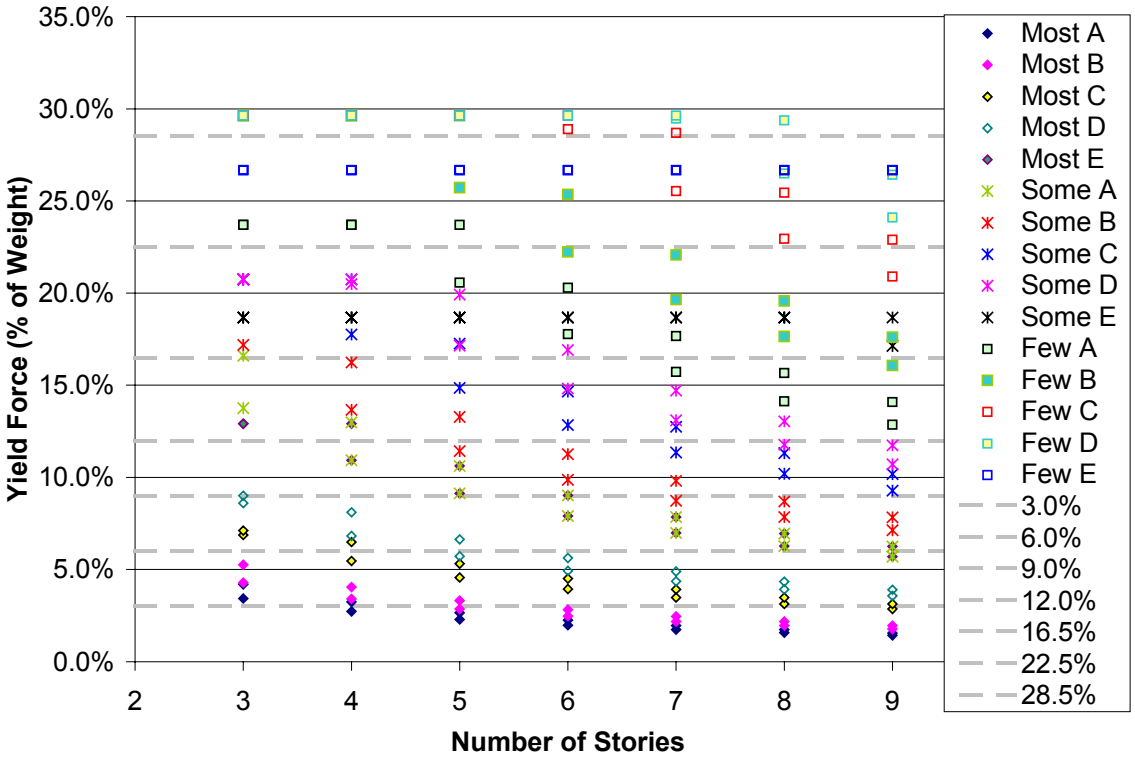

Figure 4.6 - WUS Intermediate Moment Frames (R = 5 [RC], R = 4.5 [Steel])

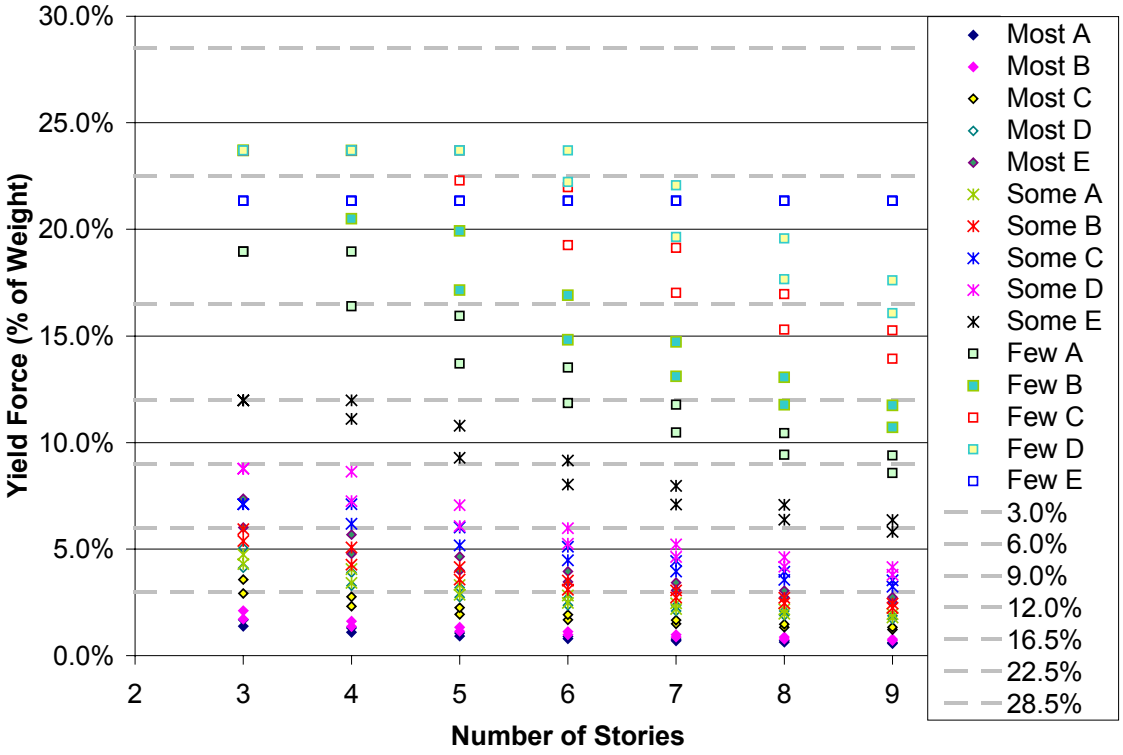

Figure 4.7 - CEUS Intermediate Moment Frames (R = 5 [RC], R = 4.5 [Steel])

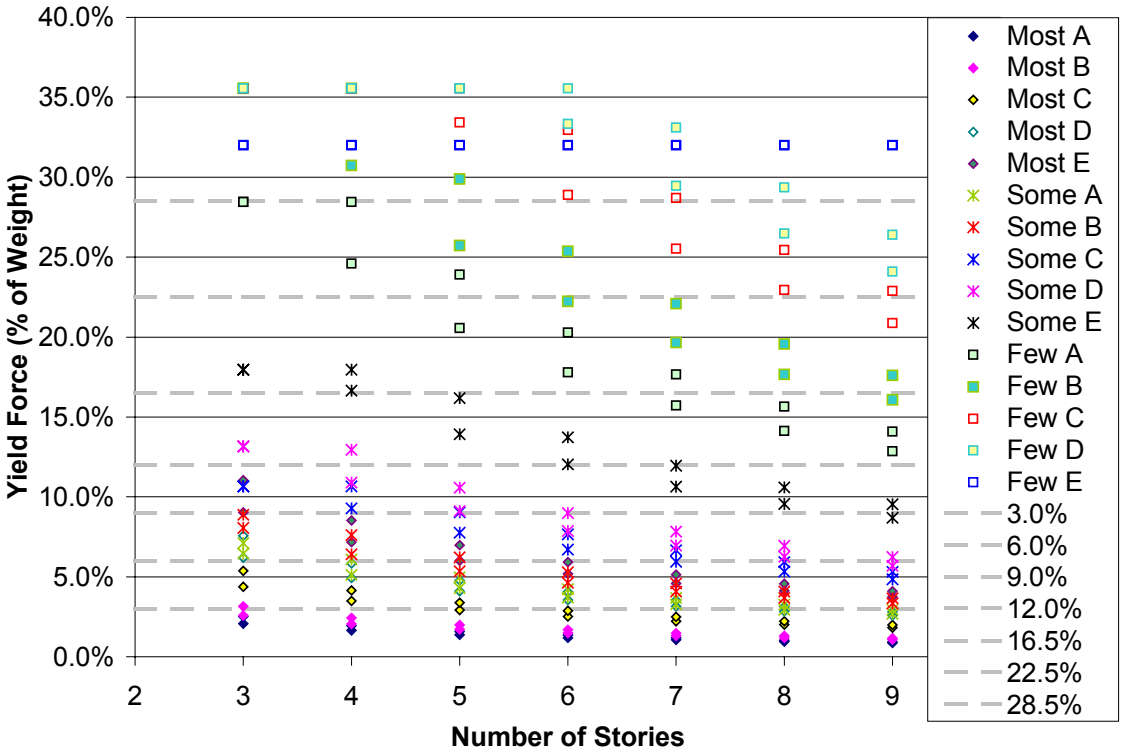

Figure 4.8 - CEUS Ordinary Moment Frames (R = 3 [RC], R = 3.5 [Steel])

To understand figures 4.5 through 4.8, a few comments must be made. First, the seismic hazards were determined rather subjectively. This is illustrated in the above figures by the most, some, and few categories. These categories are meant to represent the average levels of seismic hazard in the two regions. For example, in most of the CEUS, the seismic hazard is quite low. Consequently, the "most" category of the CEUS figures reflects this. Then, the "some" category is meant to encompass a higher average seismic hazard affecting part of the region. Finally, the "few" category is meant to encompass the highest level of seismic hazard affecting only a few areas of that region. Table 4.3 presents the S_s and S_1 values used for the subjective most, some, and few categories.

Table 4.3 – CEUS and WUS Seismic Hazards Over Most, Some, and Few Areas of the Regions.

% g	WUS			CEUS		
	Most	some	few	Most	some	few
Ss	0.4	1.4	2	0.25	0.4	1.6
S1	0.2	0.8	1.8	0.08	0.25	1.2

In Table 4.3 that the "most" acceleration values in the CEUS are much lower than those in the WUS. However, the "few" acceleration values are nearly equal between both regions. This is because of the high seismic hazards around the New Madrid and Charleston, SC regions in the CEUS.

In Figures 4.5 through 4.8, it is also important to note the types of frames examined in the permutations. For CEUS structures, a figure representing a set of permutations was created for both Ordinary and Intermediate moment frames. However, a figure representing a set of permutations was created for both Intermediate and Special moment frames for WUS structures. This was because the vast majority of moment frames in the CEUS would probably be classified as ordinary or intermediate, whereas it seemed more likely that WUS moment frames would be classified as intermediate or special due to the higher average seismicity over most of the region.

Another aspect of the figures is the site classes. For each of the three seismic hazard categories (most, some, and few), a C_s value was calculated for each site class according to Tables 4.1.2.4a and 4.1.2.4b of the NEHRP Provisions. Site Class F is not included in the figures because site-specific geotechnical investigation is required to determine the adjustment factors for such a site.

Then, there is one final comment about the figures worth mentioning before describing the yield strengths chosen for the parameter study. Each of the four figures has the number of stories on the x-axis. Since the period calculated for a three story building could have a large amount of variability based on story heights, material type, and seismic region, the story designations are somewhat subjective as well. Their primary purpose is to provide a range of periods.

Even though Figures 4.5 through 4.8 involve some subjectivity, they are still useful for determining a rational range of yield strengths. In all four figures the majority of the yield strengths occurred below about 15 per cent of the structure's weight. The minority of the yield strengths occurred above 15 per cent of the structural weight. The range of yield strengths chosen for the parameter study accounted for the distribution of yield strengths. The yield strengths chosen are plotted in the four figures above as heavy gray dashed lines. The yield strengths used were 3, 6, 9, 12, 16.5, 22.5 and 28.5 per cent

of the weight. While the above figures clearly show that there are many yield strength values that are lower than 3 per cent, models with lower yield strengths tended to collapse completely in analyses run early in the study. This can be explained by considering that the majority of the structures with yield strengths less than 3 per cent were either site class A or B (hard rock) and are in low hazard areas. Furthermore, the ground motions used in the parameter study were scaled according to PGA and the lowest ground motion scale used was 0.1g, which is quite high for a low seismic hazard area on hard rock.

One could also rationalize the yield strength choices by considering overstrength (Ω). Since the models used in the parameter study are SDOF models and real structures are MDOF, the MDOF systems must be converted. One method to do this is to construct an MDOF analytical model, run a static nonlinear pushover analysis on it, and fit a bilinear curve to the resulting pushover curve. An example of the type of result that would come from such an analysis is shown in Figure 4.9.

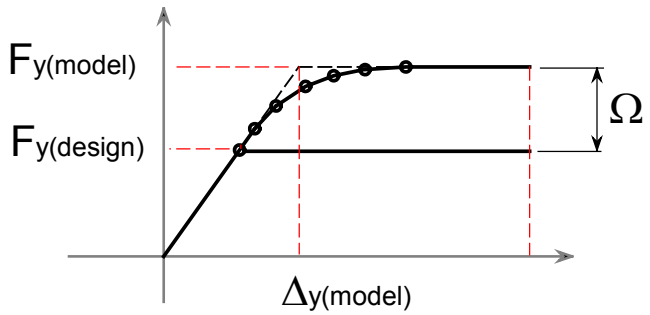

Figure 4.9 – Pushover Example

In a pushover analysis, increasing lateral loads are applied to the model until a specified displacement is reached. The MDOF model would include plastic hinges or fiber elements to mimic nonlinearity, and consequently the stiffness of the system would change as each new plastic hinge formed. The formation of plastic hinges is denoted in the above figure as small circles. If the building had been designed according to the ELF method, then the first significant yield would occur somewhere around $F_{y\ (design)}$. However, due to hinge sequencing, higher material strengths than nominal, and safety factors, the structure would more than likely reach a higher strength plateau of $F_{y\ (model)}$. Thus, the actual bilinear curve used for an SDOF nonlinear dynamic analysis would have a higher yield strength than one determined from the ELF method. The ratio of actual

strength to design strength is called overstrength (Ω). The increase in a bilinear model yield strength would be equal to Ω. Maximum expected overstrength values are provided in table 5.2.2 of the NEHRP Provisions and are in the range of two to three. So, a SDOF analytical model with a yield strength equal to 3 per cent of the weight may very well correspond to a structure that has a design yield strength of around 1.5 per cent, which is reasonable for the CEUS. At any rate, the range of the yield strength parameters chosen for this study is reasonable and adequate for showing the effects of yield strength on collapse.

4.2.5 - Rotational Forms of the Yield Strength and Stiffness

Once the stiffness and yield strength values were determined according to equations 4.8 and 4.11, they had to be converted to rotational values because the stiffness and strength were provided by rotational springs. The linear values were converted to rotational values using geometry and the assumption that $\sin\theta \approx \theta$ (small angle theory). The variables used in the rotational forms of the parameters are shown in Figure 4.1b and the derivation of them is as follows:

$$M_y = K_r \theta_y \tag{4.15}$$

$$\theta_y = \frac{\delta_y}{h} \tag{4.16}$$

$$M_y = F_y h \tag{4.17}$$

where

h = the height of the model (in.)

θ_y = the yield rotation of a column at the base

δ_y = the yield displacement measured at the top of the column

By substituting equations 4.16 and 4.17 into equation 4.13, the rotational term may be converted:

$$F_y = \frac{K_r}{h^2}\delta_y = K_e \delta_y$$

Since half of the stiffness is provided by each spring, the resulting rotational stiffness is

$$K_r = \frac{K_e h^2}{2} \tag{4.18}$$

Also, since half of the yield force is provided by each spring, then

$$M_y = \frac{F_y h}{2} \tag{4.19}$$

4.2.6 - P-Delta Parameter

P-Delta effects were included and monitored in the parameter study by specifying stability ratios (θ) for the models. The stability ratios were used to introduce P-Delta effects into the analyses because they have been shown to be good indicators of P-Delta sensitivity. Recall that the stability ratio is the ratio of geometric stiffness to lateral structural stiffness.

Even though the stability ratios were the point of variation in the parameter study, the stability ratios had to be converted to vertical loads that were applied to the structures. The method for determining the appropriate vertical load was derived from equation 4.20:

$$\theta = \frac{P}{K_e L} \tag{4.20}$$

where

θ = the stability ratio of the model

K_e = the lateral stiffness of the model

L = the height of the model (144 in.

P = the lad applied to the model to achieve a desired θ.

Since K_e was determined previously (equation 4.11) and L was constant for all models, the equation could be rearranged so that the required vertical load parameter on a structure with a given stiffness was dependent only on the choice of stability ratio. Stability ratios typically range from small values around 0.02 to 0.25. The NEHRP

Provisions in section 5.4.6.2 prescribe a maximum stability ratio of 0.25, but 0.25 is quite severe and not many realistic structures approach this upper bound. For this study, five values were chosen in a range between 0.02 and 0.2. The stability ratio parameters are listed in Table 4.4, as well as the required vertical load to achieve the prescribed stability ratios.

Table 4.4 – Vertical Loads Required to Achieve Desired Stability Ratios for Various Building Periods.

					Stability Ratio				
Stories	Kr (k*in/rad)	Ke (k/in)	ω (1/sec)	T (sec)	0.04	0.08	0.12	0.16	0.2
3	823303	79.4	8.91	0.705	457.4	914.8	1372.2	1829.6	2287.0
4	502176	48.4	6.96	0.903	279.0	558.0	837.0	1115.9	1394.9
5	342420	33.0	5.75	1.093	190.2	380.5	570.7	760.9	951.2
6	250519	24.2	4.92	1.278	139.2	278.4	417.5	556.7	695.9
7	192400	18.6	4.31	1.459	106.9	213.8	320.7	427.6	534.4
8	153103	14.8	3.84	1.635	85.1	170.1	255.2	340.2	425.3
9	125178	12.1	3.47	1.808	69.5	139.1	208.6	278.2	347.7

Notice that for a given stability ratio, the load changes as the period of the structure changes. This is in accordance with equation 4.20.

4.2.7 - Post-yield Stiffness Parameter

Recall that the models used in the parameter study employ SDOF bilinear force deformation relationships to represent realistic MDOF buildings. Since mimicking realistic MDOF structures was a goal, it was also important that the post-yield stiffness ratios for the models closely mirror the ratios one would find in an MDOF model. One way to determine the post-yield stiffness ratio for an MDOF structure is to conduct a pushover analysis and then fit a bilinear curve to the results (see Figure 4.9). Gupta and Krawinkler (1999) conducted many pushover analyses on steel moment frames and noted that the post-yield stiffness was very dependent on modeling. For example, if slab contributions are included in the analysis, then a structure will tend to have a higher post-yield stiffness ratio. Also, detailed panel zone models can greatly influence the post-yield behavior of a structure. Knowing the uncertainties involved in choosing rational post-yield stiffness ratios and considering the range of post-yield stiffness ratios seen in

work such as that of Gupta and Krawinkler, it was decided that the use of equally spaced intervals from 0.0 to 0.25 at increments of 0.05 was the most reasonable. Thus, the post-yield stiffness ratios cover a range that is rational, but at the same time can apply to a wide variety of modeling scenarios.

4.2.8 - Earthquake Parameters

The final three parameters varied in this study apply to ground motions. Naturally, the first parameter among the ground motion parameters was the various earthquakes used. Since earthquakes can have very different effects on various structures, it is important to look at as many earthquakes as possible. However, since the number of parameter combinations increases drastically with each new earthquake, only eight different earthquakes were used in this study. The earthquakes, along with pertinent information about them, are listed in Table 4.5.

Table 4.5 – Earthquakes Used for the Parameter Study

Number	Earthquake		PGA (%g)		Duration	Magnitude	Soil
	Location	Date	Horizontal	Vertical	(sec)		
1	Aqaba, Egypt	22-Nov-95	0.097	0.109	60	7.1	--
2	Cape Mendocino, CA	25-Apr-92	0.59	0.163	35.98	7.2	D
3	Chalfant Valley, CA	21-Jul-86	0.177	0.127	39.925	6.2	D
4	Kern County (Taft)	21-Aug-52	0.156	0.109	54.15	7.4	D
5	Hollister, CA	26-Jan-86	0.114	0.172	40	5.4	D
6	Izmit, Turkey	17-Aug-99	0.152	0.146	30	7.4	A
7	Kobe, Japan	16-Jan-95	0.251	0.158	40.96	6.9	E
8	Tabas, Iran	16-Sep-78	0.328	0.183	23.84	7.4	B

Accelerograms of the above earthquakes are included in Appendix A. It is important to note that when applied to the structures, all of the ground motions were scaled according to PGA. Scaling according to PGA was the only consistent option for structures with a variety of periods. While PGA was used for the parameter study, spectral acceleration scaling is more appropriate when only dealing with one structure. The set of ground motions listed in Table 4.5 showed a good amount of variation. Thus, it was hoped that the ground motion set would provide a range of responses for

comparison in the parameter study. Figures 4.10 and 4.11 show the acceleration and displacement response spectra scaled to a PGA of 0.1 g.

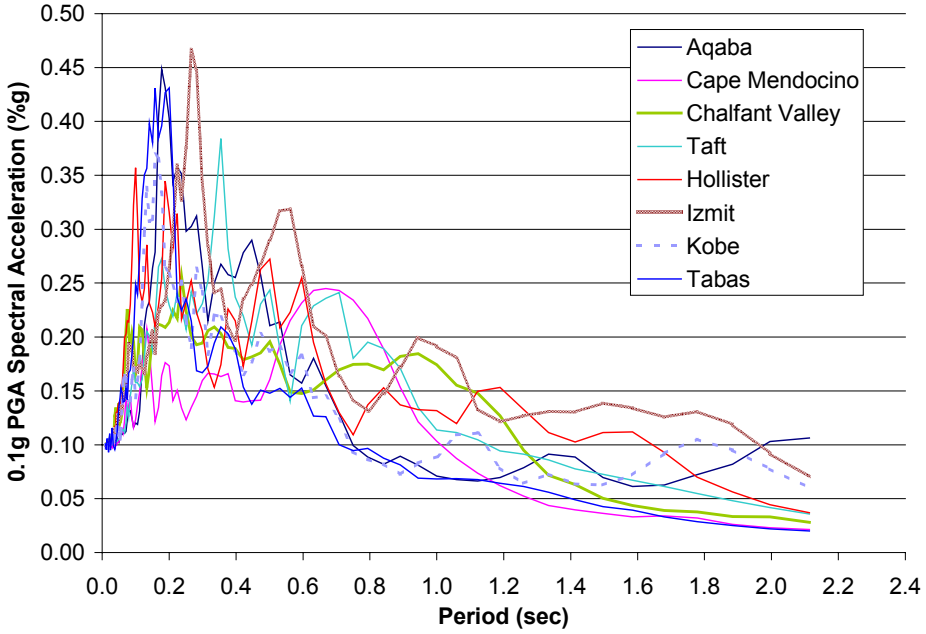

Figure 4.10 – Acceleration Response Spectrum of Parameter Study Horizontal Ground Motions

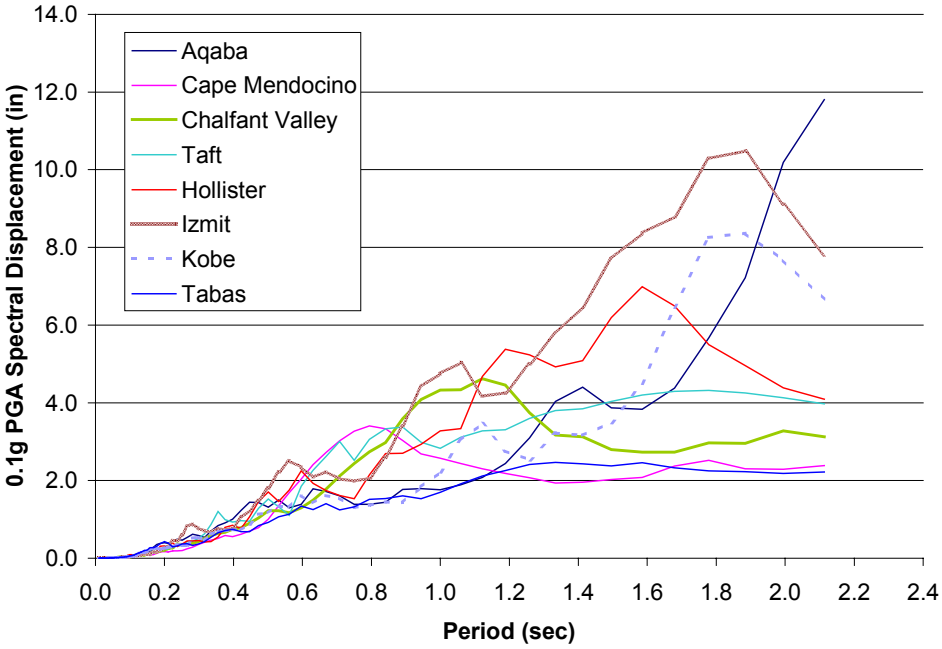

Figure 4.11 – Displacement Response Spectrum of Parameter Study Horizontal Ground Motions

The acceleration response spectrum shown in figure 4.10 reveals a reasonably banded range of acceleration values, which is what one would expect of a large set of ground motions. More importantly, the displacement response spectrum shown in figure 4.11 fills a broad spectrum of displacement demands. Thus, the ground motions used in the parameter study should provide a wide range of results for comparison.

4.2.8. 1 - Earthquake Scaling Parameters

Various earthquake intensities were used to determine their effects on the sets of models. As previously stated, each of the earthquake's lateral components used in the parameter study was scaled according to PGA. This type of scaling was used rather than response spectrum scaling because it allows for direct comparison between the results of models with differing periods. The response spectrum method of scaling would create different intensities of the same earthquake for structures with varying periods, thus causing the variation of two parameters at once.

The vertical component of the earthquakes, on the other hand, was scaled by a simple multiplier. This was done for several reasons. First and foremost, it is very difficult and may be impossible to specify beforehand the effect that vertical accelerations will have on the lateral displacement of a model. This is because the vertical accelerations cause secondary P-Delta displacements and as such are dependent on the amount of initial lateral displacement a structure undergoes. The initial lateral displacement is dependent on the yield strength, post-yield stiffness ratio, initial stiffness, and lateral ground motion characteristics. So, while it is possible to draw general conclusions about the effects of increasing the vertical accelerations, it is impossible to draw conclusions about the effects of specific vertical acceleration magnitudes on lateral displacement. In other words, scaling the vertical ground motions to a specific PGA does not enhance comparison between models in any way. In contrast, if one knows the PGA of a horizontal acceleration, the lateral displacement can be reasonably determined beforehand.

Secondly, vertical ground motion PGAs are typically in the same ranges as the lateral ground motion PGAs. So, if the vertical components are within a reasonable range

of the lateral components, then the vertical and horizontal combination is reasonable. However, if in the analyses both the vertical and horizontal accelerations are scaled together, then two parameters are being varied at once, which is unacceptable. To make the vertical components reasonable, they were scaled independently of the horizontal components, but scaled by factors that made the vertical components reasonably close to the horizontal components. All of the original vertical components had PGA values between 0.1 g and 0.2 g. Figure 4.12 shows the range of vertical PGA values according to earthquake numbers assigned in Table 4.5.

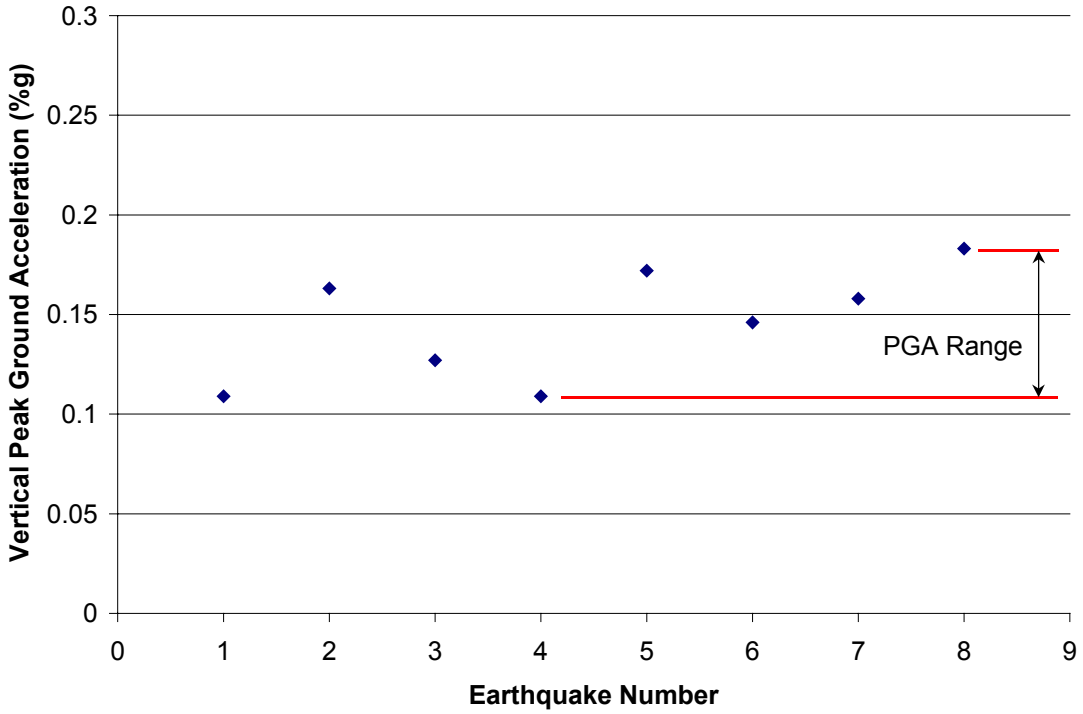

Figure 4.12 – Range of Vertical Peak Ground Acceleration Values Used in the Parameter Study

To illustrate the rationality of the vertical scaling method, consider a set of lateral ground motions scaled to 0.2 g. If the vertical components represented in Figure 4.12 are multiplied by 1.5, then the resulting range of vertical PGAs is between about 0.15 g and 0.25 g. Thus, a vertical muliplier of 1.5 is a reasonable choice.

To summarize, because it is impossible to determine beforehand the effects of vertical accelerations and since it is only necessary that the vertical components be in a reasonable range, the scaling method used for this study is to multiply the original

vertical records by between 1.5 and 2.5. Table 4.6 shows the various scale factors for the vertical components and the corresponding horizontal PGA values.

Table 4.6 – Vertical and Horizontal Ground Motion Scale Combinations

Lateral Acceleration PGA (%g)	Vertical Acceleration Multiplier 1.5	2	2.5
0.1	X		
0.2	X	X	X
0.3	X		
0.4			X

Table 4.6 is not entirely filled because the analyses were conducted incrementally and once a trend was established, extra data did not add significantly to the overall uniqueness of the results. Each "X" in the table above represents a relatively large number of analyses and so filling in the table for the sake of filling in the table would require a lot of extra computations and data for basically the same results.

4.3 - Verification of the Massless Approach

While removing the mass from the structural parameters is fundamentally sound, it seemed prudent to construct several models of both massless and mass dependent types and compare them. Both the control set and the massless set were constructed according to the "cart" method described earlier. Moreover, the physical dimensions of the frame structures was held constant between the two sets. This was done because the systems are essentially SDOF and thus the size of the physical frame does not matter as long as the flexibility of the frame does not influence the results. The structural properties used in the comparative analyses are listed in Tables 4.7 and 4.8.

Table 4.7 – Model Properties for Control Set of Models

Building Density (pcf): 9

Stories	Height (ft)	T (sec)	Weight (k)	Stiff (k/in.)	Kr (k*in./rad)	Fy (k)	My (k*in.)
3	12	0.689	3240.0	697.5	7231756.6	301	21663.5
4	12	0.868	4320.0	586.9	6085279.9	319	22946.5
5	12	1.037	5400.0	513.4	5322731.4	333	23993.8
6	12	1.200	6480.0	460.2	4771180.0	346	24884.9
7	12	1.357	7560.0	419.5	4349684.2	356	25664.0
8	12	1.510	8640.0	387.2	4014787.5	366	26358.6
9	12	1.660	9720.0	360.8	3740856.5	375	26986.9

Table 4.8 – Model Properties for Massless Set of Models

Stories	Height (ft)	T (sec)	Weight (k)	Stiff (k/in.)	Kr (k*in./rad)	Fy (k)	My (k*in.)
3	12	0.689	386.1	83.1	861784.3	36	2581.6
4	12	0.868	386.1	52.5	543871.9	28	2050.8
5	12	1.037	386.1	36.7	380575.3	24	1715.6
6	12	1.200	386.1	27.4	284282.8	21	1482.7
7	12	1.357	386.1	21.4	222144.6	18	1310.7
8	12	1.510	386.1	17.3	179410.8	16	1177.9
9	12	1.660	386.1	14.3	148595.1	15	1072.0

The control set of comparative models was assumed to be 100 ft by 100 ft in plan with twelve ft story heights. The building densities were assumed to be 9 pcf. The subsequent weights are listed in table 4.7. The weights shown in table 4.8 are merely the gravitational constant, which corresponds to a mass of one. The weight determined in each of the tables is also the force that is applied to the center of the beam for the purpose of introducing gravity induced P-Delta effects. Based on the weight and the period, which was determined using the NEHRP approximate method, the lateral stiffnesses were determined. Those stiffnesses were then converted to the rotational values used by the springs in the analysis.

Then, yield forces for the models were determined from the weight and the C_s values. For the comparative analyses, the response spectrum generated for the CEUS for structures categorized as "most" and site class D was used. The S_{DS} and S_{D1} values for the corresponding response spectrum were 0.267 and 0.128, respectively. Once the yield forces were determined, they also were converted to rotational values.

For all of the comparative models, the post-yield stiffness ratio was 5% of the initial stiffness. Also, the Chalfanta Valley and Taft earthquake records were increased

by a factor of 1.1. Finally, as with all of the models in the parameter study, the damping in the comparative models was 5% of critical.

The response histories of the three, five, seven, and nine story models are included in Appendix B. As the histories show, the nondimensional models produce the exact same results as the control set. Having proved this, the parameter study was conducted.

4.4 - Summary of Parameter Study Model Descriptions

All of the models used in the parameter study are SDOF bilinear models. Seven parameters were varied, four related to structural characteristics and three related to ground motions. Rational ranges for each of the parameters were determined. Table 4.9 summarizes the parameters.

Table 4.9 – Summary of Structural and Ground Motion Parameters

	Period (sec)	Yield Force (% of Wt)	Post-Yield Stiffness Ratio	Stability Ratio	Earthquakes	Lat. Scale (g)	Vertical Multiplier	Vertical Included?
	0.705	3	0	0.04	Aqaba, Egypt	0.1	1.5	Yes
	0.903	6	0.05	0.08	Cape Mendocino, CA	0.2	2	No
	1.093	9	0.1	0.12	Chalfant Valley, CA	0.3	2.5	
	1.278	12	0.15	0.16	Kern County (Taft)	0.4		
	1.459	16.5	0.2	0.2	Hollister, CA			
	1.635	22.5	0.25		Izmit, Turkey	*total number of vert.*		
	1.808	28.5			Kobe, Japan	*and hor. combinations*		
					Tabas, Iran	*used*		
Total:	7	7	6	5	8	6		2

The total number of ground motion and model combinations used in the analyses was 7 x 7 x 6 x 5 x 8 x 6 x 2 = 141,120. A discussion of the results and conclusions of the parameter study is included in chapter five.

5.0 Parameter Results and Discussion

5.1 – Introduction

The results of the parameter study are presented and discussed in this chapter. Recall that there were essentially seven parameters that were varied in this study. Four parameters were related to structural characteristics and three were related to ground motion characteristics. Due to the enormity of the data collected during the parameter study, only a few of the tables and figures generated are presented in this chapter. Enough of the tables and figures are included to adequately reinforce the discussion. The majority of the figures from the parameter study are included in Appendix C (available electronically), however.

Moreover, since the parameter study data set was quite large, it made more sense, at least as far as conciseness was concerned, to consider only the maximum displacement from the response histories as opposed to the entire response history. While some response histories are included in this chapter to illustrate trends in maximum displacements, figures and tables in this chapter, for the most part, will only represent maximum displacement values.

Then, before going any further, it is important to comment about how collapse was determined for the parameter study. For the bilinear models used in this study, a large arbitrary displacement of 50 inches was chosen to identify collapse. This collapse displacement identifier is not meant to be a realistic estimate of the displacement that would cause collapse, but rather an identifier alerting the sorting algorithm in the spreadsheets that a structure experiencing displacements greater than 50 inches had definitely collapsed. As will be shown, this approach to identify collapse is reasonable because the transition from stable response to collapse happens very quickly and in most cases is almost asymptotic.

This chapter is basically organized into three major sections. The first section examines the effects of the structural parameters on collapse, the second section examines the effects of structural parameters on residual displacements, and the third section encompasses ground motion parameters. The final section describes the effects

of varying both the lateral and vertical ground motion scales. It also describes the effects of including or not including vertical accelerations in an analysis.

5.2 - Effects of Structural Parameter Variation on Collapse

5.2.1 - Effects of Individual Structural Parameter Variation on Collapse

One of the first tasks of the parameter study was to examine the individual effects of the four structural parameters on collapse. Recall that the four structural parameters varied in this study were the stiffness (period), yield force (yield moment), post-yield stiffness ratio, and stability ratio. For each of the earthquakes, every possible combination of the aforementioned parameters was incorporated in an analytical model. Tables 5.1a through 5.1g present the maximum displacements resulting from structural parameter variation and the application of the Chalfant Valley (EQ 3) with a lateral ground motion scale of 0.4 g and a vertical multiplier of 2.5.

Table 5.1a – Maximum Displacements of Models Subjected to Earthquake Three (Chalfant Valley, CA) Scaled to 0.4g PGA for My = 834 k*in (Fy = 0.03*W)

1	2	3	4	5	6	7	8	9	10	11
My	post-yield	stability		Periods (sec)						
(k * in)	stiff ratio	ratio	rp	0.7051	0.9028	1.0933	1.2782	1.4586	1.6351	1.8083
834	0	0.04	-0.042	C	C	C	C	7.853	4.970	5.725
834	0	0.08	-0.087	C	C	C	C	C	C	C
834	0	0.12	-0.136	C	C	C	C	C	C	C
834	0	0.16	-0.190	C	C	C	C	C	C	C
834	0	0.2	-0.250	C	C	C	C	C	C	C
834	0.05	0.04	0.010	2.236	2.655	3.005	3.489	4.138	4.676	4.364
834	0.05	0.08	-0.033	C	C	C	9.263	11.982	5.192	5.526
834	0.05	0.12	-0.080	C	C	C	C	C	C	C
834	0.05	0.16	-0.131	C	C	C	C	C	C	C
834	0.05	0.2	-0.188	C	C	C	C	C	C	C
834	0.1	0.04	0.063	2.413	2.565	2.674	3.144	3.902	4.251	4.044
834	0.1	0.08	0.022	2.313	2.524	2.810	3.038	4.356	4.636	4.096
834	0.1	0.12	-0.023	C	C	7.491	11.612	11.639	5.839	5.289
834	0.1	0.16	-0.071	C	C	C	C	C	C	C
834	0.1	0.2	-0.125	C	C	C	C	C	C	C
834	0.15	0.04	0.115	2.606	2.596	2.750	3.014	3.472	3.844	3.650
834	0.15	0.08	0.076	2.471	2.597	2.707	3.222	3.827	4.062	3.841
834	0.15	0.12	0.034	2.385	2.555	2.622	3.186	4.303	4.430	4.051
834	0.15	0.16	-0.012	7.453	3.252	3.068	8.016	9.112	4.814	5.011
834	0.15	0.2	-0.063	C	C	C	C	C	C	C
834	0.2	0.04	0.167	2.981	2.697	2.779	2.924	3.215	3.335	3.498
834	0.2	0.08	0.130	2.690	2.635	2.787	2.985	3.334	3.609	3.660
834	0.2	0.12	0.091	2.532	2.634	2.746	3.184	3.677	3.823	3.845
834	0.2	0.16	0.048	2.449	2.590	2.569	3.369	4.016	4.150	4.033
834	0.2	0.2	0.000	2.926	2.817	3.286	5.131	5.485	4.368	4.696
834	0.25	0.04	0.219	3.435	2.895	2.815	2.962	3.112	3.190	3.369
834	0.25	0.08	0.185	3.080	2.746	2.817	2.961	3.140	3.171	3.504
834	0.25	0.12	0.148	2.778	2.679	2.826	2.949	3.185	3.377	3.665
834	0.25	0.16	0.107	2.596	2.676	2.789	3.107	3.465	3.565	3.837
834	0.25	0.2	0.063	2.510	2.634	2.756	3.387	3.897	3.800	3.993

Table 5.1b – Maximum Displacements of Models Subjected to Earthquake Three (Chalfant Valley, CA) Scaled to 0.4g PGA for My = 1668 k*in (Fy = 0.06*W)

1	2	3	4	5	6	7	8	9	10	11
My	post-yield	stability		Periods (sec)						
(k * in)	stiff ratio	ratio	rp	50.0000	50.0000	50.0000	50.0000	50.0000	50.0000	4.0120
1668	0	0.04	-0.042	C	C	C	C	15.962	4.077	4.399
1668	0	0.08	-0.087	C	C	C	C	C	9.808	3.934
1668	0	0.12	-0.136	C	C	C	C	C	C	4.012
1668	0	0.16	-0.190	C	C	C	C	C	C	C
1668	0	0.2	-0.250	C	C	C	C	C	C	C
1668	0.05	0.04	0.010	4.012	2.549	3.139	3.886	4.196	3.528	4.319
1668	0.05	0.08	-0.033	C	C	C	15.866	10.647	3.898	4.260
1668	0.05	0.12	-0.080	C	C	C	C	C	4.505	3.848
1668	0.05	0.16	-0.131	C	C	C	C	C	C	4.068
1668	0.05	0.2	-0.188	C	C	C	C	C	C	8.765
1668	0.1	0.04	0.063	2.455	2.308	2.718	3.193	3.703	3.443	3.791
1668	0.1	0.08	0.022	3.401	2.523	3.076	3.602	3.849	3.471	4.054
1668	0.1	0.12	-0.023	7.337	8.869	8.417	7.547	6.459	3.807	3.994
1668	0.1	0.16	-0.071	C	C	C	C	C	4.329	3.811
1668	0.1	0.2	-0.125	C	C	C	C	C	C	3.999
1668	0.15	0.04	0.115	2.538	2.292	2.603	3.052	3.534	3.399	3.746
1668	0.15	0.08	0.076	2.307	2.313	2.719	3.176	3.632	3.416	3.978
1668	0.15	0.12	0.034	2.886	2.504	2.969	3.342	3.723	3.462	3.988
1668	0.15	0.16	-0.012	4.743	3.691	4.061	4.407	4.476	3.893	3.733
1668	0.15	0.2	-0.063	C	C	C	C	15.272	4.287	3.858
1668	0.2	0.04	0.167	2.906	2.471	2.585	2.958	3.401	3.363	3.949
1668	0.2	0.08	0.130	2.580	2.345	2.631	3.056	3.483	3.372	4.101
1668	0.2	0.12	0.091	2.180	2.348	2.727	3.164	3.559	3.404	4.171
1668	0.2	0.16	0.048	2.505	2.493	2.853	3.273	3.632	3.641	3.900
1668	0.2	0.2	0.000	3.282	2.745	3.721	4.045	4.093	4.030	3.800
1668	0.25	0.04	0.219	3.332	2.769	2.649	2.909	3.299	3.338	4.068
1668	0.25	0.08	0.185	2.947	2.549	2.628	2.977	3.366	3.338	4.293
1668	0.25	0.12	0.148	2.613	2.410	2.663	3.062	3.430	3.408	4.348
1668	0.25	0.16	0.107	2.239	2.389	2.742	3.156	3.489	3.570	4.114
1668	0.25	0.2	0.063	2.244	2.494	2.841	3.251	3.552	3.974	3.730

Table 5.1c – Maximum Displacements of Models Subjected to Earthquake Three (Chalfant Valley, CA) Scaled to 0.4g PGA for My = 2502 k*in (Fy = 0.09*W)

1	2	3	4	5	6	7	8	9	10	11
My	post-yield	stability		Periods (sec)						
(k * in)	stiff ratio	ratio	rp	3.4163	2.8502	2.9853	3.9282	3.8955	4.7222	4.0500
2502	0	0.04	-0.042	C	3.016	13.597	12.830	7.508	5.296	4.335
2502	0	0.08	-0.087	C	C	C	C	12.167	5.545	4.976
2502	0	0.12	-0.136	C	C	C	C	C	5.553	5.147
2502	0	0.16	-0.190	C	C	C	C	C	5.477	5.320
2502	0	0.2	-0.250	C	C	C	C	C	4.852	5.366
2502	0.05	0.04	0.010	3.416	2.850	2.985	3.928	3.896	4.722	4.050
2502	0.05	0.08	-0.033	C	2.963	10.741	9.191	6.664	4.459	4.883
2502	0.05	0.12	-0.080	C	C	C	C	11.684	4.424	5.024
2502	0.05	0.16	-0.131	C	C	C	C	C	3.823	5.235
2502	0.05	0.2	-0.188	C	C	C	C	C	3.707	5.331
2502	0.1	0.04	0.063	2.444	2.519	2.742	3.313	3.502	4.518	3.851
2502	0.1	0.08	0.022	2.966	2.578	3.051	3.762	4.162	4.261	4.662
2502	0.1	0.12	-0.023	8.017	2.905	8.147	6.201	6.113	3.811	4.925
2502	0.1	0.16	-0.071	C	C	C	C	10.978	3.602	5.220
2502	0.1	0.2	-0.125	C	C	C	C	C	3.649	5.308
2502	0.15	0.04	0.115	2.865	2.458	2.665	3.198	3.478	4.336	3.875
2502	0.15	0.08	0.076	2.454	2.517	2.801	3.355	3.629	4.088	4.458
2502	0.15	0.12	0.034	2.679	2.565	3.106	3.570	4.457	3.657	4.920
2502	0.15	0.16	-0.012	5.456	2.844	4.988	5.258	5.187	3.596	5.204
2502	0.15	0.2	-0.063	C	C	C	20.678	8.067	3.593	5.286
2502	0.2	0.04	0.167	3.154	2.713	2.642	3.128	3.462	4.118	3.901
2502	0.2	0.08	0.130	2.878	2.460	2.682	3.238	3.460	3.937	4.468
2502	0.2	0.12	0.091	2.496	2.511	2.853	3.383	3.960	3.643	4.915
2502	0.2	0.16	0.048	2.507	2.544	3.126	3.551	4.197	3.589	5.188
2502	0.2	0.2	0.000	4.435	2.785	4.253	4.517	4.324	3.626	5.257
2502	0.25	0.04	0.219	3.344	2.962	2.698	3.097	3.455	3.936	3.930
2502	0.25	0.08	0.185	3.170	2.721	2.670	3.165	3.452	3.783	4.476
2502	0.25	0.12	0.148	2.902	2.460	2.730	3.267	3.621	3.639	4.908
2502	0.25	0.16	0.107	2.538	2.498	2.884	3.395	3.724	3.583	5.172
2502	0.25	0.2	0.063	2.515	2.514	3.115	3.537	3.649	3.469	5.177

Table 5.1d – Maximum Displacements of Models Subjected to Earthquake Three (Chalfant Valley, CA) Scaled to 0.4g PGA for My = 3336 k*in (Fy = 0.12*W)

1	2	3	4	5	6	7	8	9	10	11
My	post-yield	stability		Periods (sec)						
(k * in)	stiff ratio	ratio	rp	50.0000	50.0000	50.0000	50.0000	7.7995	4.0623	5.1145
3336	0	0.04	-0.042	C	13.948	2.607	5.586	5.709	4.044	4.238
3336	0	0.08	-0.087	C	C	12.861	13.683	7.972	4.229	4.618
3336	0	0.12	-0.136	C	C	C	C	8.661	4.829	4.928
3336	0	0.16	-0.190	C	C	C	C	10.477	4.409	5.125
3336	0	0.2	-0.250	C	C	C	C	C	4.034	5.131
3336	0.05	0.04	0.010	3.841	3.898	2.775	3.727	4.170	4.002	4.237
3336	0.05	0.08	-0.033	C	7.600	4.429	4.922	5.678	4.189	4.566
3336	0.05	0.12	-0.080	C	C	C	11.948	7.000	4.438	4.918
3336	0.05	0.16	-0.131	C	C	C	C	7.800	4.062	5.115
3336	0.05	0.2	-0.188	C	C	C	C	9.326	3.906	5.123
3336	0.1	0.04	0.063	3.094	2.844	2.724	3.390	3.779	3.961	4.237
3336	0.1	0.08	0.022	3.333	3.258	3.030	3.669	4.201	4.149	4.561
3336	0.1	0.12	-0.023	8.679	4.524	5.289	4.680	4.912	4.396	4.908
3336	0.1	0.16	-0.071	C	3.620	C	10.578	6.290	3.990	5.104
3336	0.1	0.2	-0.125	C	C	C	C	7.228	3.788	5.115
3336	0.15	0.04	0.115	3.278	3.038	2.850	3.222	3.797	3.921	4.236
3336	0.15	0.08	0.076	3.016	2.774	2.616	3.289	3.926	4.111	4.557
3336	0.15	0.12	0.034	2.969	2.925	3.248	3.563	4.442	4.359	4.898
3336	0.15	0.16	-0.012	5.998	3.196	4.959	4.272	4.753	3.948	5.094
3336	0.15	0.2	-0.063	C	4.535	17.793	8.995	5.658	3.709	5.107
3336	0.2	0.04	0.167	3.390	3.205	2.968	3.257	3.814	3.881	4.235
3336	0.2	0.08	0.130	3.238	2.981	2.750	3.290	3.848	4.075	4.552
3336	0.2	0.12	0.091	2.944	2.700	2.742	3.342	4.211	4.323	4.888
3336	0.2	0.16	0.048	2.679	2.679	3.018	3.414	4.592	3.913	5.084
3336	0.2	0.2	0.000	4.354	2.621	3.829	3.861	4.797	3.679	5.099
3336	0.25	0.04	0.219	3.446	3.347	3.078	3.305	3.831	3.842	4.234
3336	0.25	0.08	0.185	3.381	3.159	2.875	3.314	3.856	4.039	4.548
3336	0.25	0.12	0.148	3.199	2.922	2.745	3.343	3.995	4.288	4.878
3336	0.25	0.16	0.107	2.883	2.625	2.866	3.385	4.402	3.885	5.074
3336	0.25	0.2	0.063	2.441	2.512	3.083	3.427	4.659	3.698	5.092

Table 5.1e – Maximum Displacements of Models Subjected to Earthquake Three (Chalfant Valley, CA) Scaled to 0.4g PGA for My = 4587 k*in (Fy = 0.165*W)

1	2	3	4	5	6	7	8	9	10	11
My	post-yield	stability		Periods (sec)						
(k * in)	stiff ratio	ratio	rp	4.1460	4.3187	3.5117	3.8168	4.5399	4.3655	4.5729
4587	0	0.04	-0.042	11.070	15.590	4.955	4.247	4.854	4.237	4.637
4587	0	0.08	-0.087	C	C	6.078	4.410	5.235	4.366	4.573
4587	0	0.12	-0.136	C	C	C	7.500	4.750	4.380	4.755
4587	0	0.16	-0.190	C	C	C	10.073	4.460	4.514	4.945
4587	0	0.2	-0.250	C	C	C	C	4.009	4.481	4.991
4587	0.05	0.04	0.010	4.463	5.182	3.782	3.836	4.767	4.237	4.637
4587	0.05	0.08	-0.033	9.459	11.115	4.046	3.855	4.827	4.366	4.573
4587	0.05	0.12	-0.080	C	C	4.220	3.958	4.658	4.385	4.755
4587	0.05	0.16	-0.131	C	C	4.471	8.830	4.391	4.513	4.945
4587	0.05	0.2	-0.188	C	C	7.852	10.027	3.963	4.481	4.991
4587	0.1	0.04	0.063	3.466	3.852	3.688	3.809	4.540	4.237	4.637
4587	0.1	0.08	0.022	4.146	4.319	3.512	3.817	4.540	4.366	4.573
4587	0.1	0.12	-0.023	7.439	7.557	3.318	3.852	4.405	4.390	4.755
4587	0.1	0.16	-0.071	C	C	3.108	4.726	4.207	4.513	4.945
4587	0.1	0.2	-0.125	C	C	6.637	9.000	3.833	4.481	4.991
4587	0.15	0.04	0.115	3.400	3.884	3.716	3.665	4.409	4.237	4.637
4587	0.15	0.08	0.076	3.580	3.733	3.549	3.717	4.315	4.366	4.573
4587	0.15	0.12	0.034	3.633	3.762	3.366	3.766	4.206	4.395	4.755
4587	0.15	0.16	-0.012	5.711	5.264	3.165	4.143	4.034	4.513	4.945
4587	0.15	0.2	-0.063	C	18.465	4.909	6.009	3.785	4.480	4.991
4587	0.2	0.04	0.167	3.335	3.911	3.742	3.670	4.324	4.237	4.637
4587	0.2	0.08	0.130	3.518	3.780	3.585	3.666	4.217	4.366	4.573
4587	0.2	0.12	0.091	3.604	3.610	3.410	3.734	4.072	4.400	4.755
4587	0.2	0.16	0.048	3.410	3.392	3.220	3.748	3.942	4.513	4.945
4587	0.2	0.2	0.000	4.634	4.101	3.431	4.744	3.763	4.480	4.991
4587	0.25	0.04	0.219	3.269	3.936	3.767	3.765	4.246	4.237	4.637
4587	0.25	0.08	0.185	3.456	3.821	3.618	3.747	4.154	4.365	4.573
4587	0.25	0.12	0.148	3.624	3.673	3.453	3.757	4.026	4.405	4.755
4587	0.25	0.16	0.107	3.517	3.482	3.272	3.793	3.909	4.512	4.945
4587	0.25	0.2	0.063	3.263	3.242	3.302	4.091	3.757	4.480	4.991

Table 5.1f – Maximum Displacements of Models Subjected to Earthquake Three (Chalfant Valley, CA) Scaled to 0.4g PGA for My = 6255 k*in (Fy = 0.225*W)

1	2	3	4	5	6	7	8	9	10	11
My	post-yield	stability					Periods (sec)			
(k * in)	stiff ratio	ratio	rp	50.0000	50.0000	4.8411	4.2348	4.0067	4.4782	4.9906
6255	0	0.04	-0.042	4.221	11.748	5.474	5.234	4.426	4.237	4.637
6255	0	0.08	-0.087	C	C	6.430	6.030	4.244	4.365	4.573
6255	0	0.12	-0.136	C	C	8.471	6.477	4.226	4.480	4.755
6255	0	0.16	-0.190	C	C	C	6.423	4.103	4.509	4.945
6255	0	0.2	-0.250	C	C	C	5.724	4.007	4.478	4.991
6255	0.05	0.04	0.010	3.406	6.522	4.427	4.876	4.426	4.237	4.637
6255	0.05	0.08	-0.033	4.565	10.944	4.781	5.127	4.244	4.365	4.573
6255	0.05	0.12	-0.080	C	C	5.269	5.084	4.226	4.480	4.755
6255	0.05	0.16	-0.131	C	C	6.493	5.309	4.103	4.509	4.945
6255	0.05	0.2	-0.188	C	C	13.130	4.329	4.007	4.478	4.991
6255	0.1	0.04	0.063	3.285	4.616	4.220	4.868	4.426	4.237	4.637
6255	0.1	0.08	0.022	3.741	5.611	4.153	4.703	4.244	4.365	4.573
6255	0.1	0.12	-0.023	4.908	8.824	4.081	4.723	4.226	4.480	4.755
6255	0.1	0.16	-0.071	C	18.047	4.283	4.670	4.103	4.509	4.945
6255	0.1	0.2	-0.125	C	C	4.841	4.235	4.007	4.478	4.991
6255	0.15	0.04	0.115	3.209	4.563	4.206	4.860	4.426	4.237	4.637
6255	0.15	0.08	0.076	3.440	4.544	4.140	4.697	4.244	4.365	4.573
6255	0.15	0.12	0.034	3.996	4.718	4.059	4.529	4.226	4.480	4.755
6255	0.15	0.16	-0.012	5.216	6.933	3.961	4.363	4.103	4.509	4.945
6255	0.15	0.2	-0.063	C	14.749	3.843	4.207	4.007	4.478	4.991
6255	0.2	0.04	0.167	3.140	4.514	4.193	4.852	4.426	4.237	4.637
6255	0.2	0.08	0.130	3.363	4.500	4.127	4.690	4.244	4.365	4.573
6255	0.2	0.12	0.091	3.590	4.416	4.046	4.524	4.226	4.480	4.755
6255	0.2	0.16	0.048	4.010	4.296	3.949	4.359	4.103	4.509	4.945
6255	0.2	0.2	0.000	5.337	5.319	3.833	4.311	4.007	4.478	4.991
6255	0.25	0.04	0.219	3.076	4.467	4.180	4.845	4.426	4.237	4.637
6255	0.25	0.08	0.185	3.292	4.458	4.114	4.684	4.244	4.365	4.573
6255	0.25	0.12	0.148	3.512	4.384	4.034	4.519	4.226	4.480	4.755
6255	0.25	0.16	0.107	3.733	4.275	3.938	4.373	4.103	4.509	4.945
6255	0.25	0.2	0.063	3.942	4.129	3.824	4.408	4.007	4.478	4.991

Table 5.1g – Maximum Displacements of Models Subjected to Earthquake Three (Chalfant Valley, CA) Scaled to 0.4g PGA for My = 7923 k*in (Fy = 0.285*W)

1	2	3	4	5	6	7	8	9	10	11
My	post-yield	stability					Periods (sec)			
(k * in)	stiff ratio	ratio	rp	3.5312	5.3666	4.3925	4.5984	4.2258	4.4796	4.7551
7923	0	0.04	-0.042	3.119	7.796	4.599	4.783	4.426	4.237	4.637
7923	0	0.08	-0.087	3.947	12.028	4.190	4.780	4.244	4.365	4.573
7923	0	0.12	-0.136	C	C	4.379	4.598	4.226	4.480	4.755
7923	0	0.16	-0.190	C	C	4.793	4.568	4.103	4.509	4.945
7923	0	0.2	-0.250	C	C	7.222	4.580	4.007	4.478	4.991
7923	0.05	0.04	0.010	3.063	5.994	4.401	4.802	4.426	4.237	4.637
7923	0.05	0.08	-0.033	3.364	8.696	4.232	4.785	4.244	4.365	4.573
7923	0.05	0.12	-0.080	4.965	12.696	4.387	4.598	4.226	4.480	4.755
7923	0.05	0.16	-0.131	C	C	4.726	4.568	4.103	4.509	4.945
7923	0.05	0.2	-0.188	C	C	5.433	4.580	4.007	4.478	4.991
7923	0.1	0.04	0.063	3.011	4.829	4.318	4.821	4.426	4.237	4.637
7923	0.1	0.08	0.022	3.295	6.218	4.314	4.790	4.244	4.365	4.573
7923	0.1	0.12	-0.023	3.718	7.903	4.344	4.598	4.226	4.480	4.755
7923	0.1	0.16	-0.071	5.586	12.636	4.641	4.568	4.103	4.509	4.945
7923	0.1	0.2	-0.125	C	C	5.009	4.580	4.007	4.478	4.991
7923	0.15	0.04	0.115	2.964	4.521	4.402	4.840	4.426	4.237	4.637
7923	0.15	0.08	0.076	3.232	4.941	4.394	4.794	4.244	4.365	4.573
7923	0.15	0.12	0.034	3.531	5.367	4.393	4.598	4.226	4.480	4.755
7923	0.15	0.16	-0.012	4.248	6.809	4.546	4.568	4.103	4.509	4.945
7923	0.15	0.2	-0.063	6.612	11.840	4.826	4.580	4.007	4.478	4.991
7923	0.2	0.04	0.167	2.921	4.325	4.483	4.859	4.426	4.237	4.637
7923	0.2	0.08	0.130	3.174	4.395	4.470	4.799	4.244	4.365	4.573
7923	0.2	0.12	0.091	3.456	4.500	4.462	4.598	4.226	4.480	4.755
7923	0.2	0.16	0.048	3.766	4.692	4.466	4.568	4.103	4.509	4.945
7923	0.2	0.2	0.000	4.694	5.817	4.653	4.580	4.007	4.478	4.991
7923	0.25	0.04	0.219	2.881	4.240	4.561	4.878	4.426	4.237	4.637
7923	0.25	0.08	0.185	3.121	4.299	4.544	4.803	4.244	4.365	4.573
7923	0.25	0.12	0.148	3.388	4.346	4.529	4.598	4.226	4.480	4.755
7923	0.25	0.16	0.107	3.679	4.378	4.523	4.568	4.103	4.509	4.945
7923	0.25	0.2	0.063	3.987	4.435	4.535	4.580	4.007	4.478	4.991

In the seven tables above, the first three columns show the combinations of yield moment, post-yield stiffness ratio, and stability ratio used for each analysis. The fourth column is a calculated value, the post-yield stiffness ratio considering P-Delta effects (r_p). A derivation of the r_p value was presented in chapter 2, equation 2.10. Columns five through eleven are the maximum displacements from the response histories for each of the periods used in the study. When the displacement of a particular response history was greater than 50 inches, the letter "C" was placed in the corresponding cell, indicating that that the particular structure had collapsed

Since, only one model of each parameter combination exists, the only reasonable method to determine if any single parameter influenced collapse was to group all of the collapses that corresponded to a given period and parameter together and then compare. For example, the total number of collapses, or "C's" corresponding to a period of 0.7051 seconds and a stability ratio of 0.04 could be compared to the total number of collapses corresponding to a period of 0.7051 seconds and a stability ratio of 0.08. Furthermore, the total number of collapses using a period of 0.7051 and a stability ratio of 0.04 could be compared to the total number of collapses of the models with a period of 0.9028 and with stability ratios of 0.04. From Tables 5.1a to 5.1g, there are 42 maximum displacements that correspond with a period of 0.7051 seconds and stability ratio of 0.04, six per table. Of those 42 values, only 4 collapsed. All of the other parameters were processed similarly. While this method of processing the data did not provide detailed information about specific parameter combinations, it did provide general information on how the individual parameters affected collapse.

In the next several sections, the effects of each of the four structural parameters on collapse are discussed. Stability ratio, post-yield stiffness ratio, and yield strength will be addressed specifically, and period will be addressed in the context of the other three parameters. The results from several earthquakes are included in each of the discussions because consideration of multiple earthquakes made the results more independent of ground motion. However, the consideration of additional ground motions also meant that there were fewer conclusions that were always applicable.

5.2.1.1 – Stability Ratio

Recall that the stability ratio is a measure of P-Delta sensitivity. It is the ratio of geometric stiffness to lateral stiffness. Higher stability ratios are indicative of significant second order displacements. Limits are placed on the stability ratio in the NEHRP Provisions because second order displacements can be detrimental to structures. Also, no real structure would have a stability ratio of 0.0, because this would indicate that there was no gravity load on the given structure. As such, the range of stability ratios considered in the parameter study was between 0.04 and 0.2.

In the parameter study, for a given set of data, a given period, and stability ratio, there were 42 applicable values. When the total number of collapses caused by each of the stability ratio parameters was added together, the number of data points to be considered was condensed from 1470 to 35. For each of the seven periods, there were then five values that represented the effects of the stability ratio. Figures 5.1a through 5.1f show some of the plots created having the number of collapses categorized according to the stability ratio parameter and period. The periods of the models are shown in the legends of Figures 5.1a through 5.1f.

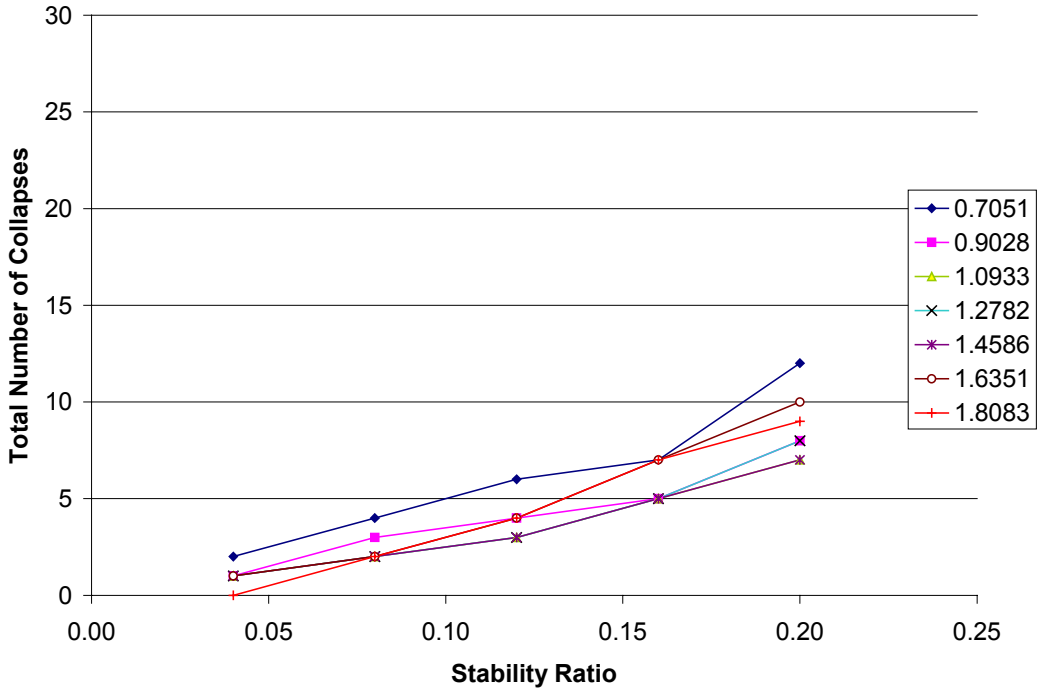

Figure 5.1a – EQ 1, Lateral Scale = 0.2 g, Number of Collapses Versus Stability Ratio, Grouped According to Period

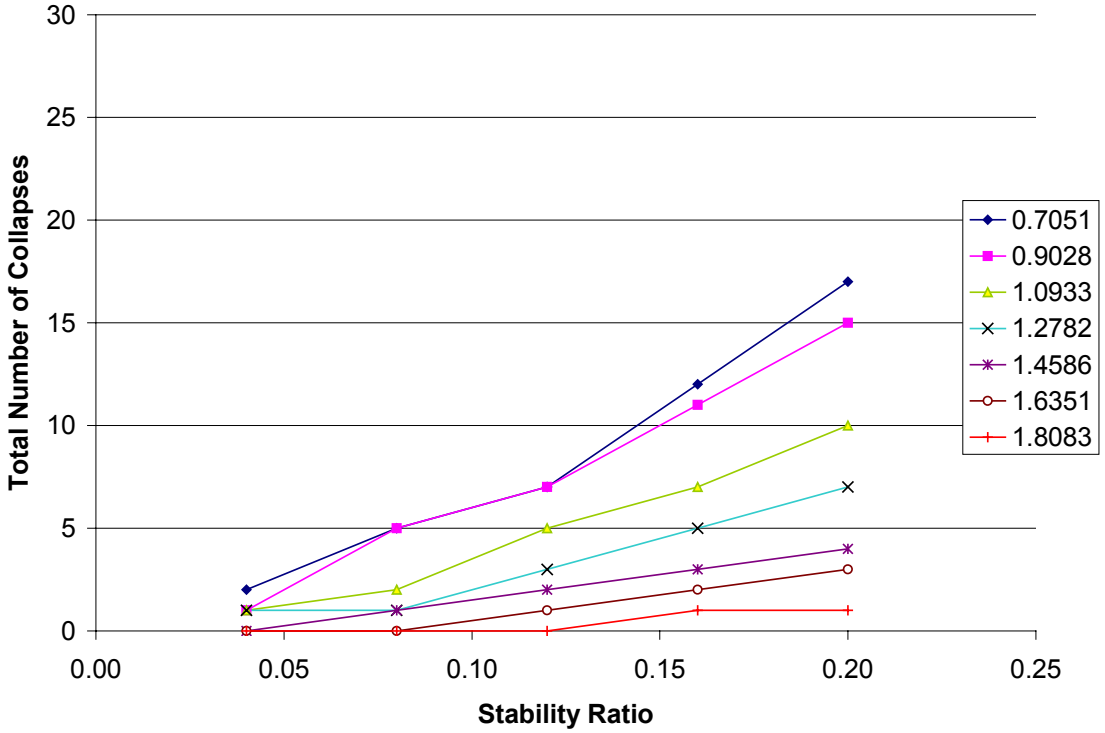

Figure 5.1b – EQ 3, Lateral Scale = 0.2 g, Number of Collapses Versus Stability Ratio, Grouped According to Period

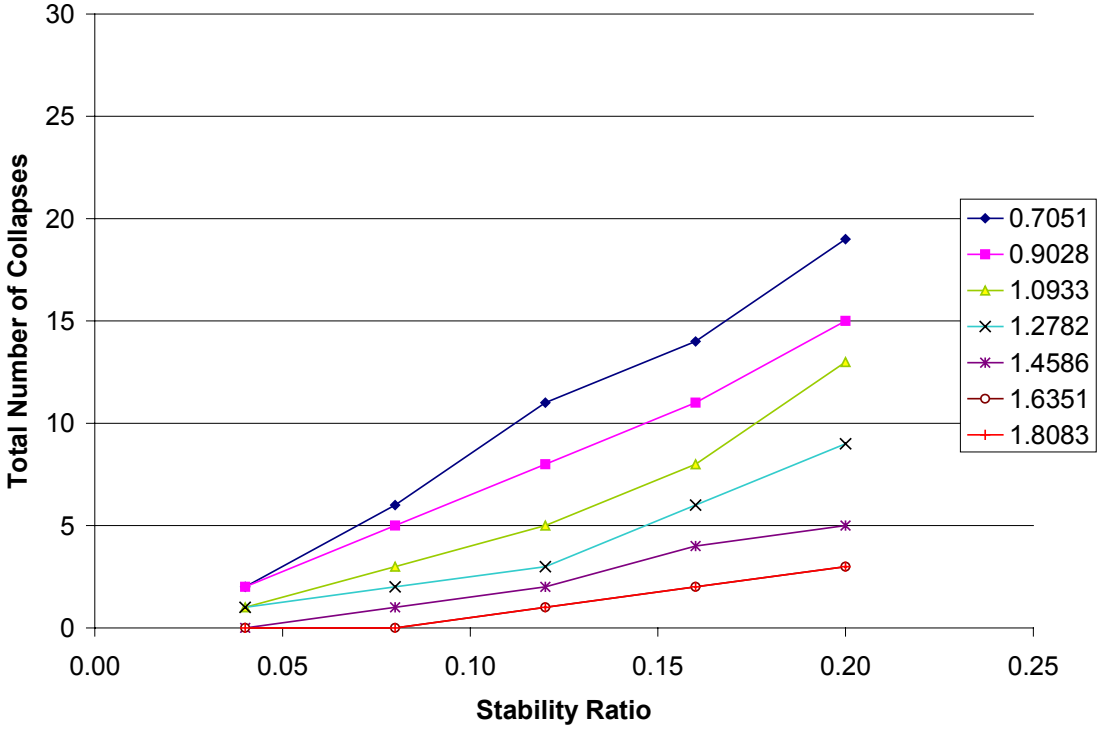

Figure 5.1c – EQ 4, Lateral Scale = 0.2 g, Number of Collapses Versus Stability Ratio, Grouped According to Period

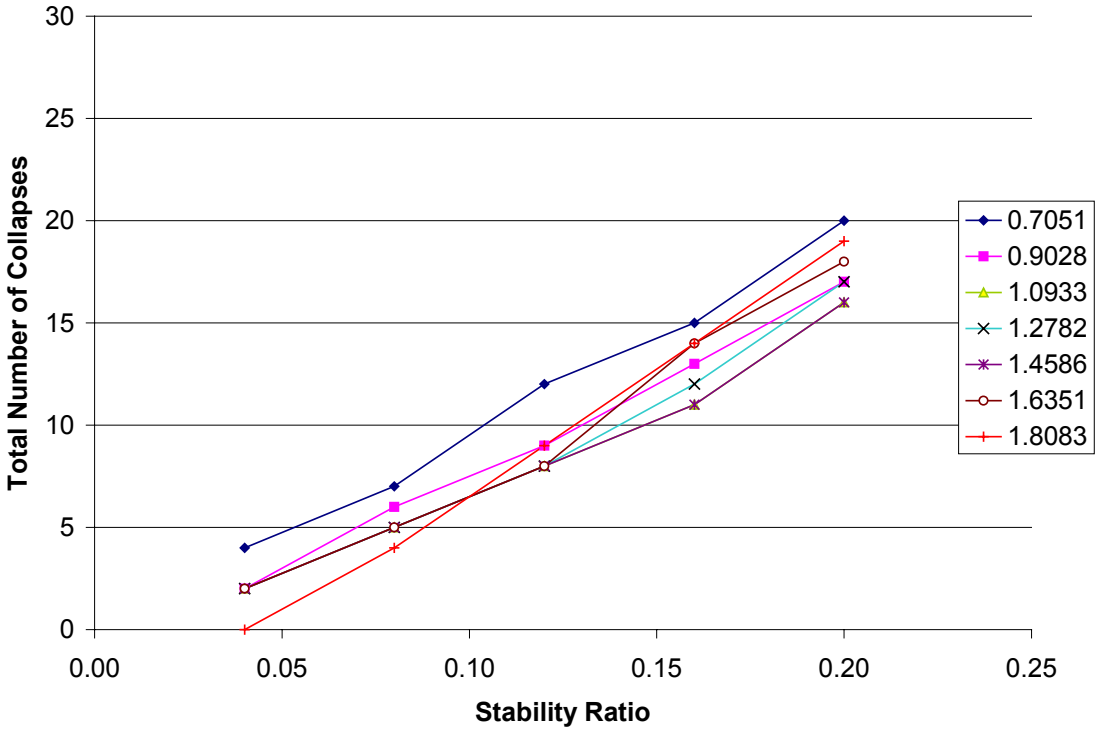

Figure 5.1d – EQ 1, Lateral Scale = 0.4 g, Number of Collapses Versus Stability Ratio, Grouped According to Period

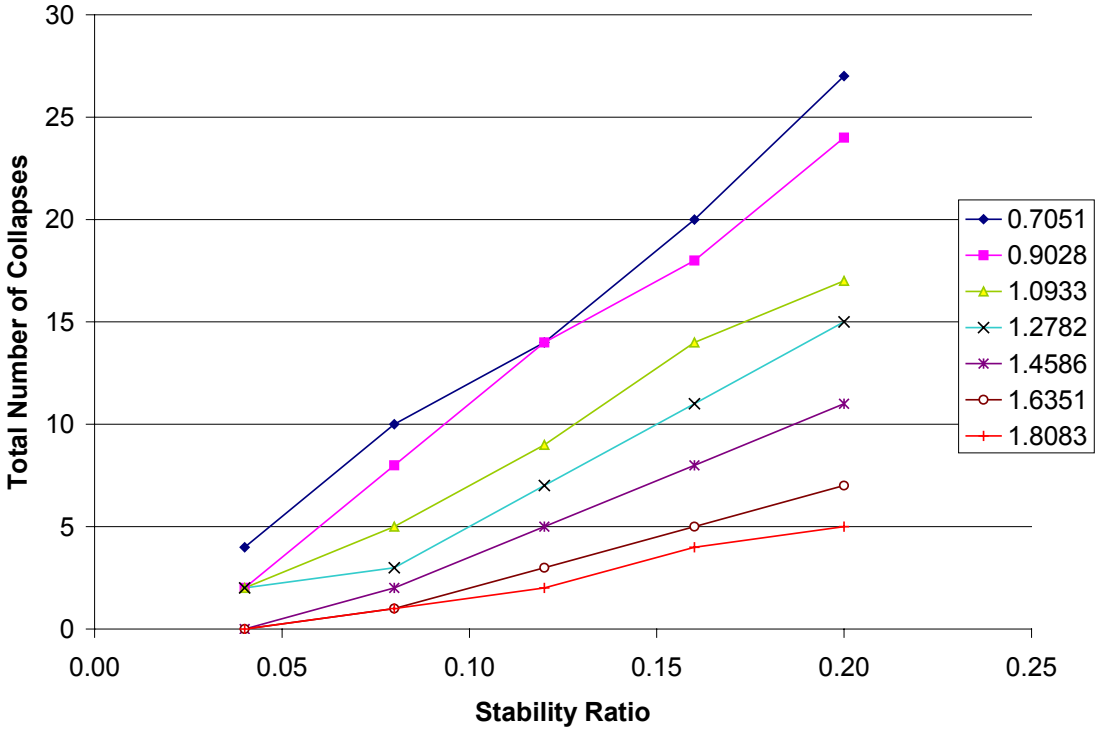

Figure 5.1e – EQ 3, Lateral Scale = 0.4 g, Number of Collapses Versus Stability Ratio, Grouped According to Period

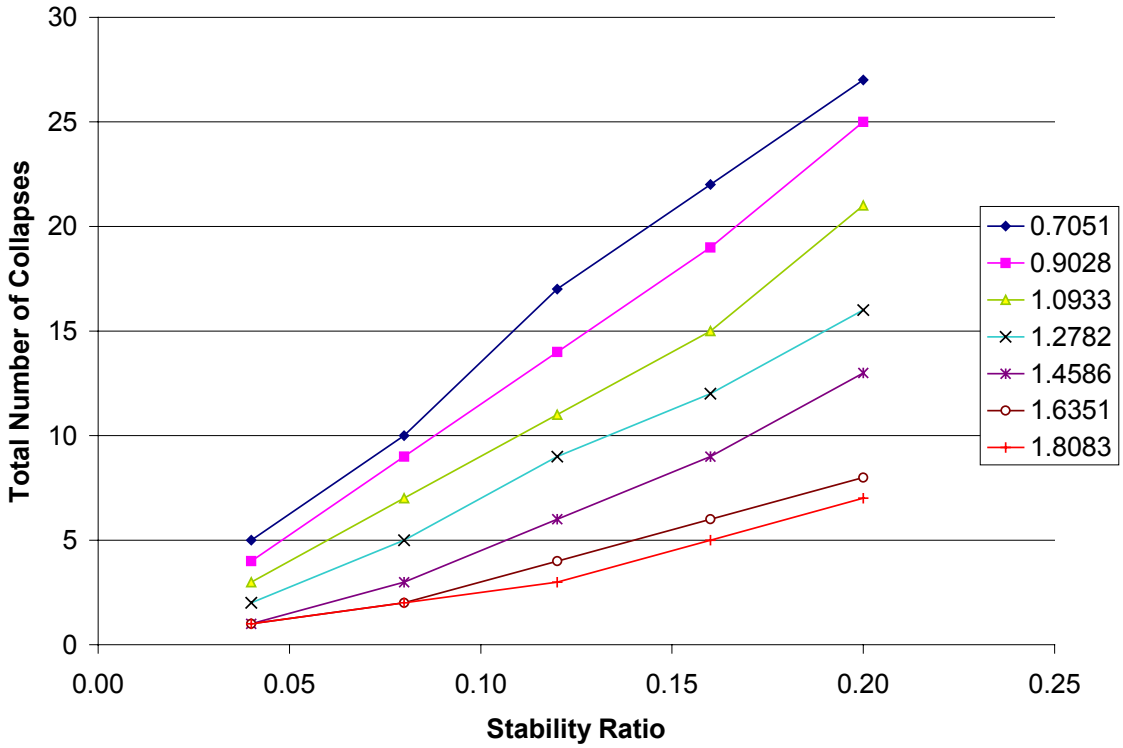

Figure 5.1f – EQ 4, Lateral Scale = 0.4 g, Number of Collapses Versus Stability Ratio, Grouped According to Period

From Figures 5.1a through 5.1f, it is clear that the number of collapses went up as the stability ratio increased. This was true for all of the models and earthquakes. The number of collapses was also related to the periods of the structures, but the influence of period on collapse is not as simple as that of the stability ratio. There are two characteristics of the periods that influenced the number of collapses in the parameter study. First, the period of vibration of a structure in conjunction with its yield strength determined the structure's yield displacement. Equation 5.1 shows this relationship:

$$\delta_y = \frac{F_y}{K} = \frac{C_s W}{\omega^2 m} = \frac{C_s g T^2}{4\pi^2} \qquad \textbf{(5.1)}$$

where,

C_s = Seismic Response Coefficient

g = gravitational constant

T = structure's period of vibration

For a given yield strength, increasing the period increased the yield displacement. Consequently, if two structures had the same yield strength and the same displacement demands, but one had a longer period, then the longer period structure would have lower ductility demands. It is assumed that structures with lower ductility demands are typically less likely to collapse than those with high ductility demands.

The second aspect of the structural period that influenced the number of collapses is the fact that the displacement demands are dependent on the period of a structure. Consider the elastic displacement spectra shown in Figures 5.2a through 5.2c, all of which have been created using five percent of critical damping.

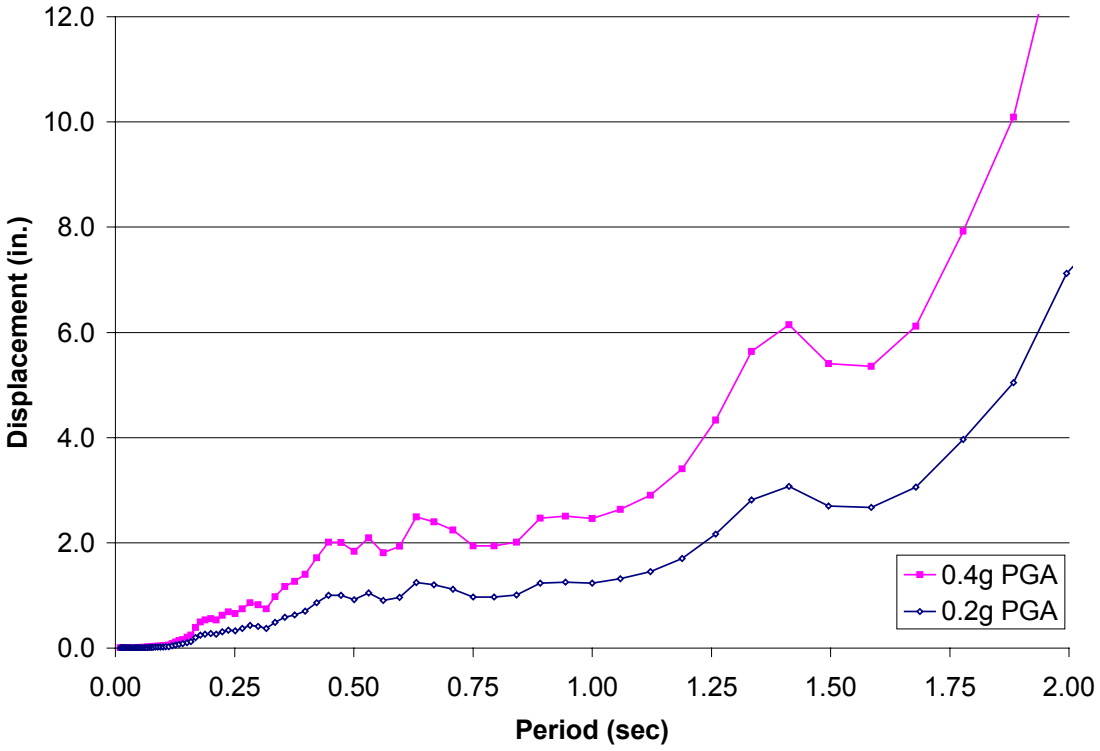

Figure 5.2a – Elastic Displacement Response Spectrum for the Aqaba Earthquake (EQ 1)

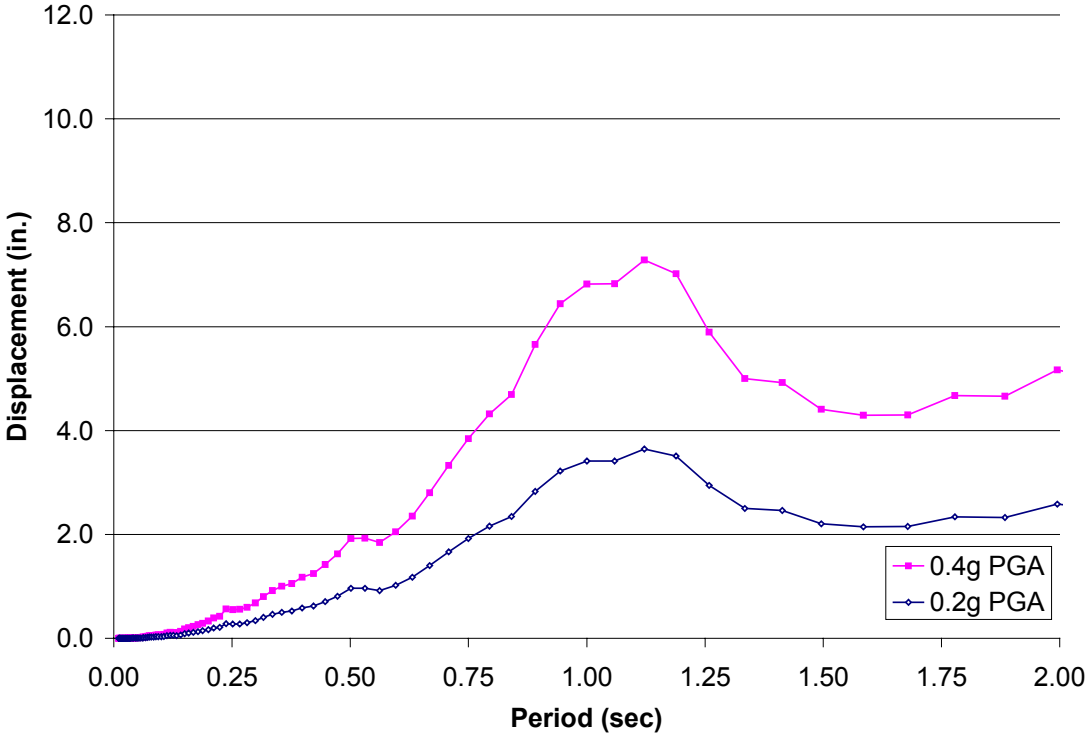

Figure 5.2b – Elastic Displacement Response Spectrum for the Chalfanta Valley Earthquake (EQ 3)

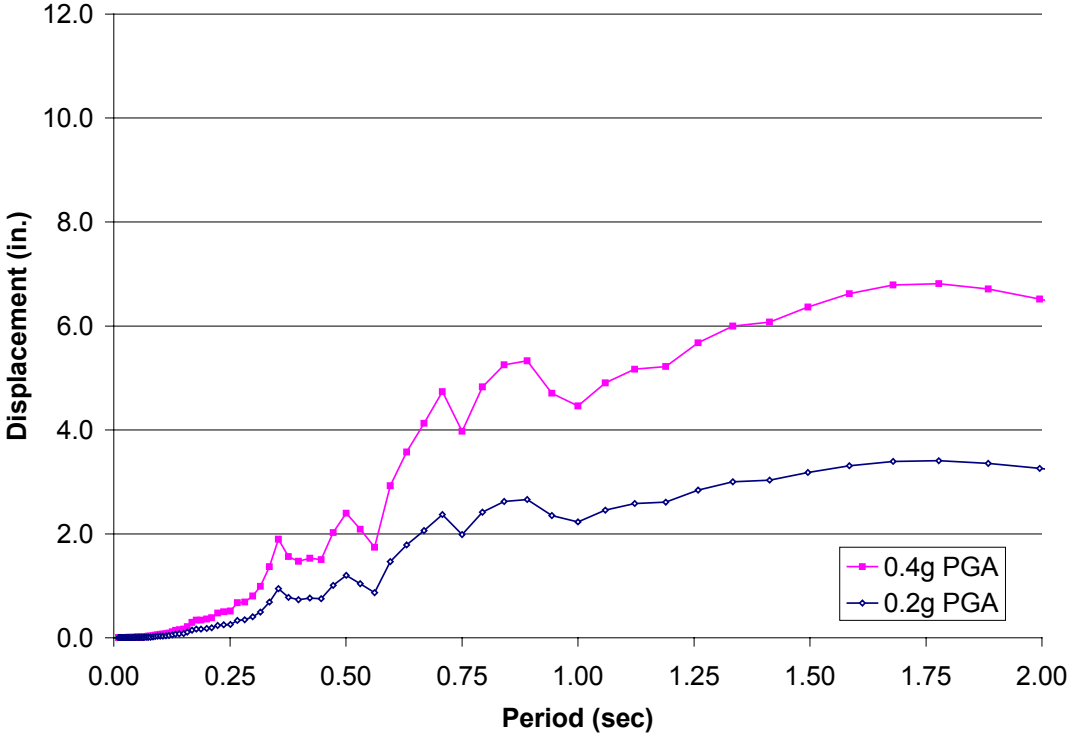

Figure 5.2c – Elastic Displacement Response Spectrum for the Taft Earthquake (EQ 4)

From Figures 5.2a through 5.2c, it is clear that the displacement demand is dependent on the period of the structure and the earthquake. In figure 5.2a, notice that the elastic displacement demands are much higher for longer period models subjected to EQ 1 than for the other two earthquakes. Also, notice in Figure 5.2b that the maximum possible displacement that a structure subjected to EQ 3 would sustain occurs in a structure with a period of about 1.0 seconds.

The period of vibration of a structure with a given yield strength influences both the yield displacement and the displacement demand. Knowing the displacement dependencies of the period makes the results of Figures 5.1a through 5.1f more understandable. Consider, for example, a series of models with a given yield strength and a range of periods. As the period increases, the yield displacement would increase as well. In order for an earthquake to cause the entire series of models to collapse, the displacement demands would have to increase at a similar rate as the yield displacements. Such a situation happened in Figures 5.1a and 5.1d. Notice that the number of collapses in Figures 5.1a and 5.1d is about the same for a given stability ratio regardless of period. This is because the displacement demands, shown in figure 5.2a, increased with the yield displacements.

In contrast, the elastic analysis displacement demands shown in Figures 5.2b and 5.2c do not continually increase with the period. Consider again a series of models with a given yield strength covering a range of periods. If this time the series of models is subjected to EQ 3 and EQ 4 as shown in Figures 5.2b and 5.2c, the displacement demands would essentially remain the same for a given period, but the yield displacements would go up. Consequently, the ductility demands would go down and, ideally, the number of collapses would go down. Such was the case in Figures 5.1b, 5.1c, 5.1e, and 5.1f. The number of collapses went down as the periods, and therefore yield displacements, went up.

Another important observation regarding Figures 5.1a through 5.1f is that the number of collapses roughly doubled as the ground motion scale doubled. This was true for all earthquakes and scales examined. Moreover, the elastic displacements exactly double as the earthquake intensity doubles, as shown in Figures 5.2a through 5.2c. The doubling elastic displacement demands, in conjunction with the doubling numbers of

collapses, show that as the ductility demands roughly double, the probability of collapse roughly doubles, too.

In conclusion, the stability ratio certainly influences collapse. It is, however, somewhat dependent on the ductility demands of the structure. For increasing ductility demands, higher stability ratios cause more collapses than if the ductility demands were lower.

5.2.1.2 – Post-yield Stiffness Ratio

The second structural parameter examined was the post-yield stiffness ratio. It is worth noting that the post-yield stiffness ratio addressed in this section is independent of P-Delta effects. The P-Delta effects are handled separately. Recall that the post-yield stiffness values ranged from 0.0 to 0.25. There were 35 displacement values that corresponded to a given post-yield stiffness ratio and structural period. As in the stability ratio section, the total numbers of collapses for each post-yield stiffness ratio and period combination were grouped together. The result was 42 grouped collapse values. Figures 5.3a through 5.3f show the effects of post-yield stiffness ratio on collapse.

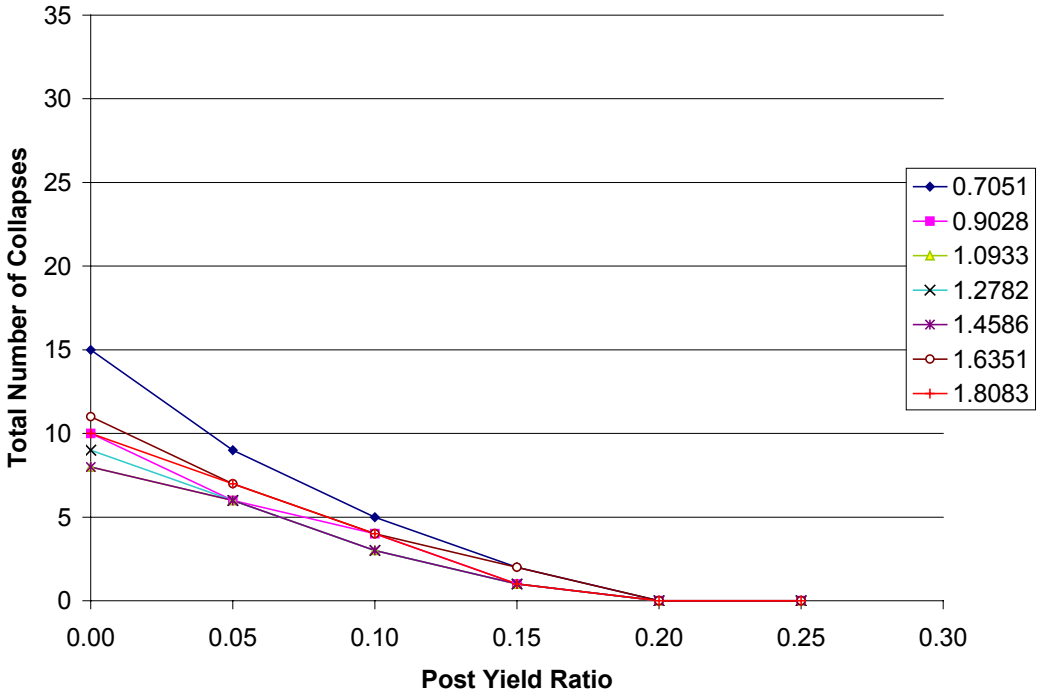

Figure 5.3a – EQ 1, Lateral Scale = 0.2 g, Number of Collapses Versus Post-yield Stiffness Ratio, Grouped According to Period

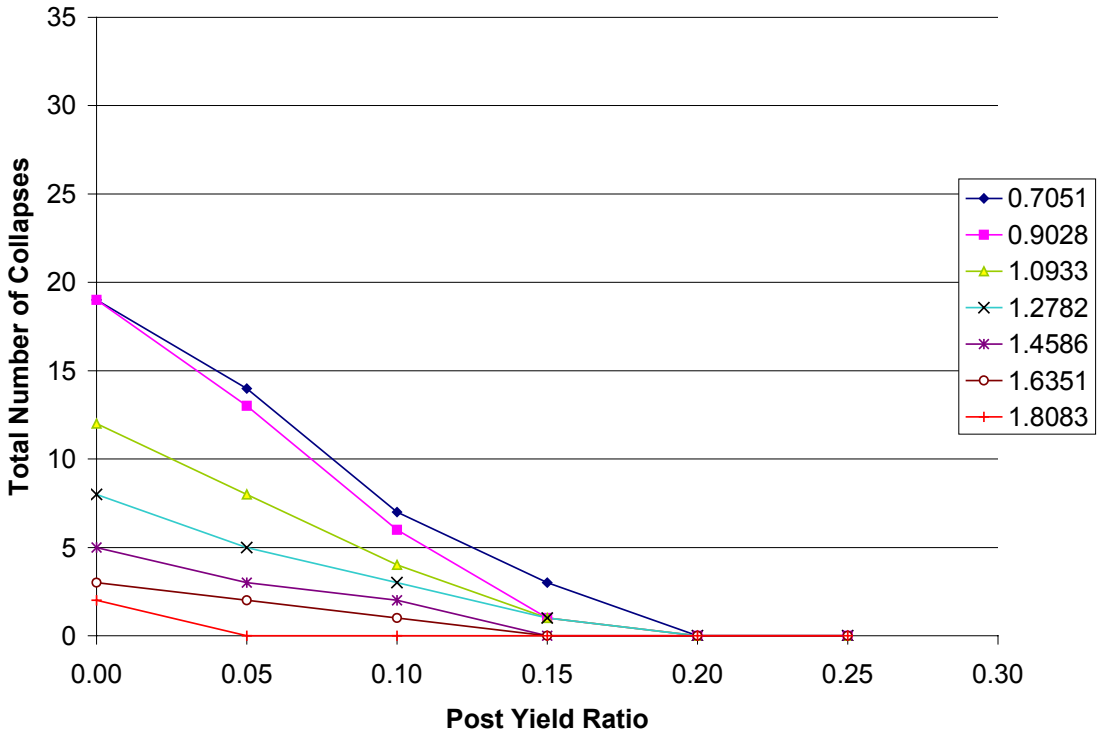

Figure 5.3b – EQ 3, Lateral Scale = 0.2 g, Number of Collapses Versus Post-yield Stiffness Ratio, Grouped According to Period

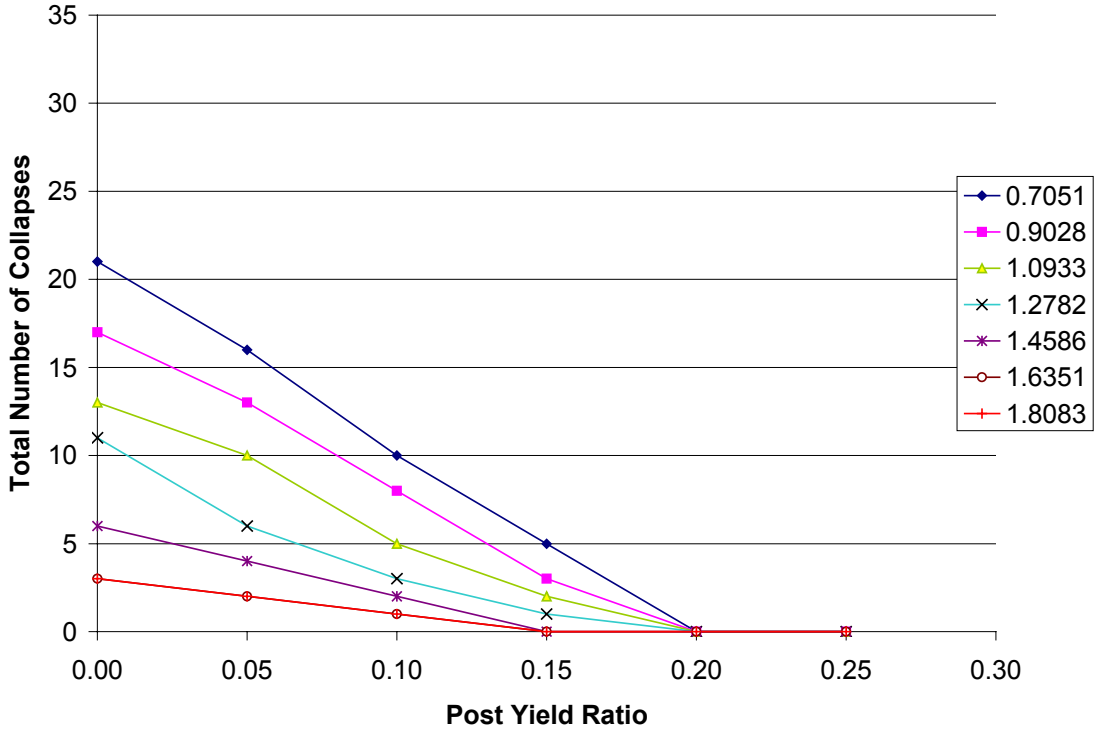

Figure 5.3c – EQ 4, Lateral Scale = 0.2 g, Number of Collapses Versus Post-yield Stiffness Ratio, Grouped According to Period

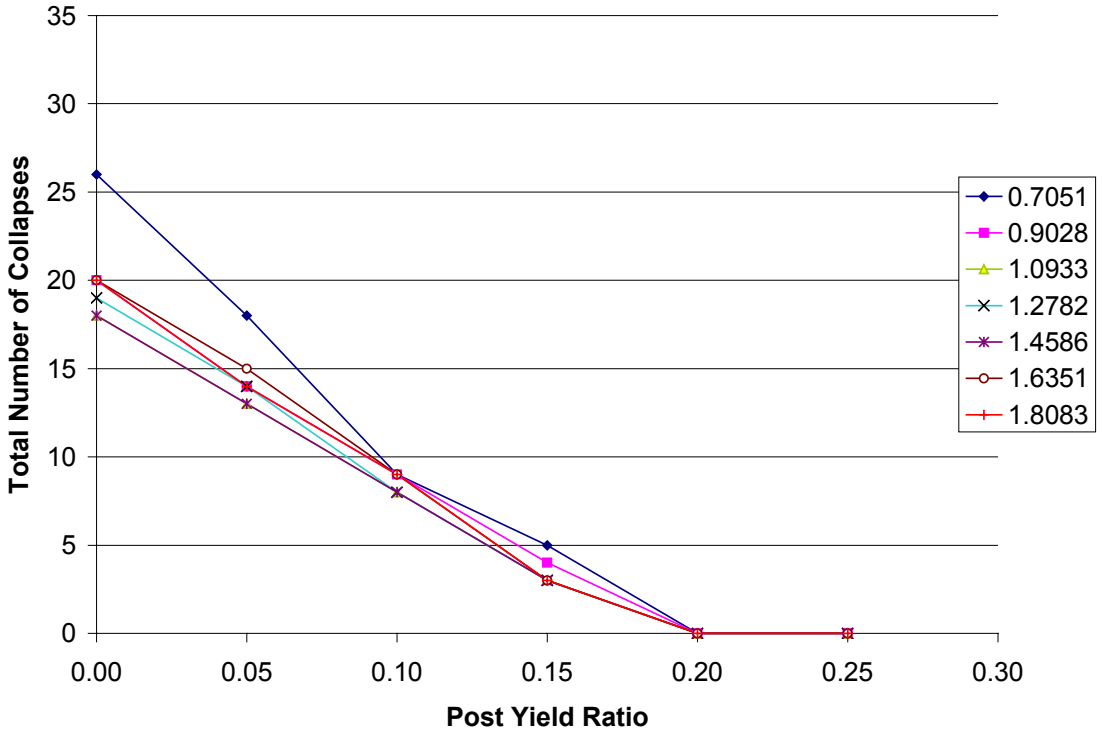

Figure 5.3d – EQ 1, Lateral Scale = 0.4 g, Number of Collapses Versus Post-yield Stiffness Ratio, Grouped According to Period

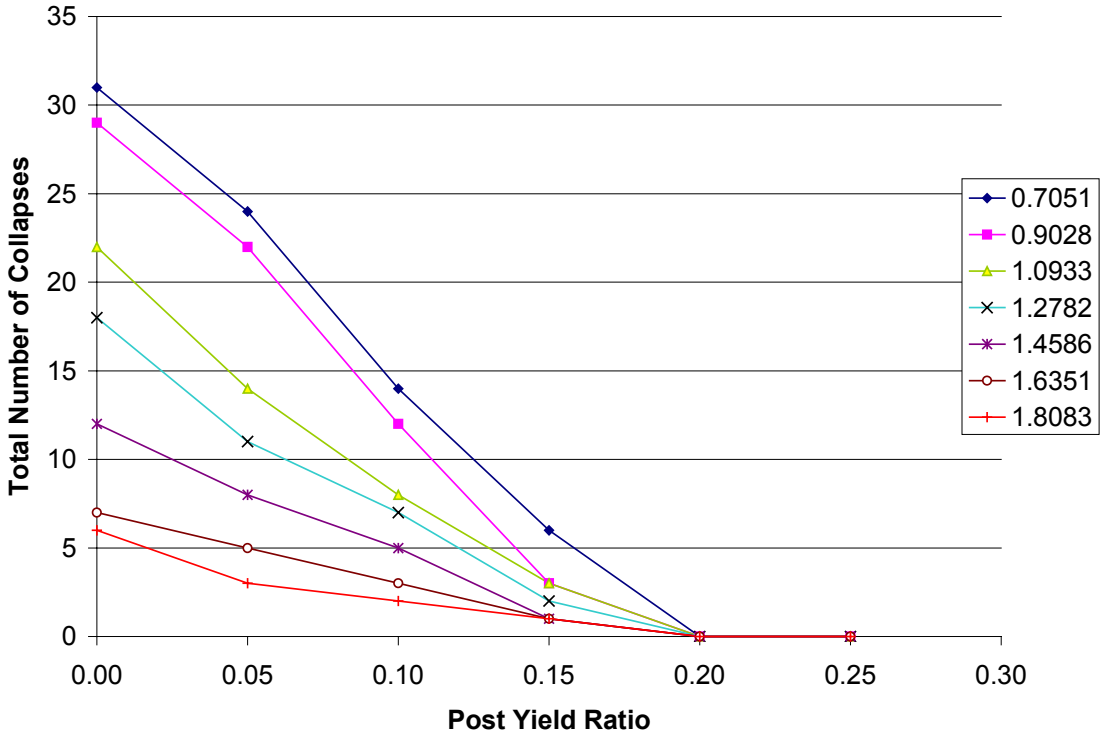

Figure 5.3e – EQ 3, Lateral Scale = 0.4 g, Number of Collapses Versus Post-yield Stiffness Ratio, Grouped According to Period

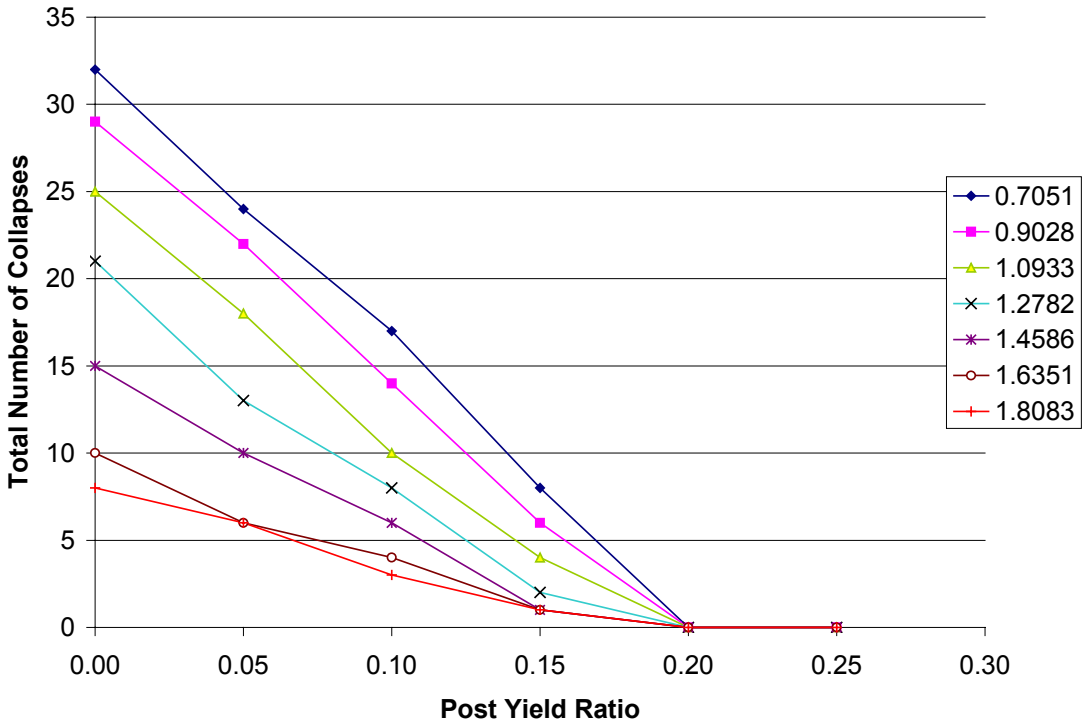

Figure 5.3f – EQ 4, Lateral Scale = 0.2 g, Number of Collapses Versus Post-yield Stiffness Ratio, Grouped According to Period

It is clear from the above figures that lower post-yield stiffness ratios result in more collapses than do higher ones. Moreover, the number of collapses seems to be dependent on the period in the same way as for the stability ratio parameter. The period influences both the displacement demands and the yield displacements

Another point worth making is that no collapses occur for structures with post-yield stiffness ratios greater than or equal to 0.2. Even for the models with yield strengths equal to three per cent of the weight (My = 834 kip-in), no collapses occur. For every earthquake at every scale this was true. A point to consider about the aforementioned is that the highest stability ratio used was 0.2. Knowing that the stability ratio reduces the effective post-yield stiffness ratio according to equation 2.10, then resulting effective post-yield stiffness ratios considering P-Delta effects (r_p) would at worst be elastic, perfectly plastic. For post-yield stiffness ratios less than 0.2, the resulting r_p values could be negative, which makes the post-yield stiffness negative. Thus, it makes sense that structures with post-yield stiffness ratios greater than or equal to 0.2 did not collapse.

5.2.1.3 – Yield Force

The final parameter requiring examination is the yield force. The yield force values were chosen based on percentages of the structure's weight. The percentages were based on reasonable values that would be close to the C_s values used in the ELF method of the NEHRP Provisions. The yield force values were given in terms of moment because the lateral strength of the models was provided by bilinear rotational springs. From Tables 5.1a through 5.1g, each table represents all of the data for a given set that had a given yield moment. The yield moments are shown in the first column. For each period, there are 30 values that correspond to a particular yield moment. Thus, there are 49 groups of values for the combinations of the yield moments and periods. The results of yield force on collapse are shown in Figures 5.4a through 5.4f.

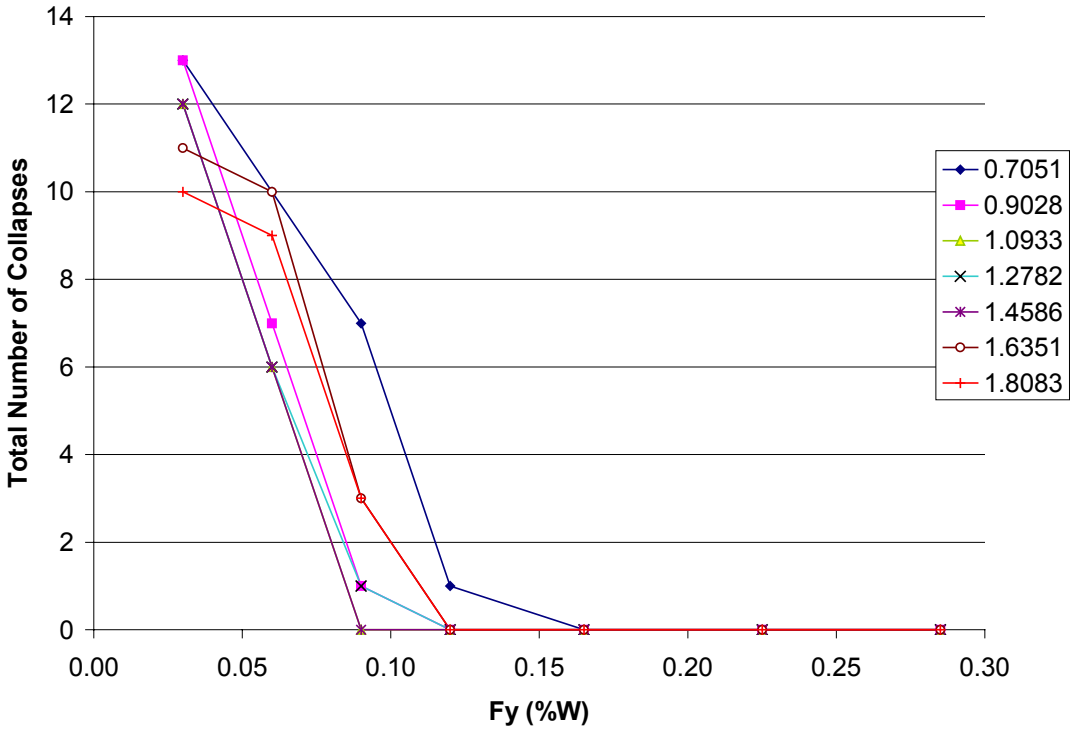

Figure 5.4a – EQ 1, Lateral Scale = 0.2 g, Number of Collapses Versus Yield Force, Grouped According to Period

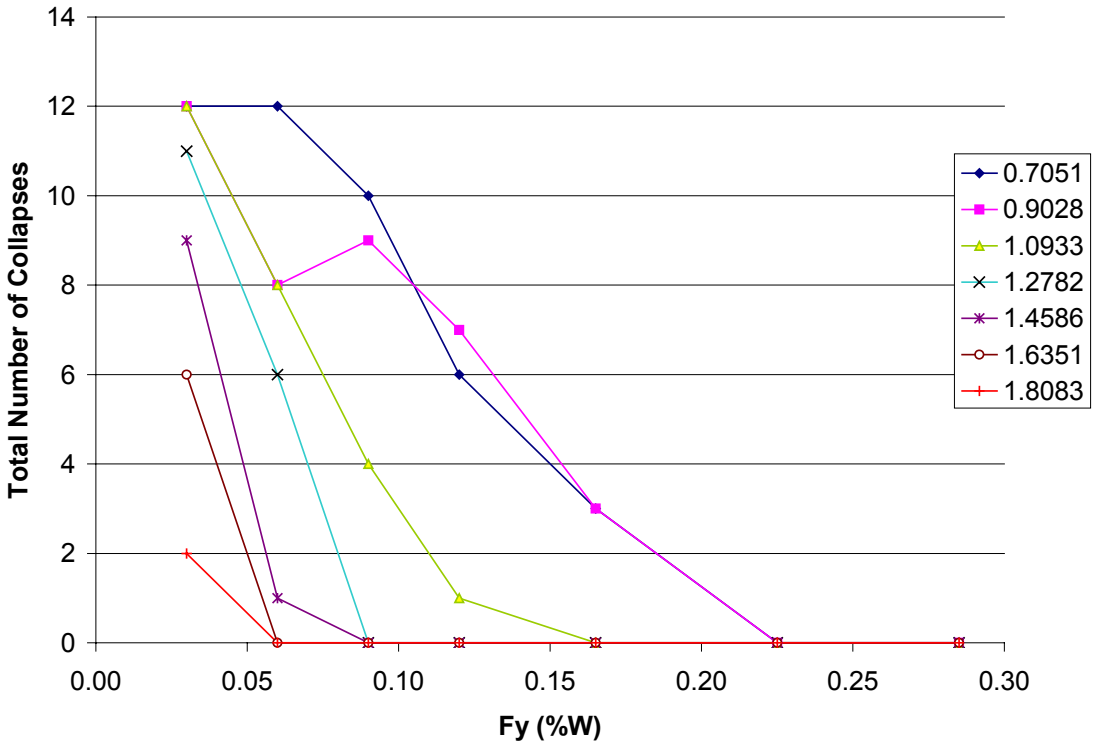

Figure 5.4b – EQ 3, Lateral Scale = 0.2 g, Number of Collapses Versus Yield Force, Grouped According to Period

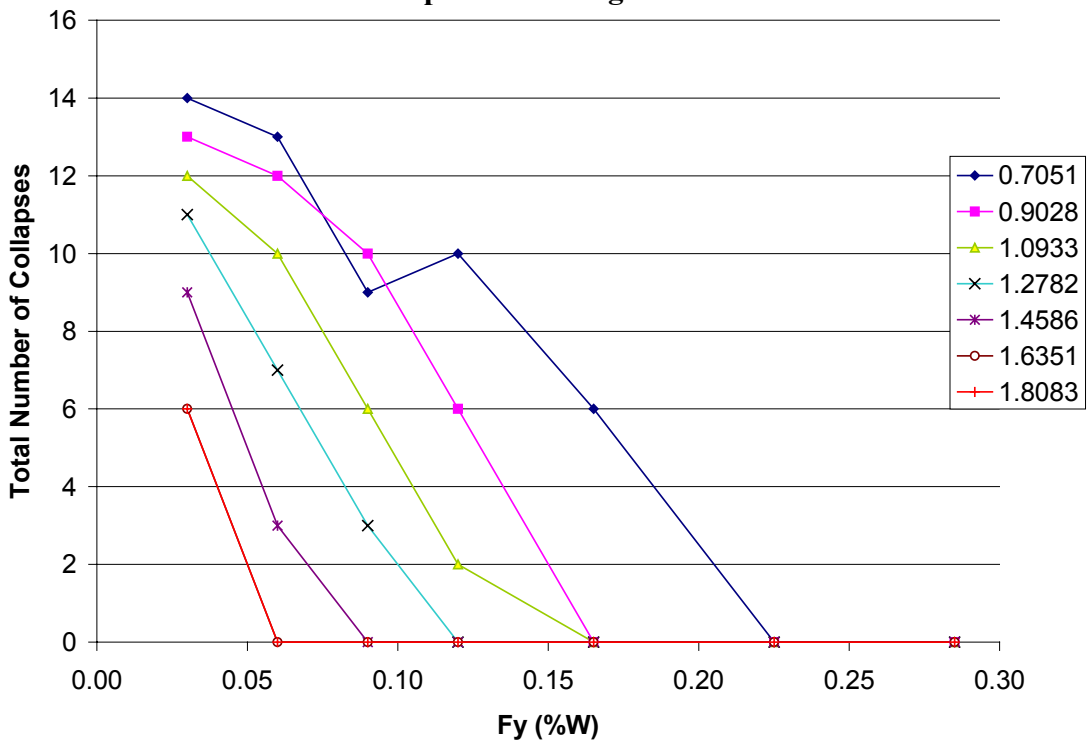

Figure 5.4c – EQ 4, Lateral Scale = 0.2 g, Number of Collapses Versus Yield Force, Grouped According to Period

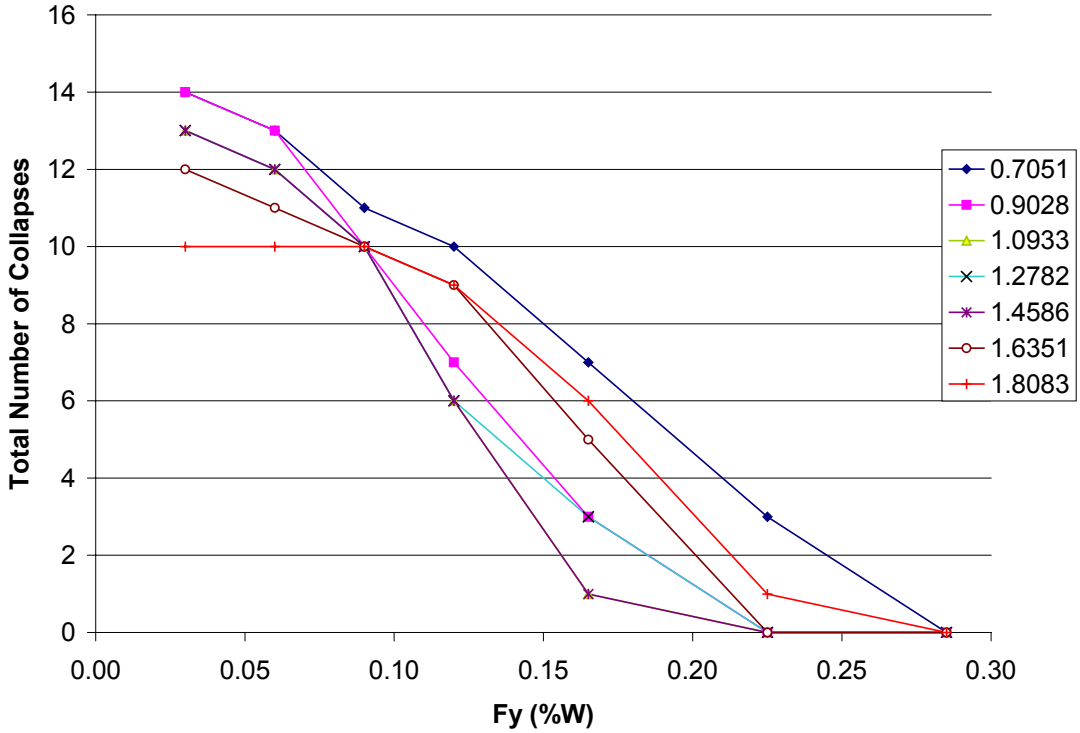

Figure 5.4d – EQ 1, Lateral Scale = 0.4 g, Number of Collapses Versus Yield Force, Grouped According to Period

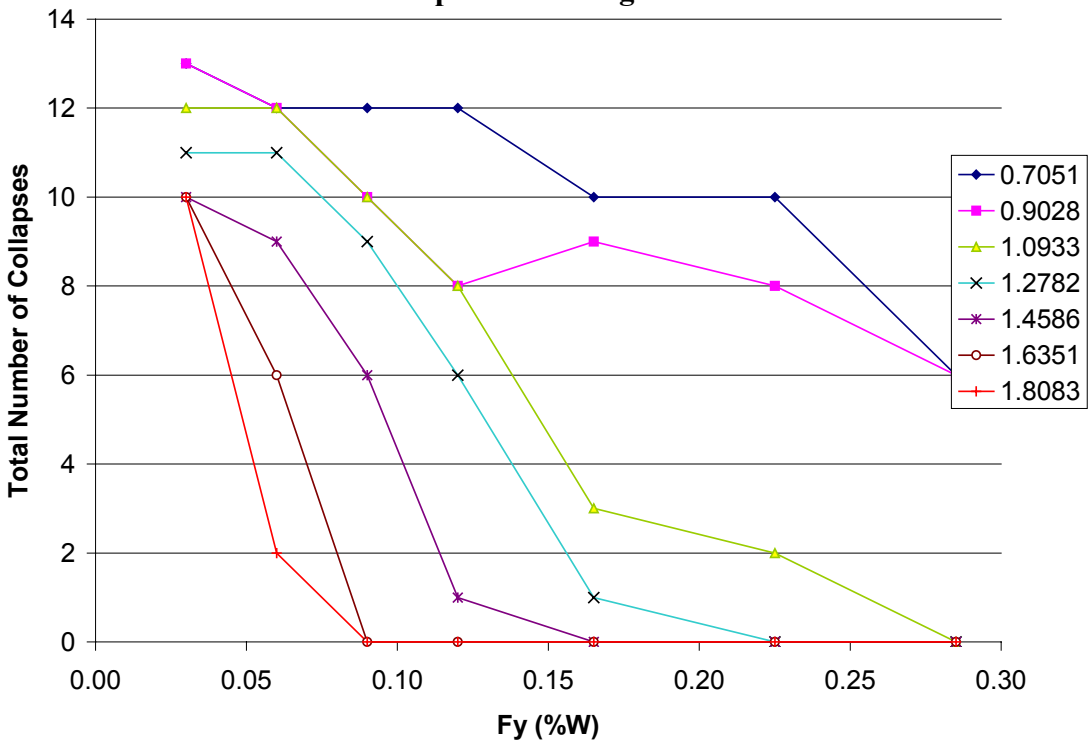

Figure 5.4e – EQ 3, Lateral Scale = 0.4 g, Number of Collapses Versus Yield Force, Grouped According to Period

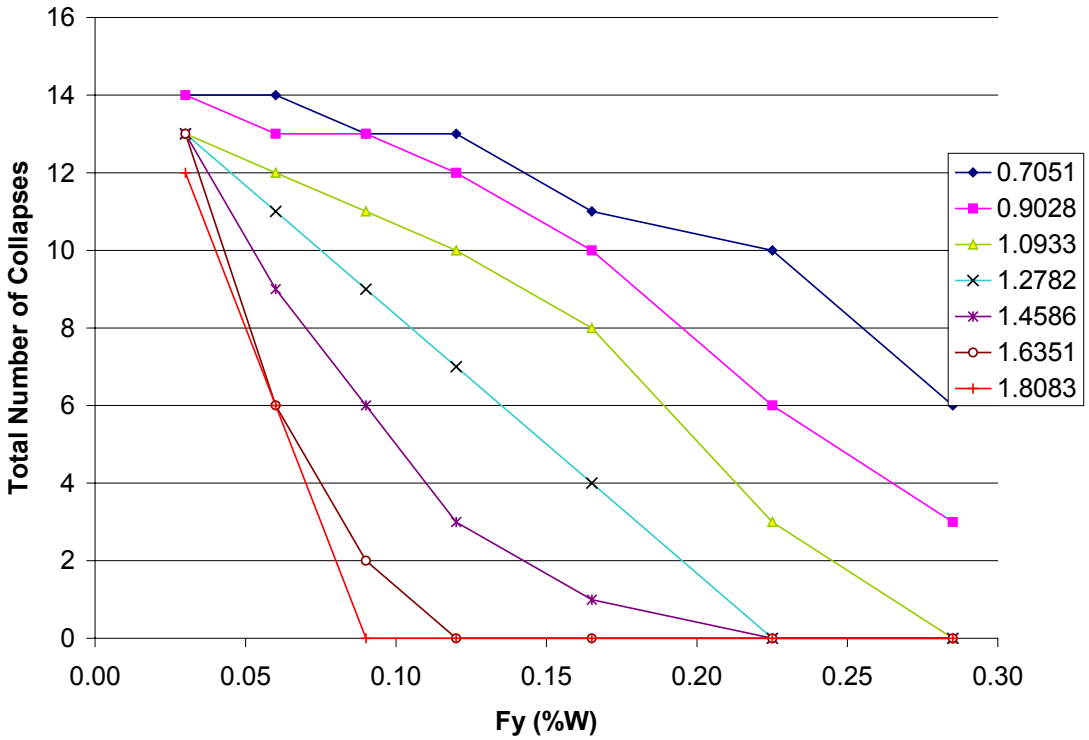

Figure 5.4f – EQ 4, Lateral Scale = 0.4 g, Number of Collapses Versus Yield Force, Grouped According to Period

In general, Figures 5.4a through 5.4f indicate that increasing the yield strength reduces the number of collapses that occur. However, in several situations, an increase in yield strength caused a collapse. Two specific cases will be examined. First, in figure 5.4b for the models with a period of 0.9028 seconds there is an increase in the total number of collapses as the strength increases from 0.06 per cent of the weight (My = 1668 kip-in) to 0.09 per cent of the weight (My = 2502 kip-in). After inspecting the data, the post-yield stiffness ratio and stability ratio of the particular models that collapsed with increasing yield strength were 0.1 and 0.16, respectively. The best way to understand what happened to these models is to examine their response histories.

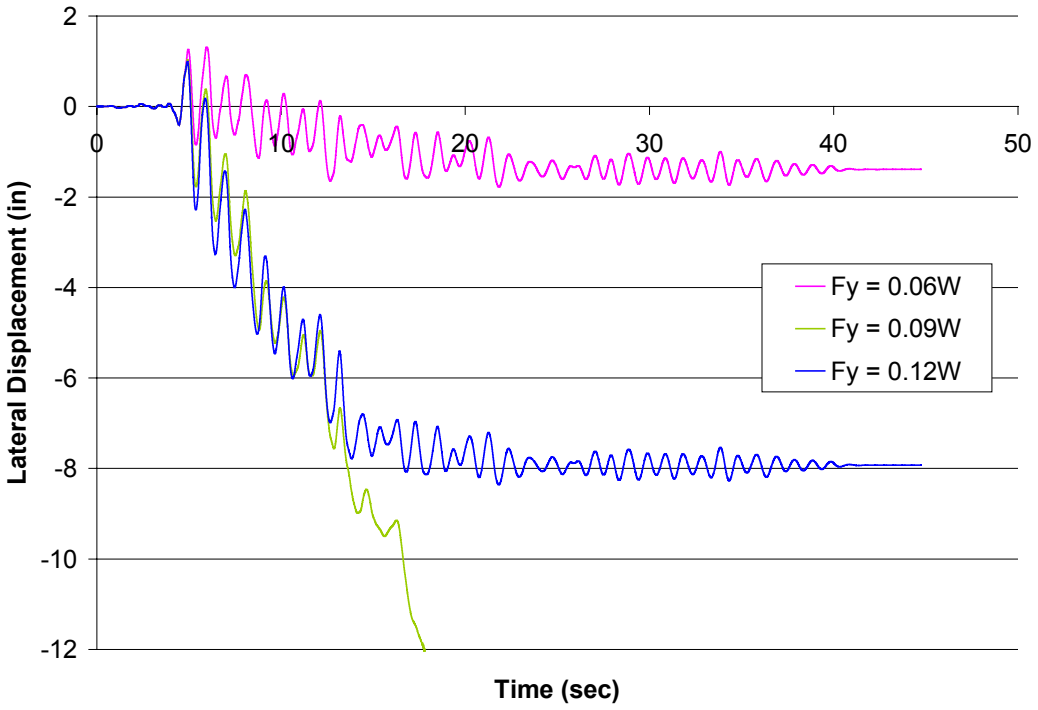

Figure 5.5 – Response History of Models with Various Yield Strengths, a Stability Ratio of 0.16, a Post-yield Stiffness Ratio of 0.1, and a Period of 0.9028 Seconds Subjected to Earthquake 3 Scaled to 0.2 g.

One of the most startling characteristics of the data shown in Figure 5.5 is that the smallest amount of displacement is associated with the lowest yield moment. It is completely counter intuitive that increasing the yield strength would either significantly increase displacements or cause collapse. It is clear from the above figure that slight changes in the amount of displacement at about five or six seconds into the response history drastically affects how the structure responds for the rest of the analysis.

Another example comes from Figure 5.4c. In this figure, the models with a period of 0.705 seconds had fewer collapses as the yield strength increased from six to nine percent of the structure's weight. As with the previous example, the problematic set of yield strengths had post-yield ratios of 0.1 and stability ratios of 0.16. The response histories of the problematic models from figure 5.4c are shown below in Figure 5.6.

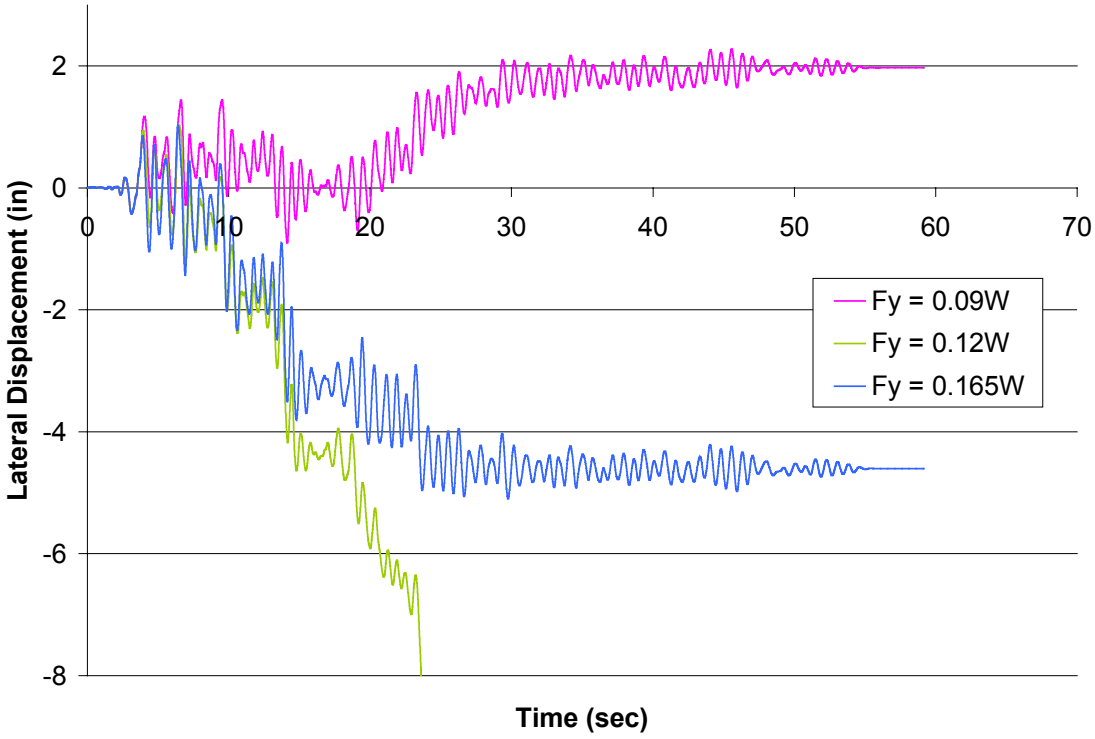

Figure 5.6 – Response History of Models with Various Yield Strengths, a Stability Ratio of 0.16, a Post-yield Stiffness Ratio of 0.1, and a Period of 0.705 Seconds Subjected to Earthquake 4 Scaled to 0.2 g.

As with the previous example, it is startling that increasing the yield strength actually causes collapse. Also, like the previous example, it seems that subtle changes in the displacements early in the response history drastically affect the rest of the response.

An important point to remember about the two examples just described is that the post-yield stiffness considering P-Delta effects is slightly negative for all of the example structures. A post-yield stiffness of 0.1 and a stability ratio of 0.16 results in an r_p value of –0.071. While it may not be clear at this point, the negative r_p value significantly increases the probability that a structure will collapse. Had the r_p values been more negative, then all of the structures would most likely have collapsed. Furthermore, had all of the r_p values been positive, all of the structures most likely would not have collapsed. However, since the r_p value is only slightly negative, then determining whether or not a model will collapse becomes nearly impossible, because survival is dependent on displacement demand, period, yield strength, ground motion intensity, and the randomness of the ground motion pulse sequences. For now, it is enough to say that

increasing yield strength generally decreases the number of collapses. However, when the r_p value is slightly negative, it is difficult to tell what will happen to a structure subjected to a particular earthquake.

5.2.2 - Effects of Combined Parameter Variation on Maximum Displacement and Collapse

While it is valuable to study the effects of individual parameters on collapse, it turns out that combinations of the parameters were much more useful for determining collapse prone behavior. For example, the r_p value, which once again is the post-yield stiffness ratio reduced by P-Delta effects, is determined with the stability ratio and post-yield stiffness ratio and thus is a sort of composite parameter. Recall that the r_p value is determined from equation 2.10. In tables 5.1a through 5.1g, r_p values have been included in the fourth column. Notice that the r_p values range from about 0.25 to about –0.25. If the rows in the tables are sorted from lowest to highest r_p value, then curves like those shown in Figures 5.7a through 5.7c result.

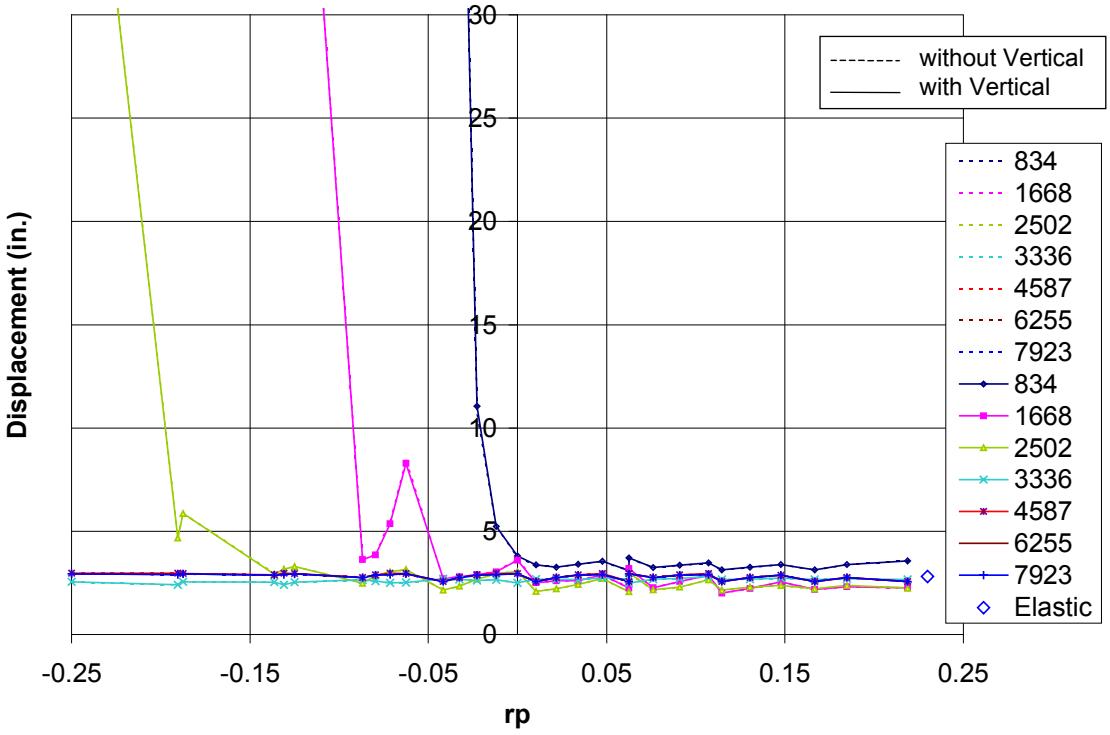

Figure 5.7a – EQ1, Lateral Scale = 0.2 g, Maximum Displacement Versus r_p for Models with a Period of 1.278 Seconds.

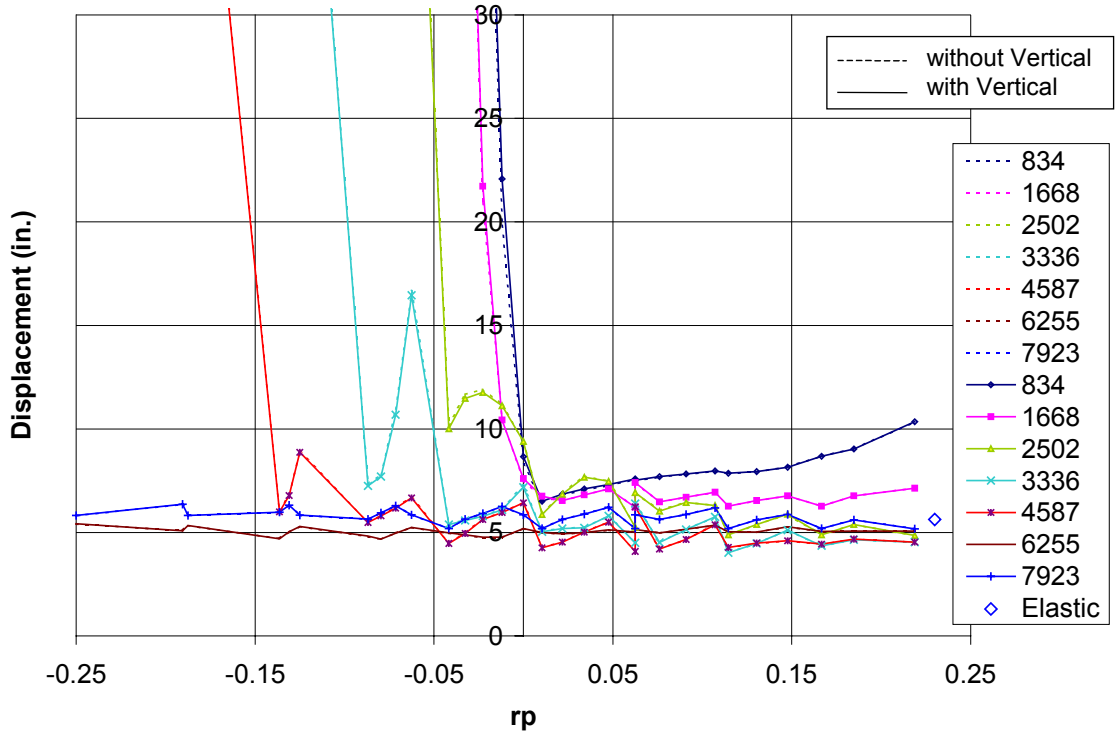

Figure 5.7b – EQ1, Lateral Scale = 0.4 g, Maximum Displacement Versus r_p for Models with a Period of 1.278 Seconds.

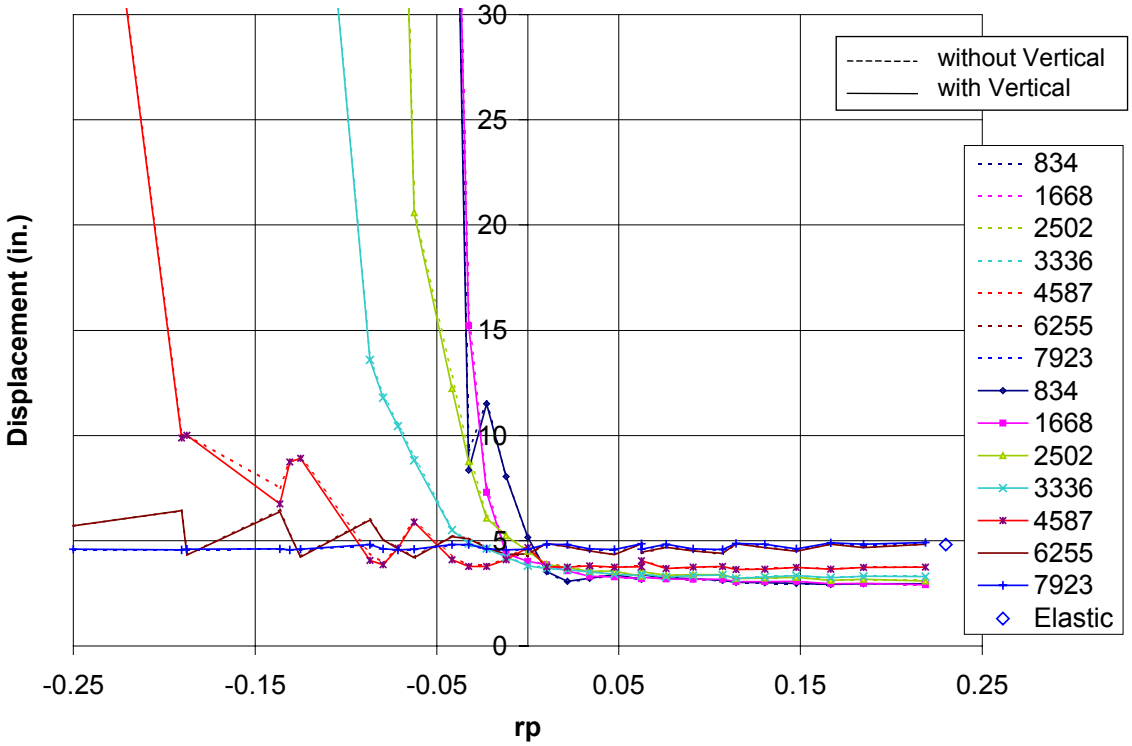

Figure 5.7c – EQ3, Lateral Scale = 0.4 g, Maximum Displacement Versus r_p for Models with a Period of 1.278 Seconds.

In Figures 5.7a through 5.7c, all of the data points represent models with periods of 1.278 seconds. Moreover, the separate curves in each figure represent the yield moments used in the parameter study. Recall that the yield moments corresponded to particular C_s values. In terms of Tables 5.1a through 5.1g, each curve is an entire column out of the appropriate table corresponding to a period of 1.278 seconds, sorted from lowest to highest r_p. As a side note, curves are also plotted in the above figures that include the effects of vertical accelerations, but vertical acceleration effects will be discussed later. For the most part, vertical accelerations had very little effect on the lateral displacements of the models shown in Figures 5.7a through 5.7c. Also shown in the figures is the maximum lateral displacement of an elastic model with the same period. The elastic value is denoted with a diamond and is located at the 0.2 r_p mark. Notice that for positive r_p values, the amount of displacement is fairly constant and in most cases close to the elastic value.

Several observations about the constant displacement values can be made at this point. First, the equal displacement concept holds true for models with positive r_p. Each of the structures undergoes about the same amount of displacement regardless of yield force, post-yield stiffness ratio, and stability ratio. However, once the r_p values become negative, many of the models quickly collapse, that is, their maximum lateral displacements exceed 50 in. Thus, the 50 in. mark used in the previous sections is an adequate measure of collapse because of the near asymptotic nature of the curves, where the transition from a non-collapsed to collapsed state is almost instantaneous.

A second observation is that displacement demand alone is not a good predictor of collapse. Consider figure 5.7a. The positive r_p displacement demand of all of the models is around 2.5 in.. However, the models with a yield moment of 834 kip-in collapse at a lower negative r_p value than the models with a yield moment of 1668 kip-in. Thus, it is clear that collapse is dependent on both r_p and the yield force and consequently any attempt to determine collapse prone structures must also consider yield force.

Yield force can be included in the three figures above by plotting ductility demand on the vertical axis as opposed to maximum displacement. Since ductility is a function of yield strength and stiffness (period), these values are indirectly included as

variables in the figures when ductility demand is plotted on the vertical axis. Consequently, the resulting figures include the effects of all of the parameters. On the horizontal axis, the r_p value is a combination of the stability ratio and the post-yield stiffness ratio. On the vertical axis, the ductility demand is a measure of earthquake intensity, yield force, and stiffness. As will be shown, the ductility demand for positive r_p values in conjunction with the r_p value at the location where the ductility demand drastically increases, called the collapse r_p value from now on, provides a fairly consistent means of determining collapse prone structures. Figures 5.8a through 5.8c plot the same data as Figures 5.7a through 5.7c, but replace maximum displacement with ductility demand.

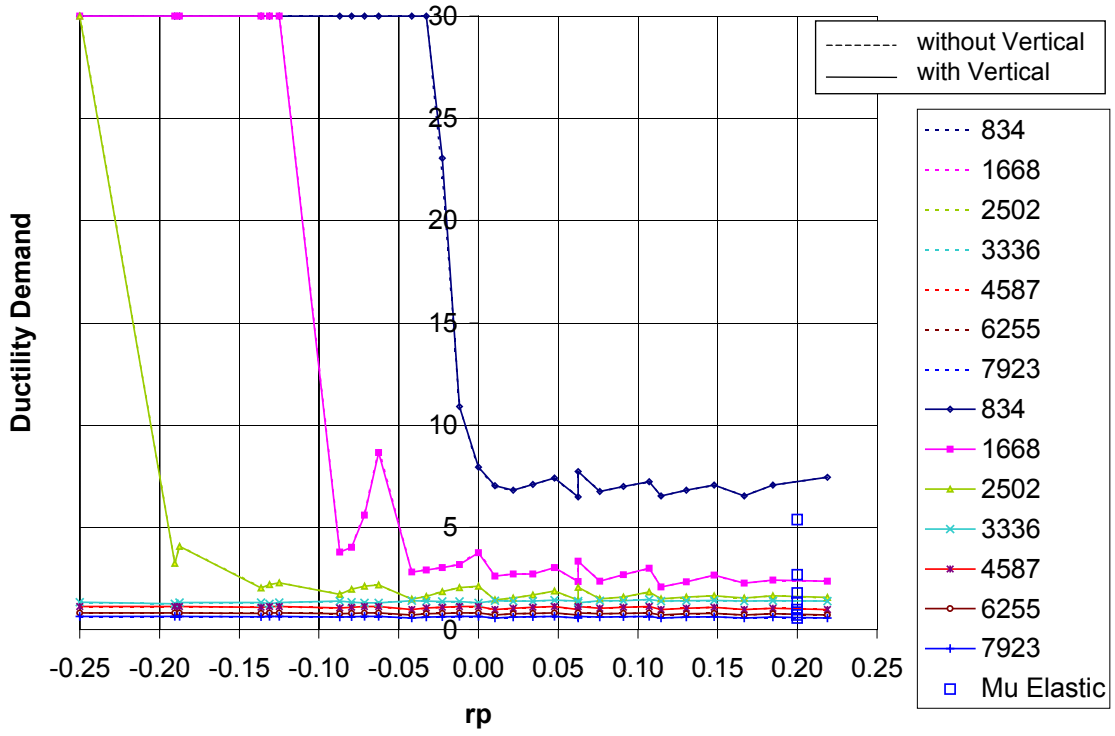

Figure 5.8a – EQ1, Lateral Scale = 0.2 g, Ductility Demand Versus r_p for Models with a Period of 1.278 Seconds.

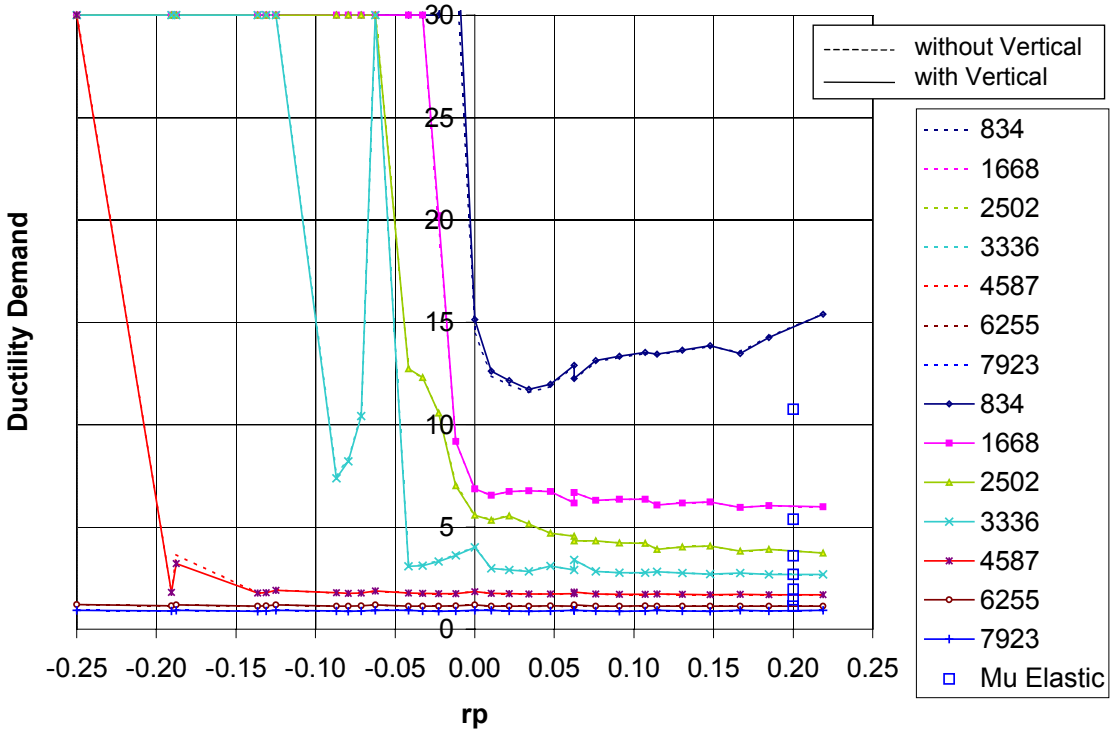

Figure 5.8b – EQ1, Lateral Scale = 0.4 g, Ductility Demand Versus r_p for Models with a Period of 1.278 Seconds.

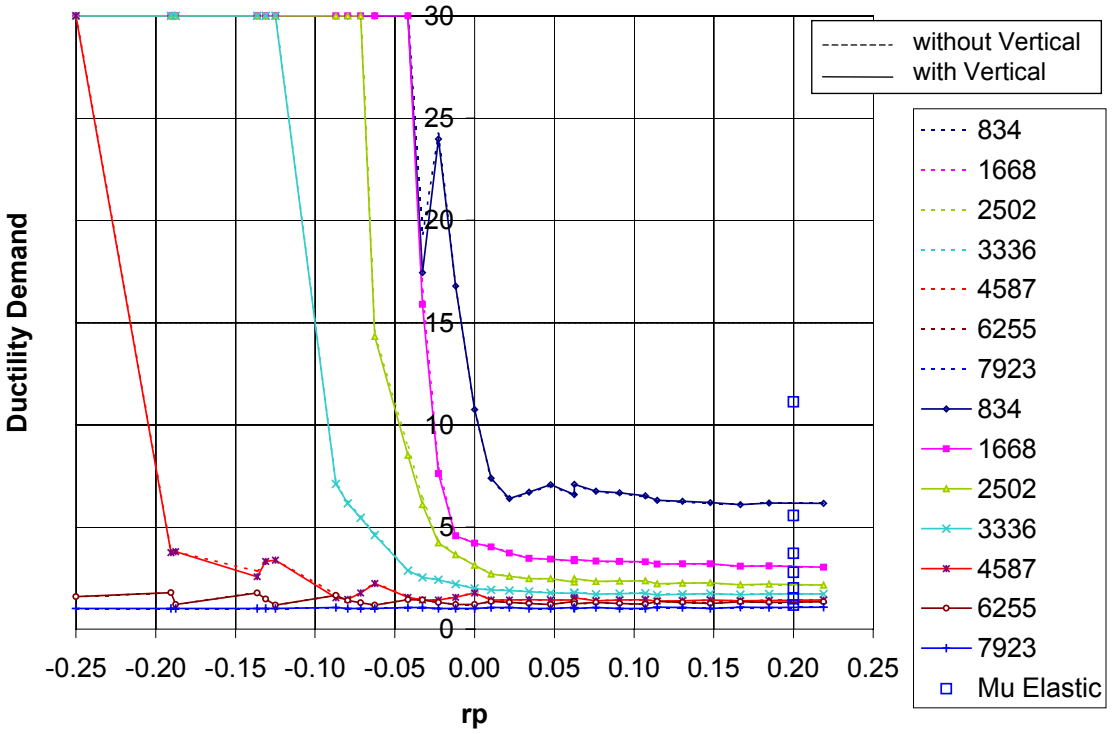

Figure 5.8c – EQ3, Lateral Scale = 0.4 g, Ductility Demand Versus r_p for Models with a Period of 1.278 Seconds.

As with the maximum displacement figures, the ductility demand figures show the demand to be fairly constant for positive r_p values. The one anomaly to this observation is the curve representing the models that have a yield moment of 834 kip-in. in Figure 5.8b. Such structures are probably unrealistic because an analysis indicating ductility demands greater than 15 would be unacceptable in a design situation. For discussion purposes, the average of the ductility demand for positive r_p values will be called the positive r_p ductility demand.

Moreover, notice that as the ductility demand for a given period and earthquake intensity goes down, the collapse r_p increases in the negative direction. For example, in Figure 5.8b, the positive r_p ductility demand for a model with a spring yield moment of 1668 kip-in. is about 7.5. The collapse r_p is about -0.025. From the same figure, a model with a spring yield moment of 2502 kip-in. has a positive ductility demand around 4.5 to 5 and a collapse r_p of about - 0.05. As the positive r_p ductility demand decreased from 7.5 to 5, the collapse r_p increased from –0.025 to –0.05. Also, notice that as the earthquake intensity increases, the ductility demand increases, which causes the collapse r_p value to shift toward zero. Consider once again the curve corresponding to a yield moment of 1668 kip-in. In Figure 5.8a, the collapse r_p is about –0.1 and the PGA is 0.2g. Then, in Figure 5.8b, the PGA was increased to 0.4g and the collapse r_p value shifted to about -0.025.

Also shown in the above figures is a set of data called “Mu Elastic,” which stands for elastic ductility demand. It was determined by dividing the elastic displacement demands shown in Figures 5.7a through 5.7c by the yield displacements of the corresponding models. It is most similar to the R values prescribed in the NEHRP Provisions. The ductility demands of models with higher yield moments tend to match the corresponding elastic ductility demands fairly closely. However, for lower yield moments, actual and elastic ductility demands tend not to agree as well.

A possible reason for the actual and elastic disagreement is because of the amount of inelastic demand in structures with lower yield moments. In the inelastic range, the period of the structure elongates because the stiffness goes down. Structures with higher ductility demands arguably spend more time in the inelastic range and thus act most of the time as structures with different periods. Consider the response histories shown in

Figure 5.9, which pertain to Figures 5.7b and 5.8b. The accelerogram of the earthquake that invoked the responses shown in Figure 5.9 is included in Appendix A, Figure A1.1.

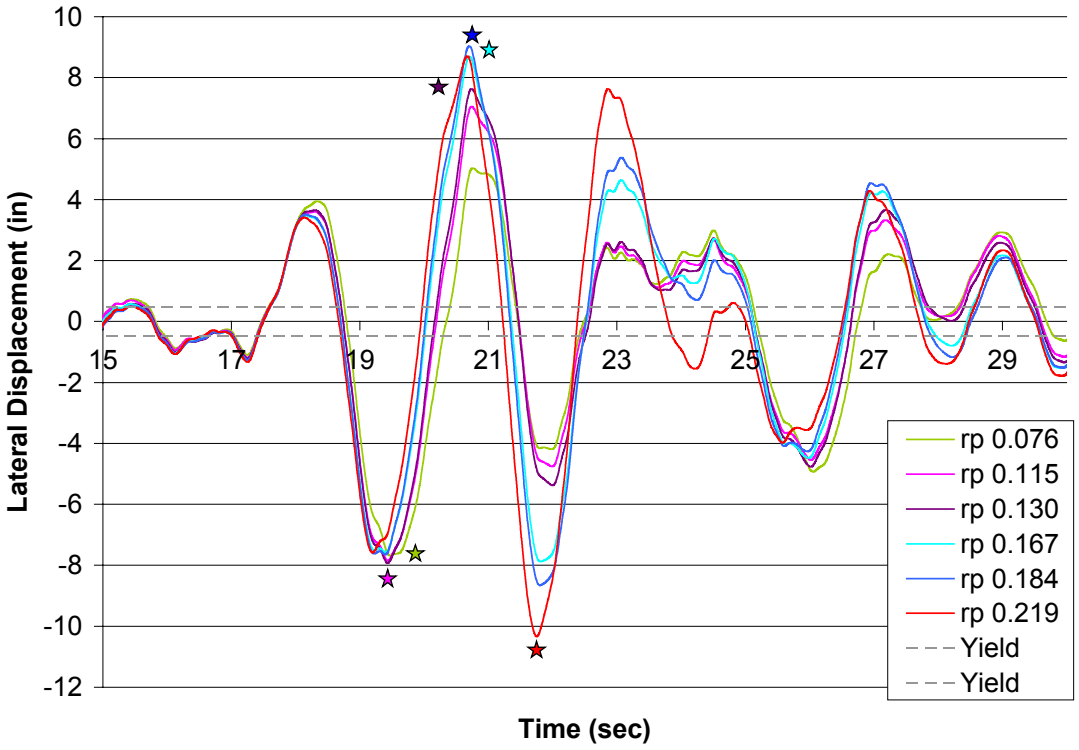

Figure 5.9 - Response Histories of Models with Periods of 1.278 Seconds Subjected to Earthquake 1 which was scaled to 0.4 g PGA.

In Figure 5.9, all of the models have yield moments of 834 kip-in ($F_y = 0.03W$). The corresponding yield displacement is shown in Figure 5.9 by the dashed lines. Then, the point of maximum displacement is denoted with a star that matches the curve where the maximum is occurring. Notice that the structure's displacements are in the inelastic range for almost every cycle of the earthquake. Also notice that the maximum displacements are not occurring in the same cycles. From Figure 5.9, it is probably safe to say that the models do not have the same effective period as a similar elastic structure because so much of the response history is inelastic. No real structure could endure that much inelasticity. In fact, the only reason that these structures did not collapse is because the ductility of the models was infinite. Thus, it seems that there is a limit to the range where the equal displacement concept is valid. From Figures 5.8a through 5.8c, it seems

that the equal displacement concept is true for structures with ductility demands less than about 10.

The disagreement may also be partially because the high ductility demands correspond with models with yield displacements less than one inch. When both the actual and elastic displacements are divided by yield displacements that are less than one in., the differences between the actual and elastic displacement would be amplified. Consider for example, the elastic displacement of Figure 5.7a, which is 2.576 inches. The actual positive r_p displacement demand of a structure with a yield moment of 834 kip-in. is around 3.5 in. and the yield displacement is 0.479 inches. Thus, when converting to ductility, the difference between the elastic and actual values is approximately doubled. The point of the previous discussion about elastic ductility demand is to point out that while the positive r_p displacements may be close to elastic displacements, differences between actual and elastic values can be amplified if one wants to try to similarly compare ductility demands.

For each of the curves shown in Figures 5.8a through 5.8c, a corresponding positive r_p ductility demand and collapse r_p value may be extrapolated. The extrapolation process is shown in Figure 5.10 using Figure 5.8b as an example.

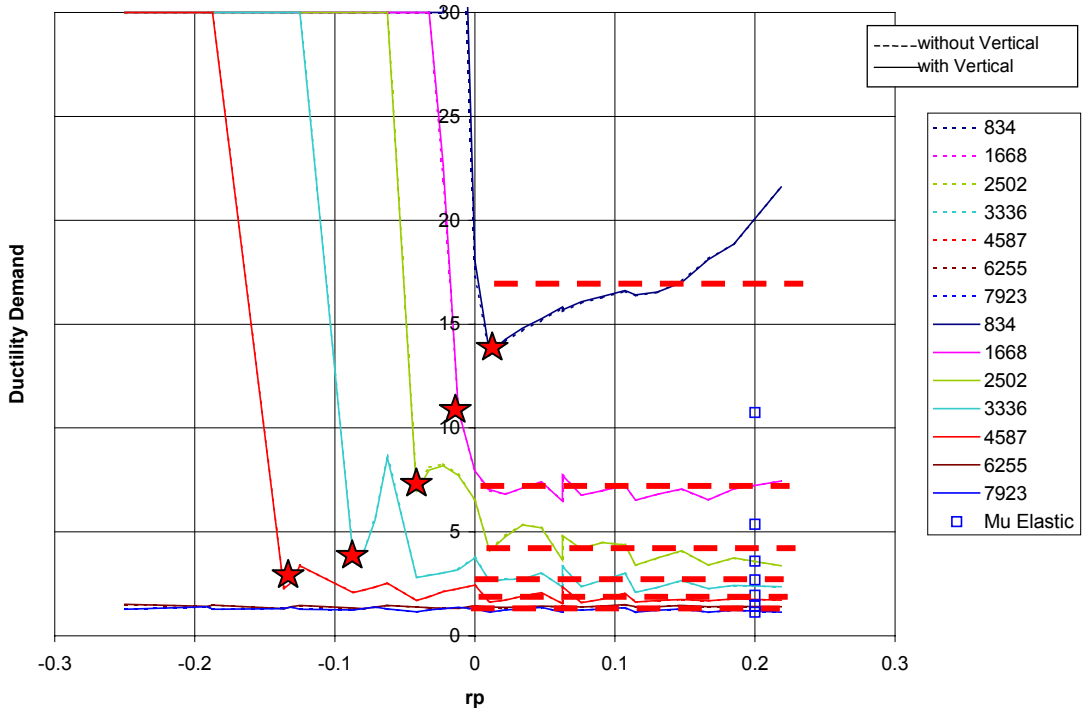

Figure 5.10 – Extrapolating Collapse r_p and positive r_p ductility demands

The thick dashed lines in the above figure represent the values used for the positive r_p ductility demand. Notice that the average value fits the data fairly well except for the 834 kip-in curve. It was explained earlier that this anomalous value was unreasonable and such a structure would never be built anyway. Then, the red stars represent the collapse r_p values. Notice that there is not a collapse r_p value for the 6255 and 7923 curves.

As is turns out, the combinations of collapse r_p and positive r_p ductility demand are fairly independent of earthquake and ground motion scale. For the eight earthquakes used in the parameter study and PGA's of 0.2g and 0.4g, a scatter plot of collapse r_p and positive r_p ductility demand revealed a fairly tight bandwidth. Besides these analyses, other models were created for the purpose of filling a broader range of negative r_p vales. These models were then subjected to earthquakes one through six at a PGA scale of 0.4 g. The resulting set of data is shown in Figure 5.11.

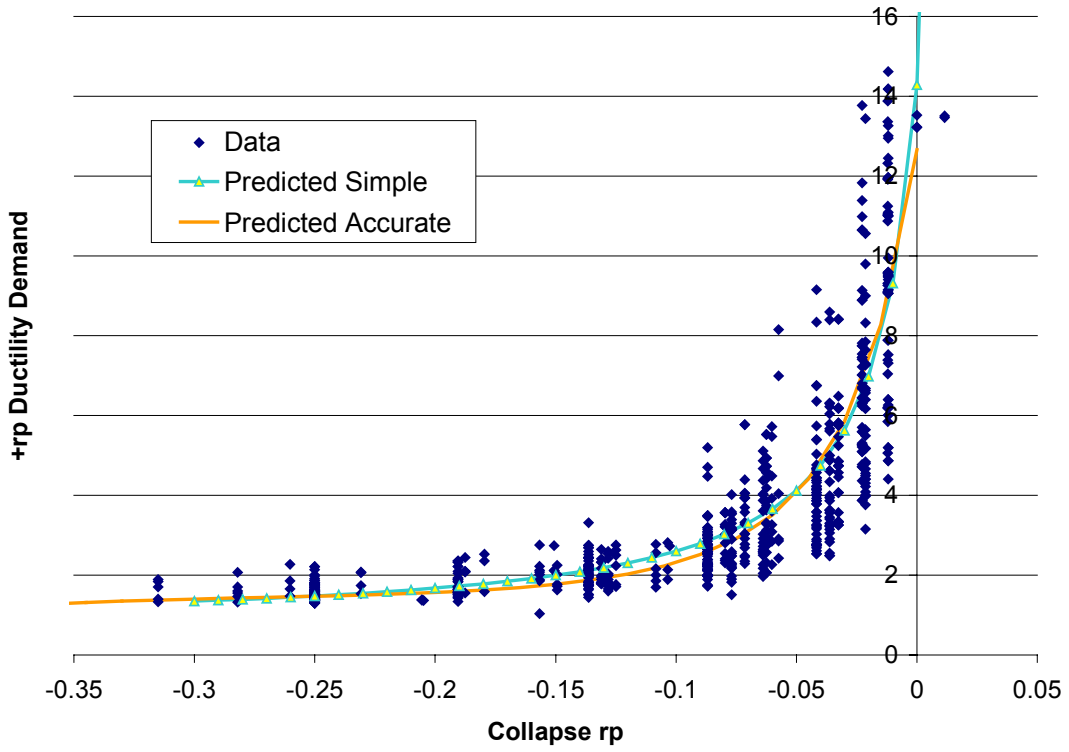

Figure 5.11 – Combinations of Collapse r_p and Positive r_p Ductility Demand Considering Multiple Ground Motions at Multiple Intensity Scales

Figure 5.11 shows that larger negative r_p values will collapse at relatively low ductility demands. As the negative r_p values approach zero from the left, the ductility values that cause collapse increase. For r_p values between 0.0 and about –0.025, collapse will not occur unless the ductility demands exceed about 10.0.

Given the distribution of the data, there were several ways that it could be interpreted. Two ways will be described next. The first method involved doing a linear regression. In order to perform a linear regression, the data had to be transformed so that there was a linear relationship between r_p and the positive r_p ductility demand (μ_{+rp}). For the transformation to be statistically accurate, the residuals had to be normally distributed about the predicted curve and the residuals needed to be small. Based on the shape of the data, it was determined that a log transformation was most applicable. After several iterations of various transformations, it was determined that the best linear fit resulted when the square root of the log of μ_{+rp} was used in conjunction with a cubic r_p polynomial.

From the linear regression, an R-sqared value of 0.85 was produced. This means that 85 per cent of the variability in the value on the vertical axis can be explained by changes in the horizontal axis value. In other words, the data correlated fairly well. Moreover, the standard deviation was a relatively low value of 0.1. The resulting equation from the regression is given by equations 5.1 and 5.2:

$$\mu_{+rp} = 10^{RP} \tag{5.1}$$

where

μ_{+rp} = positive r_p ductility demand

$$RP = \left(1.05 + 6.47 r_p + 23.04 r_p^{\,2} + 29.64 r_p^{\,3}\right)^2 \tag{5.2}$$

A slightly simpler equation, which produces about the same results, is given by equation 5.3. For statistical accuracy, equation 5.1 should be used, but equation 5.3 may be preferred because it is less complicated:

$$\mu_{+rp} = \frac{(1 - r_p)^2}{-3.95 r_p + 0.07} \tag{5.3}$$

Thus, from equation 5.1 or 5.3, if the r_p value is known, the ductility demand that would cause collapse may be estimated. From the analyses conducted, it would seem that both equations fit the data fairly well. Both equations 5.1 and 5.3 are shown in Figure 5.11.

Another way to interpret the data is to simply divide the r_p values into regions and assign acceptable ductility demand boundaries. This method is somewhat arbitrary, but given the uncertainties in nonlinear dynamic analysis, may be just as useful as the more refined regression method. Table 5.2 presents the chosen bounds, and Figure 5.12 shows plots of the bounds with the collapse data.

Table 5.2 – Collapse Prevention Ductility Demands Considering r_p

Maximum Allowable Ductility Demand		
rp range	**Average**	**Conservative**
0 to -0.025	5	4
-0.025 to -0.075	3	2.5
-0.075 to -0.15	2	1.75
> -0.15	1.5	1.25

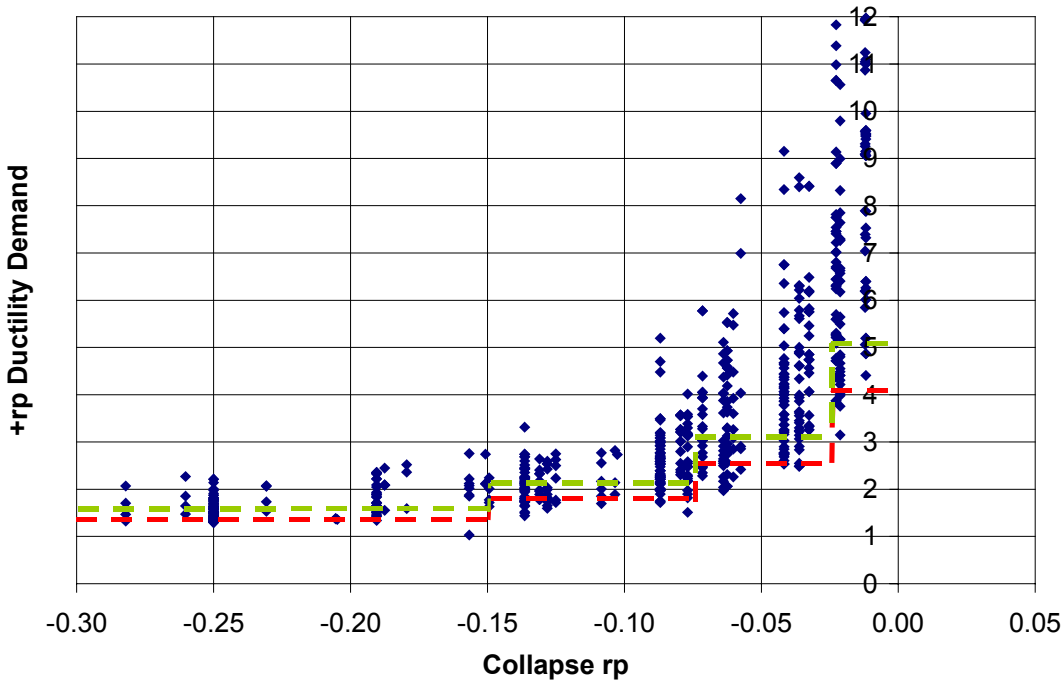

Figure 5.12 – Collapse Prevention Regions Based on Combinations of Collapse r_p and Positive r_p Ductility Demand Considering Multiple Ground Motions at Multiple Scales

While the collapse prevention bounds of Figure 5.12 are more crude than the regression fit line of Figure 5.11, both could be useful for determining collapse prevention limit states. To summarize what has been said in this section, Figures 5.8a through 5.8c showed that there is a correlation between the average ductility demand and the r_p value that causes collapse. Figure 5.11 showed the relationship to be fairly universal for all earthquakes and PGA scales. Equations 5.1 and 5.3 and Table 5.2 provide some initial attempts at providing limits for ductility demands based on r_p values.

5.3 - Effects of Structural Parameter Variation on Residual Displacements

Since the focus of this study is on collapse, residual displacements will be addressed only briefly. However, since residual displacements affect the post earthquake stability of a structure, they are worth mentioning. MacRae and Kawashima (1997) and Kawashima and Macrae (1998) argued that residual displacements should be a separate design consideration because they affect the post earthquake stability of a structure. Furthermore, Mehanny and Deierlein (2001) showed that for damaged structures the residual displacements could account for about a third of the loss of stability, whereas the damage accounted for the other two thirds. From the literature, it seems that one should consider residual displacements, not to consider how collapse prone a structure is during an earthquake, but how collapse prone a structure is after an earthquake.

To illustrate the effects of residual displacements, Figures 5.13 through 5.15 are presented. For each figure number, there is an "a" and "b" figure. The "a" figure shows the maximum ductility demand versus r_p for a given earthquake, intensity, and period. The second figure shows the residual displacements normalized by yield displacement versus r_p for the same earthquake, intensity, and period. In the residual displacement figures, the resulting values are a sort of pseudo ductility demand, which will be called normalized residual displacement. It is instructive to plot the residual displacements in this manner, because a 4 in. residual displacement in a structure with a yield displacement of 0.5 in. is much more severe than a residual displacement of 4 in. in a structure with a yield displacement of 8 inches.

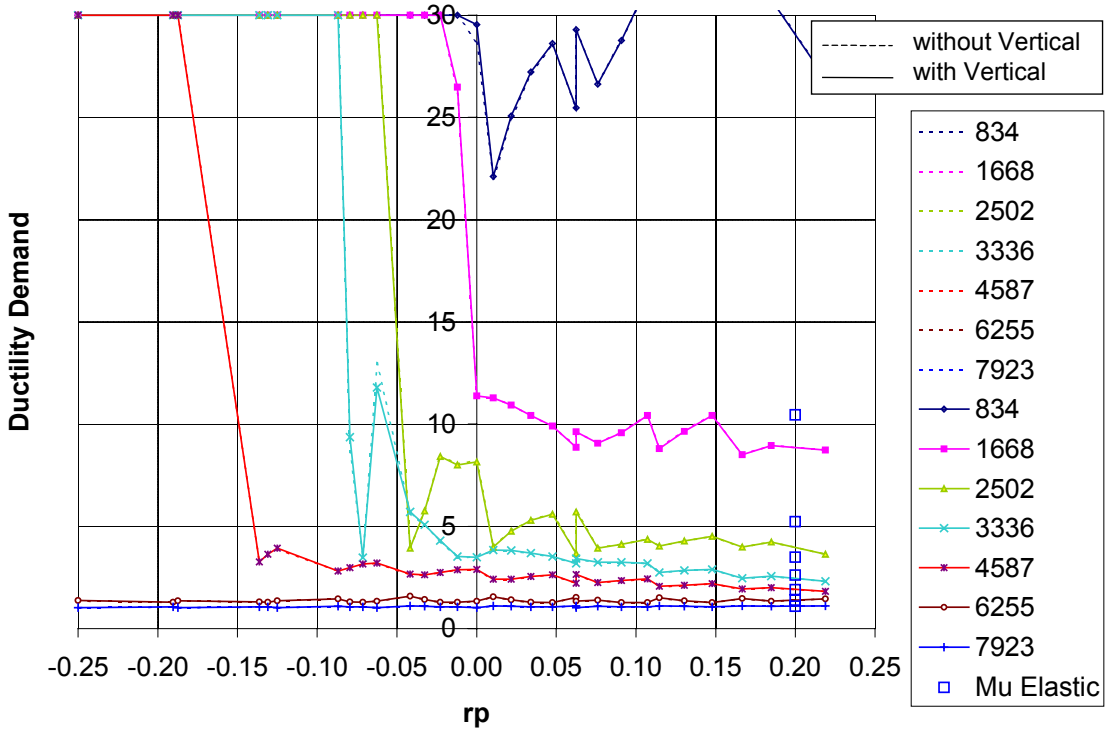

Figure 5.13a – EQ1, Lateral Scale = 0.4 g, Ductility Demand Versus r_p for Models with a Period of 0.903 Seconds.

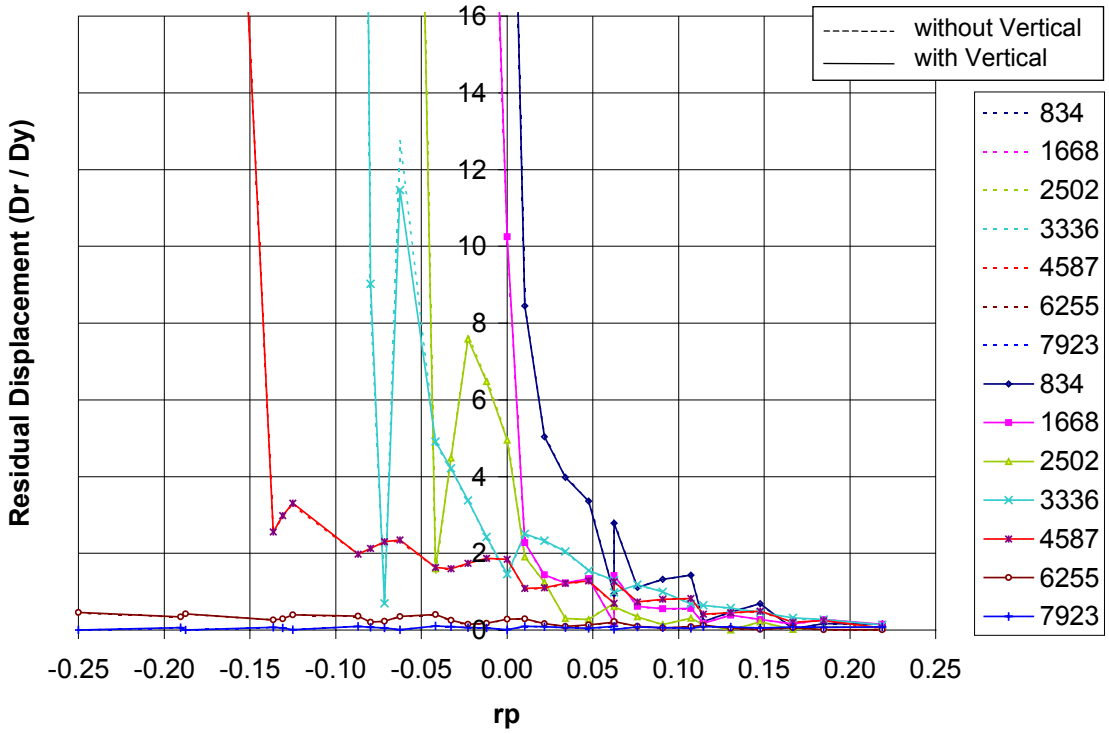

Figure 5.13b – EQ1, Lateral Scale = 0.4 g, Ratio of Residual Displacement to Yield Displacement Versus r_p for Models with a Period of 0.903 Seconds.

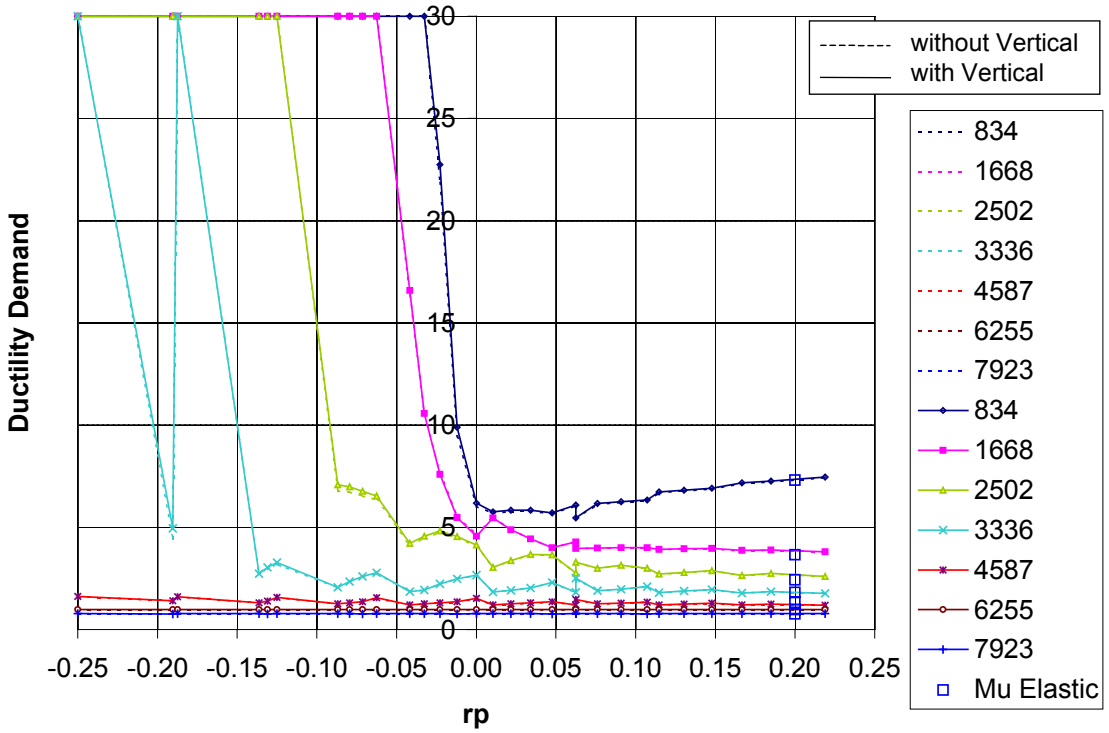

Figure 5.14a – EQ4, Lateral Scale = 0.2 g, Ductility Demand Versus r_p for Models with a Period of 1.093 Seconds.

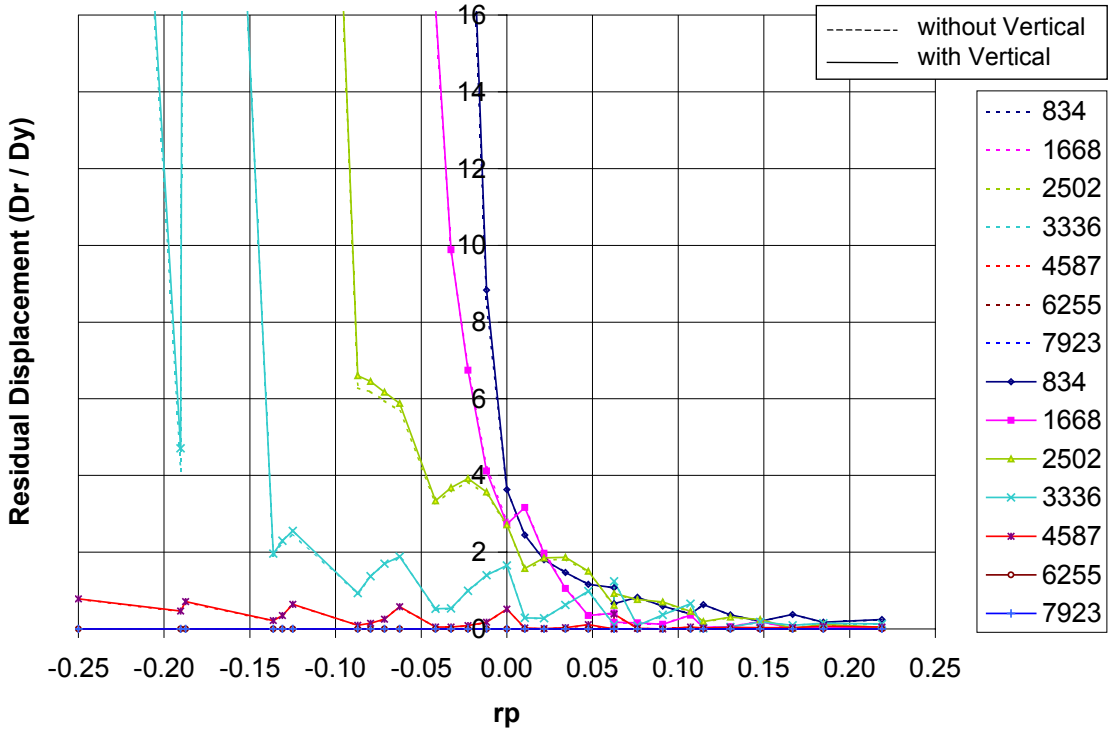

Figure 5.14b – EQ4, Lateral Scale = 0.2 g, Ratio of Residual Displacement to Yield Displacement Versus r_p for Models with a Period of 1.093 Seconds.

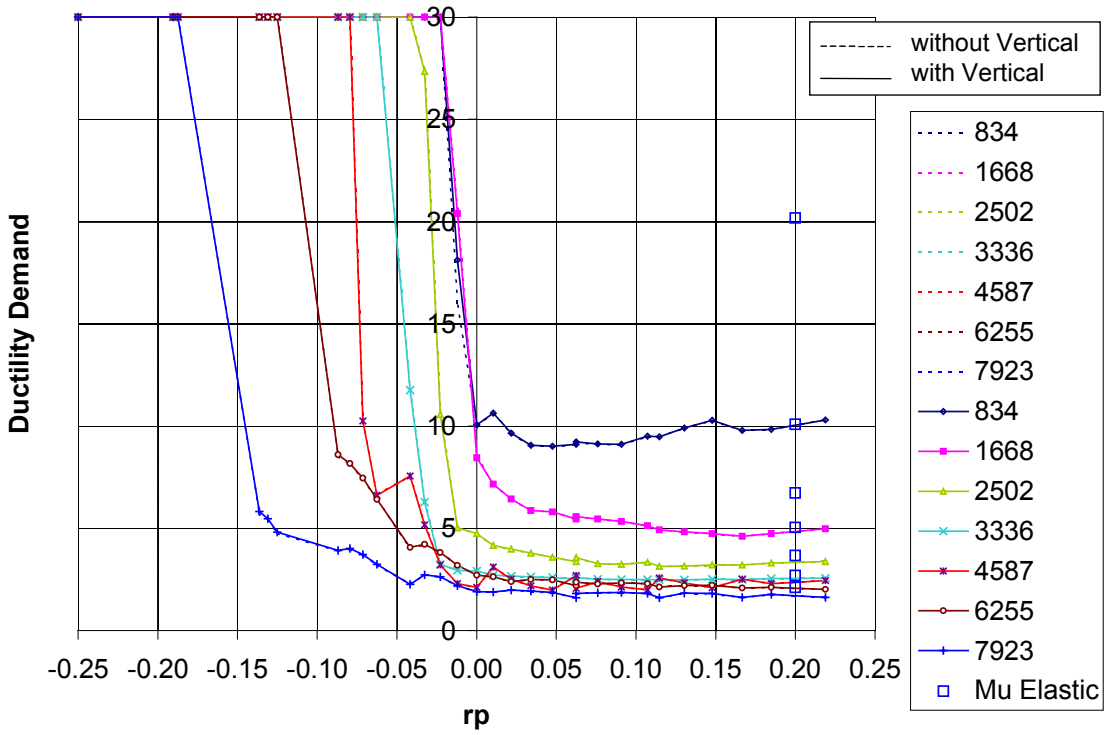

Figure 5.15a – EQ5, Lateral Scale = 0.4 g, Ductility Demand Versus r_p for Models with a Period of 1.093 Seconds.

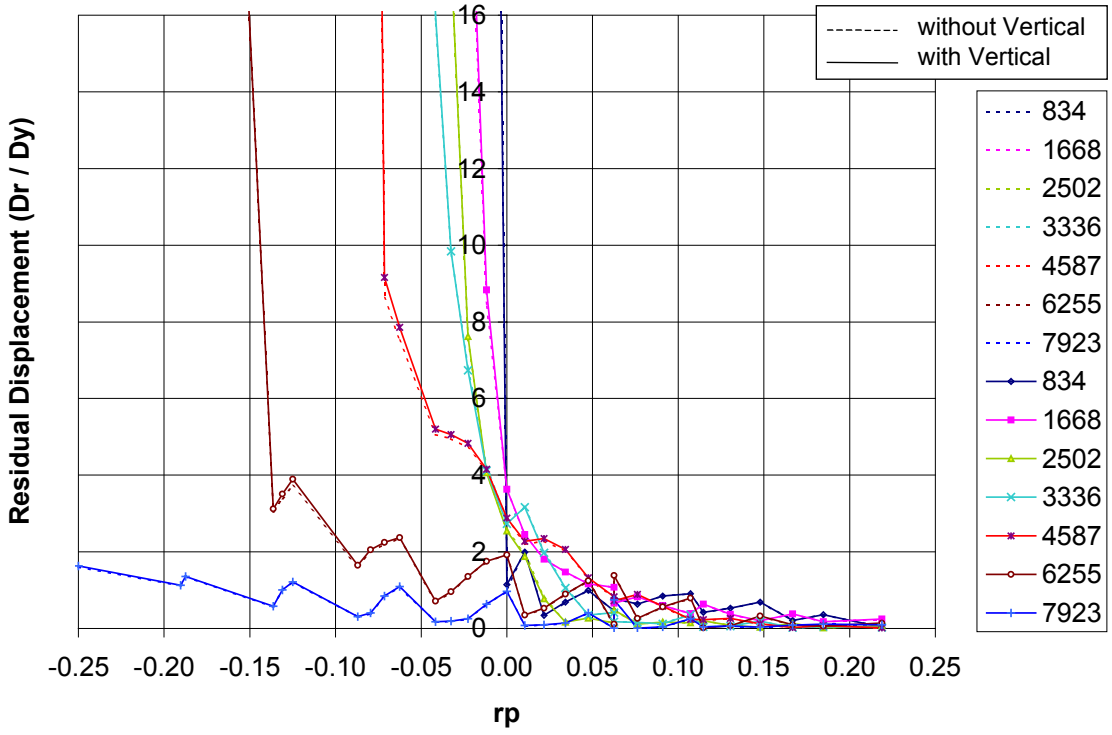

Figure 5.15b – EQ5, Lateral Scale = 0.4 g, Ratio of Residual Displacement to Yield Displacement Versus r_p for Models with a Period of 1.093 Seconds.

It is clear from Figures 5.13b, 5.14b, and 5.15b that r_p is related to residual displacements and consequently to the normalized residual displacements as well. However, the relationship between r_p and residual displacements is slightly different than the relationship between r_p and maximum displacements. Notice for example, that in the ductility demand figures, 5.13a, 5.14a, and 5.15a, the positive r_p ductility demand is for the most part constant. The ductility demand remains constant until a particular negative r_p value, where it increases drastically for small negative changes in r_p. In contrast, Figures 5.13b, 5.14b, and 5.15b show that the normalized residual displacements are small for r_p values of 0.25 and that they gradually increase for decreasing r_p values up to the point of collapse. The normalized residual displacements are not constant for positive r_p.

In regard to post earthquake stability, as the r_p values decrease, the residual displacements increase, which would adversely affect the post earthquake stability of a structure. As the normalized residual displacement figures show, the normalized residual displacements can be as high as two or three, even at a positive r_p value of 0.05. Physically, this means that a structure with a slightly better than elastic, perfectly plastic pushover curve would have permanent drifts that were twice their yield displacements. If such a structure were not in jeopardy of collapse, it at least would need to be torn down due to excessive damage.

Vertical accelerations were also considered in Figures 5.13a-b, 5.14a-b, and 5.15a-b. The vertical accelerations do tend to influence the residual displacements, but from the above figures it does not seem that the influence is very great. The influence of vertical accelerations will be addressed specifically later.

5.4 - Effects of Earthquake Parameter Variation on Maximum Displacements and Residual Displacements

Earthquake parameters were included by way of multiple earthquakes, multiple lateral and vertical scales, and including or excluding vertical accelerations. For the parameter study, eight earthquakes were used. This provided a broad range of responses for comparison. In this section, the effects of lateral ground motion scaling will be

discussed first. Then the effects of including and excluding vertical accelerations will be discussed. Finally, the effects of vertical ground motion scale will be presented.

5.4.1 – Effects of Lateral Acceleration Motion Scale on Collapse and Residual Displacements

The effects of lateral ground motion scale have been briefly discussed in the previous sections, but have not yet been formally addressed. First, to summarize what has already been said from the study of individual parameters on collapse, it was shown that as the lateral ground motion intensity increases, the number of collapses proportionally increases. Then, in the multiple parameter section, it was shown that as the lateral earthquake intensity increases, the ductility demand increases, which causes the collapse r_p to shift toward the positive direction. To more fully illustrate the increase in ductility demand and collapse r_p shift, Figures 5.16a through 5.16d show ductility demands for increasing earthquake intensity. It is important to note that for each subsequent figure, the lateral ground motion intensity increases by 0.1g.

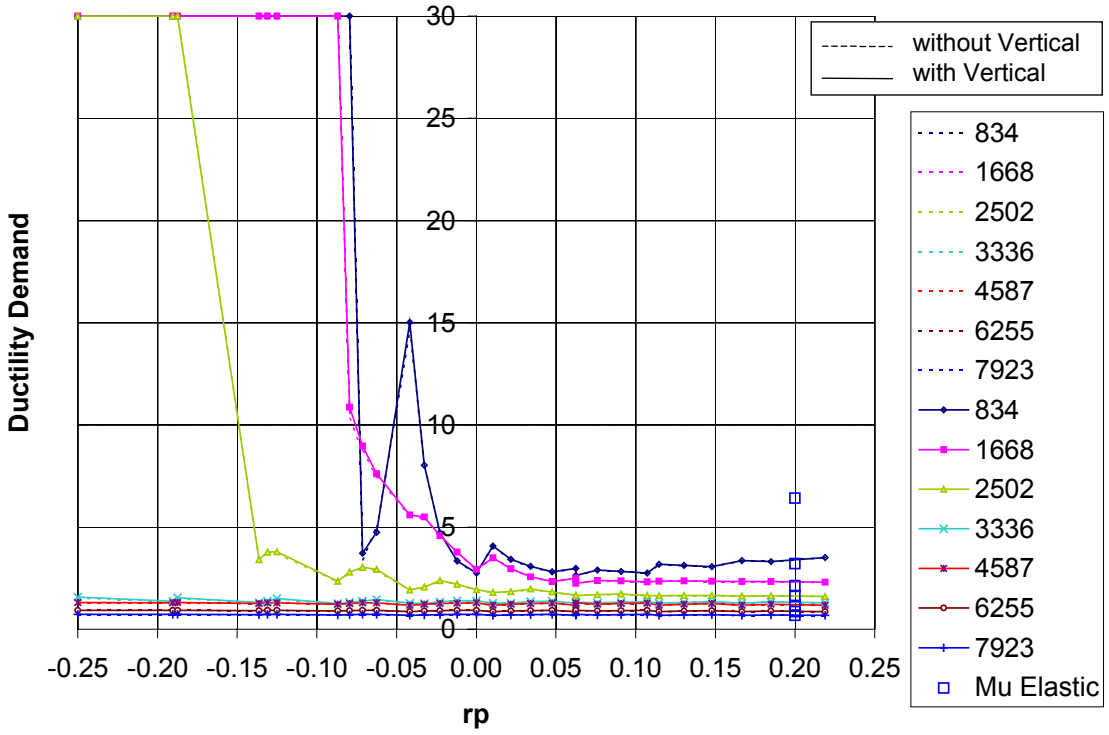

Figure 5.16a – EQ3, Lateral Scale = 0.1 g, Ductility Demand Versus r_p for Models with a Period of 0.903 Seconds.

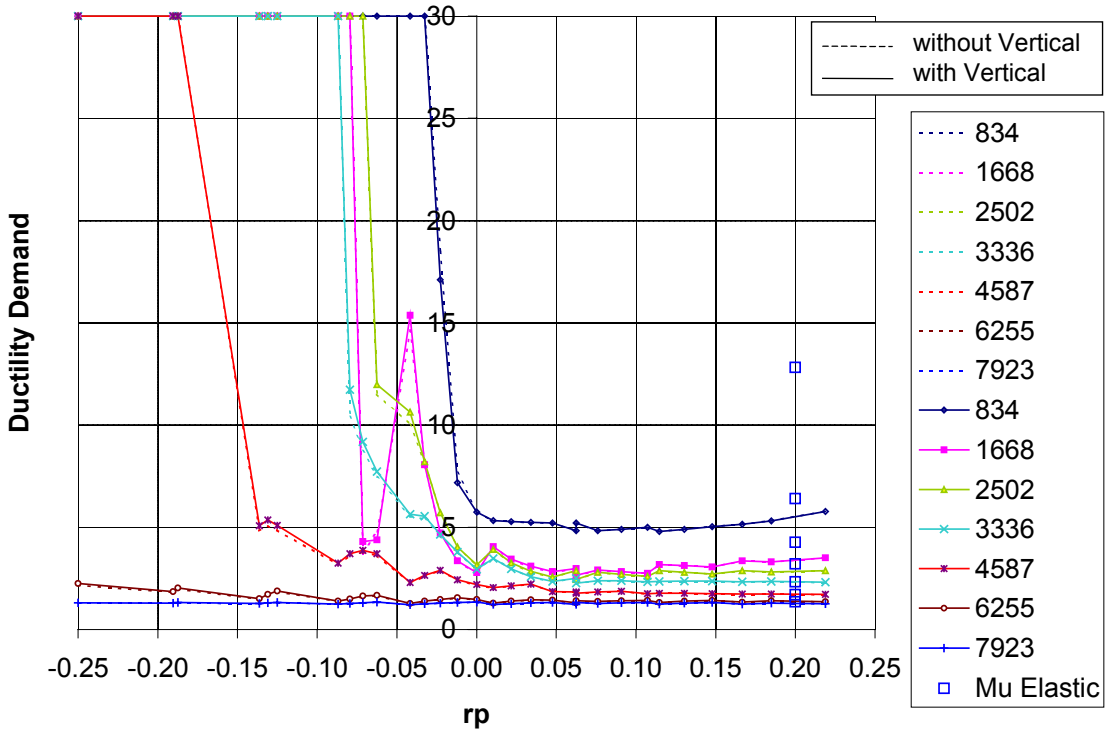

Figure 5.16b – EQ3, Lateral Scale = 0.2 g, Ductility Demand Versus r_p for Models with a Period of 0.903 Seconds.

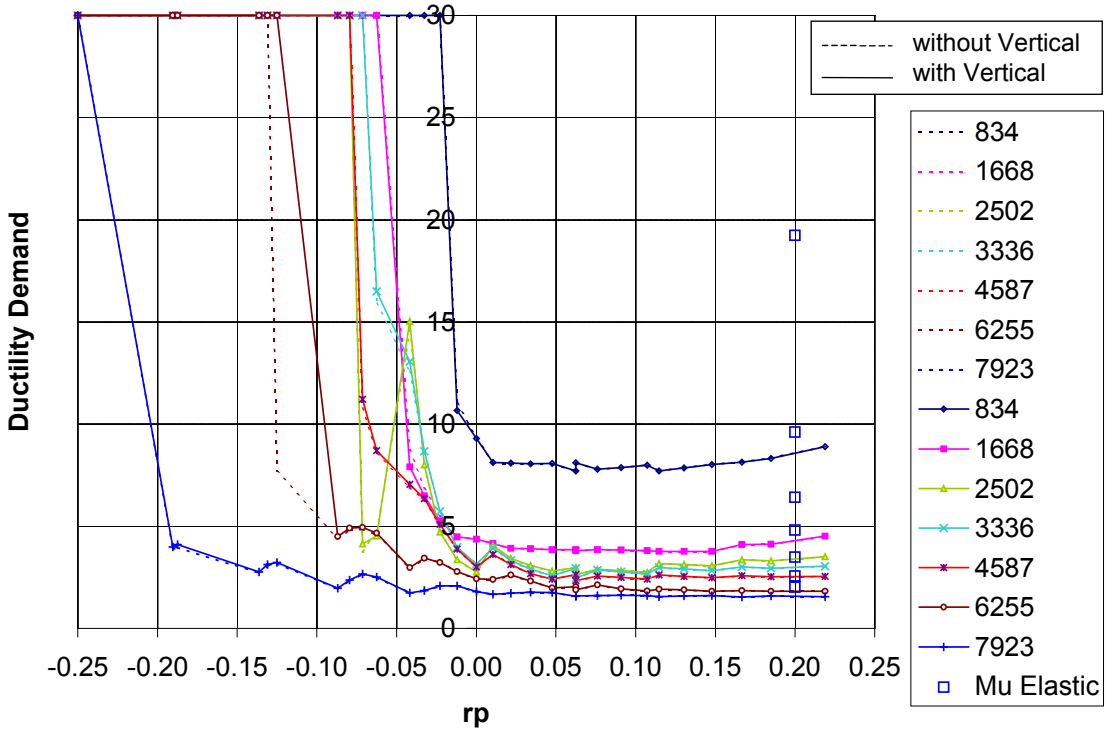

Figure 5.16c – EQ3, Lateral Scale = 0.3 g, Ductility Demand Versus r_p for Models with a Period of 0.903 Seconds.

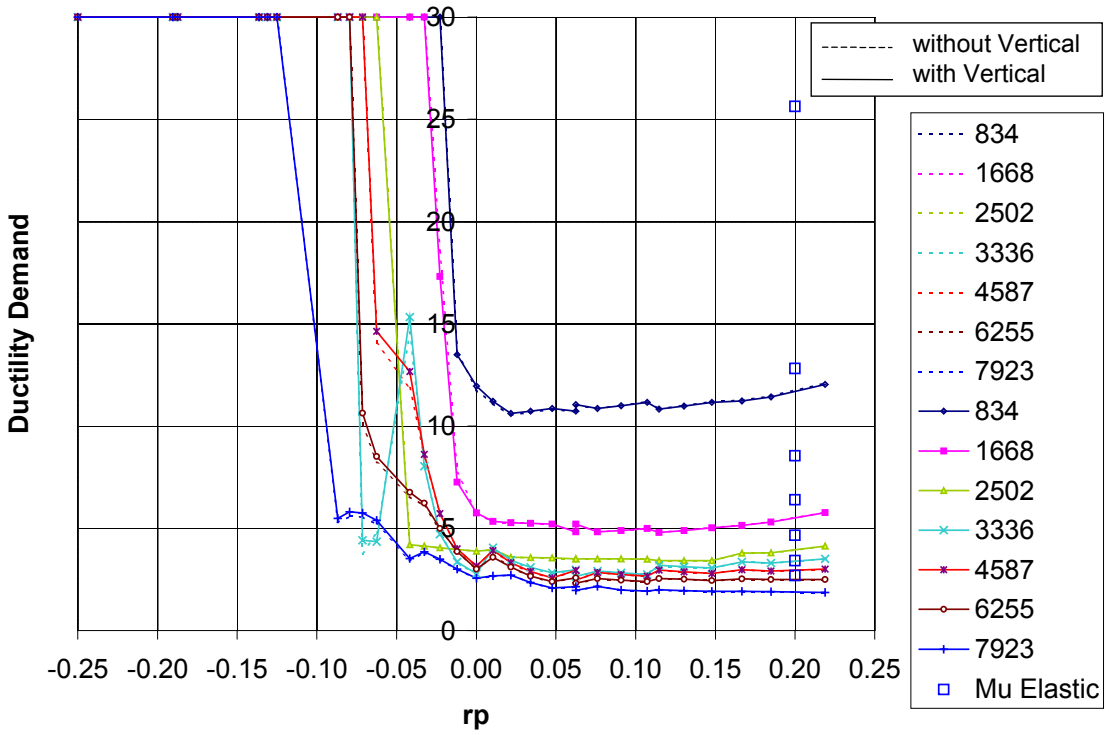

Figure 5.16d – EQ3, Lateral Scale = 0.4 g, Ductility Demand Versus r_p for Models with a Period of 0.903 Seconds.

In Figures 5.16a through 5.16d, notice that the collapse r_p for a given yield moment gets smaller (approaches zero) as the PGA increases. Also notice that the ductility demand increases for increasing PGA. These observations have been made previously, but the additional lateral scales more completely reinforce the previous observations. One new observation about the above figures is that the curves seem to keep the same shapes, but shift to different yield strengths. This observation is seen most clearly in the spike that occurs at an r_p of about -0.05. The spike occurs in higher yield moment curves as the PGA increases. For 0.1 g, the spike occurs in the models with a yield moment of 834 kip-in (Fy = 0.03W). For 0.2 g, the spike occurs in the models with a yield moment of 1668 kip-in (Fy = 0.06W). Another example of the shape carry over is seen in the hump that occurs at about –0.075 r_p. The hump is first seen in the 2502 kip-in (Fy = 0.09W) curve of the 0.1 g Figure (5.16a). It is next seen in Figure 5.16b in the 4587 kip-in (Fy = 12.5W) curve. The shape carry over was not explicitly examined in this study, but there seems to be a relationship between the shape of the curves, displacement demand, and yield force, or perhaps yield displacement.

Another observation about the shape of the curves is that some of the curves are jagged rather than smooth. It is difficult, without further investigation, to pinpoint the specific causes of the jaggedness. It is possible that the jaggedness is due to the randomness of the earthquakes. However, the jaggedness frequently occurs at the same r_p values for all yield moments. This would seem to indicate that the jaggedness is due to either the post-yield stiffness ratio or the stability ratio. Since the stability ratio affects the stiffness of a model and consequently the period of a model, it is reasonable that the jaggedness is caused by the fluctuations in period resulting from changes in the stability ratio. Further investigation is required on this subject, however.

The residual displacements were examined in a manner similar to the maximum displacements. In Figures 5.17a through 5.17d, the only difference between each figure is the lateral ground motion scale.

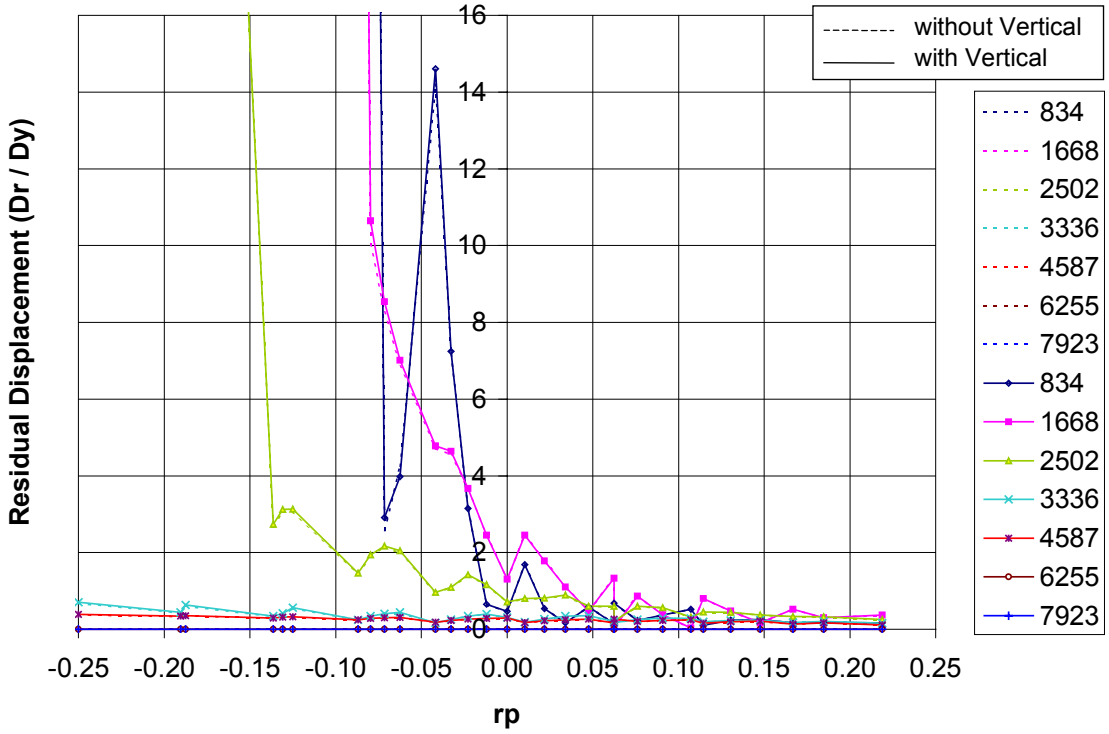

Figure 5.17a – EQ3, Lateral Scale = 0.1 g, Ratio of Residual Displacement to Yield Displacement Versus r_p for Models with a Period of 0.903 Seconds.

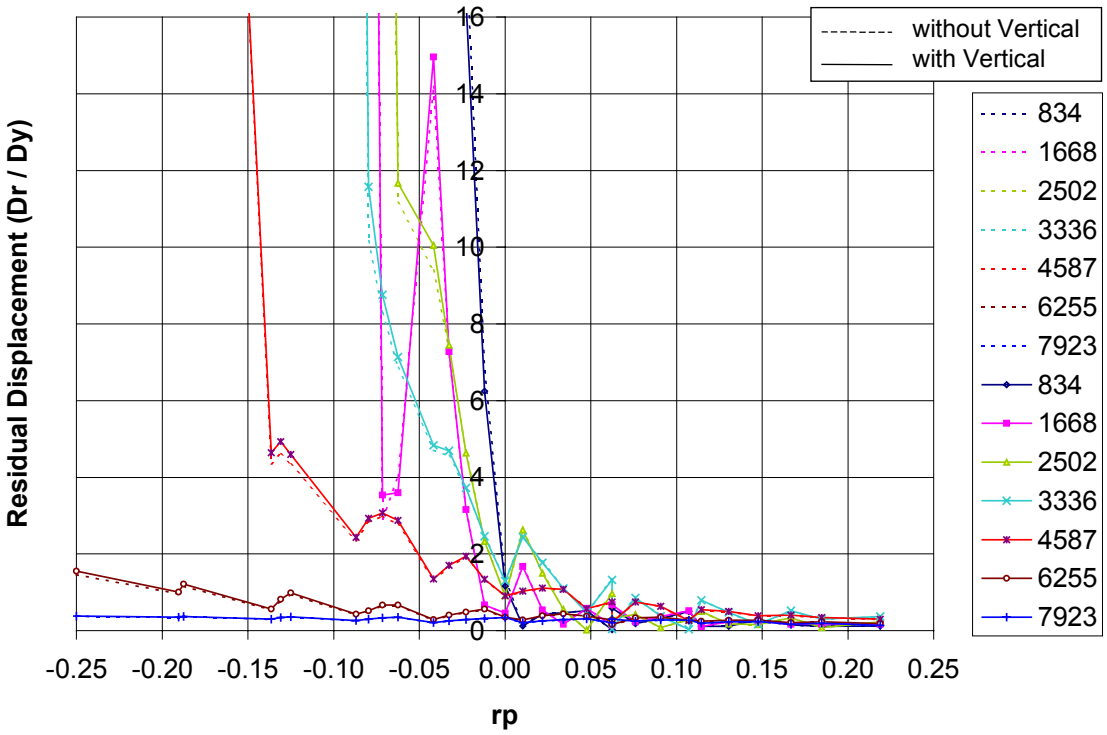

Figure 5.17b – EQ3, Lateral Scale = 0.2 g, Ratio of Residual Displacement to Yield Displacement Versus r_p for Models with a Period of 0.903 Seconds.

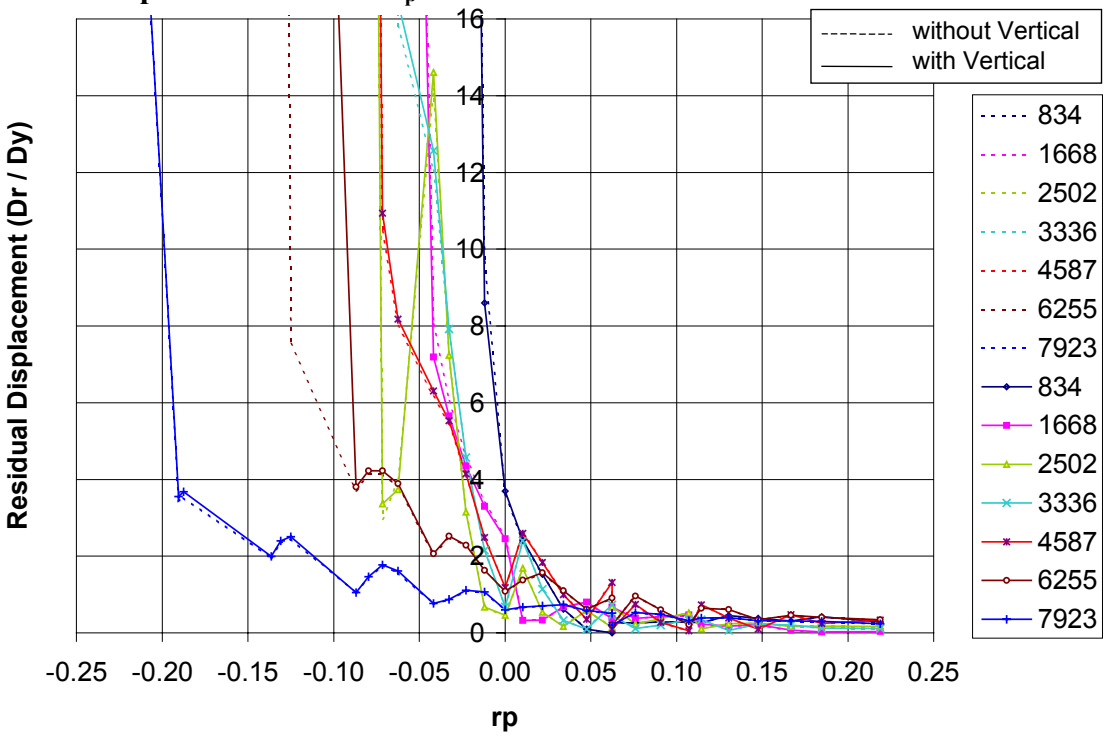

Figure 5.17c – EQ3, Lateral Scale = 0.3 g, Ratio of Residual Displacement to Yield Displacement Versus r_p for Models with a Period of 0.903 Seconds.

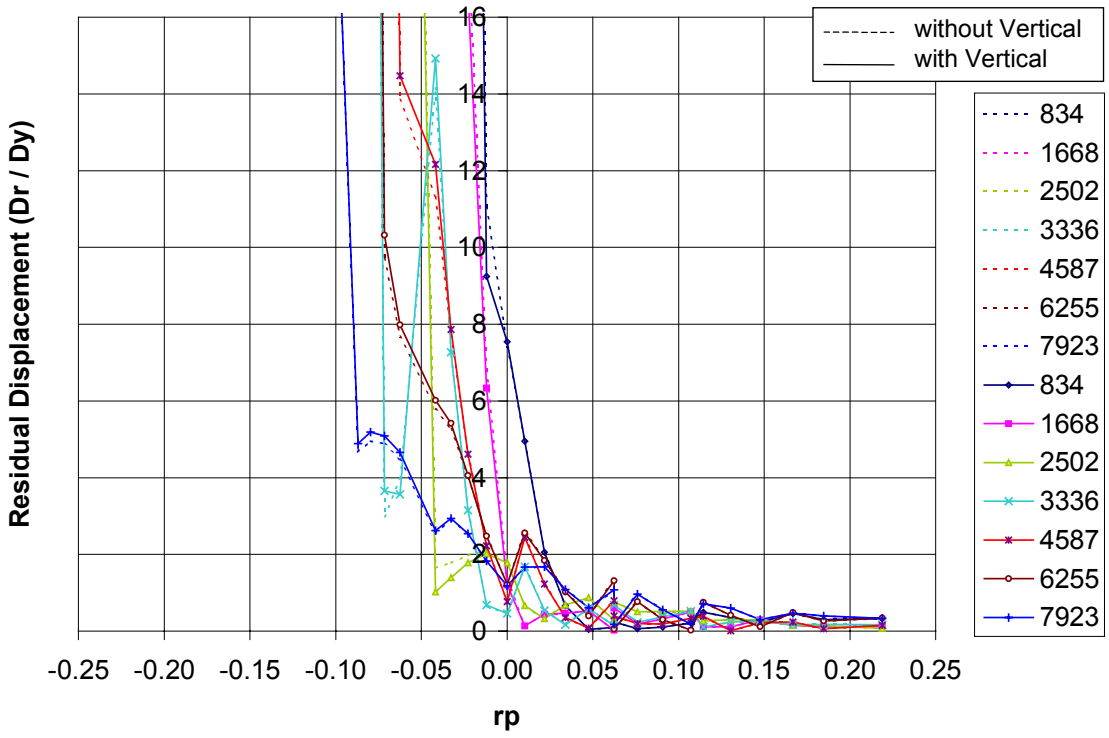

Figure 5.17d – EQ3, Lateral Scale = 0.4 g, Ratio of Residual Displacement to Yield Displacement Versus r_p for Models with a Period of 0.903 Seconds.

As has already been mentioned, the residual displacements begin to accumulate as the r_p values decrease. For lower earthquake intensities, only those structures with lower yield moments accumulate residual displacements. This is because the higher yield moment structures have higher yield displacements and thus have very few, if any, inelastic excursions. As the intensity increases, though, the displacement demands increase and consequently more models with higher yield strengths have large inelastic excursions. Thus, earthquake intensity influences residual displacements in that an earthquake must cause a certain amount of inelasticity before residual displacements will begin to accumulate. From all of the data is seems that a structure generally must have a ductility demand of at least 1.75 for residual displacements to accumulate.

From the above figures, it does seem that there is a limit to the amount of residual displacement that a structure would incur. Hardly any residual displacements accumulate, regardless of earthquake intensity, for r_p values greater than about 0.15. As the r_p values decrease and approach zero, the residual ductility demand approaches three or four. This also is relatively independent of earthquake intensity. Once the r_p value

becomes negative, the structures that were accumulating residual displacements in the positive r_p region quickly collapse.

As with the maximum displacements, the general shapes of the curves tend to carry over to other yield strengths. There is also jaggedness in the curves as with maximum displacements. Once again, it is probable that this variation is due to fluctuations in the period due to varying stability ratios.

To summarize what has just been said, for a given earthquake and period, the residual displacements are heavily dependent on r_p. Residual displacements generally accumulate for decreasing r_p. Structures that are likely to accumulate residual displacements will have ductility demands of at least 1.75. Of the structures that accumulate residual displacements, the ductility demand, which is dependent on earthquake intensity and yield displacement, may influence the residual displacements slightly, but the r_p value has a greater influence. For r_p values greater than 0.15, residual displacements will be small. For r_p values decreasing from 0.15 toward zero, the normalized residual displacements will approach between four and six. For negative r_p, the residual displacements get very high. Many structures with negative r_p values would be in danger of collapsing during the earthquake, which would make post earthquake stability a moot point.

5.4.2 – Effects of Including or Excluding Vertical Accelerations on Collapse and Residual Displacements

From the literature survey, it is clear that the influence of vertical accelerations on lateral displacements is debatable. To explore this issue, each of the structural parameter combinations and earthquake combinations used in the parameter study were analyzed once excluding vertical accelerations and once including vertical accelerations. Many of the figures used above (5.7a-c, 5.8a-c, 5.13a-b, 5.14a-b, 5.15a-b, 5.16a-d, 5.17a-d) have curves that show the effects of including and excluding vertical accelerations. While it is possible to visually see the influence of vertical accelerations in the aforementioned figures, it is more instructive to specifically examine the change in ductility demand that results from the inclusion of vertical accelerations. Figures 5.18a through 5.18d show the

changes in ductility demands that result from including vertical accelerations. In Figures 5.18a through 5.18d, there are two vertical axes corresponding to two different sets of data. The vertical axis toward the right of each figure is the ductility demand of the structures. The title of this axis has been boxed with a dashed line to indicate that it applies to the dashed line data. The thin dashed line data represents the maximum ductility demands excluding vertical accelerations. Then, the middle axis plots the change in ductility demand that comes from adding vertical accelerations. The title for this axis is on the left-hand side of the figures and is boxed with a heavy solid line to indicate that it applies to the heavy solid line data. It is important to note that the absolute value of the change in ductility demand has been plotted in the Figures 5.18a through 5.18d. This is because it is impossible beforehand to know whether vertical accelerations will increase or decrease lateral displacements, and if a structure shows sensitivity to vertical accelerations, then it is possible that vertical accelerations would be detrimental given the right earthquake. As will be shown later, vertical accelerations increased the lateral displacements about half the time and about half the time it decreased them.

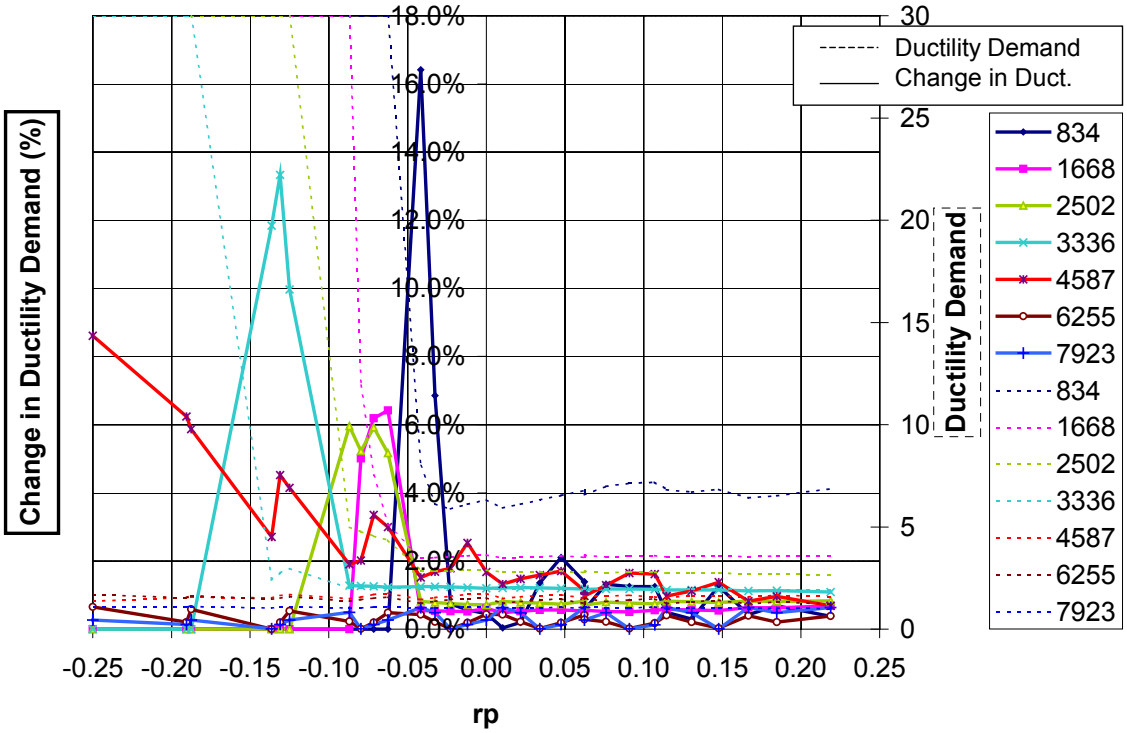

Figure 5.18a – EQ6, Lateral Scale = 0.2 g, Change in Ductility Demand Due to the Inclusion of Vertical Accelerations for Models with a Period of 1.459 Seconds.

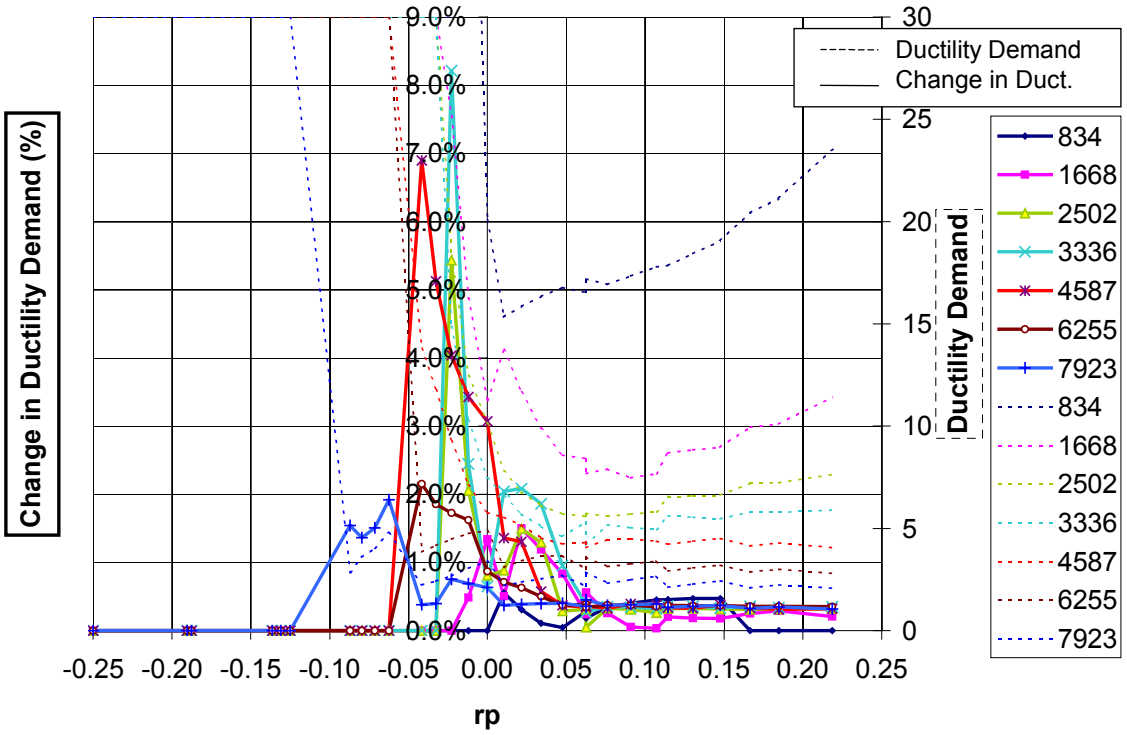

Figure 5.18b – EQ3, Lateral Scale = 0.4 g, Change in Ductility Demand Due to the Inclusion of Vertical Accelerations for Models with a Period of 0.705 Seconds.

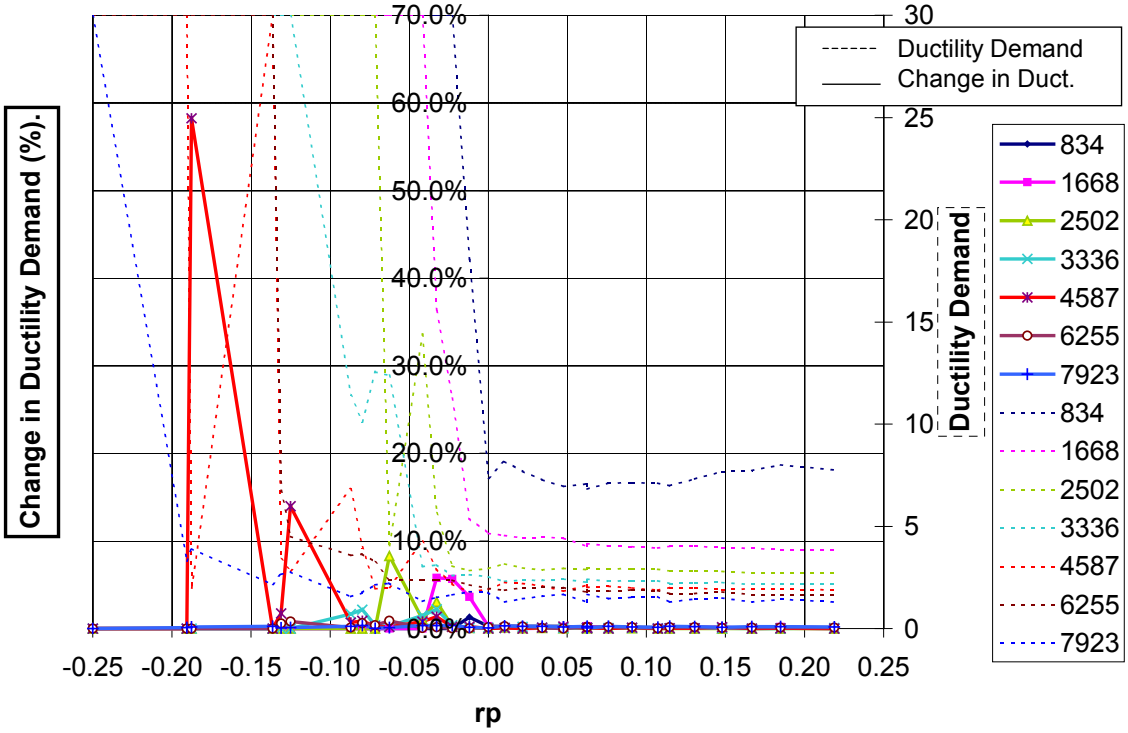

Figure 5.18c – EQ5, Lateral Scale = 0.4 g, Change in Ductility Demand Due to the Inclusion of Vertical Accelerations for Models with a Period of 1.278 Seconds.

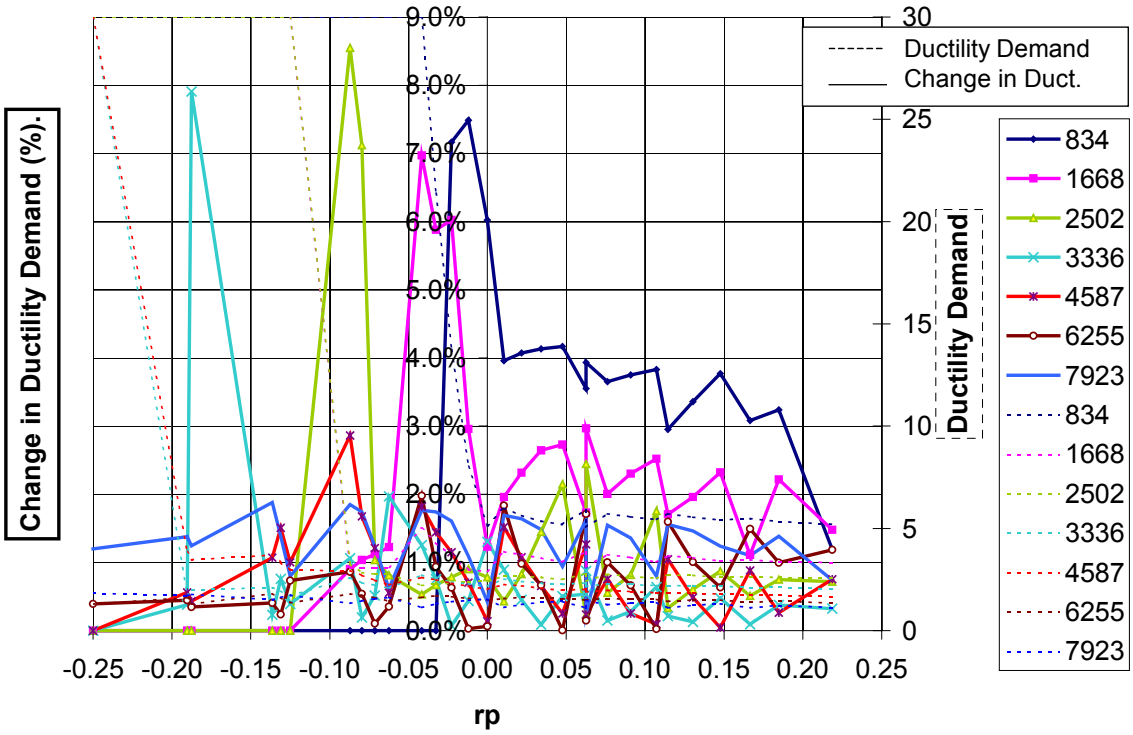

Figure 5.18d – EQ7, Lateral Scale = 0.4 g, Change in Ductility Demand Due to the Inclusion of Vertical Accelerations for Models with a Period of 1.635 Seconds.

Figures 5.18a through 5.18d were chosen as a representative sample of all of the parameter study data. Various earthquakes, intensities, and periods are shown. From the above data, several observations can be made. First, vertical accelerations did not significantly affect the lateral displacements until just before the point of collapse. For the purposes of this discussion, if the change in ductility demand was greater than about five percent, then it will be considered significant. In all four of the figures above, a spike in the change in ductility demand curves, if there was a spike, occurred in the negative r_p range just before collapse. Secondly, when the vertical accelerations did significantly affect the lateral displacements, it was generally not by more than about ten percent. There were a few cases where the change in ductility demand was much greater, Figure 5.18c for example, but that was not the norm. Third, it seems that the increase in lateral displacements is only dependent on the collapse r_p. The individual earthquakes did not have much effect on overall lateral displacement increases due to vertical accelerations. The results of four different earthquakes are shown in Figures 5.18a through 5.18d as evidence. Also, the lateral scale did not influence the amount of change

that vertical accelerations caused. In Figure 5.18a, the models were subjected to earthquake six at a lateral PGA scale of 0.2g and the average ductility demand increases caused by vertical accelerations were around ten or twelve percent, which is relatively close to the results from the other figures which had PGAs of 0.4 g. From the data of this study, it would seem that vertical accelerations do not significantly affect the lateral displacements unless the structure is near collapse. Even then, the change in lateral displacements due to vertical accelerations is on average around ten percent.

While the change in lateral displacements was relatively small, a small change could be enough to cause collapse in a building. The additional ductility demand may be just enough to fracture a critical steel connection or crush the concrete at a critical joint. To address this possibility, another set of figures was created that defined collapse as an increase greater than a specified value. Moreover, in the same figures, a structure was considered "saved" if the ductility demands decreased by a specified amount. In the figures, the number of collapses was plotted in the positive direction and the number of saves was plotted in the negative direction. This was done just to create a visual distinguishing effect for the collapses and saves. Furthermore, three changes in ductility demand values were used to determine collapses and saves, 0.5, 1.0, and 2.0. Several representative plots of the aforementioned collapse criteria are shown in Figures 5.19a through 5.19d.

One thing to keep in mind about the collapse and save figures is that the total numbers of collapses and saves represent 1470 analyses. Thus, if 20 collapses occurred for a given set of models, then 1.4 percent of the models in the set would have collapsed. This is not said to minimize the potential hazards of vertical accelerations, but to make sure that vertical accelerations are reasonably considered.

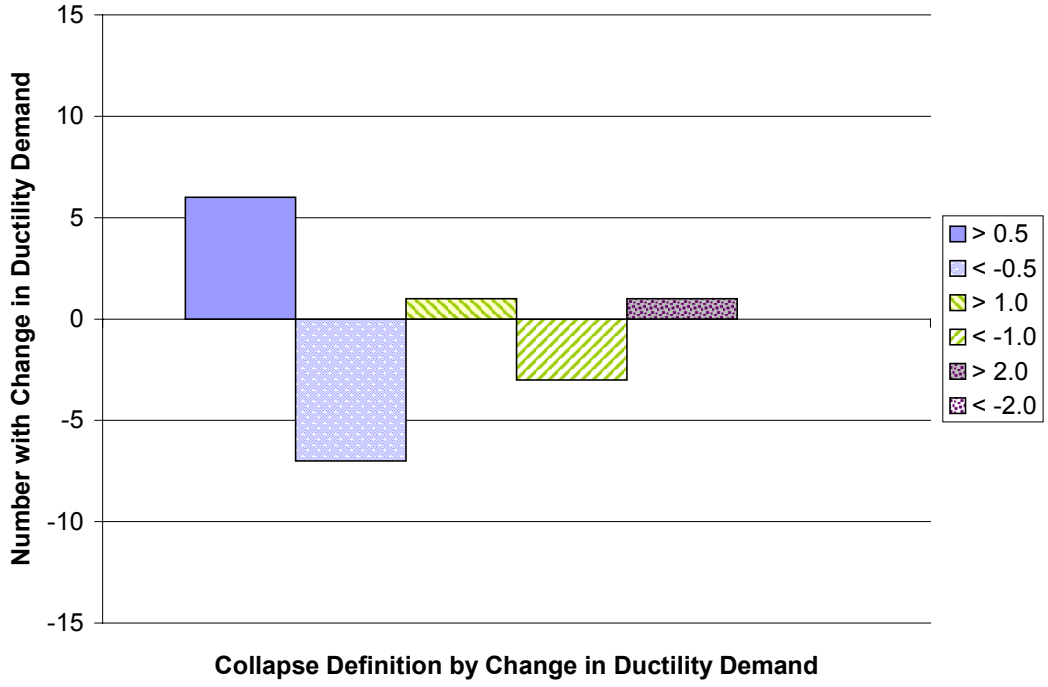

Figure 5.19a – Collapses and Saves Due to the Inclusion of Vertical Accelerations for the Set of Models Subjected to EQ 3 with a Lateral Scale of 0.2 g and a Vertical Multiplier of 1.5.

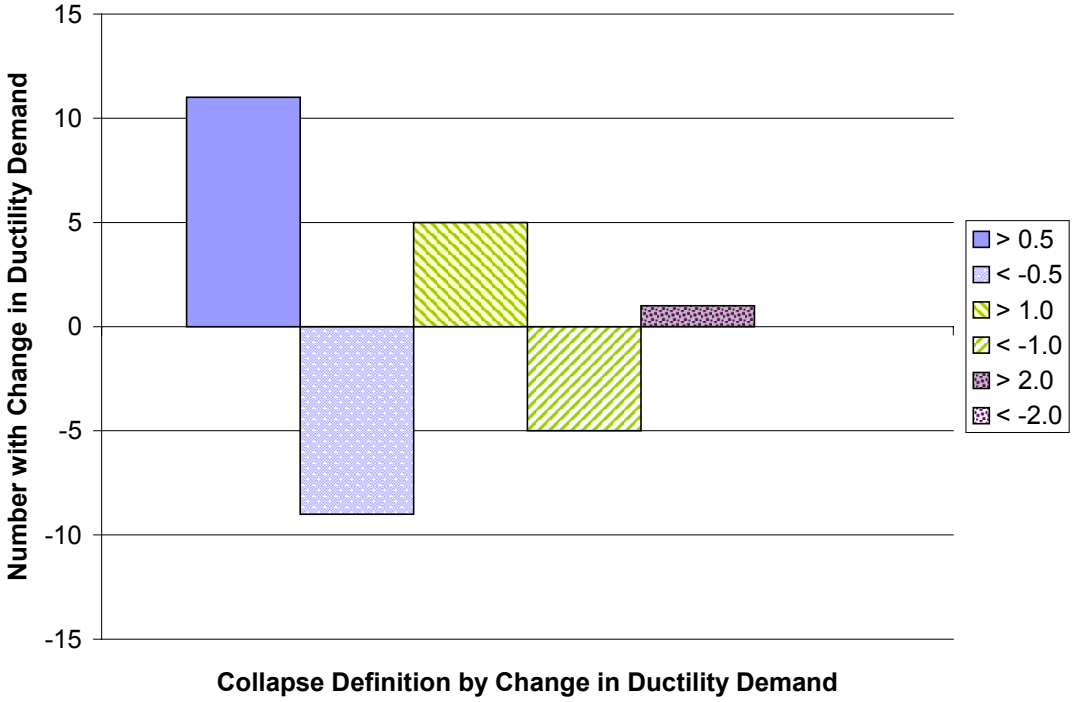

Figure 5.19b – Collapses and Saves Due to the Inclusion of Vertical Accelerations for the Set of Models Subjected to EQ 3 with a Lateral Scale of 0.2 g and a Vertical Multiplier of 2.5.

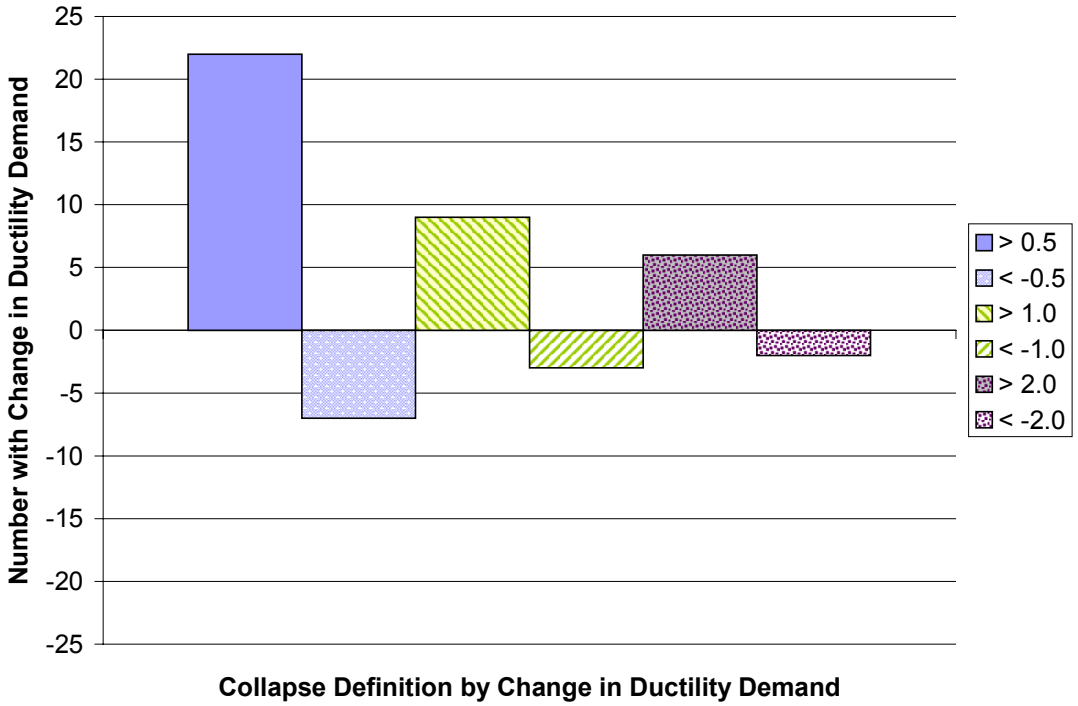

Figure 5.19c – Collapses and Saves Due to the Inclusion of Vertical Accelerations for the Set of Models Subjected to EQ 3 with a Lateral Scale of 0.4 g and a Vertical Multiplier of 2.5.

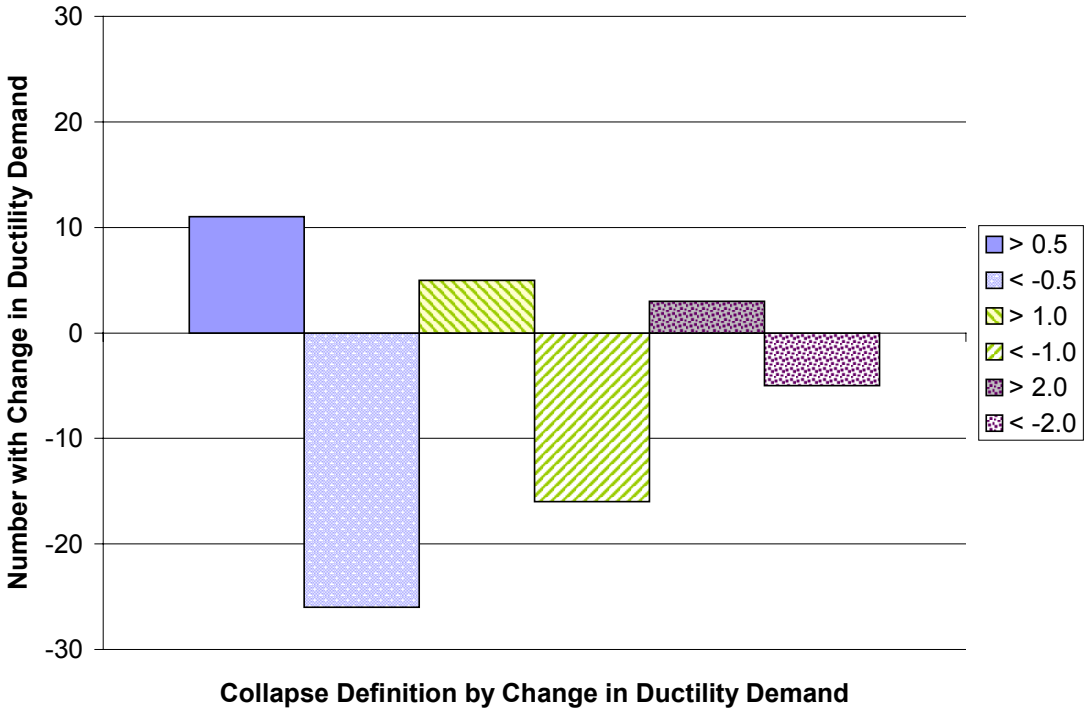

Figure 5.19d – Collapses and Saves Due to the Inclusion of Vertical Accelerations for the Set of Models Subjected to EQ 7 with a Lateral Scale of 0.4 g and a Vertical Multiplier of 2.5.

Before describing the data in Figures 5.19a through 5.19d, it is important to describe a characteristic of them. Each collapse or save category includes all of the values that pertain to it. For example, in Figure 5.19d, there were a total of eleven models for which the ductility demands increased by more than 0.5. There were not eleven models between 0.5 and 1.0 (the next category), but a total of eleven that were greater 0.5. Thus, all of the models with ductility demand increases greater than 1.0 would also be counted in the greater than 0.5 category.

From Figures 5.19a through 5.19d, it is clear that vertical accelerations would both cause structures to collapse as well as save structures from collapse in the sets of data considered. However, the numbers of collapses and saves varies from earthquake to earthquake. In Figure 5.19b, for example, there are approximately an equal number of collapses as there are saves. In Figure 5.19c, on the other hand, there are more collapses than saves. Then, in Figure 5.19d, there are more saves than collapses. This is why it was said earlier that it is impossible to predict beforehand the effects that vertical accelerations will have on a particular structure. There are too many factors that influence whether or not a structure's response will be altered by such accelerations.

Moreover, Figures 5.19a and 5.19b indicate that increasing the vertical accelerations increases both the number of collapses and saves. Thus, while is may not be clear before an analysis if the inclusion of vertical accelerations will cause a structure to collapse or be saved, it is clear that increasing the vertical acceleration magnitudes increases the probability that a collapse or save could occur.

Vertical accelerations also had an effect on residual displacements. The effects of vertical accelerations on residual displacements were examined in a manner similar to the examination of ductility demand increases shown in Figures 5.18a through 5.18d. Five representative examples of residual displacement changes due to the inclusion of vertical accelerations are shown in Figures 5.20a through 5.20e.

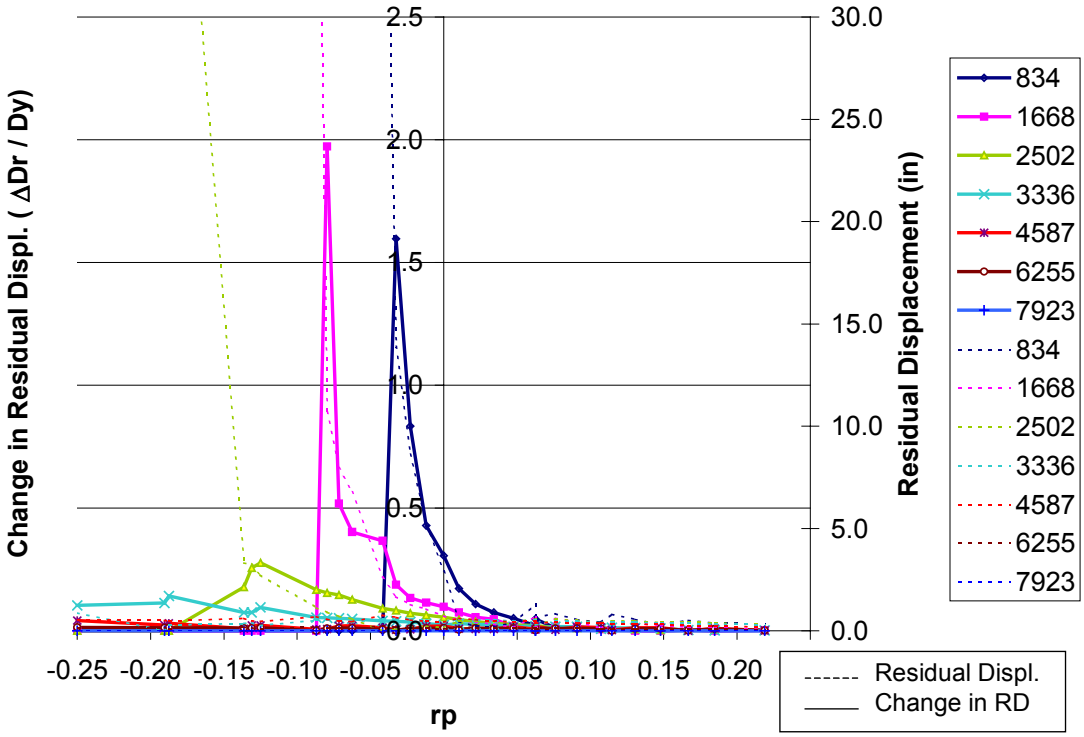

Figure 5.20a – EQ2, Lateral Scale = 0.2 g, Change in Residual Displacements Due to the Inclusion of Vertical Accelerations for Models with a Period of 0.903 Seconds.

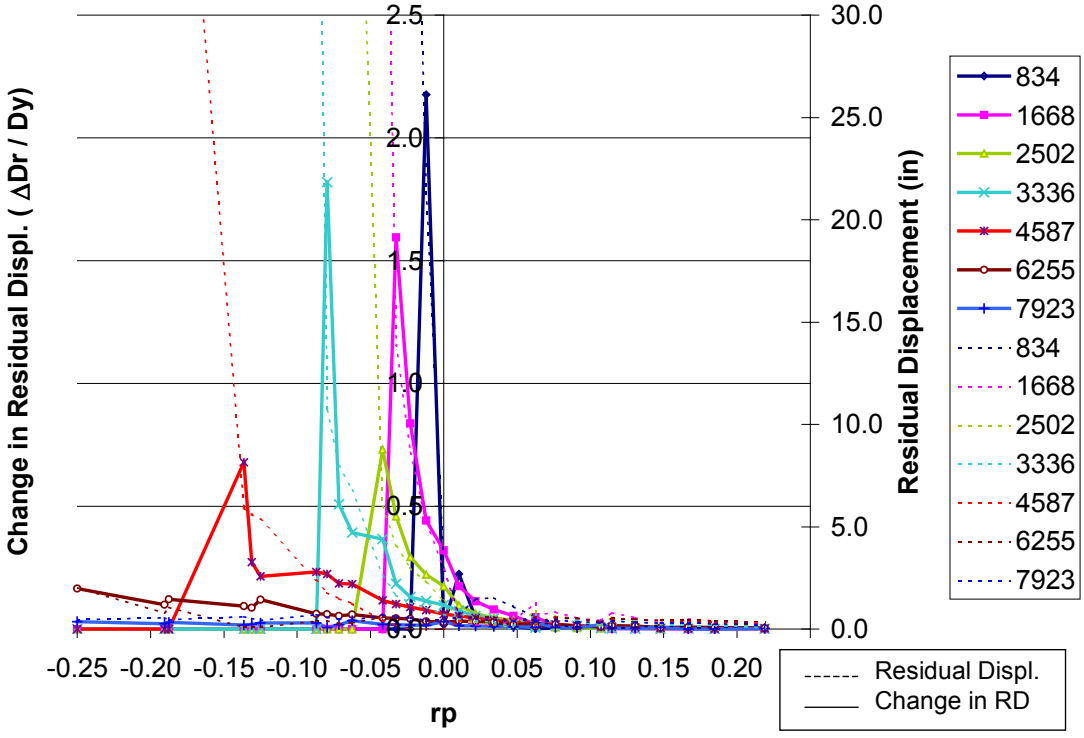

Figure 5.20b – EQ2, Lateral Scale = 0.4 g, Change in Residual Displacements Due to the Inclusion of Vertical Accelerations for Models with a Period of 0.903 Seconds.

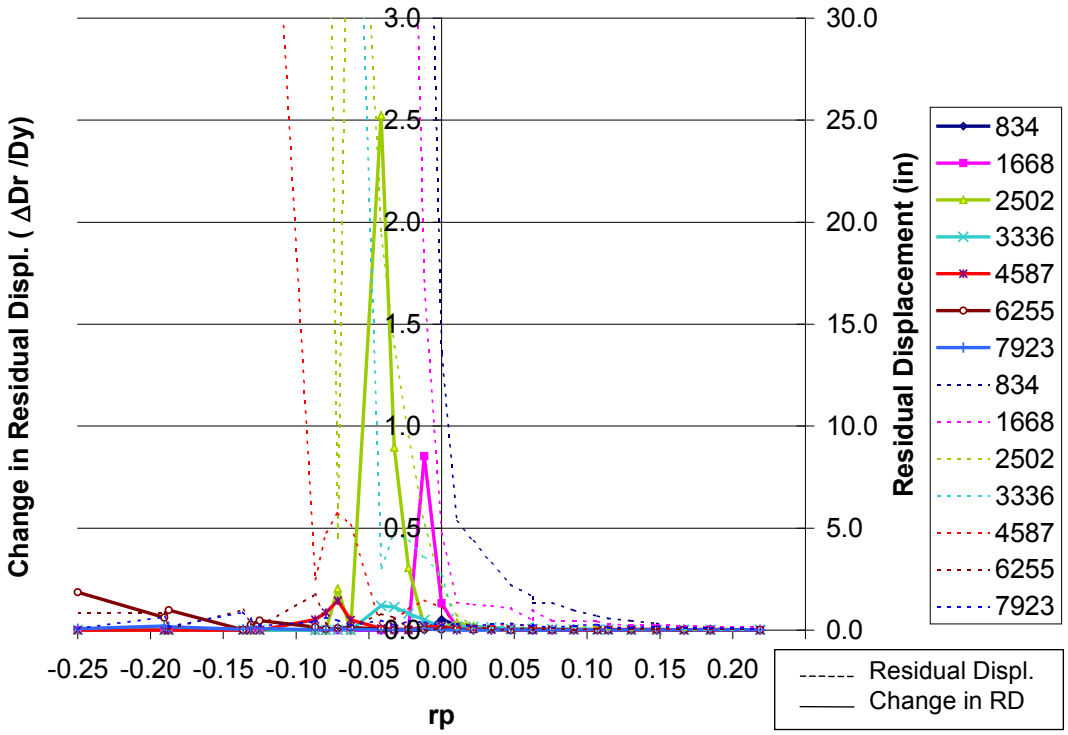

Figure 5.20c – EQ4, Lateral Scale = 0.2 g, Change in Residual Displacements Due to the Inclusion of Vertical Accelerations for Models with a Period of 0.705 Seconds.

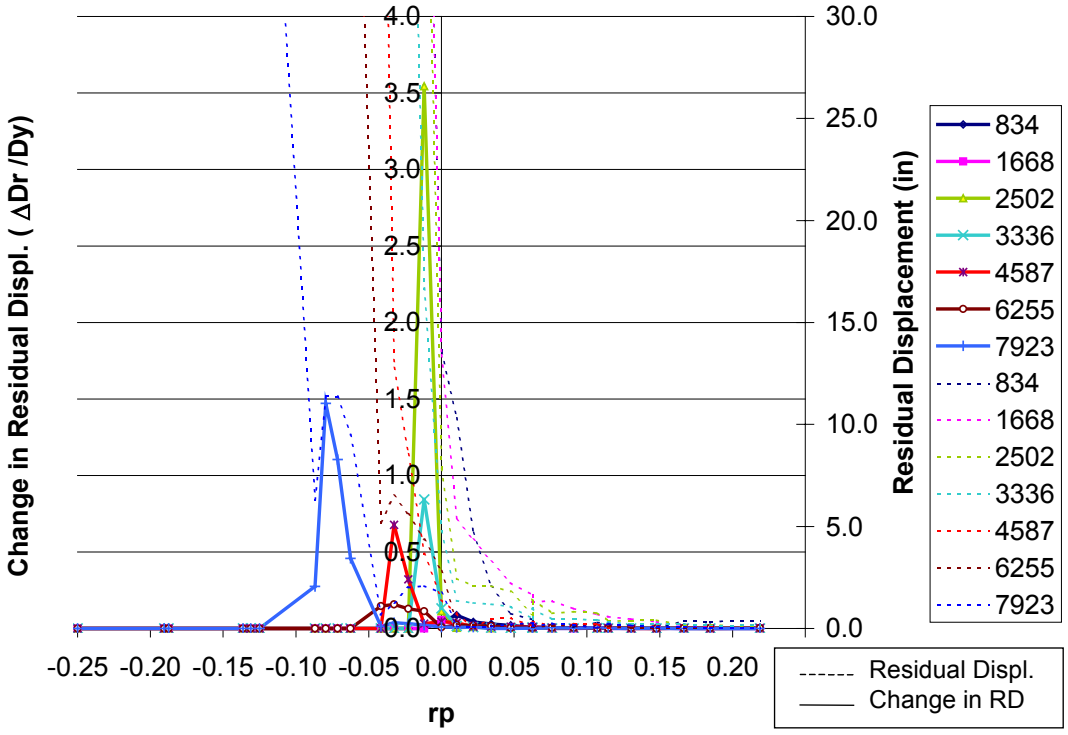

Figure 5.20d – EQ4, Lateral Scale = 0.4 g, Change in Residual Displacements Due to the Inclusion of Vertical Accelerations for Models with a Period of 0.705 Seconds.

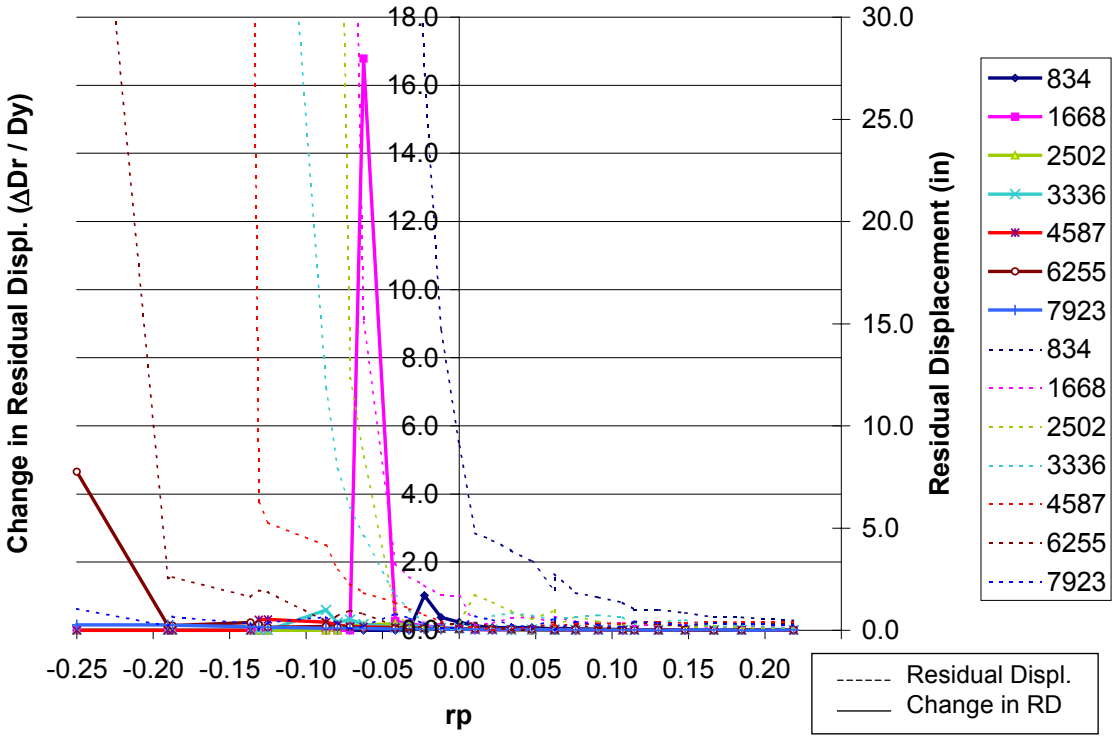

Figure 5.20e – EQ6, Lateral Scale = 0.4 g, Change in Residual Displacements Due to the Inclusion of Vertical Accelerations for Models with a Period of 1.635 Seconds.

Figures 5.20a through 5.20e are very similar to 5.18a through 5.18d, except that the right hand vertical axis plots residual displacement and the center axis plots the normalized change in residual displacement. As with the maximum displacements, vertical accelerations do not significantly affect the residual displacements until close to the point of collapse. Moreover, the residual displacements typically change, either increase or decrease, on the order of one to two times the yield displacement if they are significantly affected by vertical accelerations. While a change by a factor of one or two may seem small, a building with a residual displacement that is equal to two times the yield displacement would most likely need to be torn down and may have severely diminished post earthquake stability. Furthermore, there are some extreme cases where the change factor in normalized residual displacements in much higher than one or two. An example of an extreme case is shown in Figure 5.20e. In this figure, the change in residual displacement due to the inclusion of vertical accelerations is 16 times the yield displacement for the structure with a 1668 kip-in yield moment and an r_p of –0.0625.

An important point to make about the effect of vertical accelerations on both maximum and residual displacements is that structures should ideally be designed so that they would not come close to the point of collapse. Consequently, a well-designed structure should rarely, and possibly never, be significantly affected by vertical accelerations. This assumes, however, that the hazards and risks of a given region are known exactly and that there are no shortcomings in the current design philosophies. While the hazards and risks may be known with a fairly high degree of certainty in the Western United States and the current design philosophies have been iteratively improved with each new earthquake, the same cannot be said about structures in the central and eastern United States (CEUS). There is much more uncertainty regarding the definition of a well designed CEUS structure.

Furthermore, the above statements have been based on SDOF models with bilinear stiffness. The results may be very different for MDOF models incorporating degrading strength and stiffness.

5.4.3 – Effects of Vertical Acceleration Scale on Collapse and Residual Displacements

In addition to including vertical accelerations, several sets of models were analyzed for varying vertical earthquake scales. Recall that multipliers ranging from 1.5 to 2.5 were used to scale the vertical accelerations. In Figures 5.21a through 5.21c and Figures 5.22a through 5.22c, the effect of increasing vertical multipliers is seen. Three of the figures show the effects of increasing vertical accelerations on maximum lateral displacements and three show the effects of increasing vertical accelerations on residual displacements. All six of the figures involve earthquake three, which had an unscaled vertical PGA of 0.127 g. After multiplying the vertical PGA by 1.5, 2.0, and 2.5, the resulting values were 0.191, 0.254, and 0.318, respectively.

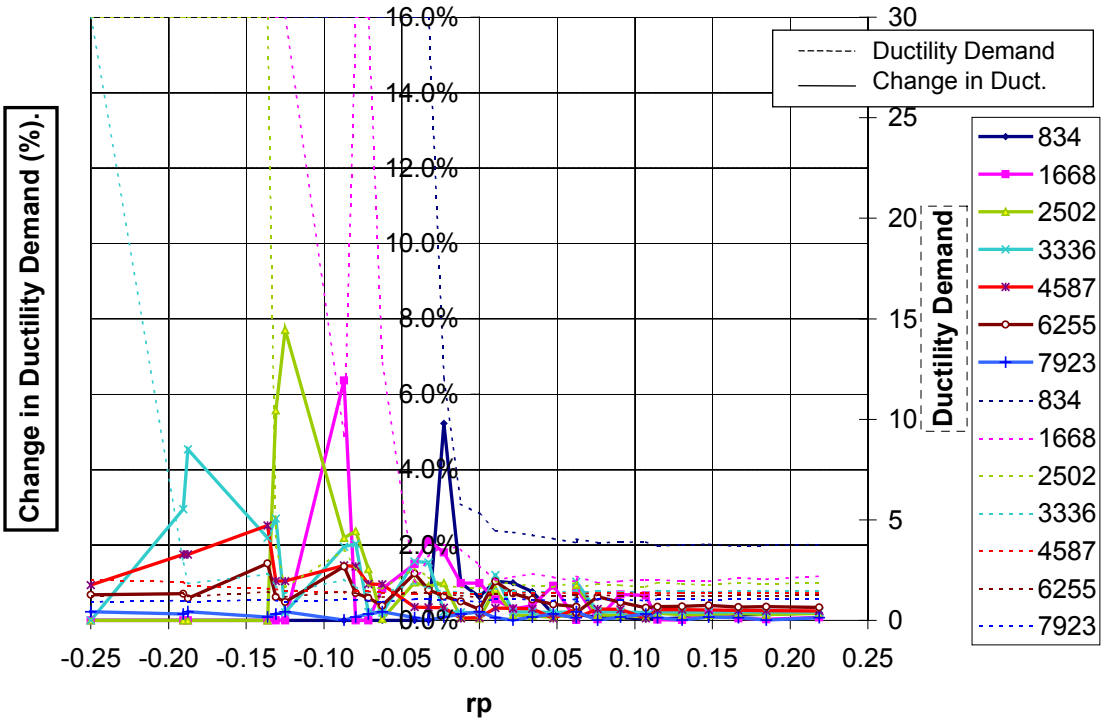

Figure 5.21a – EQ3, Lateral Scale = 0.2 g, Vertical Multiplier = 1.5, Change in Ductility Demand Due to the Inclusion of Vertical Accelerations for Models with a Period of 1.093 Seconds

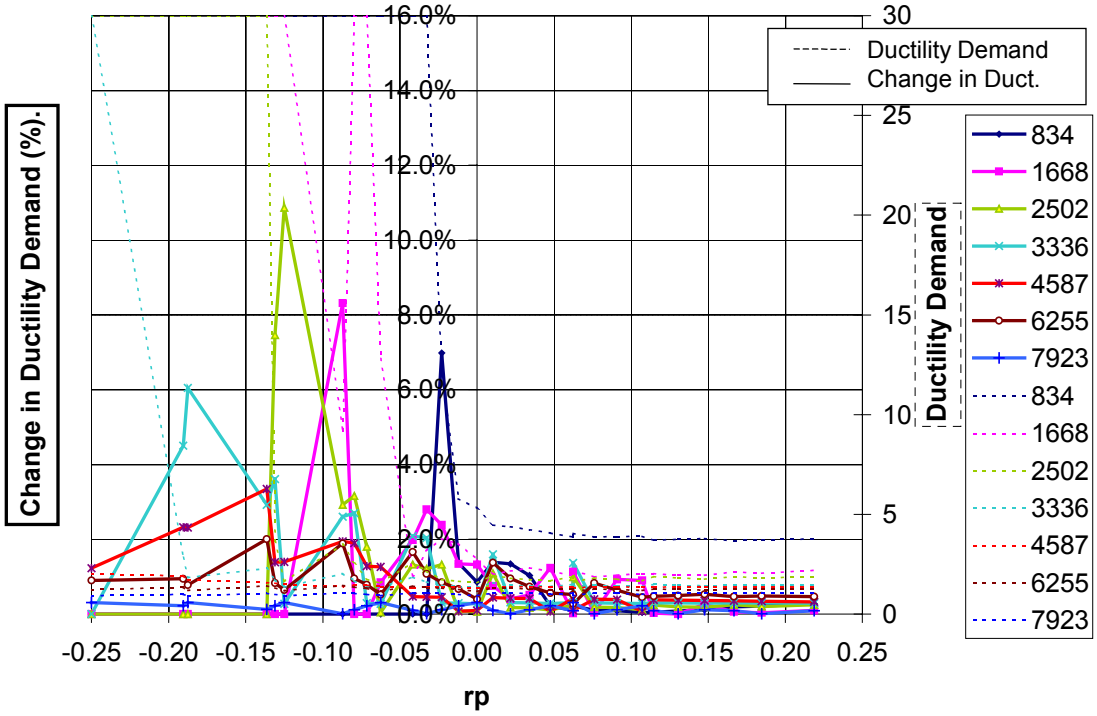

Figure 5.21b – EQ3, Lateral Scale = 0.2 g, Vertical Multiplier = 2.0, Change in Ductility Demand Due to the Inclusion of Vertical Accelerations for Models with a Period of 1.093 Seconds.

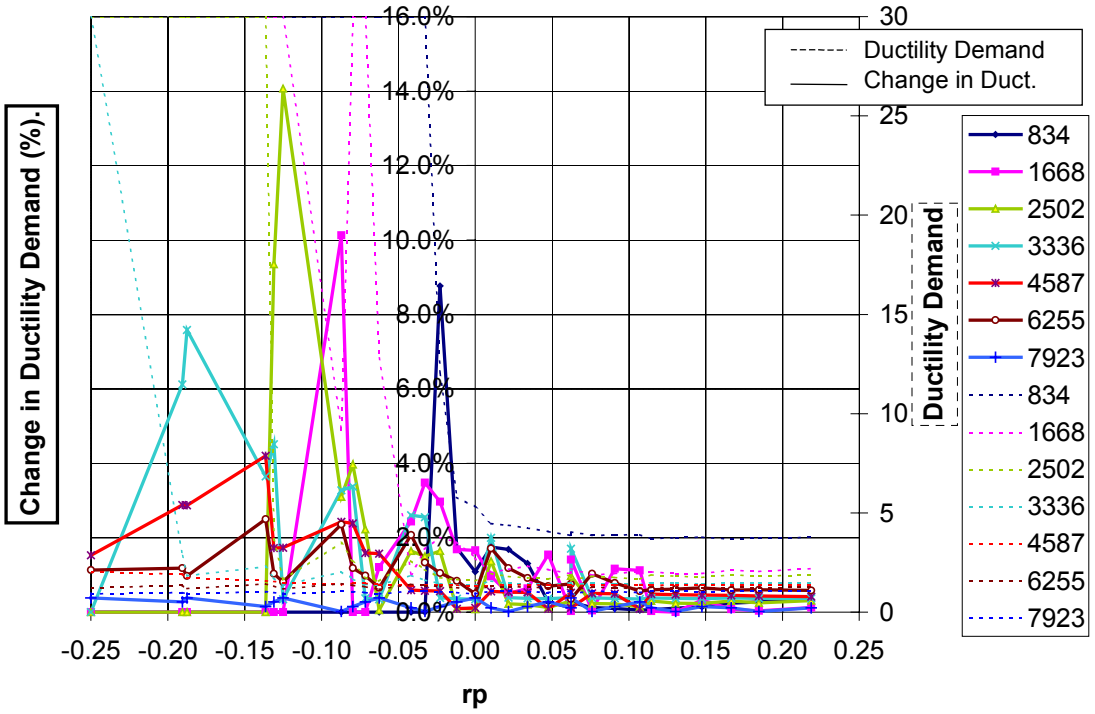

Figure 5.21c – EQ3, Lateral Scale = 0.2 g, Vertical Multiplier = 2.5, Change in Ductility Demand Due to the Inclusion of Vertical Accelerations for Models with a Period of 1.093 Seconds.

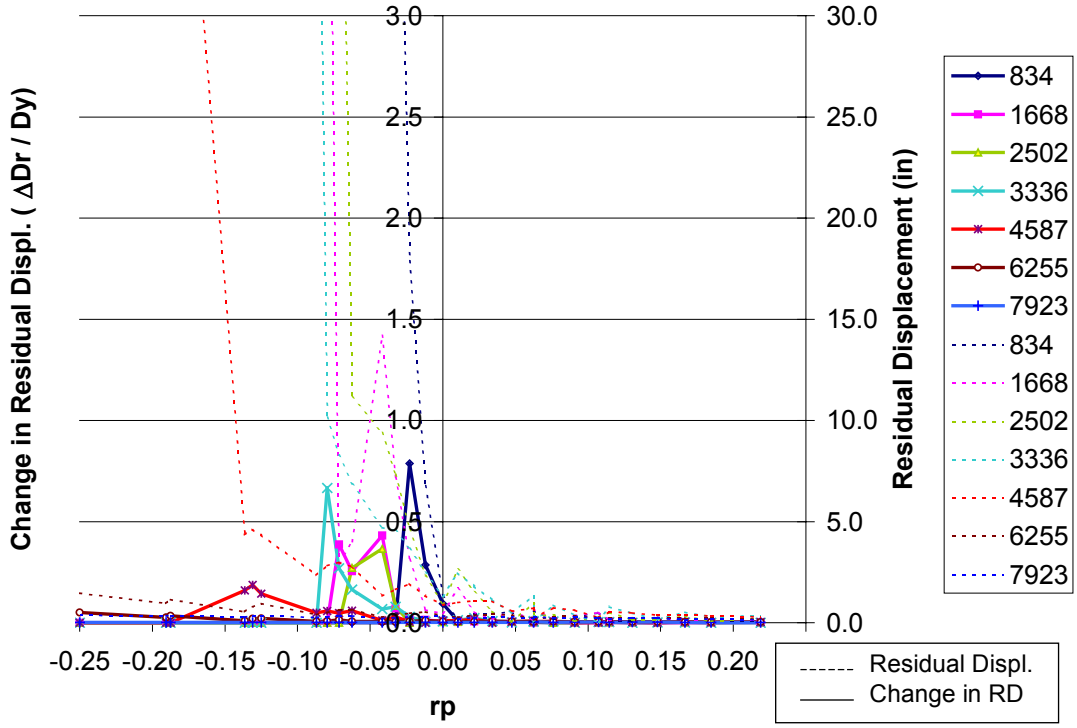

Figure 5.22a – EQ3, Lateral Scale = 0.2 g, Vertical Multiplier = 1.5, Change in Residual Displacements Due to the Inclusion of Vertical Accelerations for Models with a Period of 0.903 Seconds.

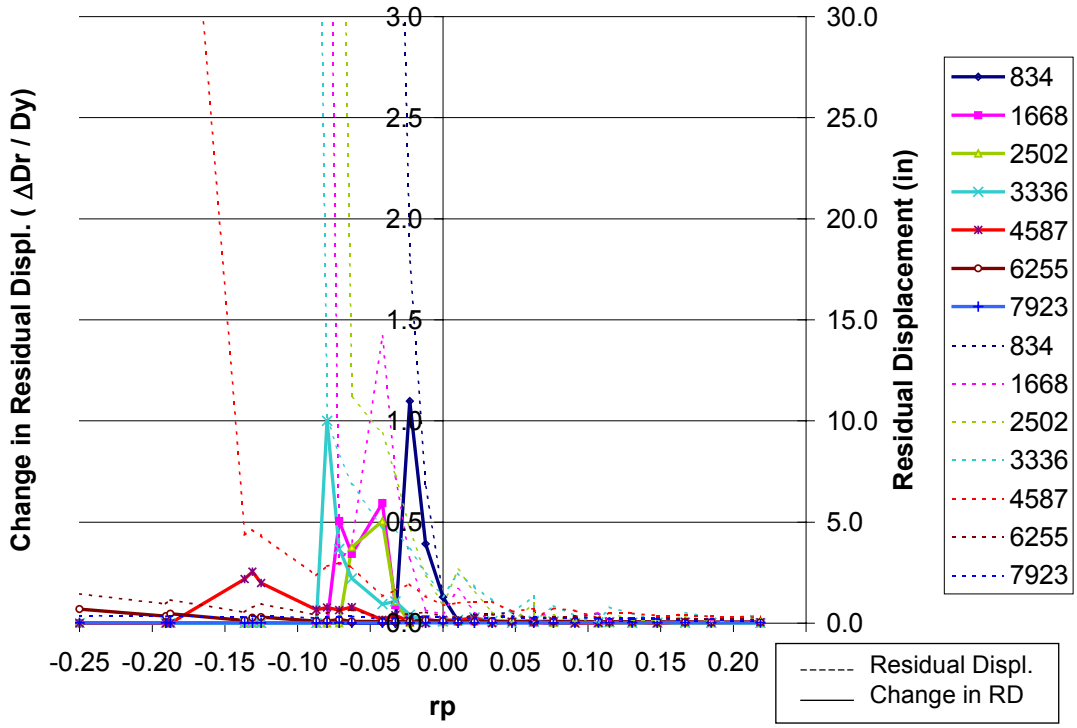

Figure 5.22b – EQ3, Lateral Scale = 0.2 g, Vertical Multiplier = 2.0, Change in Residual Displacements Due to the Inclusion of Vertical Accelerations for Models with a Period of 0.903 Seconds.

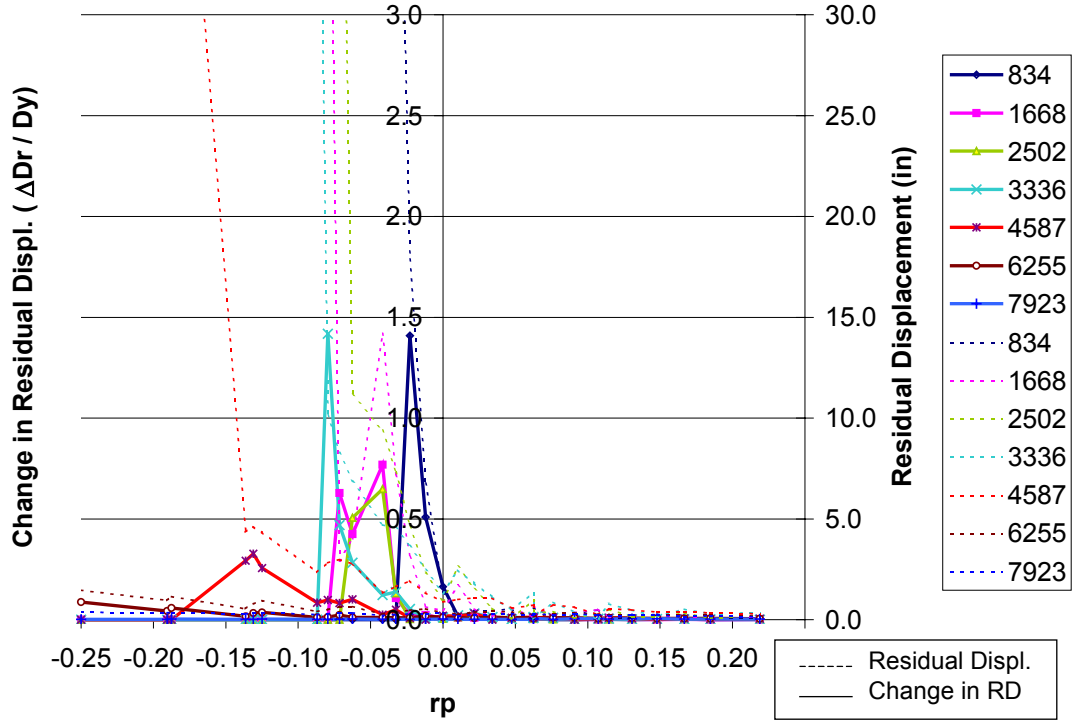

Figure 5.22c – EQ3, Lateral Scale = 0.2 g, Vertical Multiplier = 2.5, Change in Residual Displacements Due to the Inclusion of Vertical Accelerations for Models with a Period of 0.903 Seconds.

Notice that in all six of the figures, the maximum values increase as the vertical accelerations increase. Also notice, though, that as the vertical accelerations increase from 0.191 g to 0.318 g the change in ductility demand increases from an average of about six percent to an average of about ten percent. Then, similarly, the change in residual displacements normalized by yield displacement increase from about 0.5 to about 1.0. Thus, while the value changes increase by about 50 percent, the values are still relatively small whereas the vertical ground motion has increased significantly in magnitude. If one considers the case of Figure 5.20e, where the vertical multiplier was 2.5, then a 50 percent decrease in the normalized change in residual displacements would drop the maximum value from 16 to about 8. Such a reduction would be significant, but it is important to remember that such a structure is on the verge of collapsing regardless of vertical accelerations. Thus, it is good to be able to reduce the amount of lateral displacement or the residual displacements caused by vertical accelerations, but a structure should ideally never be on the verge of collapse anyway.

5.5 – Chapter Summary

The results of the parameter study were discussed in this chapter. Due to the large amount of information presented, several points are worth reiterating. First, from the individual parameter study, it was shown that all four of the structural parameters influence collapse. Increasing the stability ratio in general caused more collapses. Decreasing the post-yield stiffness ratio generally caused more collapses. If the yield strengths were increased, the number of collapses could be reduced. Finally, the period influenced collapse in that it, coupled with the earthquake intensity, influenced the inelastic displacement demands, which influence collapse.

After examining the parameters individually, it was then shown that combinations of the structural parameters proved to be better indicators of collapse potential. From this portion of the discussion, the collapse r_p and positive r_p ductility demand values were introduced. It was shown that these values could reasonably determine the collapse potential of a structure, independent of earthquake frequency content and magnitude.

Then, in regard to residual displacements, it was shown that residual displacements increase for decreasing r_p. For the most part, there was a ceiling on the amount of residual displacement that a structure would incur at a given r_p value. Consequently, increasing the intensity of a ground motion did not generally increase the residual displacements, but instead caused structures with higher yield moments to have them and be at the ceiling values.

In the final section of this chapter, the effects of ground motion parameter variation was discussed. First, it was shown that increasing the lateral ground motion generally caused an increase in the number of structure collapses. Second, vertical accelerations typically only increase the lateral displacements at the r_p value just before a structure is going to collapse.

It is clear from the results of the parameter study that certain factors influence collapse and residual displacements. Some parameters proved to be more influential than others. While this study does shed some light into the nature of collapse and the factors that influence it, it is the author's contention that much more work could be done in this area to more fully understand why one building would collapse as opposed to another.

6.0 Incremental Dynamic Analysis Description

6.1 – Introduction

Incremental dynamic analysis (IDA) is a procedure for conducting nonlinear dynamic analyses, whereby a model with material and geometric nonlinearity is subjected to a particular accelerogram in increasing intensity increments. The intensity may be measured a variety of ways, but is typically measured by the peak ground acceleration (PGA), peak ground velocity (PGV), or spectral acceleration. Any measure of earthquake intensity that may be monotonically scaled can be used. For this study, PGA was used because the same scaling procedure could be used for structures with different periods. For each increment of the IDA, a response value was recorded. This response value is called a damage measure according to the IDA paradigm. In IDA, there are many ways to measure damage, just as there are many ways to measure intensity. Damage measures used in this study were interstory drift ratio, ductility demand, the Park and Ang damage index, and the Kumar and Usami damage index. The details of these damage indices are presented in chapter two.

IDA basically served two purposes in this study. First, it was a means of testing the hypotheses developed during the parameter study. In the parameter study it was found that decreasing the r_p, particularly in the negative range, decreased the ductility demand which corresponded to collapse. This phenomenon is shown in Figure 5.11 of chapter five. For a structure with a given r_p value, there was a range of ductility demand that would likely cause collapse. IDA provided a good way to look at intensity ranges, and consequently ductility ranges, where collapse might occur.

Second, it was a means of contrasting the responses of reasonable Central and Eastern United States (CEUS) and Western United States (WUS) structures subjected to a variety of earthquake intensities. A goal of this study was to determine the performance of CEUS and WUS structures subjected to increasingly severe earthquakes. The main range of ground motion intensities of interest for this study was between the probable 10 percent and 2 percent in 50 earthquake events. The reason that this range was significant

is because it covers the range of intensities that have been used in design codes within the last ten years.

In the IDA study, five representative sites were chosen in both the CEUS and WUS. The sites were chosen based on population and seismicity. In the WUS, Los Angles, San Francisco, Seattle, and Salt Lake City were chosen. For all four of the aforementioned sites it was decided that moment frames would be used. The Seismic Use Group for each of the sites and height of the structures dictated that special moment frames were required (R = 8). To add some variety to the WUS sites, the fifth site in the WUS was also based on a San Francisco location, however an R of six rather than an R of eight was used. In the CEUS, six sites were originally chosen -- Memphis, Charleston SC, New York City, Boston, Chicago, and Washington D.C. However, the seismic hazards associated with Washington D.C. and Chicago were approximately equal and so those two sites were condensed to one.

In the following sections, the details of the IDA will be described.

6.2 – Model Descriptions

Before describing how the IDA model structural properties were determined, it is important to mention that there is a large amount of subjectivity associated with the determination process. The seismic hazard, for example, of each CEUS and WUS site did not correspond to the hazard of a particular latitude and longitude. Rather, an estimate of the average seismic hazard over the entire city was used. Thus, in most of the cities there are some places that would have higher seismic hazards and some that would have lower seismic hazards than the values used to generate the models used in the IDA. Then, with regard to post-yield stiffness ratio, it was assumed that most structures would have at least a slight amount of strain hardening and thus have post-yield stiffness ratios slightly greater than zero. No actual measurements on existing buildings were used, however. Nor were multiple static pushover analyses conducted on MDOF structures to get an idea of the range of post-yield stiffnesses for the cities in question. The values were determined based on best estimates.

Even though there is a large amount of subjectivity in the parameters used in the IDA, the parameters used are reasonable. Just as the periods of the models used in the

parameter study may not exactly correspond with structures between three and nine stories, so the parameters used in the IDA may not exactly correspond to actual or MDOF analytical structures, but the models are reasonable and are useful.

The structural properties of the models used in the IDA were determined using the Equivalent Lateral Force Method (ELF) of the NEHRP Provisions and the ASCE 7-02 (ACSE 2002) wind provisions. As in the parameter study, four structural characteristics were required to define each of the models -- period (stiffness), yield force (yield moment), post-yield stiffness ratio, and stability ratio (P-Delta effects). Unlike the parameter study, though, fewer models were created because IDA required more analyses to be conducted on each model. The number of parameters and their determination are described at length in the following sections; however, a brief overview is in order first.

For each site, four different structural periods of vibration were used. The periods corresponded to buildings that would be three, five, seven, and nine stories in height. For each of the building heights, or periods, two different post-yield stiffnesses were used to show the influence of slight changes in that parameter. Based on the four building heights and two post-yield stiffness ratios, eight different structures resulted. To those eight structures, two different stability ratios were applied. Thus, some variability in the P-Delta effects was also included. The stability ratios dictated the vertical load applied to the structures. In sum, sixteen structures were analyzed for each of the five WUS and CEUS sites.

6.2.1 – Overview of Parameter Determination

Most of the structural parameters used in the IDA were determined by considering both the NEHRP seismic provisions and the ASCE 7-02 wind provisions. The only parameter chosen, rather than determined, was the post-yield stiffness ratio. The strength of the models was generally controlled by seismic designs. The stiffness for each story was determined by using the maximum of the required seismic, wind, and stability stiffnesses. The stability ratios were determined according to the resulting maximum stiffnesses and reasonable distributions of the structure's weight. In the following sections, the details of determining the IDA structural parameters are presented.

6.2.2 – Constructing the Design Response Spectrum

In order to calculate the seismic strength and stiffness of the models, it was first necessary to construct a design response spectrum for each site. The design response spectrum was basically the range of C_s values as a function of structural period. The C_s values were calculated according to equations 4.9 and 4.10 of this thesis. These equations required the importance factors (I), spectral acceleration values (S_{ds} and S_{d1}) , and response modification factors (R). As with the parameter study, the importance factor for all models was 1.0. Next, the short period and one second period spectral acceleration values were determined from seismic hazard maps. Table 6.1 below shows the acceleration values used in the IDA.

Table 6.1 – PGA, Short Period Spectral Acceleration, and One Second Spectral Acceleration Values for Selected WUS and CEUS Sites.

City	10% Probability of Exceedance in 50 yr PGA (%g)	2% Probability of Exceedance in 50 yr PGA (%g)	2% Probability of Exceedance in 50 yr 0.2 sec (S_S) (%g)	1 sec (S_1) (%g)
Western United States				
Los Angeles	0.6	1.2	2.4	0.8
San Francisco	0.6	0.8	2.4	1.2
Seattle	0.3	0.6	1.25	0.45
Salt Lake City	0.15	0.2	1.4	0.6
Central and Eastern United States				
Memphis	0.4	1.4	2.4	0.9
Charleston	0.15	1.2	1.5	0.4
Boston	0.03	0.15	0.26	0.08
New York City	0.04	0.2	0.4	0.09
Washington D.C.	0.02	0.08	0.2	0.07
Chicago	0.02	0.08	0.18	0.07

As has already been mentioned, the spectral acceleration and PGA values were determined somewhat subjectively. The second and third columns of Table 6.1 show the earthquake PGAs that have a 10 percent and 2 percent probability of occurring in 50 years. Notice that the 2 percent in 50 year PGAs for the CEUS sites are about 4 or 5 times higher than the 10 percent in 50 year PGAs. Then, notice that the increases are not nearly as dramatic for the WUS sites. The last two columns of Table 6.1 show the short (S_s) and one second (S_1) spectral acceleration values chosen for the 2 percent in 50 year

events. The values from the 2 percent in 50 year columns were used to construct design acceleration spectrums.

Based on the spectral acceleration values of Table 6.1, site amplification factors were determined. For the IDA, it was assumed that all of the models would be constructed in areas classified as site class C, which is defined as "very dense soil and soft rock" (NEHRP 2000). The site amplification factors, F_a and F_v, were determined from tables 4.1.2.4a and 4.1.2.4b of the NEHRP Provisions. Then, the design spectral acceleration values, S_{DS} and S_{D1}, were determined from equations 6.1 and 6.2 below.

$$S_{DS} = \frac{2}{3} F_a S_s \tag{6.1}$$

$$S_{D1} = \frac{2}{3} F_v S_1 \tag{6.2}$$

The amplification factors determined from the aforementioned tables, as well as the resulting design spectral acceleration values, are presented in Table 6.2 below.

Table 6.2 – Spectral Acceleration Values for Selected WUS and CEUS Sites Modified by Site Amplification Factors.

City	Site Factors		2% Probability of Exceedance (%g)		Design Spectral Accelerations		Seismic Design Category
Western United States	**Fa**	**Fv**	**Ss**	**S1**	Sds	Sd1	
Los Angeles	1	1.3	2.40	1.04	1.60	0.69	D
San Francisco	1	1.3	2.40	1.56	1.60	1.04	E
Seattle	1	1.35	1.25	0.61	0.83	0.41	D
Salt Lake City	1	1.3	1.40	0.78	0.93	0.52	D
Central and Eastern United States							
Memphis	1	1.3	2.40	1.17	1.60	0.78	E
Charleston	1	1.3	1.50	0.52	1.00	0.35	D
Boston	1.2	1.7	0.31	0.14	0.21	0.09	B
New York City	1.2	1.7	0.48	0.15	0.32	0.10	C
Washington D.C.	1.2	1.7	0.24	0.12	0.16	0.08	A
Chicago	1.2	1.7	0.22	0.12	0.14	0.08	A

From the design spectral acceleration values, each site was assigned to a particular Seismic Design Category according to section 4.2 of the NEHRP Provisions. The Seismic Design Categories dictated the types of structures that could be built on a particular site. Table 5.2.2 of the NEHRP Provisions provides a variety of framing systems and related limitations based on the Seismic Design Categories. For example, if one wanted to build a steel moment frame in a Seismic Design Category D area, a special

moment frame could be used regardless of height. An intermediate moment frame could be used as long as it is less than 35 ft high and an ordinary moment frame is not permitted. The Seismic Design Categories in conjunction with the desired framing system were used to determine the Response Modification Coefficients (R) and Deflection Amplification Factors (C_d). The R and C_d values were determined from Table 5.2.2 of the NEHRP Provisions. It was assumed that steel moment frames were used on each of the sites. The resulting R and C_d values used in the IDA are shown in Table 6.3 below.

Table 6.3 – Response Modification Coefficients and Deflection Amplification Factors for Selected WUS and CEUS Sites

City		
Western United States	**R**	**Cd**
Los Angeles	8	5.5
San Francisco	8	5.5
Seattle	8	5.5
Salt Lake City	8	5.5
Central and Eastern United States		
Memphis	8	5.5
Charleston	8	5.5
Boston	4.5	4
New York City	8	5.5
Washington D.C.	3.5	3
Chicago	3.5	3

Most of the structures in the study required special moment frames for which R was 8 and C_d was 5.5. In fact, all of the structures in the WUS were special moment frames. Consequently, another series of models was created based on an R of 6 for the San Francisco site to provide some variety to the types of structures in the WUS.

As stated earlier, the design response spectrums were created according to equations 4.9 and 4.10. The shape of the design response spectrums is shown in Figure 6.1.

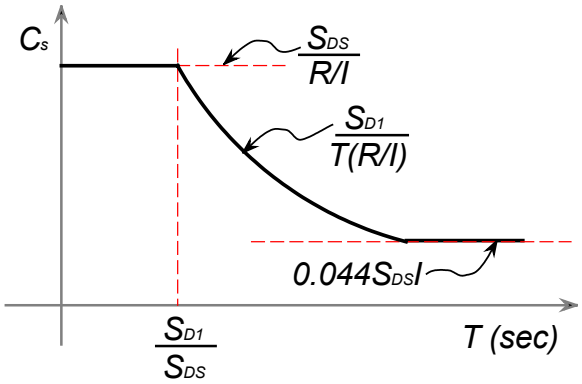

Figure 6.1 – Seismic Design Response Spectrum

6.2.3 – Calculating the Approximate Periods

The next step toward determining the seismic yield strengths was to approximate values for the periods of the structures. As in the parameter study, the initial periods of the models were determined using the NEHRP approximate formulas. The approximate period formulas can be found in Section 5.4.2 of the Provisions, or equations 4.3 and 4.4 of this thesis. Recall that the approximate formulas were a lower bound estimate of a building's period and that some of the conservatism could be removed by multiplying by the "coefficient for the upper limit on calculated period", C_u. C_u factors were determined from table 5.4.2 of the NEHRP Provisions. For the IDA study, periods were determined for buildings that were three, five, seven, and nine stories tall. It was assumed that the story height of all the models was 12 feet. In general, the C_u values resulted in CEUS approximate periods that were about 20 percent longer than their WUS counterparts. The approximate period values were required to calculate the Seismic Response Coefficients (C_s).

6.2.4 – Determining the Seismic Response Coefficients

With the approximate periods (T) and the design response spectra, the Seismic Response Coefficients (C_s) were calculated. The C_s values, in practical terms, basically specify the lateral yield strength of a building as a fraction of its design weight. The C_s values used for each of the sites are presented in Table 6.4.

Table 6.4 – Seismic Response Coefficients for Selected WUS and CEUS Sites

City	Design Force / Wt (Cs) Number of Stories			
Western United States	**3**	**5**	**7**	**9**
Los Angeles	25.0%	16.6%	14.1%	14.1%
San Francisco (R = 8)	37.7%	25.1%	19.2%	15.7%
San Francisco (R = 6)	53.3%	37.1%	28.2%	22.8%
Seattle	14.9%	9.9%	7.6%	7.3%
Salt Lake City	18.9%	12.5%	9.6%	8.2%
Central and Eastern United States				
Memphis	28.3%	18.8%	14.4%	14.1%
Charleston	12.7%	8.8%	8.8%	8.8%
Boston	5.8%	3.9%	2.9%	2.4%
New York City	3.0%	2.8%	2.8%	2.8%
Chicago	5.5%	3.6%	2.8%	2.3%
Washington D.C.	5.5%	3.6%	2.8%	2.3%

Notice that there are two entries for San Francisco. The only difference between the two sites is the R value. Then, notice that the C_s values for Boston, New York City, Chicago, and Washington D.C. sites are quite low, in most cases less than five percent of the building weight. While these values are low, they are higher than would be required by wind design and thus reasonable.

Notice also, in Table 6.4, that some of the sites have the same C_s values for increasingly taller buildings. This was because of the lower bound on the C_s values for increasingly larger period buildings.

Once the C_s values were determined, it was time to determine the stiffnesses of the models.

6.2.5 – Period (Stiffness) Determination

The stiffnesses used for the SDOF models in the IDA were determined from MDOF approximations. The approximate MDOF structures were derived from seismic and wind lateral force distributions and seismic and wind drift requirements as well as building weight and geometry assumptions and stability requirements. The SDOF models were based on MDOF buildings that were 150 ft square in plan. Moreover, as has

already been mentioned, the floor heights of the MDOF buildings were assumed to be 12 feet. It was furthermore assumed that the buildings would have densities of 9 pcf.

6.2.5.1 – Seismic Force Lateral Stiffness Determination

The MDOF model stiffnesses based on seismic considerations were determined from the required force distribution and drift limitations of the ELF method in the NEHRP Provisions. The seismic lateral force distribution was determined according to section 5.4.3 of the NEHRP provisions. The base shear (V), which was determined according to equations 4.7 and 4.8, was distributed along the height according to equations 6.1 and 6.2.

$$F_x = C_{vx} V_b \tag{6.1}$$

and

$$C_{vx} = \frac{w_x h_x^k}{\sum_{i=1}^{n} w_i h_i^k} \tag{6.2}$$

where

C_{vx} = vertical distribution factor,

V_b = base shear

w_i and w_x = the portion of the total gravity load of the structure, W, assigned to level i or x,

h_i and h_x = the height from the base to level i or x,

k = exponent related to structural period, usually between 1 and 2

n = number of stories

The k value used in equation 6.2 is 1.0 when the period of the structure in question is less than 0.5 seconds and 2.0 when the period is greater than 2.5 seconds. For intermediate structural periods, one may linearly interpolate between 1.0 and 2.0 or just use 2.0. For this study, the k value was conservatively assumed to be 2.0.

In the IDA study, all of the story heights were equal and all of the story weights were assumed to be equal. Consequently, equation 6.2 was reduced to equation 6.3:

$$C_{vx} = \frac{x^2}{\sum_{i=1}^{n} i^2} \tag{6.3}$$

where

x = Story or Level Number

In equation 6.3, the distribution of the seismic forces became independent of story height and mass. The next step was to determine the total seismic shear at each level of the structure based on the force distribution. The percentage of the shear acting at a given level, $C_{vtotal\text{-}x}$, was the sum of the seismic forces acting at that level and above that level. Equation 6.4 describes the total shear force at a given level, x, as a percentage of the total base shear:

$$C_{vtotal-x} = \frac{\sum_{k=1}^{n-x+1} (n-k+1)^2}{\sum_{i=1}^{n} i^2} \tag{6.4}$$

The values of $C_{vtotal\text{-}x}$ varied from 1.0 at the first floor to the reciprocal of the denominator of equation 6.4 at the roof.

Once the shear force distributions were determined, it was necessary to determine the allowable drift values. The total allowable drift for a given story was determined from section 5.2.8 of the NEHRP Provisions. Section 5.2.8 stipulates that a given story may have a total drift, including inelastic displacement, equal to two percent of the story height. The two percent limitation applies to structures above four stories tall in seismic use group one. Other drift limitations apply to other types of structures and seismic use groups, but the two percent value was used for the IDA in this study. Since the allowable drift included inelastic displacement, the allowable drift values were divided by the deflection amplification factor, C_d, to get the allowable elastic displacements, δ_{allow}. The allowable elastic displacement for a model is given by equation 6.5:

$$\delta_{allow} = \frac{0.020 h_x}{C_d} \tag{6.5}$$

The required story stiffnesses, then, became the story shear divided by the allowable displacement. The seismic story stiffnesses, K_{sx}, are given by equation 6.6.

$$K_{sx} = \frac{V_b C_{vtotal-x} C_d}{0.02 h_x} \quad \textbf{(6.6)}$$

6.2.5.2 – Wind Force Lateral Stiffness Determination

Next, the stiffnesses based on wind force distributions and deflection limitations were determined. It was important to determine the wind force lateral stiffness requirements because in some situations the wind forces can control the stiffness values, particularly in the low seismic hazard areas. As with the seismic story stiffness calculations, it was first necessary to determine the distribution of the forces over the height of the structures. The forces applied to the structures were determined according to ASCE 7-02 section 6.5, which provides wind pressure values. The pressure values at a given level were determined according to equation 6.7:

$$q_z = 0.00256 K_z K_{zt} K_d v^2 I \quad \textbf{(6.7)}$$

where

q_z = pressure at level z (psf)

K_z = velocity pressure exposure coefficient

K_{zt} = topographic factor

K_d = wind directionality factor

v = three second gust wind velocity (mph)

I = importance factor

It was assumed that the models would be designed for 100 mph 3-sec wind gusts and exposure B. Moreover, the importance factor and topographic factor were both assumed to be 1.0. Then, the directionality factor was assumed to be 0.85. The K_z value varied with the height.

The total force at a given story was equal to the integral of the pressure over the area enclosed by the tributary height and width. It was assumed that the width of the

buildings was constant, and thus only K_z varied with the height. The total wind force became an integral of K_z as a function of height over the tributary height. Another way to present equation 6.7, which considers the fact that only K_z varies in a given frame, is presented in equation 6.8:

$$q_z(h) = C_{wind} K_z(h) \tag{6.8}$$

where

$$C_{wind} = 0.00256 K_{zt} K_d v^2 I$$

Thus, the force at level z is given by equation 6.9

$$F_z = C_{wind} L_{trib} \int_{trib-height} K_z(h) dh \tag{6.9}$$

where,

L_{trib} = the tributary width

The tributary height for each floor was assumed to cover half the story below and half the story above the level in question. The tributary width was considered to be the entire building width. Figure 6.2 shows the vertical distribution of K_z for an arbitrary exposure.

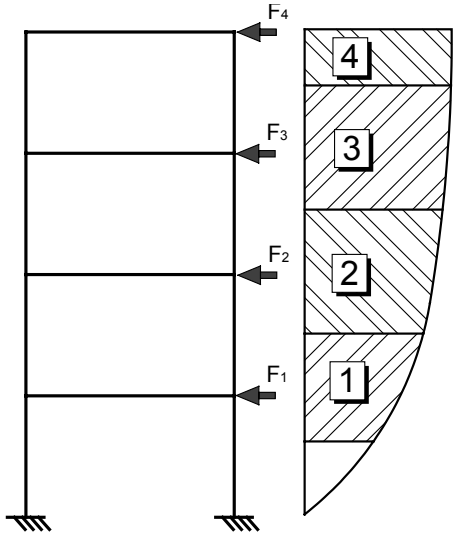

Figure 6.2 – ASCE 7-02 General Wind Force Distribution

Notice that for each level of the structure the vertical tributary width covers half the story above and below the level in question. Moreover, the roof tributary width only covers half the story below it and no force is applied as a result of wind pressures acting at half the first story height down. Equations for K_z as a function of height are provided in ASCE 7-02 Table 6-4. In ASCE 7-02, the equations for K_z are C6-3a and C6-3b. The ASCE equations are presented in this thesis as equations 6.10 and 6.11:

$$Kz(h) = 2.01\left(\frac{h}{z_g}\right)^{\frac{2}{\alpha}}, \text{ for } 15\,ft \le h \le z_g \qquad \textbf{(6.10)}$$

$$Kz(h) = 2.01\left(\frac{15}{z_g}\right)^{\frac{2}{\alpha}}, \text{ for } h < 15\,ft \qquad \textbf{(6.11)}$$

where,

h = height at which the pressure is being calculated (in feet)

α and z_g are given in table 6.5

Table 6.5 – Wind Pressure Constants

Exposure	α	z_g (ft)
A	5	1500
B	7	1200
C	9.5	900
D	11.5	700

Figure 6.3 shows plots of equation 6.10 and the resulting simplified forms of the equation for the various exposures shown in Table 6.5.

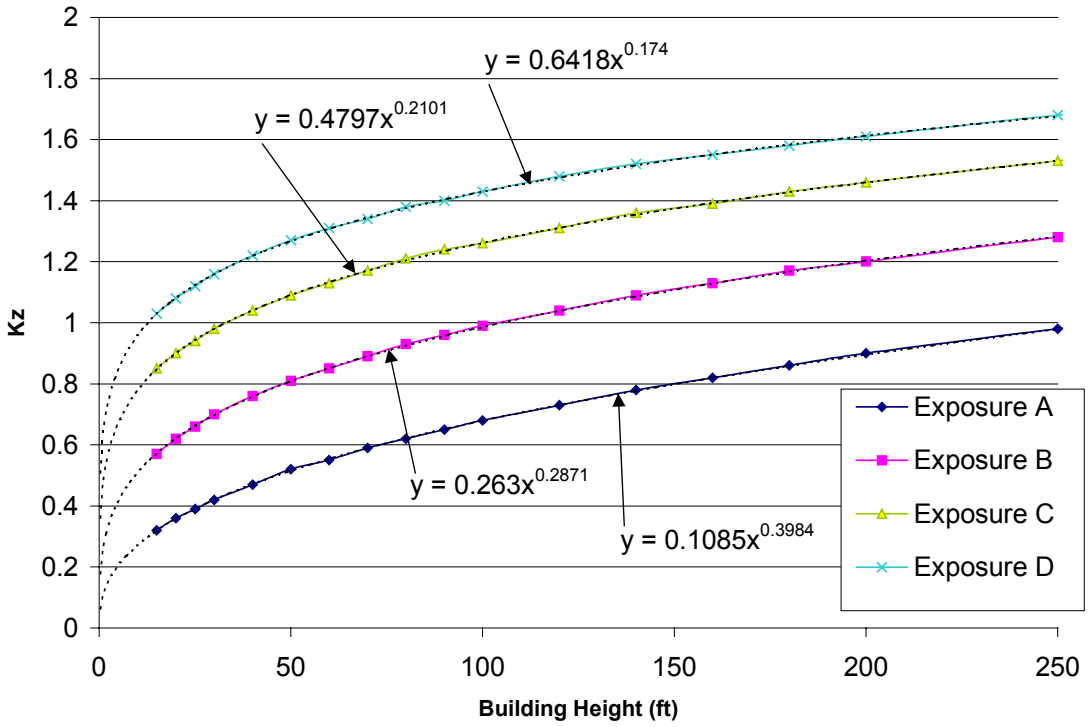

Figure 6.3 – Equations for the Velocity Pressure Exposure Coeffiecients, K_z

From Figure 6.3, it is clear that as the exposures go from A to D, the wind pressure increases. The equations determined from figure 6.3 were used in conjunction with equation 6.9 to determine the design forces at each floor. After calculating the story forces, it was necessary to convert the distributed forces to story shears. The story shears included all of the forces applied at that level up to the roof. The total shear at a given story was described by equation 6.12:

$$V_{wind-x} = C_{wind} L_{trib} \int_{(x-0.5)h_{st}}^{Roof-Ht} K_z(h)dh \qquad \textbf{(6.12)}$$

where

$V_{wind\text{-}x}$ = story shear at level x

h_{st} = height of a story

The limits of integration went from half a story below the story in question to the roof. Once the wind story shears were determined, the allowable story drifts were then

determined. It was assumed that the allowable story drifts due to wind would be equal to the story height divided by 400.

Finally, to determine the required stiffness due to wind, the wind story shears were augmented by a factor of 0.8 and divided by the allowable drifts. The 0.8 factor was used because stiffness demands for wind are based on serviceability requirements. It is common to use a wind with a 10 year mean recurrence interval to satisfy these demands. Table C6-3 of ASCE 7-02 indicates that the ratio of the 10 year wind to the unfactored design level wind is approximately 0.8. The resulting equation for the required stiffness due to wind is given by equation 6.13:

$$K_{wind-x} = \frac{0.8 \cdot C_{wind} L_{trib}}{\left(\frac{h_{st}}{400}\right)} \int_{(x-0.5)h_{st}}^{Roof-Ht} K_z(h)dh \qquad \textbf{(6.13)}$$

6.2.5.3 – Stability Stiffness Determination

In Section 5.4.6.2 of the NEHRP Provisions, a limit is placed on the maximum stability ratio that a story may have. The limit is given by equation 2.27 in chapter two of this thesis. By substituting equation 2.5 and 2.7 into equation 2.27, the minimum stiffness of a story required by stability considerations is given by equation 6.14:

$$K_{\theta x} = \frac{P_x \beta_x C_d}{0.5 h_x} \qquad \textbf{(6.14)}$$

where

$K_{\theta x}$ = stiffness required at level x due to stability requirements.

P_x = total gravity load acting on level x.

β_x = ratio of shear demand to shear capacity of level x.

C_d = deflection amplification factor.

h_x = height of story x.

It is important to note that in equation 6.14 it is assumed that $0.5/\beta C_d$ is always less than 0.25. This assumption is accurate for all values of C_d pertaining to moment frames as long as β is greater than 0.67. When β is less than 0.67, the stability ratios are limited to 0.25. The value of β may also be conservatively assumed to be 1.0. For the IDA analysis β was chosen to be 0.9 to be on the conservative side, but not overly conservative.

The vertical load, P_x, was determined assuming that the weight of the structure was evenly distributed throughout. Thus, the total weight acting on a given level is given by equation 6.15:

$$P_x = W\frac{n-x+1}{n} \tag{6.15}$$

where

n = number of stories

W = total weight of the building

6.2.5.4 – Total Required Stiffness and Period Determination Considering Seismic Forces, Wind Forces, and Stability

The actual stiffness values used for the approximate MDOF models were taken as the largest stiffness values produced from equations 6.6, 6.13, and 6.14 for each story. In general, the story stiffnesses of structures with C_s values less than five percent were controlled by stability in at least some of the stories. Wind never controlled for the structures examined in this study.

Once the story stiffnesses were determined, a global stiffness matrix, which incorporated each story's stiffness, was created. The global stiffness matrix was essentially that of a shear building, in which each floor of the building has a single lateral degree of freedom. Then, a mass matrix based on an assumed equal distribution of the building's mass was created. The mass value for each floor was given by equation 6.16.

$$m_x = \frac{W}{n \cdot g} \tag{6.16}$$

where

n = total number of stories.

With the global stiffness matrix and the mass matrix, the frequencies, or eigenvalues, were then determined. The fundamental frequency in conjunction with equation 6.17 was used to determine the stiffnesses of the SDOF models, K_{SDOF}.

$$K_{SDOF} = m_{SDOF}\,\omega^2_{MDOF\_1} \quad \textbf{(6.17)}$$

where,

m_{SDOF} = mass of the SDOF model

ω_{MDOF_1} = fundamental frequency of the MDOF model.

As in the parameter study, the mass of the SDOF IDA models was a unit mass, so the SDOF stiffness values were equal to the squares of the MDOF fundamental frequencies. The resulting SDOF lateral stiffnesses are presented in Table 6.6.

Table 6.6 – SDOF Lateral Stiffness Values Based on Approximate MDOF Models

City	Lateral Stiffness (k / in.) Number of Stories			
Western United States	**3**	**5**	**7**	**9**
Los Angeles	50.30	22.55	14.37	11.51
San Francisco (R = 8)	75.81	33.98	19.54	12.81
San Francisco (R = 6)	101.09	45.31	26.06	17.08
Seattle	29.89	13.40	7.70	5.97
Salt Lake City	37.91	16.99	9.77	6.69
Central and Eastern United States				
Memphis	56.86	25.49	14.66	11.51
Charleston	25.51	11.93	8.98	7.19
Boston	9.34	5.21	3.73	2.94
New York City	11.04	7.00	5.12	4.04
Chicago	6.76	3.88	2.80	2.21
Washington D.C.	6.76	3.88	2.80	2.21

For most of the models in the IDA, the lateral stiffnesses result in structural periods that are longer than the approximate period formulas presented in the NEHRP Provisions. Furthermore, the periods that result for the Boston, New York City, Chicago, and

Washington D.C. sites are much longer than the NEHRP approximate formulas. All of the periods determined for the IDA models are presented in Table 6.7. Also included in Table 6.7 are derived C_u values. The derived C_u values are included to show how much longer the actual periods were compared to the approximate formula of equation 4.3.

Table 6.7 – IDA Model Structural Periods and Derived C_u Values.

City	Period Based on Approximate MDOF Shear Building				Determined Cu		Ta - Steel Moment Frame	
					0.492	0.741	0.970	1.185
Western United States	**3**	**5**	**7**	**9**	**3**	**5**	**7**	**9**
Los Angeles	0.886	1.323	1.658	1.852	1.800	1.786	1.710	1.562
San Francisco (R = 8)	0.722	1.078	1.421	1.756	1.466	1.455	1.466	1.481
San Francisco (R = 6)	0.625	0.933	1.231	1.520	1.270	1.260	1.270	1.283
Seattle	1.149	1.717	2.264	2.571	2.335	2.317	2.335	2.169
Salt Lake City	1.021	1.524	2.010	2.429	2.073	2.058	2.073	2.049
Central and Eastern United States								
Memphis	0.833	1.245	1.641	1.852	1.693	1.680	1.693	1.562
Charleston	1.244	1.819	2.097	2.343	2.527	2.456	2.163	1.976
Boston	2.056	2.752	3.254	3.664	4.176	3.715	3.357	3.091
New York City	1.891	2.375	2.776	3.125	3.842	3.207	2.863	2.636
Chicago	2.417	3.189	3.758	4.231	4.910	4.305	3.876	3.569
Washington D.C.	2.417	3.189	3.758	4.231	4.910	4.305	3.876	3.569

Notice that the derived C_u values for the Los Angeles, San Francisco, and Memphis sites are relatively close to the 1.4 value prescribed by Table 5.4.2 of the NEHRP Provisions. However, the derived C_u values for all of the other sites are significantly larger, especially for the Boston, Chicago, and Washington D.C. sites. The high derived C_u values do not necessarily mean that the calculated periods are wrong, however. The commentary of the NEHRP Provisions admits that the approximate period equations have been tailored to high seismic areas. Furthermore, the approximate period equations are not intended to be limits on the actual periods of structures, but on the periods used in the initial design phase where the C_s values are being calculated. Consequently, it is entirely likely that CEUS structures would be quite flexible and still meet all seismic, wind, and stability requirements.

6.2.6 – Stability Ratio Determination

The stability ratios used in the IDA were determined from the story stiffnesses of the approximate MDOF structures and the weight distribution. The stability ratio for each story (θ_x) of the MDOF structures was given by equation 6.18.

$$\theta_x = \frac{P_x}{K_{\max -x} \cdot h_x} \tag{6.18}$$

where

$K_{max\text{-}x}$ = maximum stiffness at level x based on equations 6.6, 6.13, and 6.14.

P_x = total weight acting on level x (equation 6.13)

Using equation 6.18 and building densities of 9 pcf, all resulting stability ratios were less than 0.19. The stability ratios for a given building were highest for the first floor and decreased in higher stories. This trend may not seem logical at first, but is easily explainable. The vertical load at a level, x, is determined according to equation 6.15 and the lateral stiffness at level x is determined according to equation 6.6. Equation 6.6 has all constant terms except for $C_{vtotal\text{-}x}$. Thus, the lateral stiffness at a level, x, is proportional to $C_{vtotal\text{-}x}$. For the purposes of this discussion, $C_{vtotal\text{-}x}$ will be called Ke^*_x. Then, the geometric stiffness has all constant terms except for the part given by equation 6.19:

$$Kg^*_x = \frac{n - x + 1}{n} \tag{6.19}$$

K_g, then, is given by

$$K_g = \frac{W}{h_x} Kg^*_x \tag{6.20}$$

Also, K_e is given by

$$K_e = \frac{V_b C_d}{0.02 h_x} Ke^*_x \tag{6.21}$$

The stability ratio for level x, θ_x, then becomes

$$\theta_x = \frac{0.02}{C_s C_d}\left(\frac{Kg^*_x}{Ke^*_x}\right) \quad \textbf{(6.22)}$$

Define θ_0 as

$$\theta_0 = \frac{0.02}{C_s C_d} \quad \textbf{(6.23)}$$

Equation 6.22 becomes

$$\theta_x = \theta_0\left(\frac{Kg^*_x}{Ke^*_x}\right) \quad \textbf{(6.24)}$$

To see the variation of Kg^*_x and Ke^*_x, consider a five story building with a C_s of 0.06 and a C_d of 3. The resulting θ_0 value is 0.111. The values for Kg^*_x and Ke^*_x for the five story building are shown in Table 6.8. Also, shown in table 6.8 is the ratio of Kg^*_x and Ke^*_x as well as the resulting stability ratios for each floor.

Table 6.8 – Stability Ratios for a Five Story Building

Story	Ke*	Kg*	Kg* / Ke*	θ
5	0.455	0.200	0.440	0.049
4	0.745	0.400	0.537	0.060
3	0.909	0.600	0.660	0.073
2	0.982	0.800	0.815	0.091
1	1.000	1.000	1.000	0.111

As Table 6.8 clearly shows, the stability ratios decrease in the higher stories of a building. For the IDA it seemed reasonable to use the worst case first floor value (θ_0) and a value that would occur in the middle stories. For each of the models, stability ratios of $1.0\theta_0$ and $0.7\theta_0$ were used. The stability ratios used in the IDA analysis corresponding to the first floors are presented in table 6.9.

Table 6.9 – Stability Ratios Used in the IDA Study.

City	Stability Ratios at the First Floor			
Western United States	**3**	**5**	**7**	**9**
Los Angeles	0.029	0.044	0.052	0.052
San Francisco (R = 8)	0.019	0.029	0.038	0.046
San Francisco (R = 6)	0.014	0.022	0.028	0.035
Seattle	0.049	0.074	0.096	0.100
Salt Lake City	0.039	0.058	0.076	0.089
Central and Eastern United States				
Memphis	0.026	0.039	0.051	0.052
Charleston	0.057	0.083	0.083	0.083
Boston	0.139	0.139	0.139	0.139
New York City	0.101	0.101	0.101	0.101
Chicago	0.185	0.185	0.185	0.185
Washington D.C.	0.185	0.185	0.185	0.185

Notice that the only sites with relatively high stability ratios are those corresponding to areas of low to moderate seismic hazard, in particular Boston, New York City, Chicago, and Washington D.C. Since the dimensions and weights of similar height buildings are the same for CEUS and WUS sites, the increase in stability ratio was due solely to lower stiffnesses in the CEUS models.

To achieve the stability ratios of Table 6.9 in the SDOF analyses, vertical loads were applied to the models determined from equation 6.23:

$$P_{SDOF} = \theta_{MDOF} h_{SDOF} K_{SDOF} \quad \textbf{(6.23)}$$

where

P_{SDOF} = vertical Load Applied to SDOF Model

θ_{MDOF} = a stability ratio determined from the MDOF approximate models

h_{SDOF} = height of the SDOF model

K_{SDOF} = lateral stiffness of the SDOF model

It is important to note that the stability ratios used in the SDOF IDA were determined from the MDOF structures. This is because the equivalent SDOF stiffnesses based on the fundamental frequency would result in unacceptably high and erroneous stability ratios. For example, consider the Boston five story building. The stiffness of the

first floor was almost 700 kips per in. and the total weight of the building was 12150 kips. Since the story height was 12 ft, the resulting first floor stability ratio was 0.121. However, if the K_{SDOF} value of 256 kips per in. is used to determine the stability ratio, then 0.33 results, which is unacceptable and fundamentally wrong.

6.2.7 – Post-yield Stiffness Ratio Choice

The post-yield stiffness values used were 0.05 and 0.07. Both values are reasonable estimates for MDOF models. Moreover, these values were chosen because lower post-yield stiffness ratios are more likely to result in negative r_p values which is where collapses occur. In order for an r_p value to become negative, the stability ratio must exceed the post-yield stiffness ratio.

6.2.8 – Rotational Forms of the Yield Force and Lateral Stiffness

As in the parameter study, the yield force and lateral stiffness values had to be converted to rotational values. The values of Tables 6.4 and 6.6 were converted to those of Table 6.10 according to section 4.2.5 of this work.

Table 6.10 – Yield Moments and Rotational Spring Stiffnesses for Selected WUS and CEUS Sites

City	Yield Moment (kip-in.) Number of Stories				Rotational Spring Stiffness (k / in.) Number of Stories			
Western United States	**3**	**5**	**7**	**9**	**3**	**5**	**7**	**9**
Los Angeles	6958	4624	3914	3914	521509	233750	148944	119346
San Francisco (R = 8)	10488	6969	5325	4355	786043	352320	202620	132786
San Francisco (R = 6)	14826	10324	7829	6338	1048057	469759	270160	177048
Seattle	4134	2748	2099	2030	309882	138895	79879	61911
Salt Lake City	5244	3485	2663	2275	393021	176160	101310	69370
Central and Eastern United States								
Memphis	7866	5227	3994	3914	589532	264240	151965	119346
Charleston	3529	2446	2446	2446	264534	123667	93090	74591
Boston	1613	1072	819	670	96861	54044	38647	30488
New York City	831	783	783	783	114426	72535	53128	41922
Chicago	1518	1009	771	630	70070	40256	28979	22866
Washington D.C.	1518	1009	771	630	70070	40256	28979	22866

6.2.9 – Summary of SDOF Structural Parameter Determination Procedure

The general procedure for determining the structural properties for a given site was as follows:

1) Determine both the seismic base shear and the allowable seismic story drift

A) Construct the design response spectrum for the site according to equations 4.9 and 4.10 (see figure 4.1).

B) Determine the approximate building period according to equation 4.3 and Table 5.4.2 of the NEHRP Provisions.

C) Determine C_s using the design response spectrum and approximate structural period. The seismic base shear is determined from equation 4.8. The seismic base shear determined in this step will be the yield force of the structure assuming that the actual period of the structure is greater than or equal to the approximate period determined in step B.

D) Determine the allowable story drift from Table 5.2.8 of the NEHRP Provisions.

2) Determine the required seismic lateral stiffness for each story of the structure from the base shear and allowable drift determined in step 1.

A) Distribute the base shear to the stories of the structure according to equations 6.1 and 6.2.

B) Determine the total story shear at each level according to Section 5.4.4 of the NEHRP Provisions and equation 6.4.

C) Determine the required seismic lateral stiffness of each story as the story shear divided by the allowable story drift (equation 6.6).

3) Determine both the wind forces and the allowable wind drifts

A) Determine an appropriate wind force distribution according to Section 6.5 of ASCE 7-02. The K_z term shall be determined according to equations C6-3a and C6-3b and Table 6-4. The resulting wind force distribution shall be a function of the height of the structure.

B) Determine the allowable story drift as h/400 (common practice)

4) Determine the required wind lateral stiffness for each story of the structure from the wind forces and allowable wind drifts determined in step 3.

A) Determine the total story shear at each level by integrating the wind force distribution equation (6.10).

B) Determine the required wind lateral stiffness of each story as the total wind shear at that level divided by the allowable wind drift (equation 6.11).

5) Determine the required stability ratio lateral stiffness from equation 6.12.

6) Determine the Global Stiffness Matrix.

A) Determine the required stiffnesses per floor as the maximum per floor stiffnesses from steps 2, 4, and 5.

B) Create a global stiffness matrix for a shear building (one lateral DOF per floor) which is based on the maximum required story stiffnesses

7) Determine the distribution of the mass to each of the floors according to equation 6.14.

8) Determine the Structural Properties of the SDOF model.

A) Calculate the frequencies of the MDOF system by calculating the eigenvalues of the matrix $K*M^{-1}$.

B) Assuming a mass of 1.0, determine the stiffness of the SDOF system according to equation 6.15.

C) If the fundamental period of vibration of the MDOF system is less than the approximate formula, then the C_s value needs to be recalculated using the new period. If the fundamental period of vibration is greater than or equal to that of the MDOF system, then use the C_s value determined in step 1.

D) The yield strength of the system is determined from equation 4.8. It may be appropriate to increase the yield strength determined in equation 4.8 by a certain amount to account for overstrength.

E) The vertical load applied to the system to achieve a desired stability ratio is determined from equation 6.16.

F) Choose a value for the post-yield stiffness ratio.

6.3 – Damage Measures

Four damage measures were used in the IDA study. Multiple damage measures were useful because the different damage measures represented different types of structures and different types of materials.

6.3.1 – Interstory Drift Ratio

The Interstory Drift Ratio (IDR) was used because the NEHRP Provisions put limitations on the amount of interstory drift a structure can sustain. Thus, the IDR provided a way to see if the NEHRP limits were violated. If the limits were violated, it was possible to see the level of intensity that caused the violation. The NEHRP story drift limitations are presented in table 5.2.8 of the Provisions. In general, the drift ratio limitations are between 1 and 2.5 percent of a given story height, depending on the type of structure and the seismic use group.

A possible shortcoming of the IDR values, as they relate to this study, is that the SDOF IDR values may not have indicated the true severity of a given drift value. This is because the lateral displacements of the SDOF models used in the IDA corresponded to the lateral displacements at the roof of the MDOF equivalent structure. The SDOF IDR does not take into account that the interstory drift ratios of an MDOF structure would mostly likely be higher than the roof drift ratios. Consider Figure 6.4.

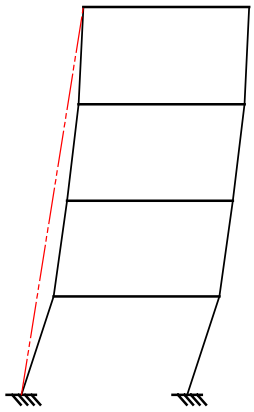

Figure 6.4 – Roof Drift Ratio versus Interstory Drift Ratio.

Notice that the drift ratio of the first story is higher than the drift ratio of the roof. In the case of Figure 6.4, it may be true that the drift limits of the SDOF model, which mimicked the roof displacement of a MDOF model, would not be violated, but could be violated if one considered the MDOF first floor IDR. Knowing the possible limitations of the IDR values, they were still generally useful for determining damage to the structures.

6.3.2 – Ductility Demand

The ductility demand was used because it, in conjunction with $r_{p,}$ can indicate possible collapse risks. From the parameter study, for a given r_p value, there was a range of ductility demand that tended to cause collapse. Recall that the r_p values were dependent both on the post-yield stiffness ratio and the stability ratio. In the IDA study, all structures had a post-yield stiffness ratio of 0.05 or 0.07. However, the stability ratios were primarily dependent on the stiffnesses. For the WUS models, the stability ratios were very small, and consequently only one of the WUS r_p values was negative. In the context of the parameter study, this meant that all but one of the WUS structures should never be in danger of collapse. However, in the CEUS models, many of the stability ratios were greater than 0.05 and 0.07, which meant that the r_p values for many CEUS models were negative and in danger of collapse given sufficient ductility demand. The IDA study provided a way to see the point where the negative r_p structures actually collapsed or at least the point where the deflections became excessive. In this manner, the IDA provided a way to see if the observations from the parameter study held true

Ductility demand was also useful because the deflection amplification factors used to create the models are a sort of ductility capacity measurement. Thus, if a structure's ductility demand exceeds the C_d value, then it may be significantly damaged and in danger of collapse.

6.3.3 – Park and Ang Damage Index

The Park and Ang (PA) damage index was used because it has been shown to be a reasonable measure of damage by many researchers (Cosenza 1993). Moreover, it is useful because it monitors damage due to maximum deflections as well as cyclic fatigue. Ductility demand and IDR only measures damage due to maximum displacements.

The PA equation is given by equation 2.46 in chapter two of this thesis. The calculation of the PA damage index was not as straightforward as one might think. The basic procedure, however, is relatively simple. The maximum displacement portion of the index was simply the maximum roof displacement of the structure. During the course of an analysis, each time the displacement reached a new maximum, the damage index increased as well.

Then, the energy related portion of the index increased each time the models yielded. To determine if the model was yielding at a particular time step, the base shear and roof displacement from the previous time step, in conjunction with the base shear and roof displacement of the current time step, were used to calculate the stiffness of the system. The system was yielding if the stiffness was equal to the post-yield stiffness ratio times the initial stiffness. The determination of the energy portion of the damage index was actually more complicated than this, however, because vertical accelerations and P-Delta effects augmented the shape of the force deformation curve for each of the models. Consider the force deformation relationship shown in Figure 6.5 for example.

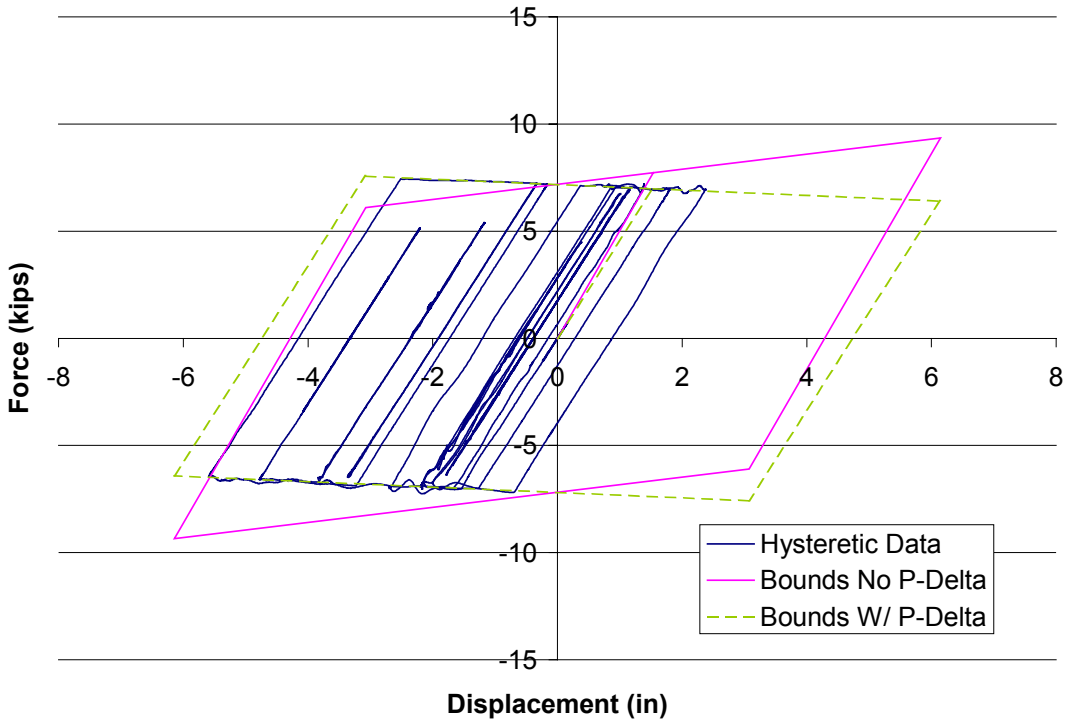

Figure 6.5 – Base Shear versus Roof Displacement

First, since each of the analyses in the IDA included P-Delta effects, the force deformation curves generally followed the shape of the hysteretic loop denoted with the dashed line. This was one augmentation of the force deformation relationship. Then, the effects of the vertical accelerations further augmented the force deformation relationship. The effects of vertical accelerations are more visible when the yielding portions of the hysteretic curve are examined more closely, as in Figure 6.6.

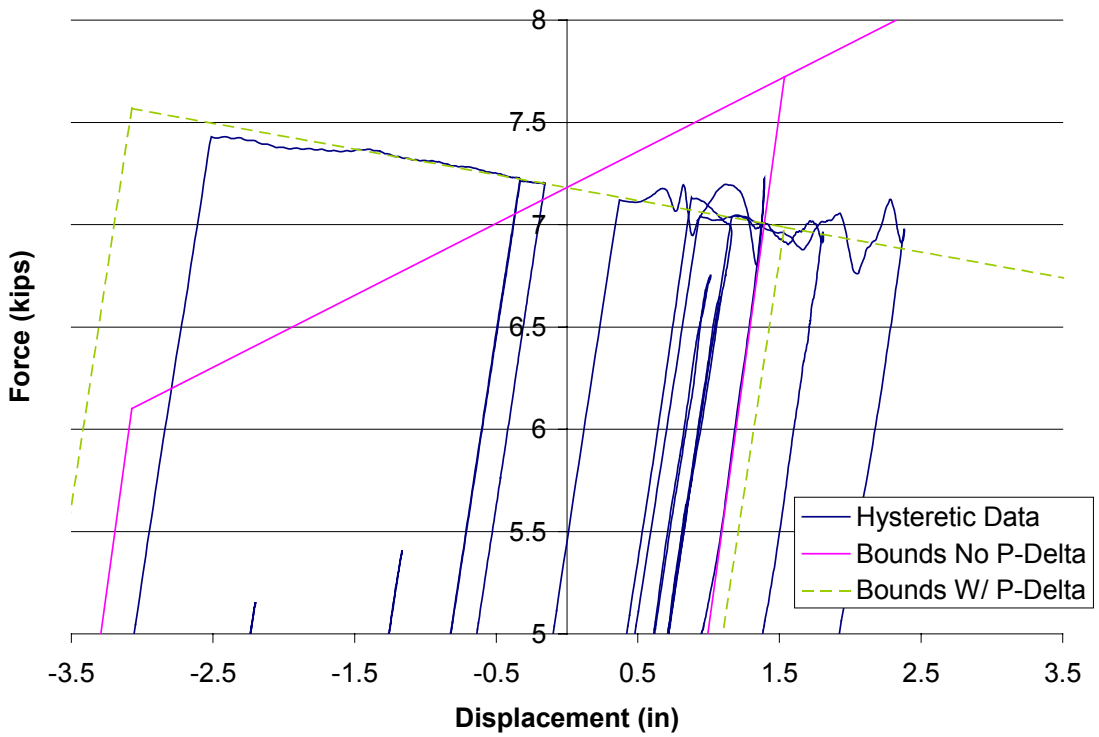

Figure 6.6 – Yielding Portion of Base Shear versus Roof Displacement History (Closer View of Figure 6.4)

In the yielding portions of the curve shown in Figure 6.6, the vertical accelerations increasingly caused fluctuations in the base shear values and consequently in the determination of the stiffness values. Thus, the stiffness based on base shear and roof displacement was not reliable for calculating the PA damage index. It was possible from figures like 6.5 to determine the yielding regions by visual inspection, but it was impractical to visually inspect every hysteresis history for every model at every earthquake scale used. The determination of energy dissipation had to be automated to be efficient and useful. A more stable response was available in the moment rotation relationship in the rotational springs. The spring moment rotation relationship corresponding to the analysis represented in Figure 6.5 is shown in Figure 6.7.

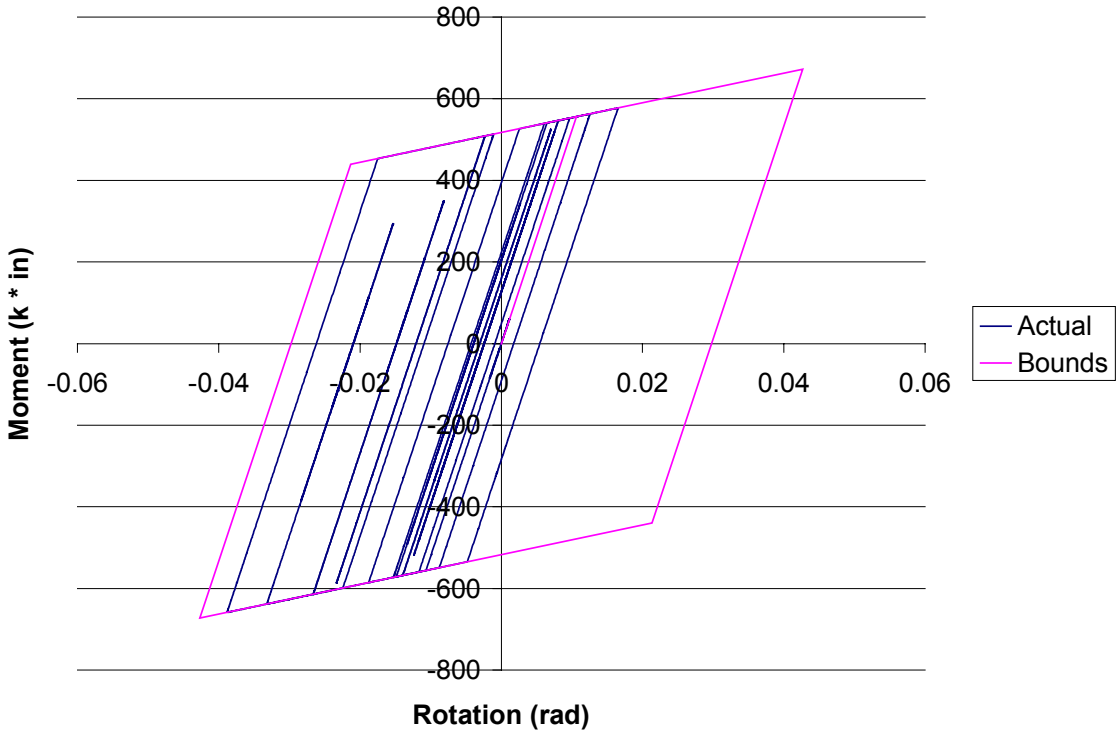

Figure 6.7 – Rotational Spring Moment-Rotation Relationship

From Figure 6.7, it is clear that the moment-rotation relationship was much more stable than the base shear versus roof displacement relationship of Figure 6.5. Thus, the moment-rotation relationship was used to determine the times when the models were yielding. When the rotational spring stiffness changed to the post-yield stiffness, the PA damage index was increased.

To summarize, calculating the PA damage index required the base shear, roof displacement, spring moment, and spring rotation response histories. The damage was calculated from the base shear and roof displacement response histories, but the spring moment and spring rotation histories were used to determine when the models were yielding.

6.3.4 – Kumar and Usami Damage Index

The final damage index used in the IDA was the Kumar and Usami (KU) index. The KU damage index was used because, like the PA damage index, it measured both

maximum displacement and cyclic fatigue damage. However, the KU index was different than the PA index in that the maximum displacement term considered the history of loading whereas the PA index did not. The PA index is only dependent on the single maximum displacement achieved during a given earthquake. Thus, the maximum displacement term of the PA index would be the same for an earthquake that had one maximum displacement excursion of 10 in. or 20 maximum displacement excursions of 10 inches. The KU index, on the other hand, takes the loading history into account in both the maximum displacement term and the energy related terms. Kumar and Usami (1996) experimentally examined damage imposed on steel box columns through cyclic loading. They found that loading history influenced damage. In fact, they found that more damage accumulated for consistently increasing cyclic displacements rather than for a similar series of high constant cyclic displacements. Thus, the KU index provided another interpretation of how damage accumulates in structures. The procedures for determining yield events for the KU index were similar to those for the PA index. Thus, like the PA index, the KU index calculations required the base shear, roof displacement, spring moment, and spring rotation response histories.

7.0 Incremental Dynamic Analysis Results and Discussion

7.1 - Introduction

Incremental Dynamic Analysis (IDA) was used in this research to both test the hypotheses of the parameter study, which were presented in chapter five, and to examine the performance of structures designed for the Central and Eastern United States (CEUS) and Western United States (WUS) over a range of reasonable earthquake intensities. The CEUS and WUS models were proportioned using the Equivalent Lateral Force (ELF) method as described in the NEHRP Provisions. Single-degree-of-freedom (SDOF) representations of multi-degree-of-freedom (MDOF) structures were used for the IDA. SDOF models were created to represent three, five, seven, and nine story steel moment frames for each of five sites for both the CEUS and WUS. Only a representative sample of the results is presented in this chapter, the majority of the results are included as figures in Appendix D (available electronically).

Damage in the models was measured using ductility demands, drift ratios, the Park and Ang (PA) damage index, and the Kumar and Usami (KU) damage index. Multiple damage measures (DM) were used because damage accumulates differently between various structural types and materials. Moreover, multiple DMs provide a higher level of confidence in either the adequacy or inadequacy of a particular structure.

In the IDA study, collapse was defined similarly to the definition used by FEMA 350 (2000). In the course of an IDA, a structure was considered collapsed if the slope of the Intensity Measure (IM) versus DM curve approached zero. In other words, a model was considered collapsed when small increases in intensity resulted in large increases in damage.

This chapter is organized into two sections. The first section describes the results of the core IDA study comprised of the set of models, earthquakes, and scale factors described in chapter six. Based on trends observed in the core data, it was decided that a few additional IDA analyses with strength variations should be examined. A discussion of the data collected beyond the core set of data is included in the second section of this chapter. Nonlin (Charney 1997) was used to generate the additional IDA data included in

section two, because it provided quick graphical feedback on the changes of various earthquake and structural parameters. All eight earthquakes from the parameter study were used in the second section.

7.2 - Core IDA Results

As previously mentioned, the core IDA data set consisted of SDOF analytical models representative of three, five, seven, and nine story buildings. Five sites were chosen in both the CEUS and WUS to provide a range of structural characteristics and responses. In the CEUS, Memphis, TN, Charleston, SC, Boston, MA, and New York City, NY were used. The fifth site was a composite site representing both Washington D.C. and Chicago, IL. The seismic hazards associated with Chicago and Washington D.C. were very similar, so the two sites were merged to make one. Then, in the WUS, Los Angeles, CA, San Francisco, CA, Seattle, WA, and Salt Lake City, UT were used. A fifth site was included in the WUS set by adding another model designed for San Francisco, which was based on a lower R value than the original design. A summary of the structural parameters associated with the core set of IDA models is presented in Tables 6.3, 6.4, and 6.5.

The core set of IDA models was subjected to three earthquake records. From the parameter study, the Taft (EQ 4) and Hollister (EQ 5) ground motions were used. The lateral ground motion from these earthquakes was scaled in the IDA. The vertical ground motion was included, but was used at the original scale. Then, a ground motion from the 1994 Northridge earthquake (EQ 9) was used. This ground motion was chosen because it had a strong vertical component. The vertical PGA was 0.544g. The recording station of the Northridge accelerograms was at Coldwater Canyon in North Hollywood.

The lateral ground motions were scaled according to PGA rather than according to spectral acceleration. Spectral acceleration is the scaling procedure of choice when using IDA in design situations. This is what is advocated by FEMA 350 (FEMA 2000a). So, an explanation of the PGA scaling choice is in order. In a design situation, IDA is carried out on a single building using a suite of ten to twenty ground motions. In such a situation, scaling according to spectral acceleration greatly reduces the dispersion in the

set of IDA curves created from the suite of earthquake ground motions (Vamvatikos 2002a). However, if one is interested in a family of buildings, say all of the buildings in New York City less than ten stories high, then scaling according to the spectral acceleration becomes problematic. PGA scaling provides a means of scaling that is applicable to all structures and at the same time not specifically tailored for the response of one structure.

For each of the sites, the ground motions were scaled from zero to a level that was about twice the PGA of a probable two percent in fifty year earthquake. Thus the range of PGA values used at a given site was proportional to the seismic hazard for that site. The probable two percent exceedance in fifty year and ten percent exceedance in fifty year PGA values for the sites used in the IDA are listed in Table 6.1.

7.2.1 – Core IDA Results using Ductility Demands as a Damage Measure

To begin this discussion, the CEUS models and results will be addressed first. The order of discussion will be the highest CEUS seismic hazard sites to the lowest CEUS seismic hazard sites. In general, the CEUS models had lower yield strengths, lower stiffnesses, and higher stability ratios than their WUS counterparts. Also, the deflection amplification factors, C_d, were generally less than those in the WUS. The lower deflection amplification factors meant that CEUS structures should have lower ductility capacities.

Of the CEUS models, the Memphis and Charleston sets of buildings were designed for the highest seismic forces. In fact, the Memphis family of models was stiffer and stronger than the Los Angeles family of buildings. The Charleston family of models was slightly less stiff and strong, but were still comparable to moderate hazard WUS designs. The stability ratios of the Memphis buildings were all less than 0.052 and the post-yield stiffness ratios were either 0.05 or 0.07, which meant that the post-yield stiffness ratios considering P-Delta effects (r_p) were rarely negative. Moreover, when they were negative, it was very slightly. The smallest r_p value for the Memphis sites was –0.002. For the Charleston buildings the stability ratios were higher, but the post-yield

stiffness ratios remained the same. Consequently, about half the combinations of stability ratio and post-yield stiffness ratio resulted in negative r_p values for the Charleston sites. Of those r_p values that were negative, the smallest r_p for the Charleston sites was –0.036. Based on the results of the parameter study, it would seem that very few of the Memphis models and perhaps half of the Charleston models would be in danger of collapse.

As it turned out, the IDA did indeed verify the aforementioned statement. The results of several of the Memphis and Charleston IDAs using ductility demand as the damage measure are shown in Figures 7.1a through 7.1d. Each figure in the 7.1 series corresponds to a single structure with a given yield strength and stiffness. The other two structural parameters used to define the models, post-yield stiffness ratio and stability ratio, were left as variables. Each curve in a figure corresponds to a combination of post-yield stiffness ratio and stability ratio. The names of the curves shown in the legend indicate the post-yield stiffness ratios and stability ratios used for that IDA series. For example, in Figure 7.1a, the first curve shown in the legend has the name, "R0.05ST0.022," which corresponds to a post-yield stiffness ratio of 0.05 and a stability ratio of 0.022. From the naming scheme, it is easy to quickly identify those structures that had negative r_p values. If the stability ratio is larger than the post-yield stiffness ratio then r_p for that series was negative. For each stability ratio and post-yield stiffness ratio combination, two IDAs were conducted, one that included vertical accelerations and one that did not. The series that included vertical accelerations was distinguished by adding a "V" to the end of the series name in the legend. Also shown in the 7.1 series of Figures are the PGA levels corresponding to the probable two percent in fifty year (2/50) earthquake and the probable ten percent in fifty year (10/50) earthquake of that particular site.

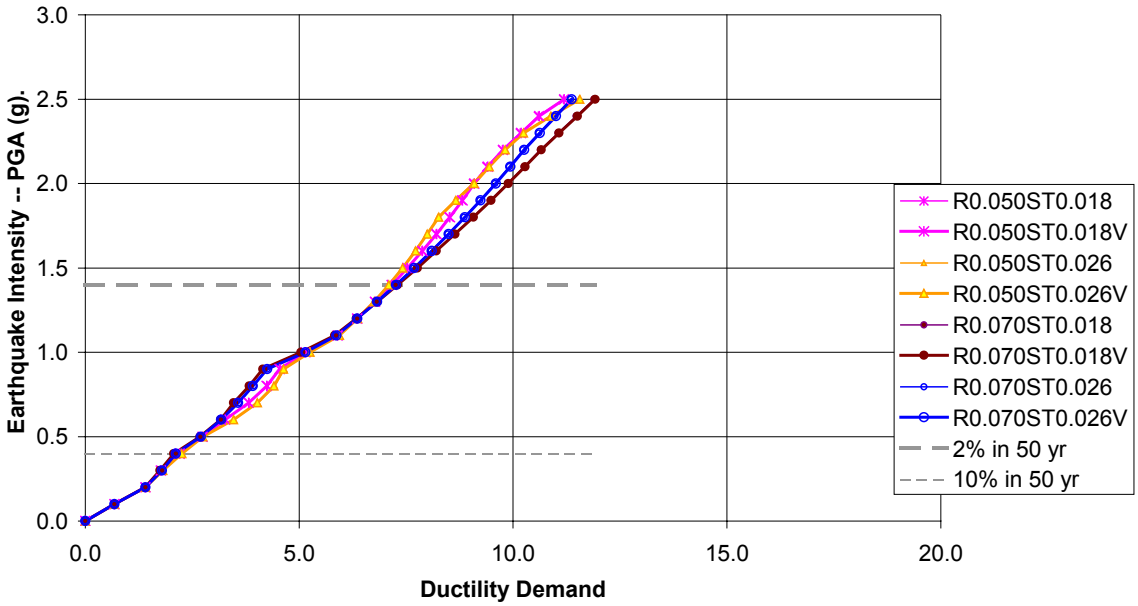

Figure 7.1a – Ductility Demands of the Memphis 3 Story Models Subjected to the Taft Earthquake (EQ 4).

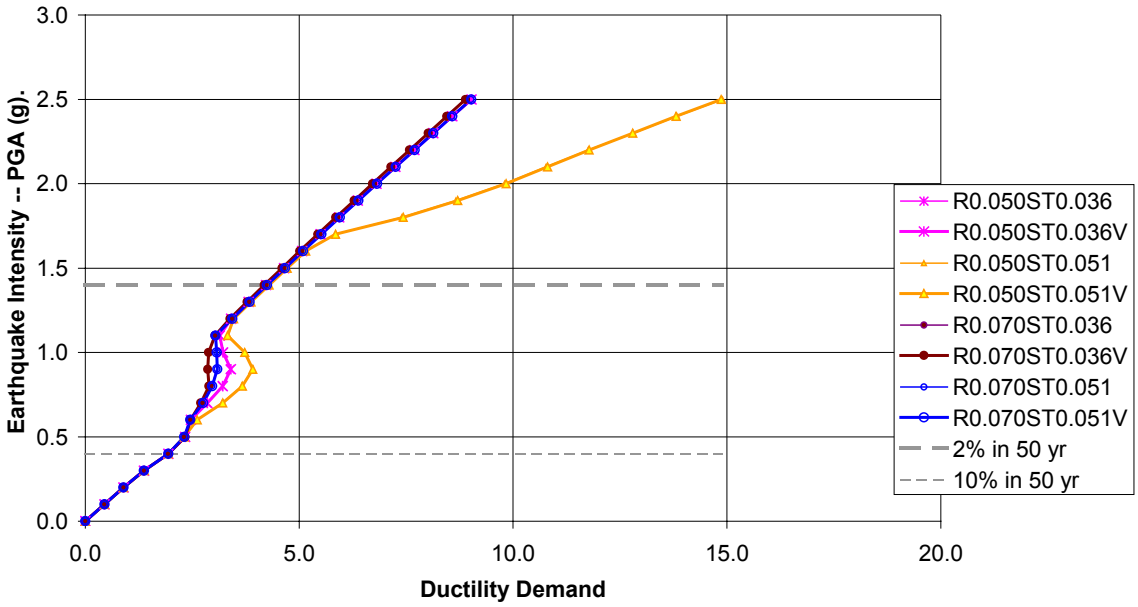

Figure 7.1b – Ductility Demands of the Memphis 7 Story Models Subjected to the Taft Earthquake (EQ 4).

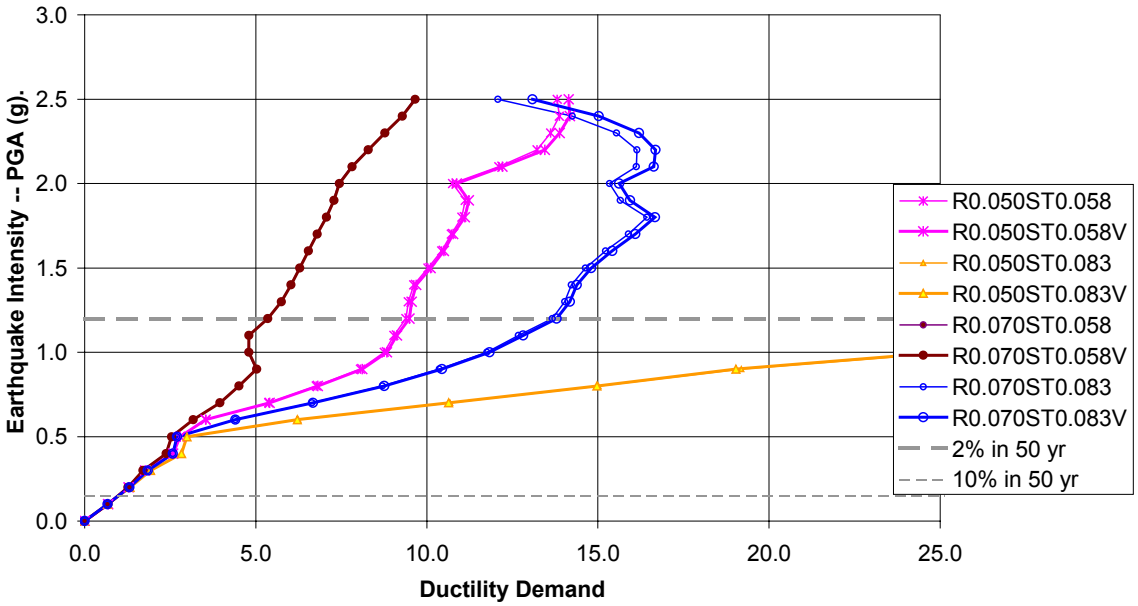

Figure 7.1c – Ductility Demands of the Charleston 5 Story Models Subjected to the Hollister Earthquake (EQ 5).

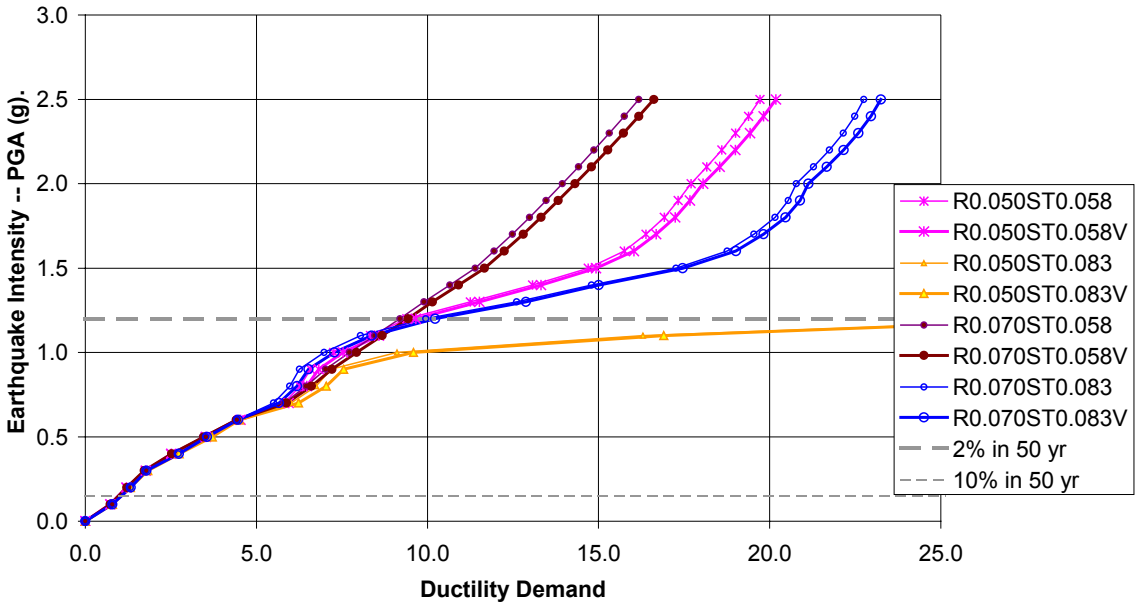

Figure 7.1d – Ductility Demands of the Charleston 5 Story Models Subjected to the Northridge Earthquake (EQ 9).

Several observations about the 7.1 series of figures are worth mentioning. First, if the deflection amplification factors (C_d), used to design the structures, are truly indicative of the ductility capacity and if a damage-based collapse rule is used, then it is likely that the majority of the Memphis and Charleston buildings would either collapse or be close

to collapsing in the event of the 2/50 earthquake. The C_d value used for both the Memphis and Charleston sites was 5.5. The ductility demands at the 2/50 level were at least close to 5 for most of the curves in the 7.1 figures. It is likely that if a ductility demand greater than 5.5 would be considered collapsed, that one around 5 would be close to collapse.

Another observation regarding the Memphis and Charleston sites is that the IDA curves in a given 7.1 figure generally followed a common linear path when the r_p values were positive. There may have been some weaving and slight deviation from the common path, but the positive r_p IDA curves generally followed it. This is because the common linear paths coincided with the equal displacement line.

For those models with positive r_p, not only did the IDA curves follow the equal displacement line, but they also continued on the equal displacement line indefinitely. For the bilinear models used in this study, a model would never collapse, that is, the slope of the IDA curve would never approach zero if the r_p value was not less than zero. This is because the bilinear models used in this study had infinite ductility capacity. Only a model that could account for damage in the structural properties of a model would have finite displacement limitations if the r_p value were positive.

While the positive r_p IDA curves in the 7.1 series of figures generally followed the equal displacement line, the negative r_p IDA curves tended to deviate from it. The effect of negative rp is seen most clearly in Figure 7.1b. In this figure, only the "R0.050ST0.051" IDA curve deviated from the common path. Moreover, this is the only IDA curve in that figure that had a negative r_p value. In the IDA curves, increasingly smaller r_p values in the negative range generally increased the ductility demands, or decreased the slope of the IDA curves.

The results of the Charleston buildings, in Figures 7.1c and 7.1d, clearly show the effects of decreasing r_p in the negative range. In Figures 7.1c and 7.1d, only one of the IDA curves has a mostly linear slope. The linear curve happens to correspond to models that had a positive r_p value. All of the other IDA curves in Figures 7.1c and 7.1d have nonlinear slopes and negative r_p values. Furthermore, the smaller the negative r_p value, the higher the ductility demands.

While all of the structures might be considered collapsed at the 2/50 intensity according to a damage-based rule, only the model, "R0.050ST0.083", which corresponds to a negative r_p value of –0.036, of Figures 7.1c and 7.1d would likely be considered collapsed according to an intensity-based collapse rule. The slope of the R0.050ST0.083 curves is quite flat by the time that 1.0g PGA is reached. Notice that a PGA 0f 1.0g is less than that of the probable 2/50 event.

Finally, from the 7.1 figures it would seem that vertical accelerations were not influential unless the r_p values were negative. From Figures 7.1a and 7.1b corresponding to the Memphis sites, the change in ductility demand due to the inclusion of vertical accelerations was negligible. Recall that the vast majority of the Memphis models had positive r_p values. On the other hand, about half of the Charleston models had negative r_p values and vertical accelerations did affect the Charleston sites to some extent. The changes in ductility demands resulting from the inclusion of vertical accelerations in the analyses of Figure 7.1c are shown in Figure 7.2a. The changes in ductility demands resulting from the inclusion of vertical accelerations in the analyses of Figure 7.1d are shown in Figure 7.2b. Positive changes in ductility demand indicate an increase in ductility demand due to vertical accelerations, and negative changes indicate a decrease.

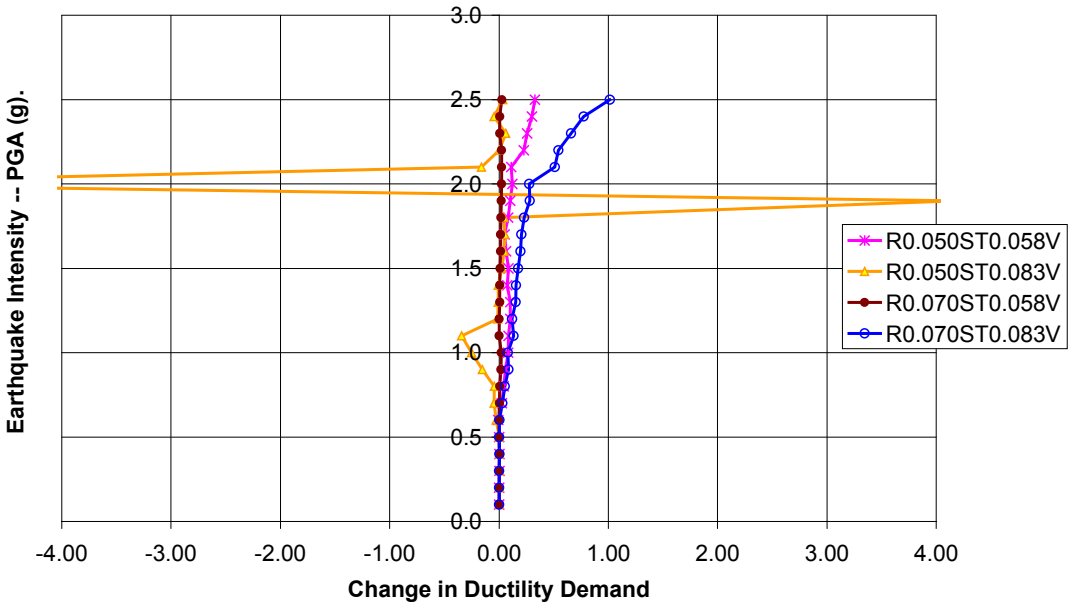

Figure 7.2a – Change in Ductility Demands for the Charleston 5 Story Models Subjected to the Hollister Earthquake (EQ 5).

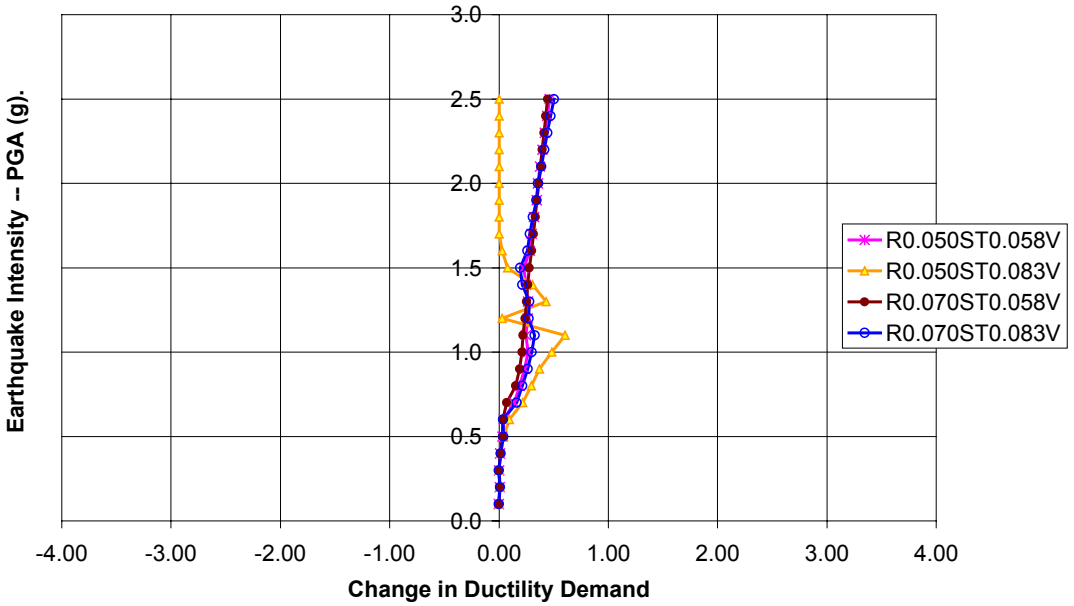

Figure 7.2b – Change in Ductility Demands for the Charleston 5 Story Models Subjected to the Northridge Earthquake (EQ 9).

From Figures 7.1a and 7.1b, it seems that vertical accelerations generally changed the ductility demand by about 0.5 to 1.0. In Figures 7.1a and 7.1b, the change is positive, that is, vertical accelerations increased the ductility demands. A positive change did not always occur, however. Curves with negative changes in ductility demands will be shown later. It is worth pointing out that the only real deviation from the 0.5 to 1.0 change in the ductility demand occurred at 2.0g PGA in figure 7.1a. This anomaly occurred at an unreasonably high intensity range because the structure had collapsed at about 1.0g PGA. Thus, this spike in ductility demand change should be disregarded.

While there was an increase in ductility demand for both Figures 7.1a and 7.1b, the increase was rather small and occurred at an intensity that was higher than the 2/50 earthquake. Thus, it would generally seem that vertical accelerations did not significantly alter the lateral displacements for the CEUS structures designed for high seismic hazards when the r_p values were positive, and marginally altered displacements when the r_p values were negative.

The observations regarding the Memphis and Charleston ductility demand are instructive. However, it is important to examine the ductility demands of the other structures as well. The ductility demands of several of the New York City and Boston models are shown in Figures 7.3a through 7.3d. These models were designed for moderate seismic hazard. The New York City buildings were required to be special moment frames (R = 8, C_d = 5.5) and the Boston buildings were required to be intermediate moment frames (R = 5.5, C_d = 4). The stability ratios of the Boston and New York City buildings were generally higher than those of the Memphis and Charleston models. In fact, all of the Boston and New York City models had negative r_p values.

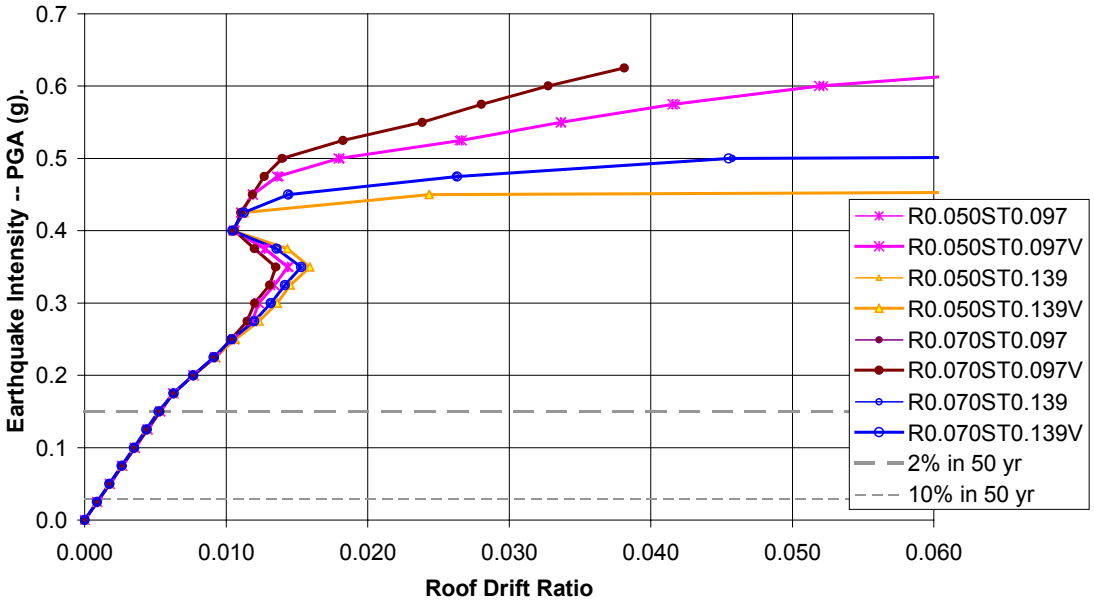

Figure 7.3a – Ductility Demands of the Boston 3 Story Models Subjected to the Taft Earthquake (EQ 4).

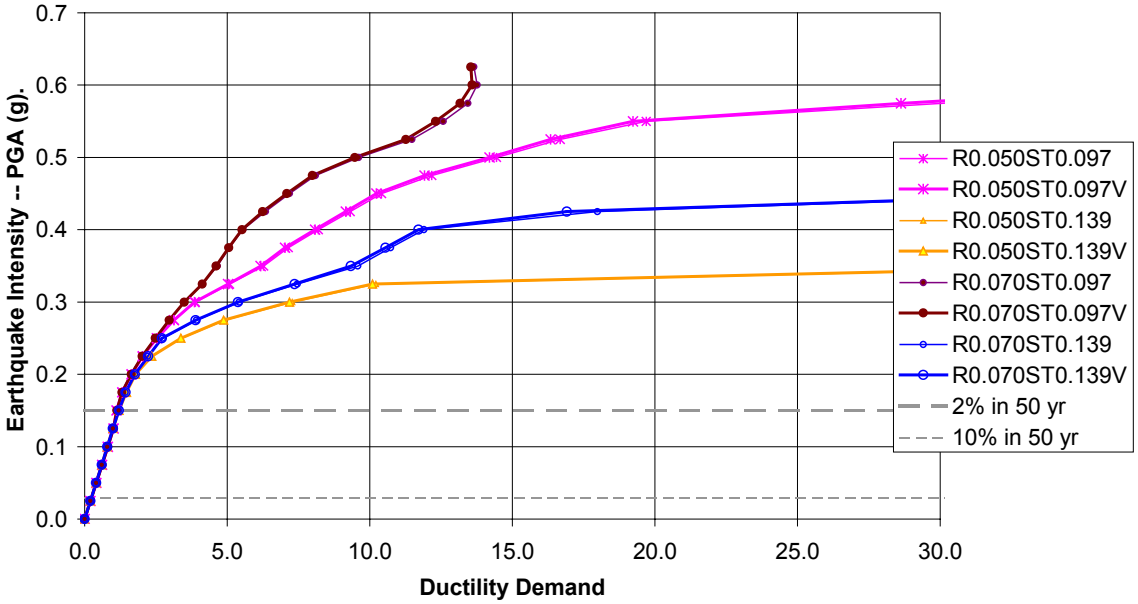

Figure 7.3b – Ductility Demands of the Boston 7 Story Models Subjected to the Taft Earthquake (EQ 4).

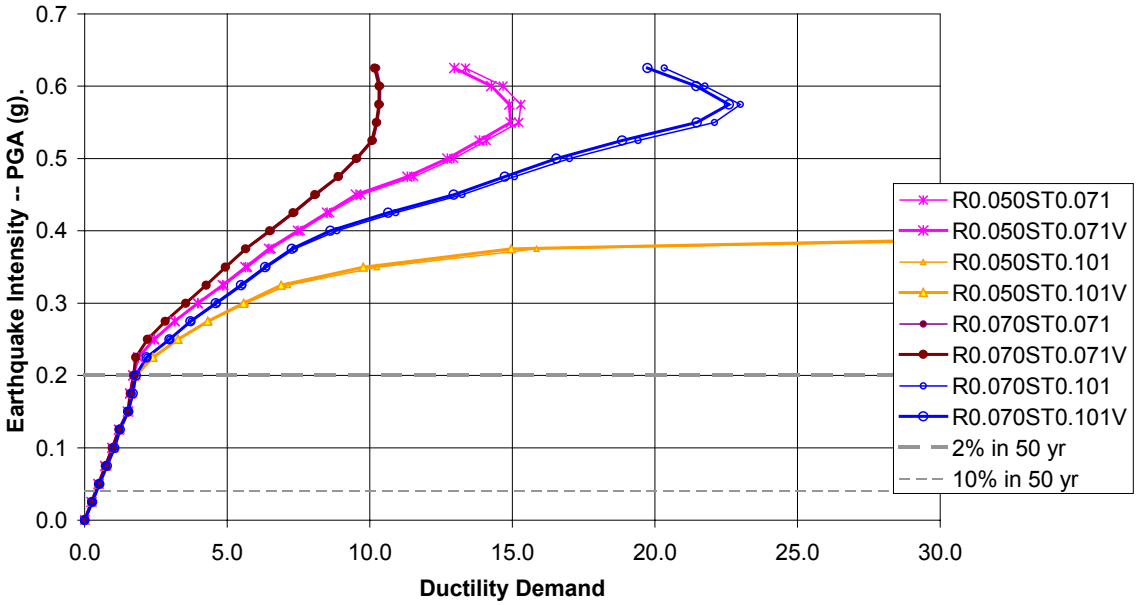

Figure 7.3c – Ductility Demands of the New York City 5 Story Models Subjected to the Taft Earthquake (EQ 4).

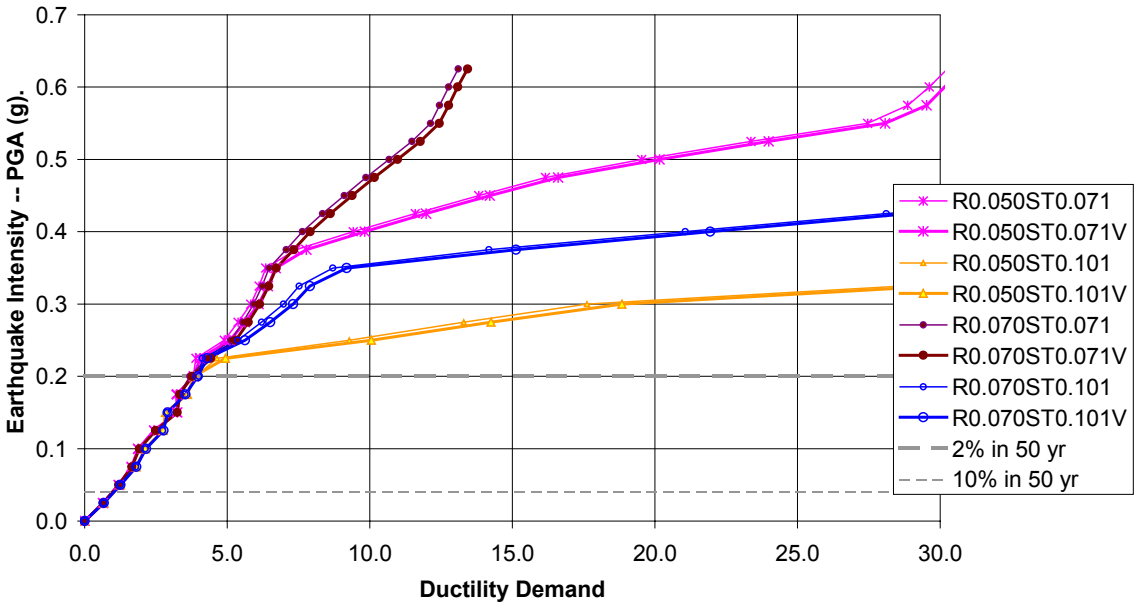

Figure 7.3d – Ductility Demands of the New York City 3 Story Models Subjected to the Northridge Earthquake (EQ 9).

If using a damage-based rule to determine collapse, all of the Boston and New York City Models shown in Figures 7.3a through 7.3d would not collapse in the event of the 2/50 earthquake. Even if using an intensity-based rule to determine collapse, none of the models would be considered collapsed at the 2/50 PGA. The models do collapse, but at intensities that are higher than the 2/50 PGA.

Considering vertical accelerations, the ductility demands of the moderate hazard CEUS structures changed about the same amount as the Charleston site ductility demands. However, there was one difference between the moderate seismic hazard CEUS sites and the Charleston sites. In the moderate seismic hazard CEUS sites, as the ground motion intensities increased, there tended to be a spike in the influence of vertical accelerations at a given intensity and then the vertical accelerations did not influence the models any more. The spikes occurred most frequently in the models with the smallest r_p values, that is, the most negative. This was the case in the parameter study as well. Several plots of the change in ductility demand due to the inclusion of vertical accelerations for the Boston and New York City analyses are shown in Figures 7.4a through 7.4d.

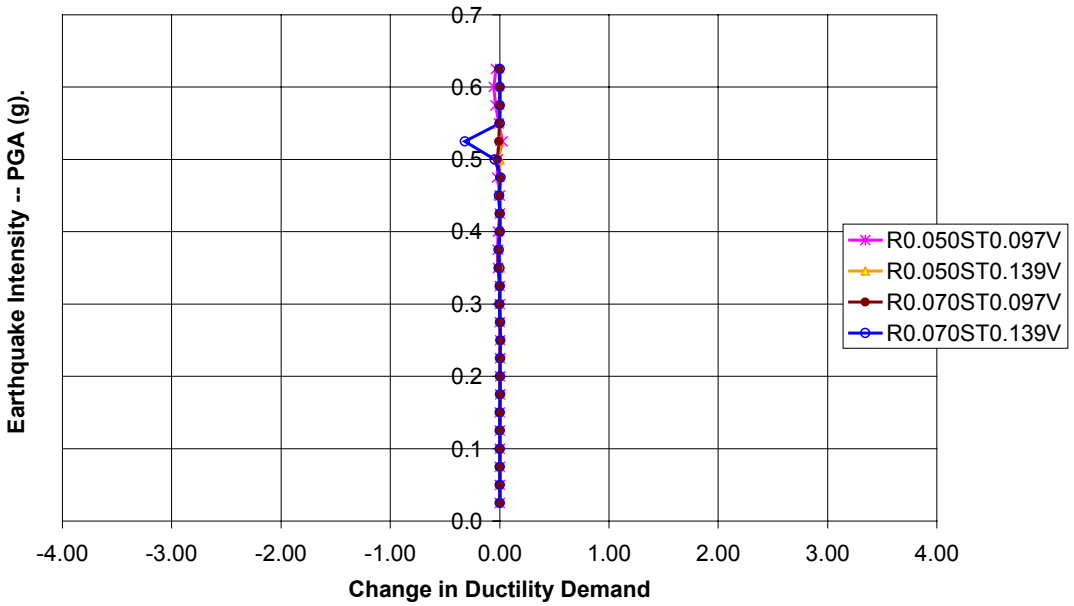

Figure 7.4a – Change in Ductility Demands of the Boston 3 Story Models Subjected to the Taft Earthquake (EQ 4).

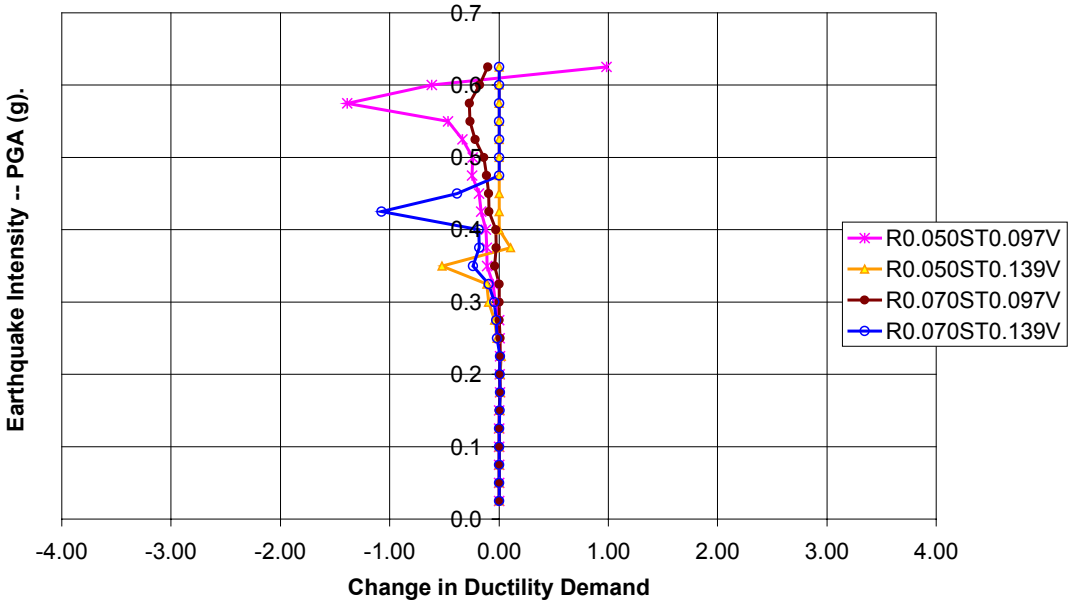

Figure 7.4b – Change in Ductility Demands of the Boston 7 Story Models Subjected to the Taft Earthquake (EQ 4).

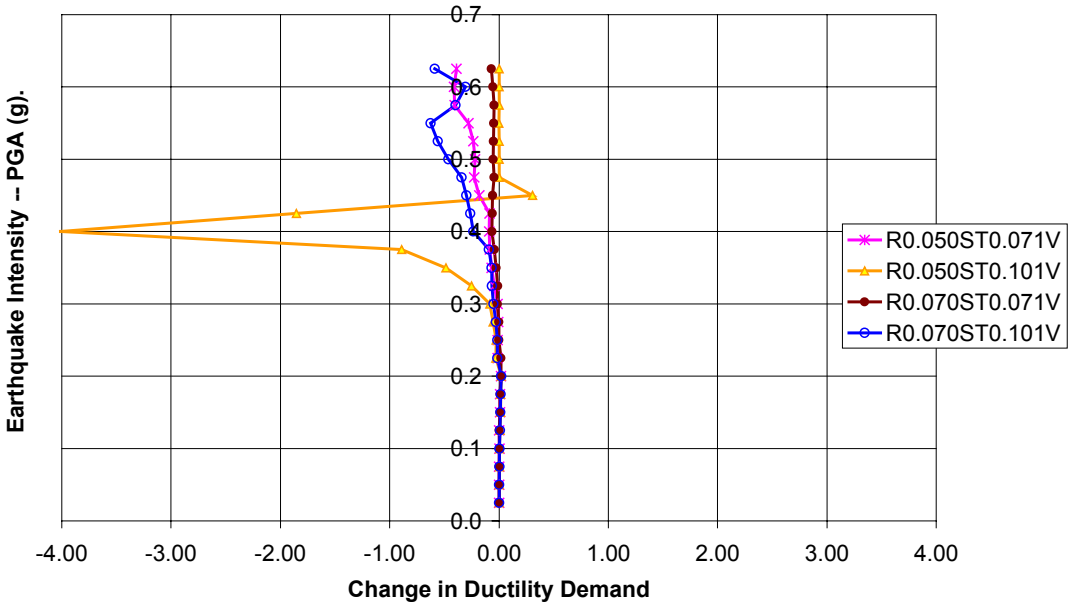

Figure 7.4c – Change in Ductility Demands of the New York City 5 Story Models Subjected to the Taft Earthquake (EQ 4).

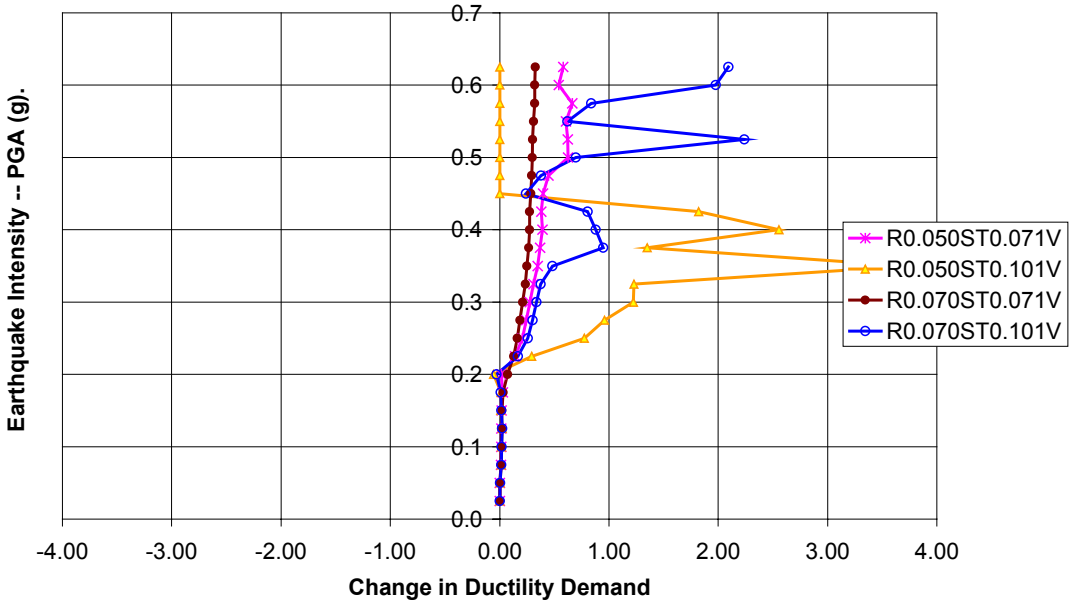

Figure 7.4d – Change in Ductility Demands of the New York City 3 Story Models Subjected to the Northridge Earthquake (EQ 9).

The change in ductility demand for the moderate hazard CEUS structures was generally between 0.5 and 1.0. However, there were some exceptions. The structures with stability ratios of 0.097 and 0.101 experienced larger ductility demand changes than the other models in some situations. In Figures 7.4c and 7.4d, for example, the ductility

demands of the R0.050ST0.101 models changed by a value of about 4.0 due to the inclusion of vertical accelerations. It is worth noting that in Figure 7.4c the vertical accelerations decreased the ductility demands of the R0.050ST0.101 model by about 4.0. Then, they increased the ductility demands of the R0.050ST0.101 model by about 4.0 in Figure 7.4d. Figures 7.4c and 7.4d illustrate the fact that it is impossible to predict whether vertical accelerations will reduce or increase displacements before an analysis.

Figures 7.3b, 7.4b, 7.3c, and 7.4c reinforce the observation in the parameter study that vertical accelerations cause the largest increases in ductility demand at the point just before collapse. The spikes in the "Change in Ductility Demand" plots correspond with the PGA intensities at the points just before collapse.

The last of the CEUS sites was the low seismic hazard site representing Chicago and Washington D.C. These models were comparable in strength to the Boston models; however, they had lower ductility capacities and were less stiff. It was assumed that the low seismic hazard CEUS structures would be ordinary steel moment frames. Thus, the deflection amplification factor was equal to three for these models. Three IDA plots from the low seismic hazard site are shown in Figures 7.5a through 7.5c.

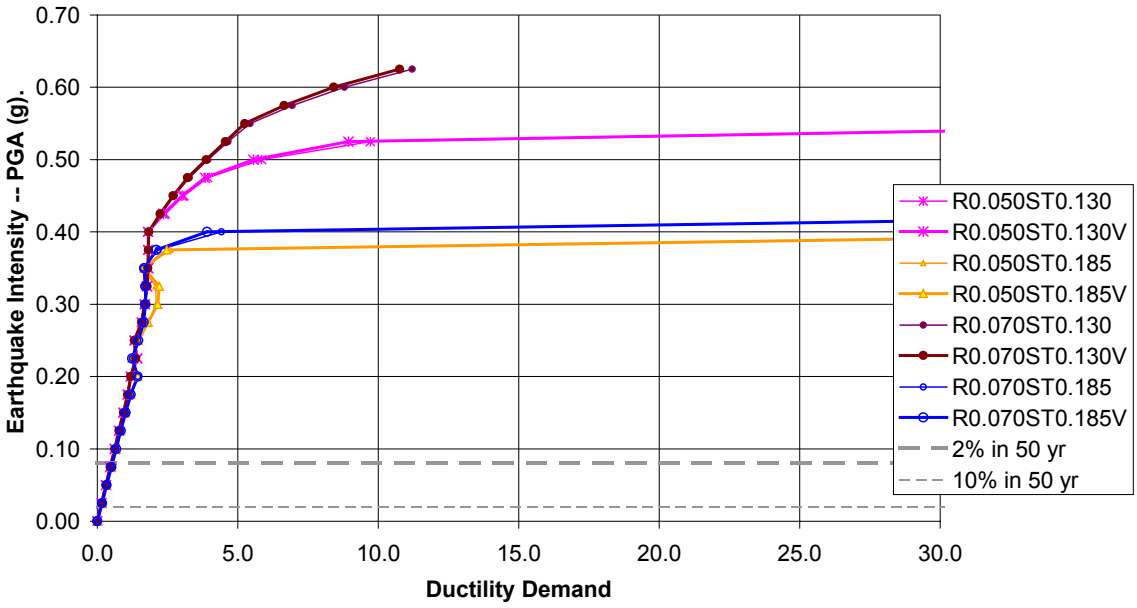

Figure 7.5a – Ductility Demands of the Chicago and Washington D.C. 3 Story Models Subjected to the Taft Earthquake (EQ 4).

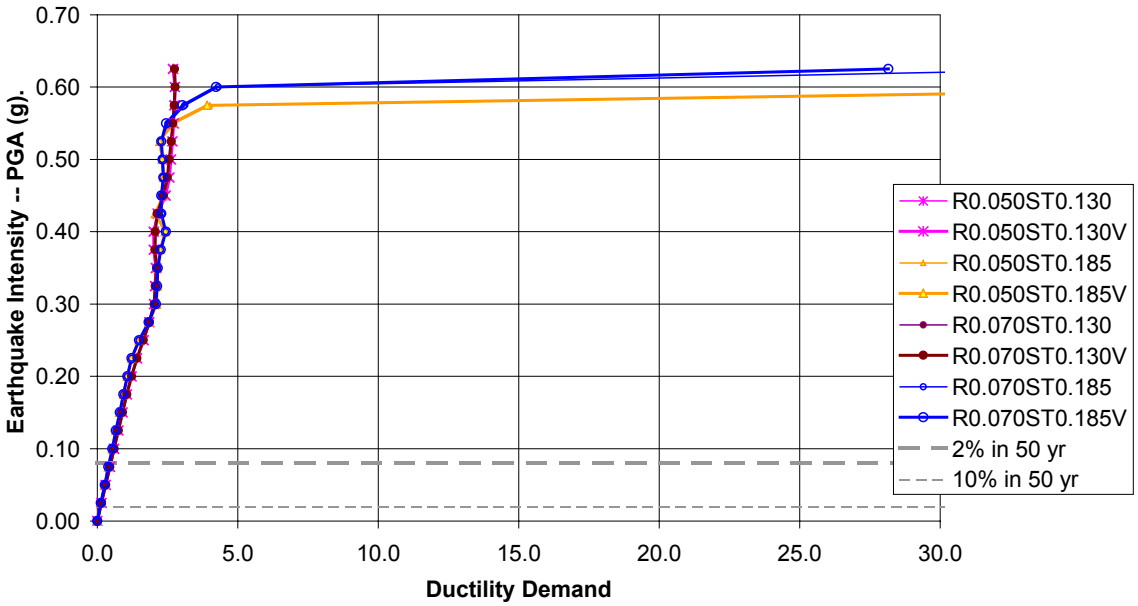

Figure 7.5b – Ductility Demands of the Chicago and Washington D.C. 3 Story Models Subjected to the Hollister Earthquake (EQ 5).

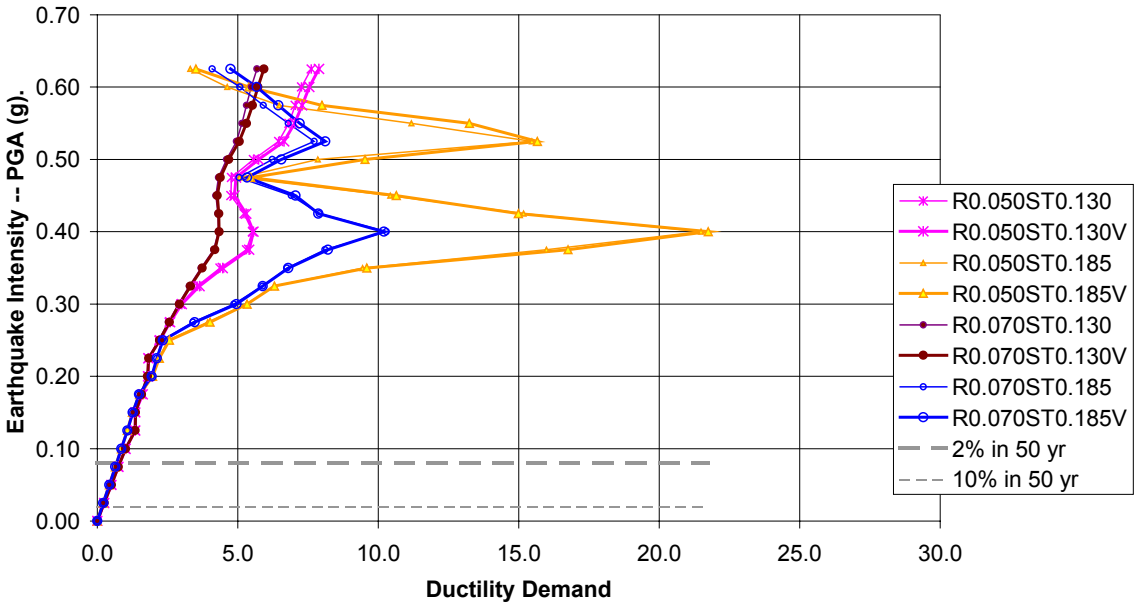

Figure 7.5c – Ductility Demands of the Chicago and Washington D.C. 3 Story Models Subjected to the Northridge Earthquake (EQ 9).

Notice that the 2/50 earthquake PGA level is quite low compared to all of the other sites discussed thus far. Furthermore, notice that there is a range of collapse intensities, but that the average collapse intensity of the CEUS models is about equal to the average collapse intensities of the Boston models shown in Figures 7.3a and 7.3b.

Based on the CEUS data, it seems that there was a relationship between the collapse intensity and the yield force. Structures with higher yield forces tended to collapse at higher PGA values than lower yield force structures. Both the Boston and Chicago/Washington D.C. models had about the same yield strengths and collapse PGA values. The New York City models had the lowest yield strengths of the CEUS models and thus generally had collapse intensities that were lower than all of the other CEUS models. This issue is discussed further in section two of this chapter.

As with the other CEUS models, vertical accelerations increased the lateral displacements in some situations. As with the other CEUS models, the ductility demands were changed, on average, between 0.5 to 1.0.

In contrast to the CEUS models, the WUS models had higher yield strengths, higher stiffnesses, and lower stability ratios. Based on the seismic design categories of the WUS models, all were designed as special steel moment frames. Thus, the R values were all 8 and the C_d values were all 5.5. The WUS IDA figures created from the Los Angeles and San Francisco sites closely resemble the Memphis IDA Figures 7.1a and 7.1b. Moreover, the Seattle and Salt Lake City IDA figures resemble the Charleston figures. Thus, only a few of the WUS figures are required to show the trends typical to all WUS structures. An example from each of the WUS sites is provided in Figures 7.6a through 7.6d.

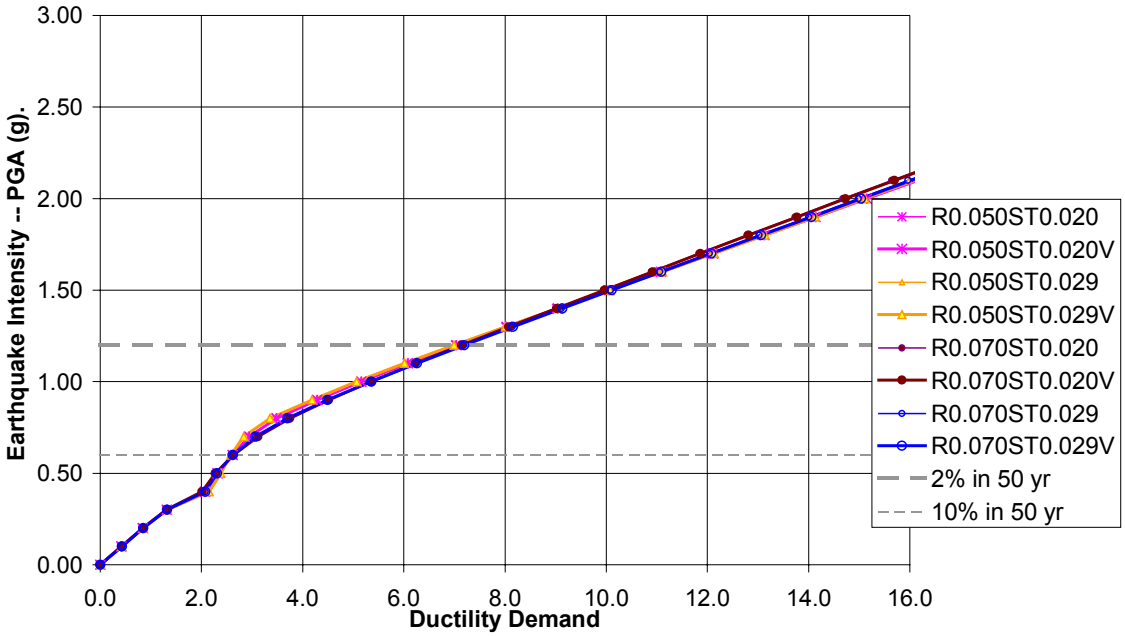

Figure 7.6a – Ductility Demands of the Los Angeles 3 Story Models Subjected to the Northridge Earthquake (EQ 9).

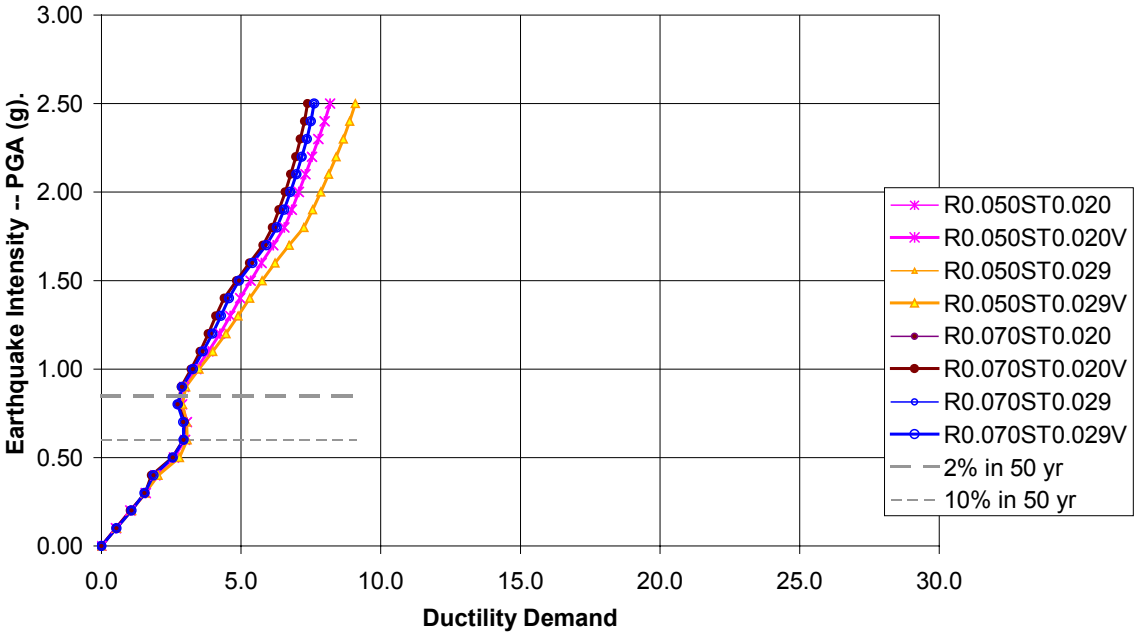

Figure 7.6b – Ductility Demands of the San Francisco A 5 Story Models Subjected to the Hollister Earthquake (EQ 5).

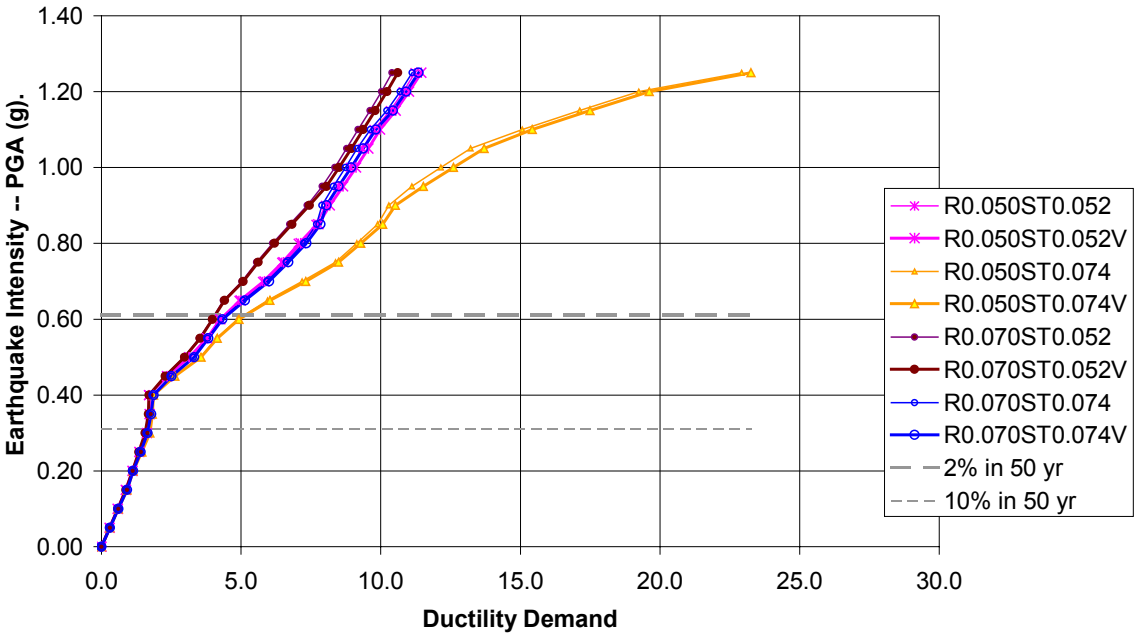

Figure 7.6c – Ductility Demands of the Seattle 5 Story Models Subjected to the Northridge Earthquake (EQ 9).

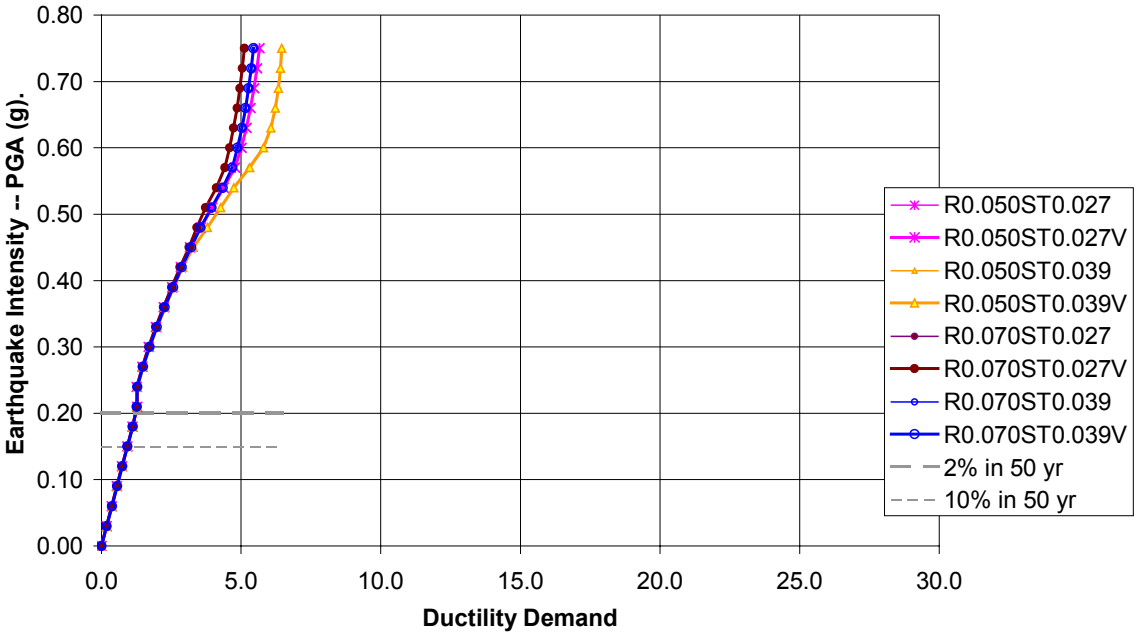

Figure 7.6d – Ductility Demands of the Salt Lake City 3 Story Models Subjected to the Taft Earthquake (EQ 4).

Of the WUS structures shown in Figures 7.6a through 7.6d, it would seem that the Los Angeles and Seattle structures would be in danger of collapsing according to a damage-based rule if the probable 2/50 earthquake were to occur. This is assuming that the ductility limit was the C_d value, 5.5. On the other hand, the San Francisco and Salt Lake City buildings have relatively low ductility demands. As has been stated earlier, the difference in ductility demands is likely related to yield strength. The higher the yield strength, the lower the ductility demands and higher the collapse intensity.

Of the WUS models, none of the models were significantly affected by vertical accelerations. However, the Seattle models were moderately influenced by vertical accelerations. As in the other models, those Seattle models that were affected had negative r_p values. It is important to note that the Charleston models were more affected by vertical accelerations than the Seattle models. Moreover, the Seattle models were more affected by vertical accelerations than the Salt Lake City models. From the data, it seems that this was most likely because of the strengths of the models. Of the three sites just described, the Salt Lake City models had the highest yield strengths, the Seattle models were in the middle, and the Charleston models had the lowest yield strengths.

7.2.2 – Summary of Core IDA Ductility Demand Results

From the core IDA study using ductility demand to measure damage, several observations were applicable to all structures. First, bilinear models with positive r_p values will never collapse according to an intensity-based collapse rule. Second, bilinear models with a negative r_p will almost always collapse at a given intensity according to an intensity-based collapse rule. Vertical accelerations can at least moderately affect the ductility demands of a model with a negative r_p value as the earthquake intensity approaches the collapse intensity. In general, increasing stability ratio or decreasing the post-yield stiffness ratio will increase the ductility demands of the IDA. Increasing the strength of a model will generally increase the intensity at which collapse occurs.

7.2.3 – Core IDA Results using Roof Drift Ratio as a Damage Measure

The second DM used in the IDA was the roof drift ratio. The roof drift ratio IDA figures basically show the same information as in the ductility demand figures, but scaled differently. Moreover, the limitations on the drift ratio provide another DM whereby the adequacy or inadequacy of the models can be assessed. Since the shapes of the roof drift ratio IDA figures are similar to the ductility demand figures that have already been presented, only a few of the roof drift ratio figures are presented in this section. The figures are included primarily to show how the drift values are the ductility values normalized to a different scale and to show how the drift limits impose a different damage-based collapse rule on the models. Figures 7.2a through 7.2e show the roof drift IDA figures that correspond to several of the IDA figures in the ductility demand section. For the IDA study, a structure was considered collapsed if the roof drift ratio reached a value of 0.02.

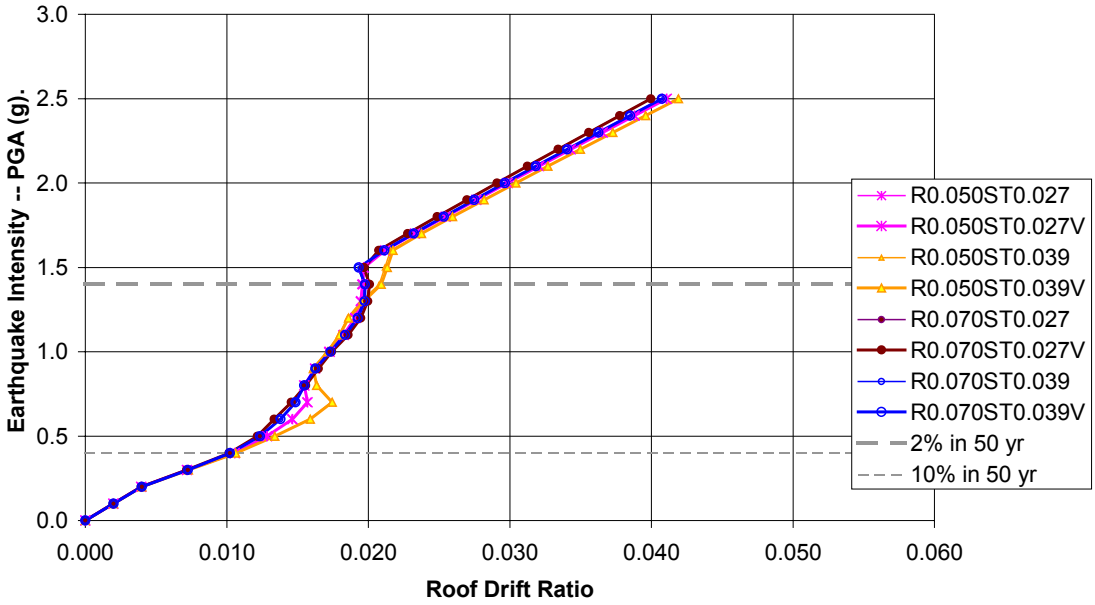

Figure 7.7a – Roof Drift Ratio of the Memphis 5 Story Models Subjected to the Taft Earthquake (EQ 4) – Corresponds to Figure 7.1a.

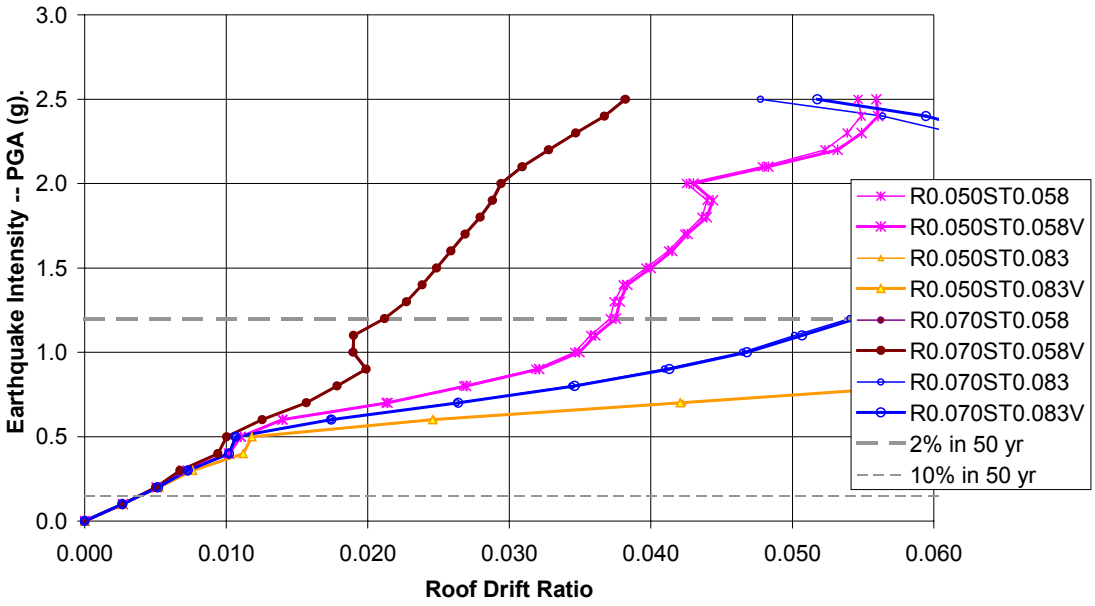

Figure 7.7b – Roof Drift Ratio of the Charleston 5 Story Models Subjected to the Hollister Earthquake (EQ 5) – Corresponds to Figure 7.1c.

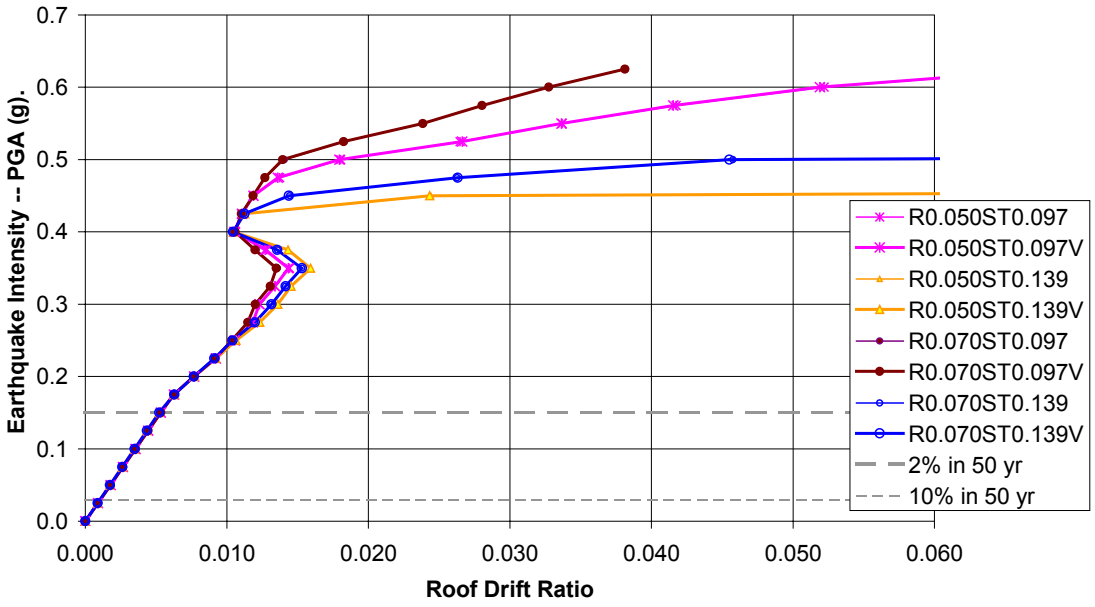

Figure 7.7c – Roof Drift Ratio of the Boston 3 Story Models Subjected to the Taft Earthquake (EQ 4) – Corresponds to Figure 7.3a.

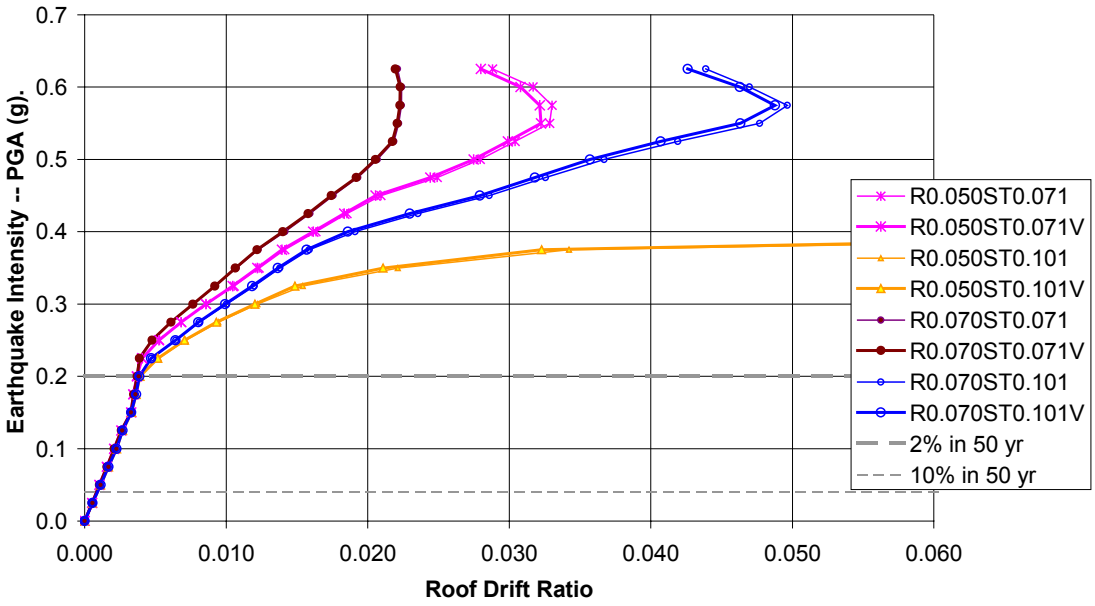

Figure 7.7d – Roof Drift Ratio of the New York City 5 Story Models Subjected to the Taft Earthquake (EQ 4) – Corresponds to Figure 7.3c.

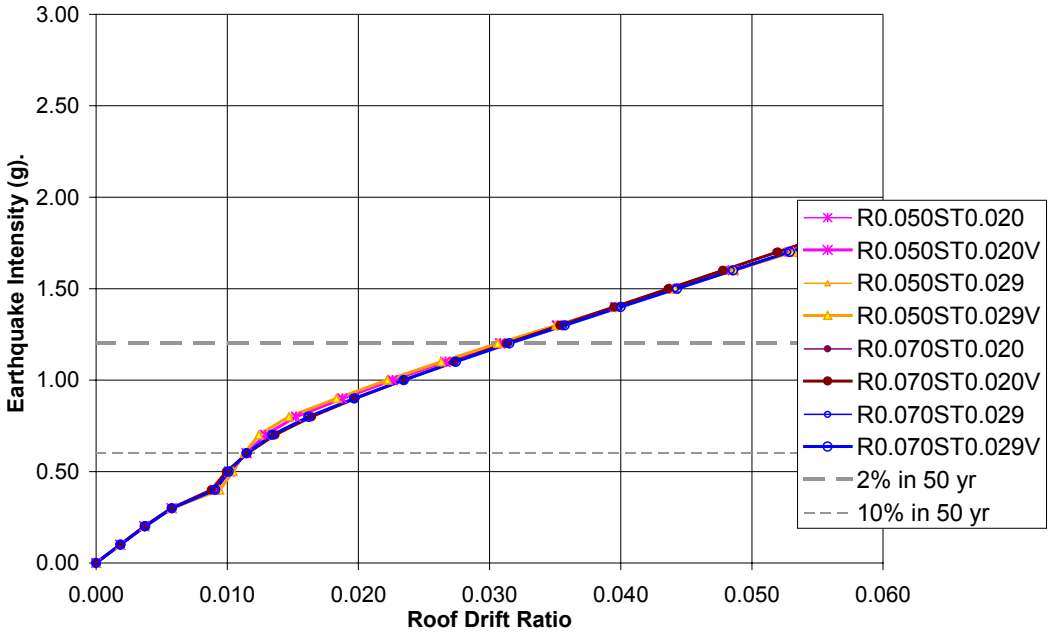

Figure 7.7e – Roof Drift Ratio of the Los Angeles 3 Story Models Subjected to the Northridge Earthquake (EQ 9).

Figures 7.7a through 7.7e are similar in shape to their corresponding ductility demand figures. However, the limits of the ductility demand based collapse rule are different than the limits of the roof drift ratio collapse rule. Consequently, a model may

be deemed collapsed according to the ductility demand rule, but not according to the roof drift rule, and vice versa. Table 7.1 shows a comparison of the two damage-based collapse rules for the data shown in Figures 7.7a through 7.7e. The limits for the ductility demands were the C_d values and the limit for the roof drift ratios was 0.02.

Table 7.1 – Comparison of Ductility Demand and Roof Drift Ratio Collapse Rules

Site and Model	Earthquake	Cd	Collapsed at 2/50 level?		Collapse Intensity -- PGA (%g)	
			μ Demand	Roof Drift	μ Demand	Roof Drift
Memphis 3 Story	Taft (EQ 4)	5.5	No	Yes	1.5	1.05
Charleston 5 Story	Hollister (EQ 5)	5.5	Yes	Yes	0.6	0.6
Boston 3 Story	Taft (EQ 4)	4	No	No	0.45	0.45
New York City 5 Story	Taft (EQ 4)	5.5	No	No	0.3	0.35
Los Angeles 3 Story	Northridge (EQ 9)	5.5	Yes	Yes	0.6	0.6

In Table 7.1, there are three places where the two damage-based collapse rules do not agree. The places of discrepancy have been shaded. Table 7.1 illustrates the need for multiple limit state checks in an IDA analysis. One damage measure may be more appropriate for a given type of structure, but multiple ones provide a higher level of confidence in the results.

7.2.4 – Core IDA Results Using the Park and Ang Damage Index as a Damage Measure

For each of the core IDA models, a Park and Ang (PA) damage index was also calculated. This provided yet another limit whereby the collapse risk could be assessed. The models were considered collapsed when the index reached value of 1.0. As an aside, Fajfar (1992) has suggested that a structure is unrepairable when the PA damage index is greater than 0.4. While a PA damage index of 1.0 indicated collapse, the models had values that were much greater than 1.0. This was because the models were infinitely ductile. They could deform well beyond the ductility limit. Material models that account for damage were not used in this study. The results of one model from each site for both the WUS and CEUS are shown in Figures 7.8a through 7.8j.

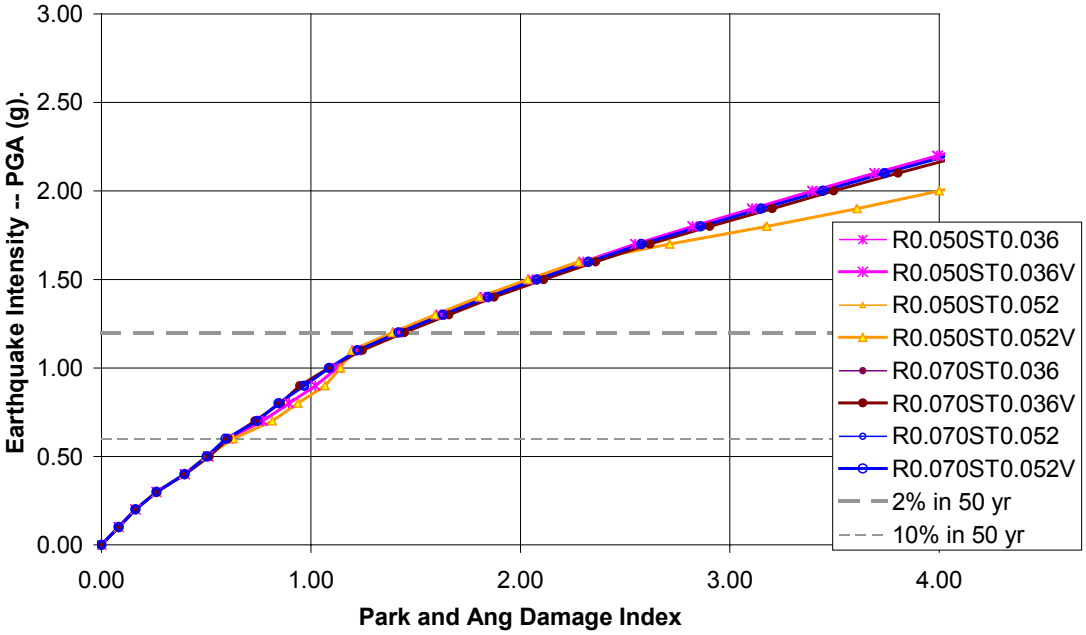

Figure 7.8a – Park and Ang Damage Indices of the Los Angeles 7 Story Models Subjected to the Taft Earthquake (EQ 4).

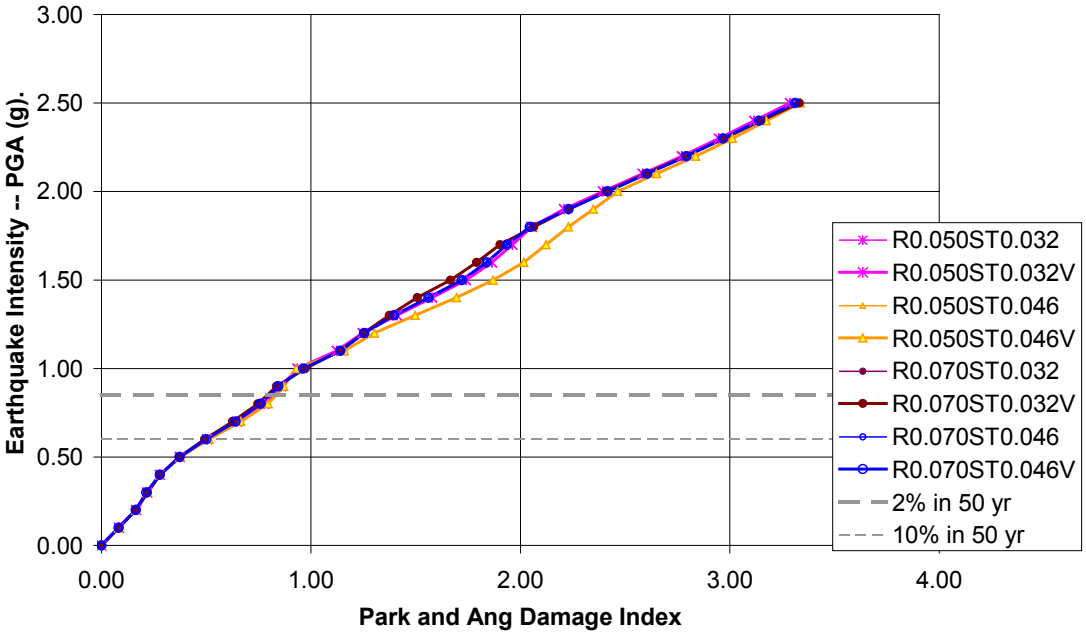

Figure 7.8b – Park and Ang Damage Indices of the San Francisco A 9 Story Models Subjected to the Hollister Earthquake (EQ 5).

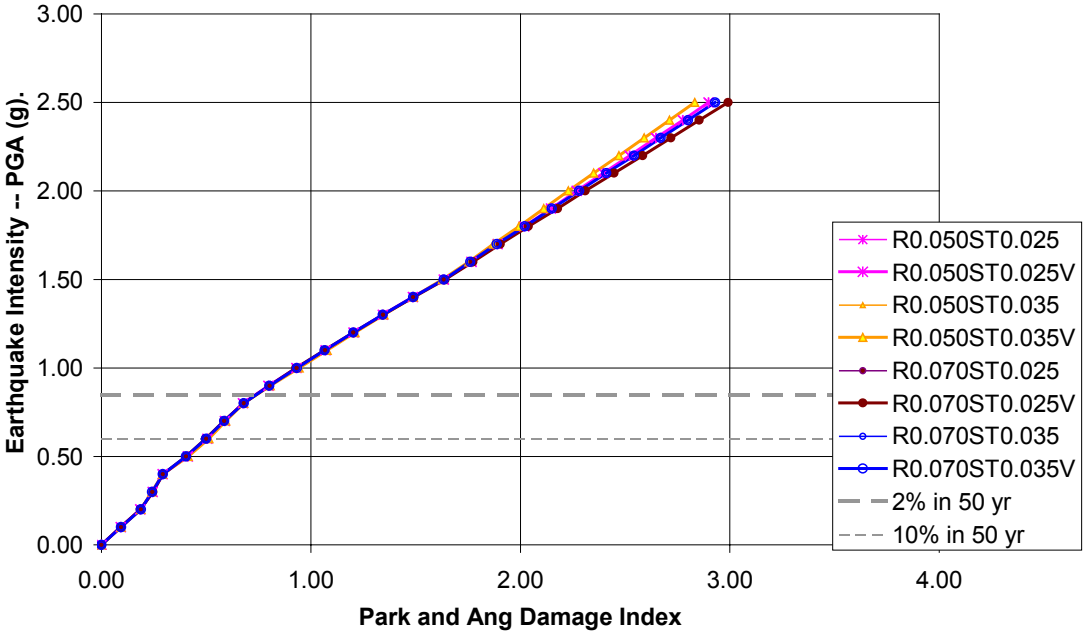

Figure 7.8c – Park and Ang Damage Indices of the San Francisco B 9 Story Models Subjected to the Hollister Earthquake (EQ 5).

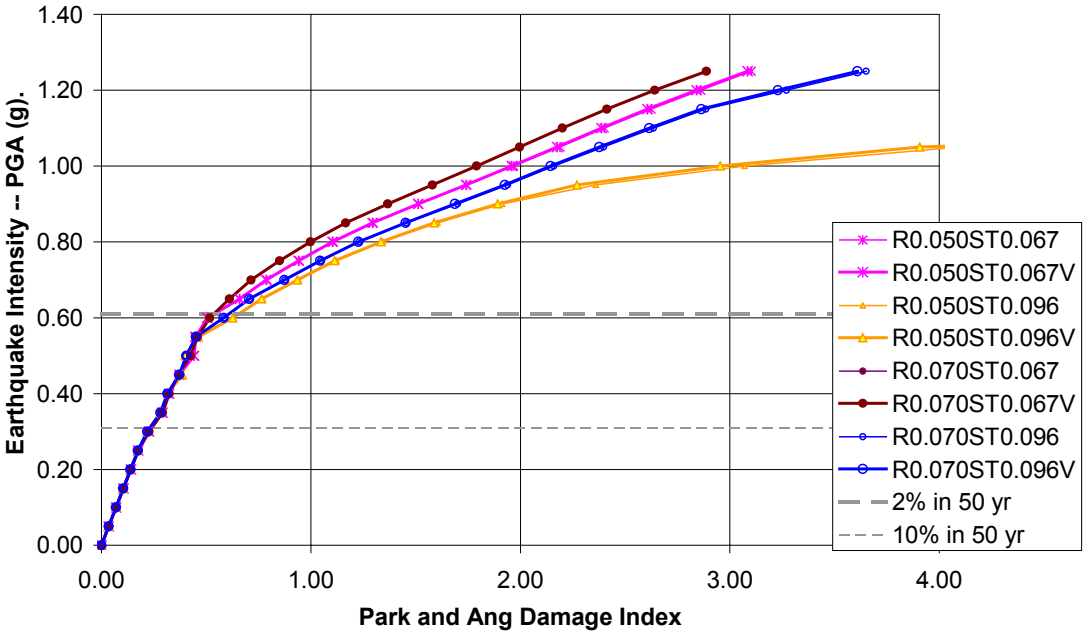

Figure 7.8d – Park and Ang Damage Indices of the Seattle 7 Story Models Subjected to the Taft Earthquake (EQ 4).

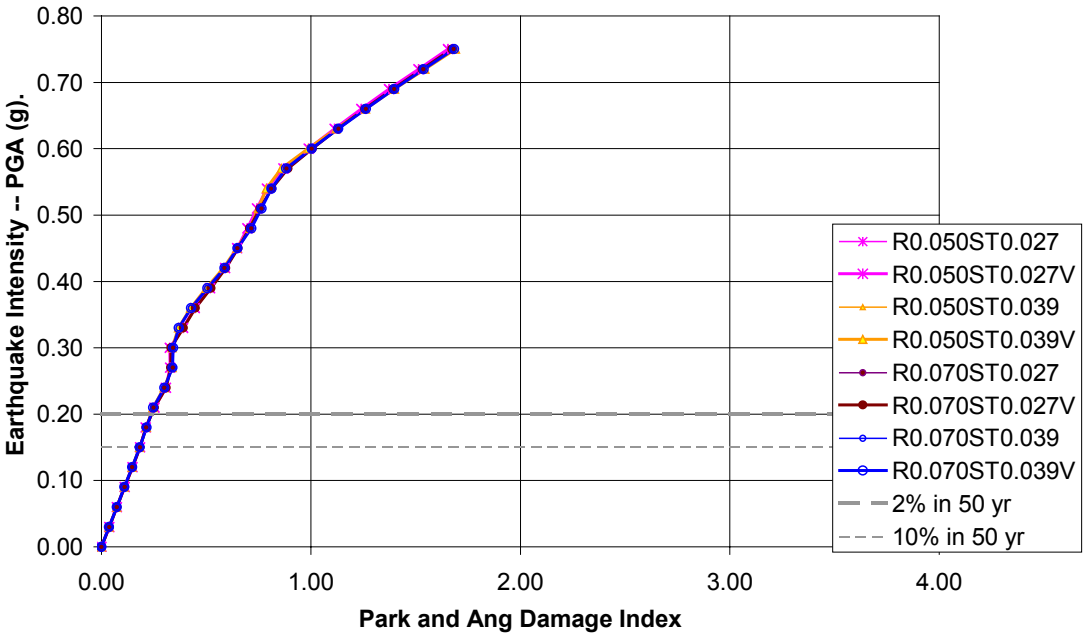

Figure 7.8e – Park and Ang Damage Indices of the Salt Lake City 3 Story Models Subjected to the Northridge Earthquake (EQ 9).

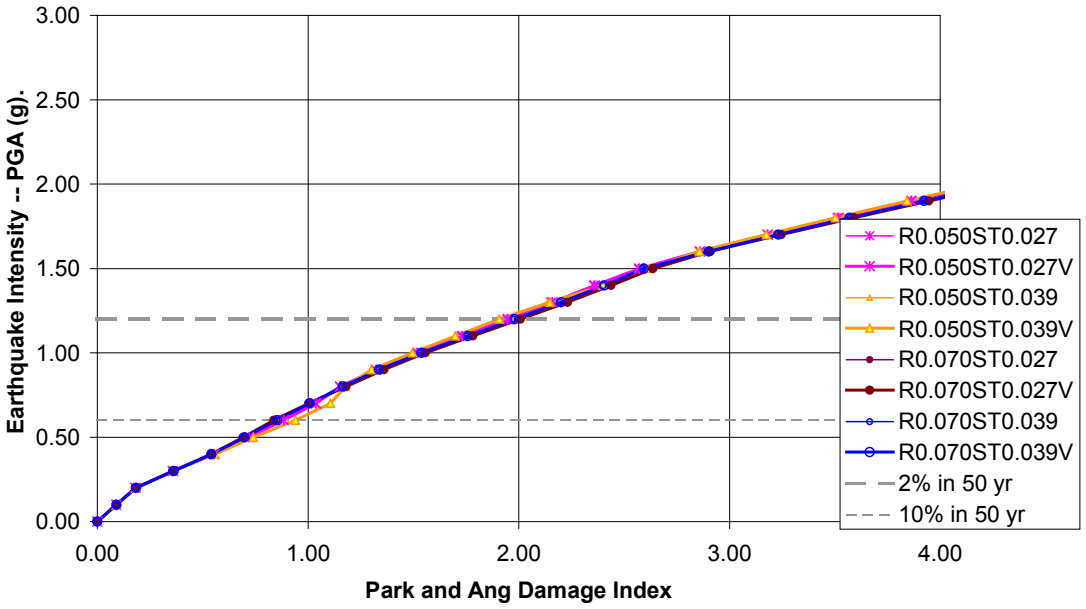

Figure 7.8f – Park and Ang Damage Indices of the Memphis 5 Story Models Subjected to the Taft Earthquake (EQ 4).

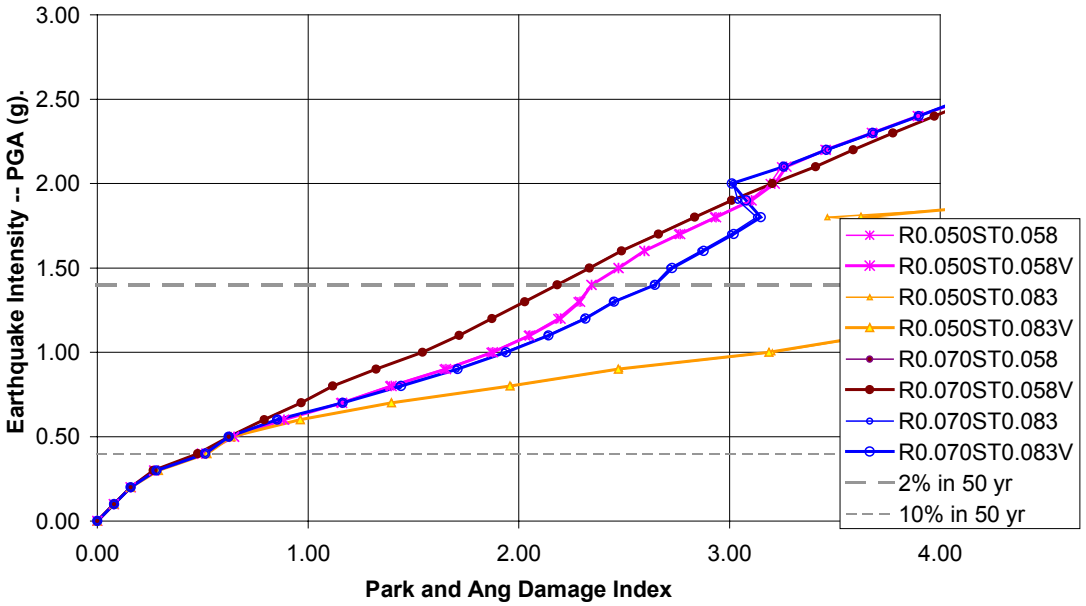

Figure 7.8g – Park and Ang Damage Indices of the Charleston 7 Story Models Subjected to the Hollister Earthquake (EQ 5).

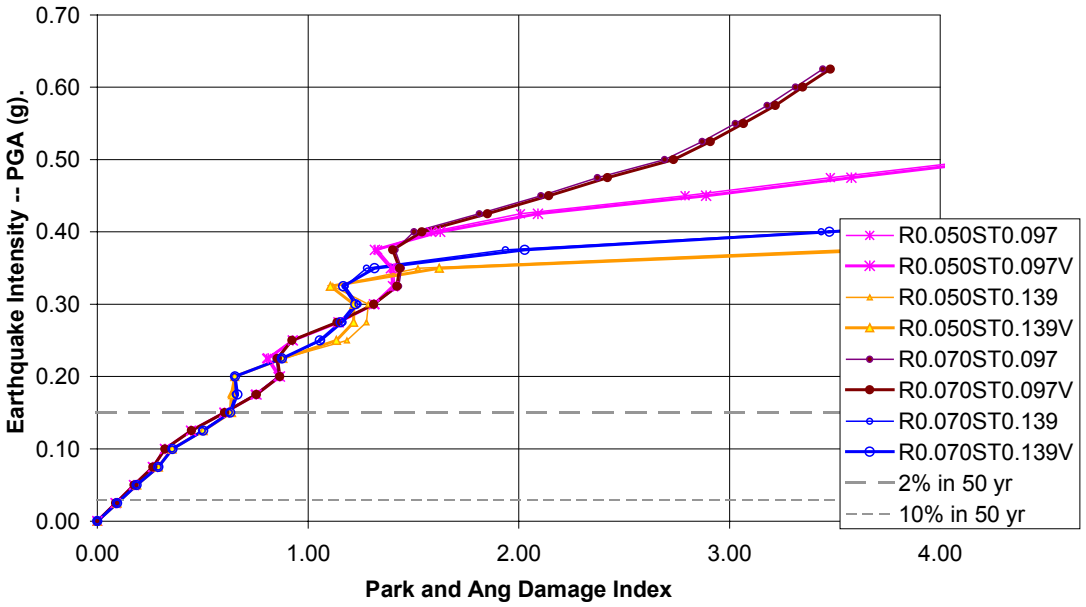

Figure 7.8h – Park and Ang Damage Indices of the Boston 3 Story Models Subjected to the Northridge Earthquake (EQ 9).

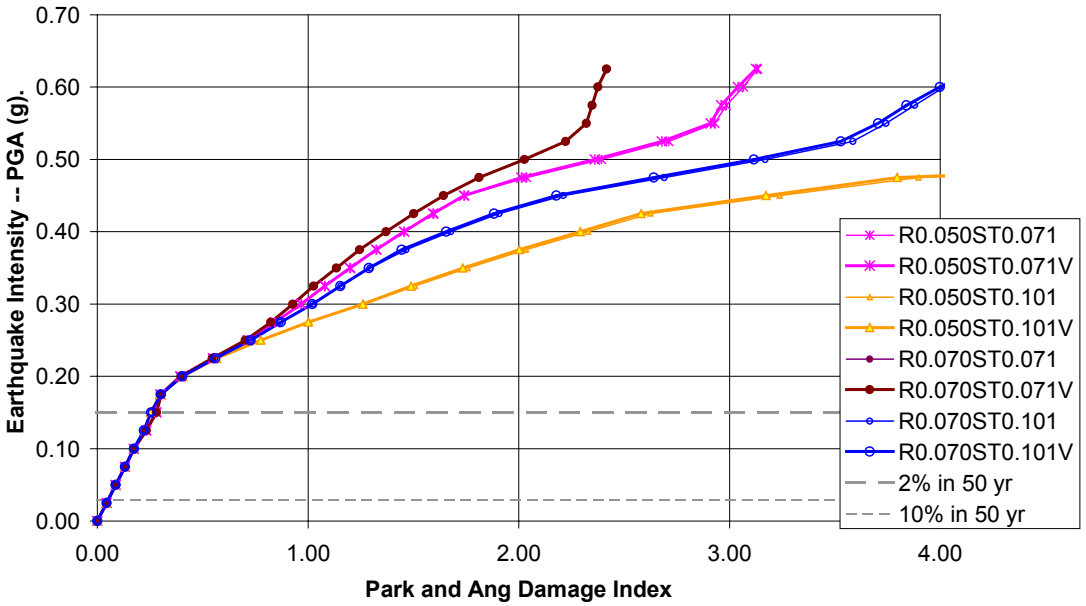

Figure 7.8i – Park and Ang Damage Indices of the New York City 9 Story Models Subjected to the Taft Earthquake (EQ 4).

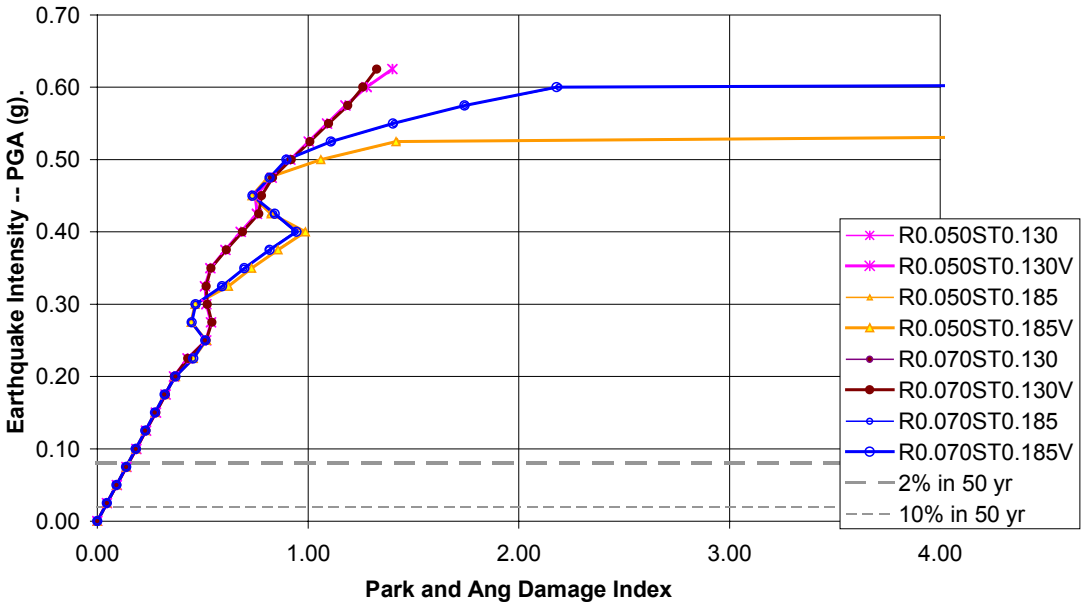

Figure 7.8j – Park and Ang Damage Indices of the Chicago/Washington D.C. 7 Story Models Subjected to the Hollister Earthquake (EQ 5).

Like the roof drift ratio IDA plots, the PA damage index IDA plots are somewhat similar to the ductility demand figures. This is because the first term in the PA damage index is related to ductility capacity and it dominates the PA damage index. The second term in the PA index is the cyclic energy dissipation term. It has a modifier, the β term, which

reduces the effects of the energy dissipation on damage accumulation. The value of β used for this study was 0.15, which is typical. While a multiplier reduces the energy dissipation term, the total index should effectively report damages higher than would be reported from just considering ductility demand. A discussion of the PA damage index IDA results will follow the presentation of the Kumar and Usami damage index results.

7.2.5 – Core IDA Results using the Kumar and Usami Damage Index as a Damage Measure

The Kumar and Usami (KU) damage index, like the PA damage index, was developed to account for both maximum ductility demand damage and cyclic energy dissipation damage. Unlike the PA damage index, however, the KU damage index only accumulates damage in the maximum ductility term when a yield event is occurring. Thus, the KU damage index provides another perspective on the collapse risks associated with the WUS and CEUS structures examined in the IDA. The results of one model from each site for both the WUS and CEUS are shown in Figures 7.9a through 7.9j.

Before presenting the figures, it is important to note that the constants used to calculate the KU damage index were different than typical constants prescribed by Kumar and Usami. The values used for β and c were 0.22 and 0.95, respectively. Kumar and Usami used a range for β between 0.1 and 0.2. They used a range for c between 1.0 and 2.0. Thus, the values used in this study were outside the range prescribed by the developers of the index. However, the values for the KU constants used in this study are reasonable. The procedure for choosing the KU damage index constants was as follows:

1) Examine the response histories and the moment-rotation hysteresis histories of several of the models subjected to several of the earthquakes.
2) Use the following subjective criteria to choose the KU damage index constants
    - At the point where a model exceeds the ultimate ductility capacity, it should have a damage value of 1.0.
    - If the model is subjected to many small nonlinear hysteretic cycles, it should have a damage value approximately equal to 1.0.

- If a model is subjected to a few large nonlinear hysteretic cycles, but does not exceed the ductility capacity, it should have a damage value approximately equal to 1.0.

3) Iteratively change the KU damage index constants until the criteria in step 2 are reasonably satisfied.

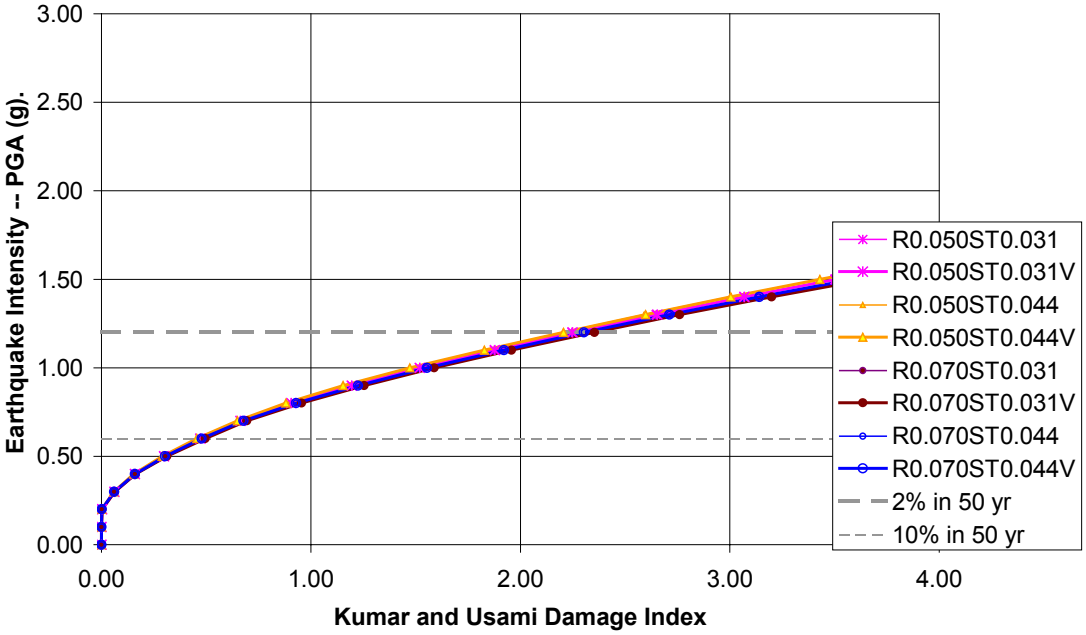

Figure 7.9a – Kumar and Usami Damage Indices of the Los Angeles 7 Story Models Subjected to the Taft Earthquake (EQ 4).

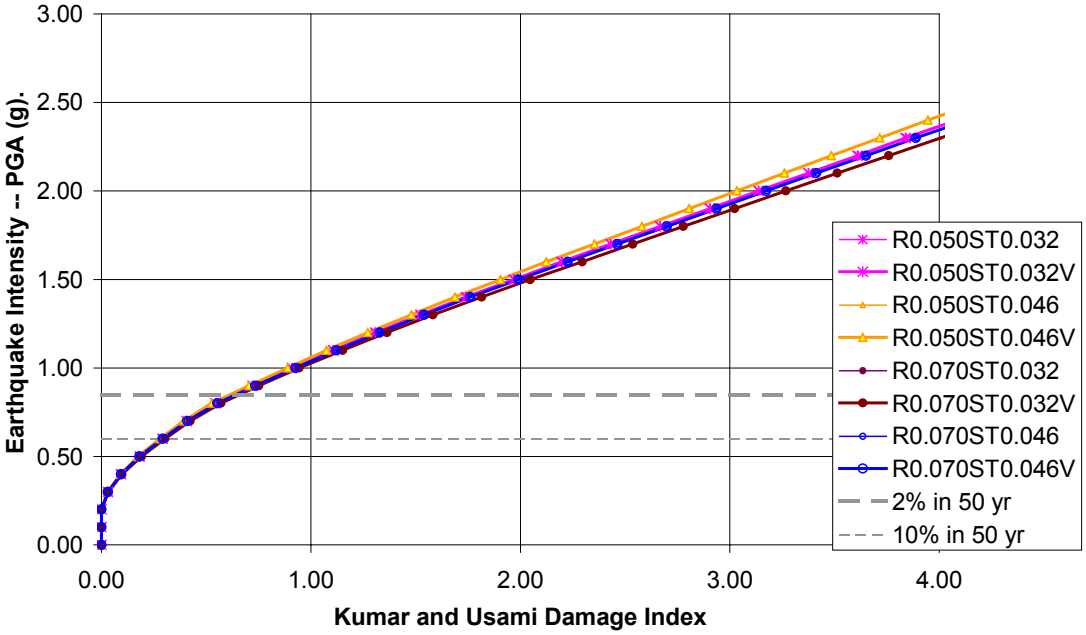

Figure 7.9b – Kumar and Usami Damage Indices of the San Francisco A 9 Story Models Subjected to the Hollister Earthquake (EQ 5).

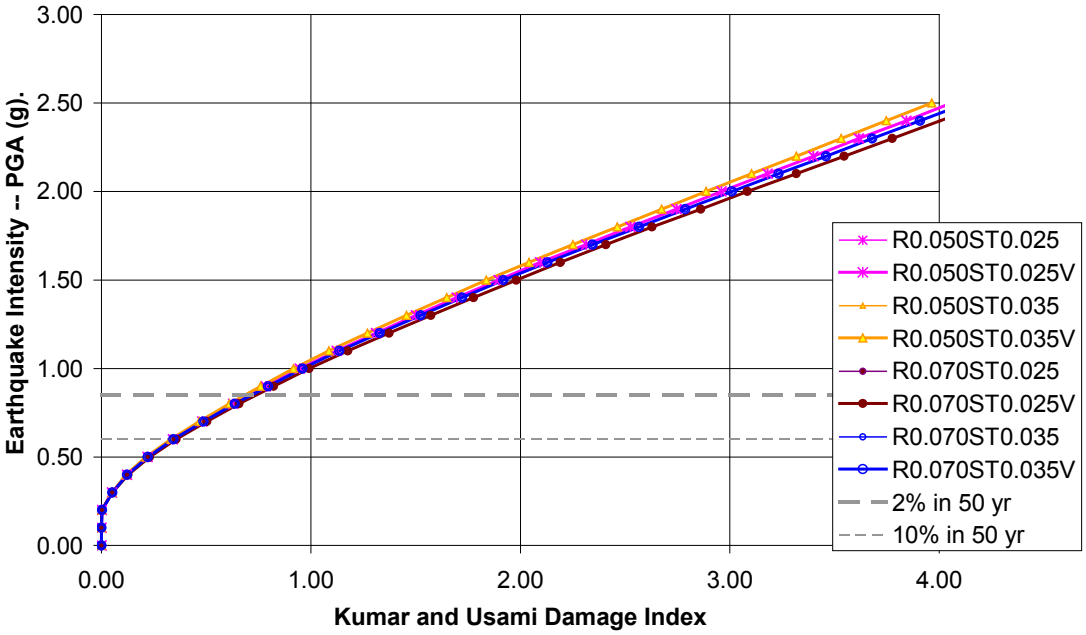

Figure 7.9c – Kumar and Usami Damage Indices of the San Francisco B 9 Story Models Subjected to the Hollister Earthquake (EQ 5).

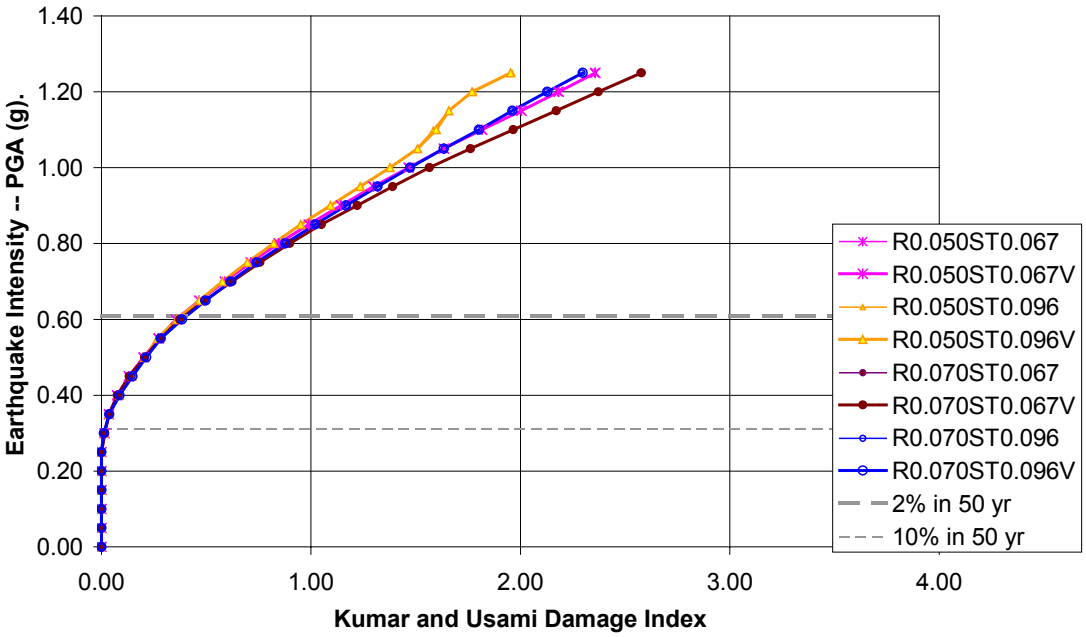

Figure 7.9d – Kumar and Usami Damage Indices of the Seattle 7 Story Models Subjected to the Taft Earthquake (EQ 4).

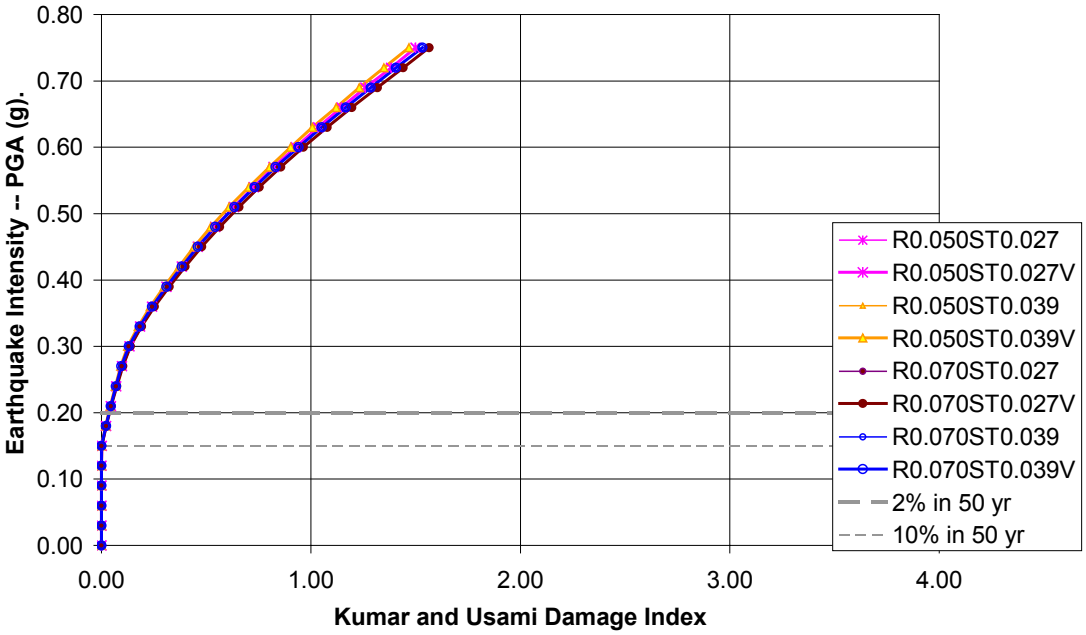

Figure 7.9e – Kumar and Usami Damage Indices of the Salt Lake City 3 Story Models Subjected to the Northridge Earthquake (EQ 9).

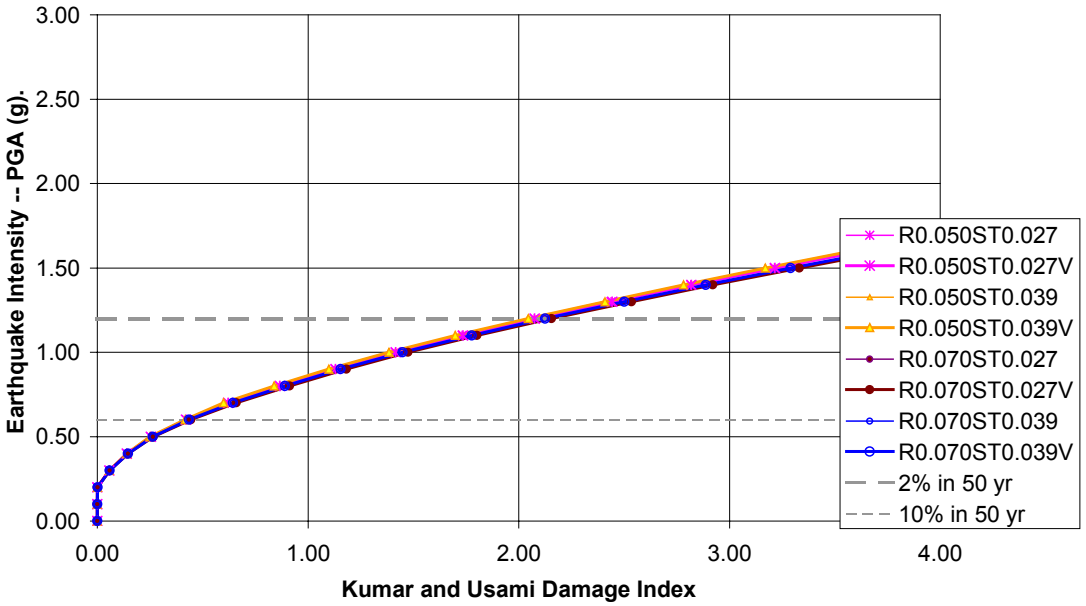

Figure 7.9f – Kumar and Usami Damage Indices of the Memphis 5 Story Models Subjected to the Taft Earthquake (EQ 4).

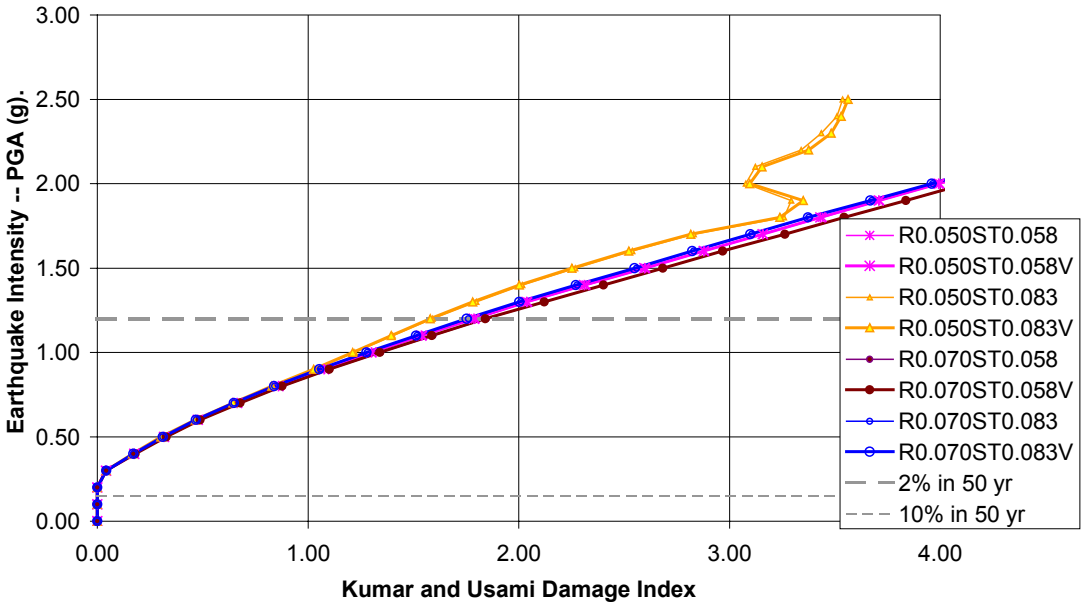

Figure 7.9g – Kumar and Usami Damage Indices of the Charleston 7 Story Models Subjected to the Hollister Earthquake (EQ 5).

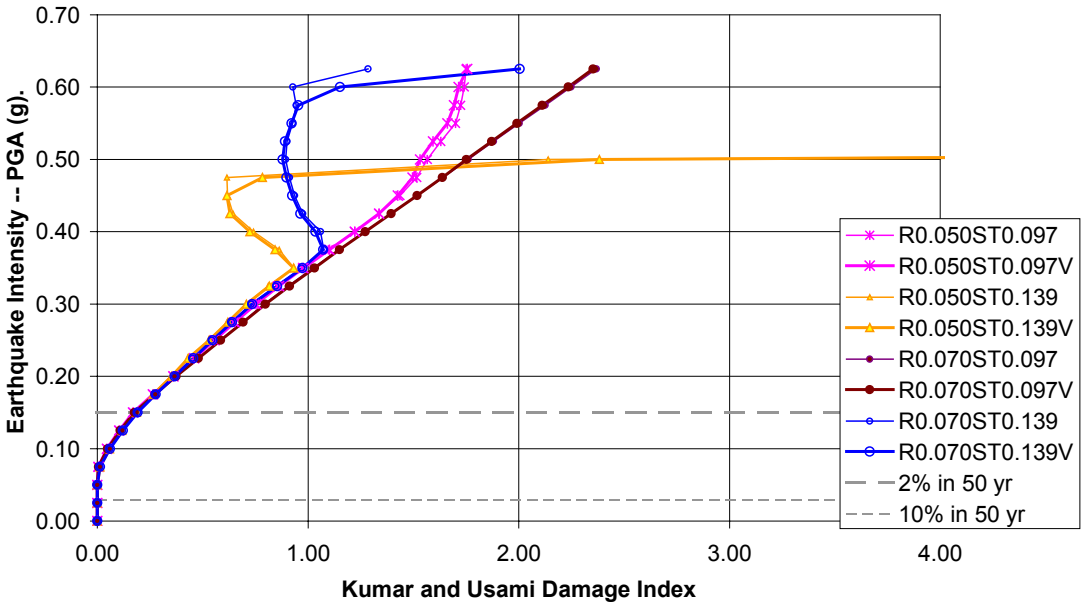

Figure 7.9h – Kumar and Usami Damage Indices of the Boston 3 Story Models Subjected to the Northridge Earthquake (EQ 9).

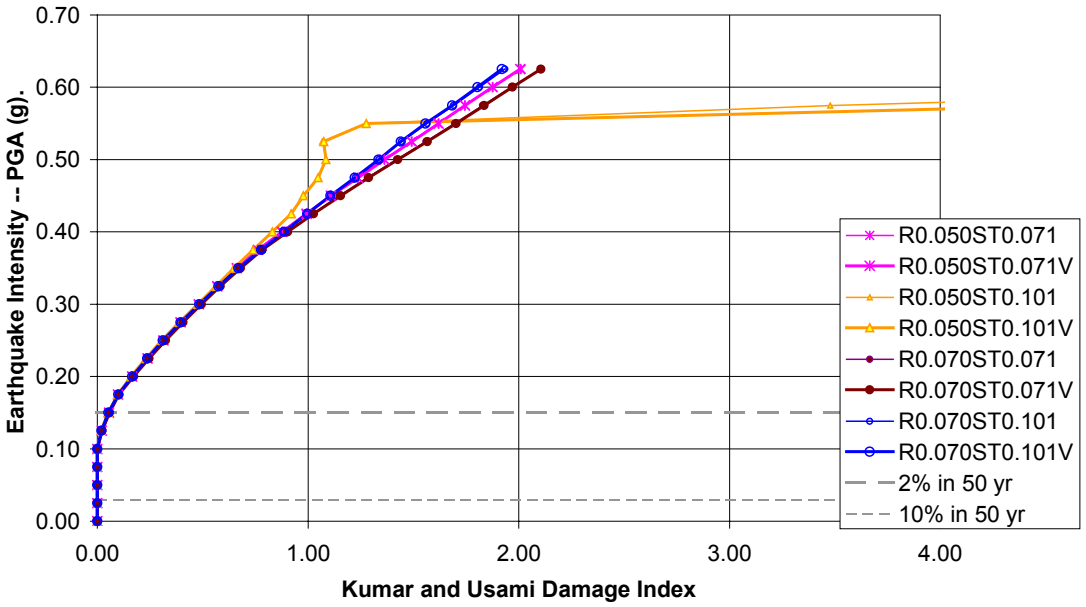

Figure 7.9i – Kumar and Usami Damage Indices of the New York City 9 Story Models Subjected to the Taft Earthquake (EQ 4).

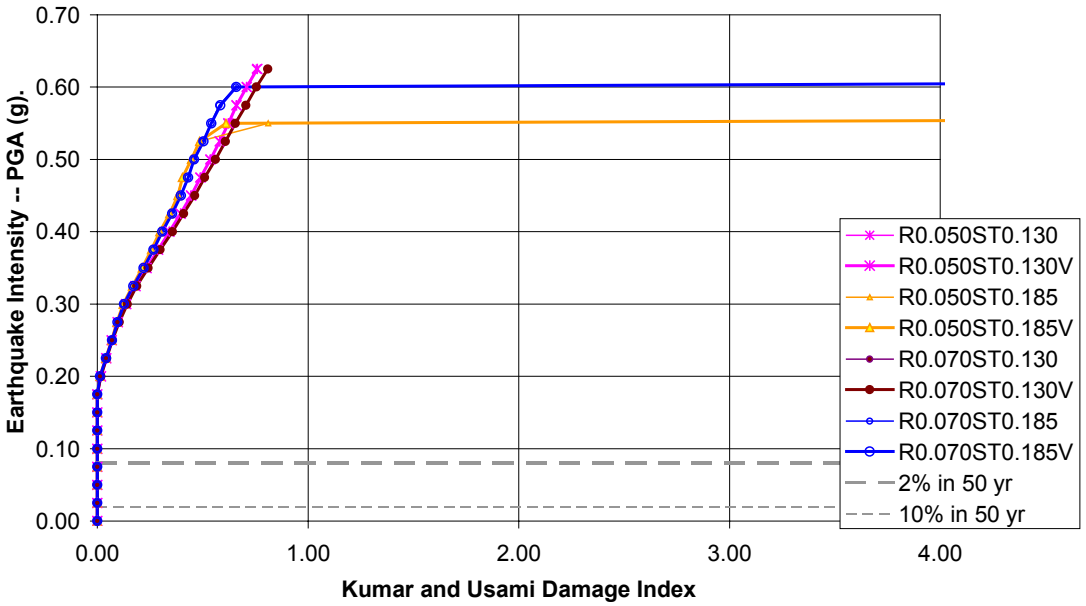

Figure 7.9j – Kumar and Usami Damage Indices of the Chicago/Washington D.C. 7 Story Models Subjected to the Hollister Earthquake (EQ 5).

Notice in Figures 7.9a through 7.9j that no damage accumulates until a certain PGA value is reached. As said before, this was because the maximum ductility term of the KU damage index does not accumulate damage unless the member in question is yielding. The results from the KU damage index IDA figures is presented comparatively with PA damage index results in section 7.2.6.

7.2.6 – Comparison of the Park and Ang and the Kumar and Usami Damage Index Results

While the PA and KU damage indices are calculated differently, they produced similar results in many situations. Table 7.2 summarizes the IDA Figures 7.8a through 7.8j and 7.9a through 7.9j. At points where the two indices produced very different results, the cells in Table 7.2 have been shaded.

Table 7.2 - Comparison of the Park and Ang and the Kumar and Usami Damage Index Results

Site and Model	Earthquake	Cd	DM at 2/50 level		PGA (%g) at DM = 1.0	
			PA	KU	PA	KU
LA 3 Story	Taft (EQ 4)	5.5	0.7	1.5	0.85	1
San Fran. A 9 Story	Hollister (EQ 5)	5.5	0.9	0.8	1	1.05
San Fran. B 9 Story	Hollister (EQ 5)	5.5	0.8	0.85	1.05	1
Seattle 7 Story	Taft (EQ 4)	5.5	0.65	0.4	0.72	0.85
Salt Lake City 3 Story	Northridge (EQ9)	5.5	0.3	0.1	0.5	0.5
Memphis 5 Story	Taft (EQ 4)	5.5	2.4	3	0.7	0.85
Charleston 7 Story	Hollister (EQ 5)	5.5	1.9	1.75	0.75	0.9
Boston 3 Story	Northridge (EQ9)	4	0.7	0.25	0.25	0.35
New York City 9 Story	Taft (EQ 4)	5.5	0.3	0.2	0.28	0.41
Chicago / D.C. 7 Story	Hollister (EQ 5)	3	0.15	0	0.5	0.55

It would seem that the LA, San Francisco, and Seattle WUS models described in Table 7.2 would be in danger of collapse if the probable 2/50 earthquake event were to occur. They would certainly be unrepairable. Then, the Memphis, Charleston, and Boston CEUS models described in Table 7.2 would similarly be in danger of collapse in the event of the probable 2/50 earthquake. The rest of the models described in Table 7.2 would not be in danger of collapse and the damage sustained would be repairable.

7.3 - Supplemental IDA Results

After examining the core IDA results, it seemed that strength and r_p values were the most important factors influencing the collapse intensity levels. Thus, supplemental IDAs were conducted to specifically look at these parameters more closely. It also seemed important to examine strength variations because the core IDA models assumed an overstrength of 2.0. Since real structures may have more or less overstrength, it was important to understand the effects of strength on the collapse intensities of the models. The models chosen for the supplemental IDAs are shown in Table 7.3.

Table 7.3 – Supplemental IDA Models with Corresponding C_s and r_p Values.

Site and Model	2.0 Cs	rp
LA 5 Story	0.166	0.006
Charleston 3 Story	0.127	-0.007
New York City 3 Story	0.03	-0.023
Boston 5 Story	0.039	-0.103

The models used in the supplemental IDA were chosen based on r_p. The r_p values in Table 7.3 decrease going down in the table. The C_s values shown in Table 7.3 are the actual values used in the core IDA, but are twice as high as was required. Once again, the higher yield strengths were used to account for overstrength. In the supplemental IDA, the strengths of the four models shown in Table 7.3 were varied. The values for the yield strengths in the supplemental IDA were 1.0, 2.0, and 3.0 times C_s. To conduct the supplemental IDA, Nonlin was used, for reasons discussed earlier. Also, all of the earthquakes were used in the supplemental IDA because it was easy to do so in Nonlin. It is important to note that Nonlin does not include vertical accelerations. So, no conclusions regarding vertical accelerations can be drawn from this section. The ductility demand results for each of the models are presented in Figures 7.10 through 7.13.

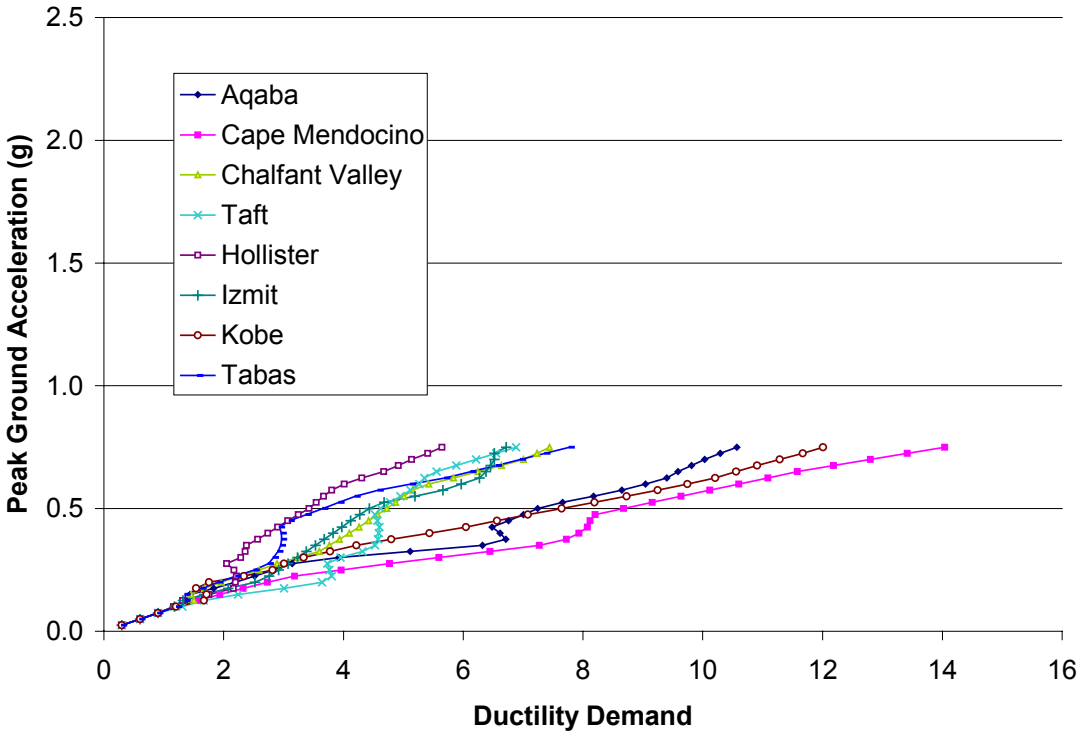

Figure 7.10a – IDA Ductility Demands of the Los Angeles 5 Story Model with a r_p value of 0.006 and a Yield Force Equal to 1.0C_s.

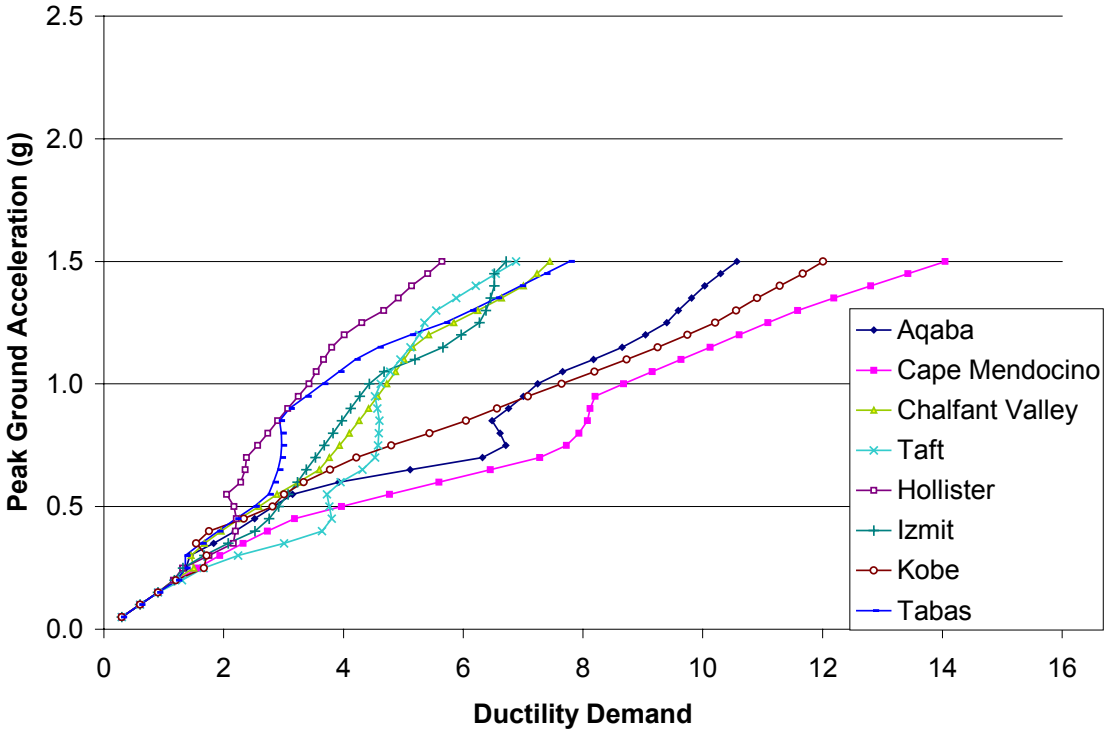

Figure 7.10b – IDA Ductility Demands of the Los Angeles 5 Story Model with a r_p value of 0.006 and a Yield Force Equal to 2.0C_s.

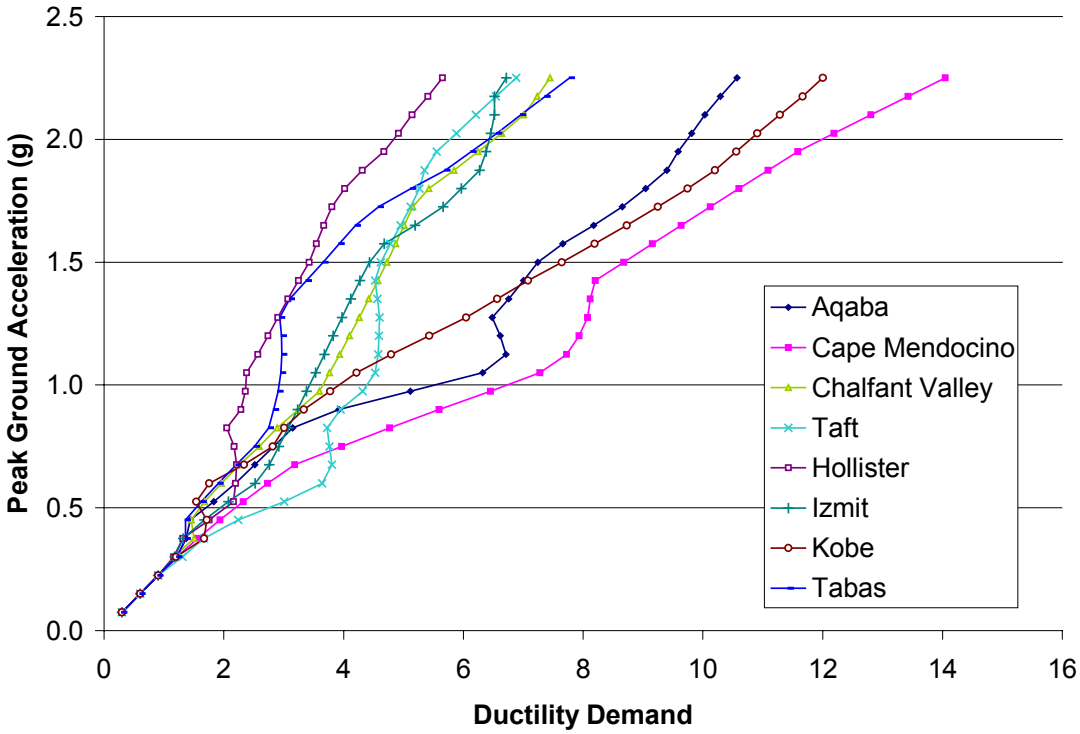

Figure 7.10c – IDA Ductility Demands for the Los Angeles 5 Story Model with a r_p value of 0.006 and a Yield Force Equal to 3.0C_s.

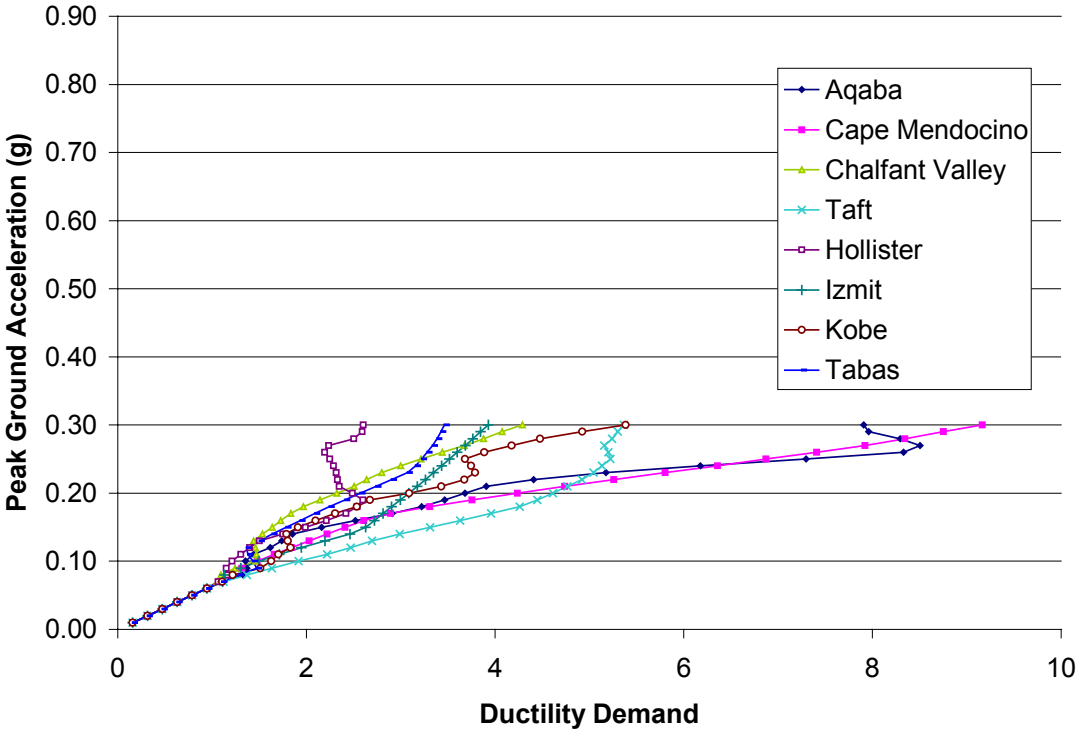

Figure 7.11a – IDA Ductility Demands for the Charleston 3 Story Model with a r_p value of -0.007 and a Yield Force Equal to 1.0C_s.

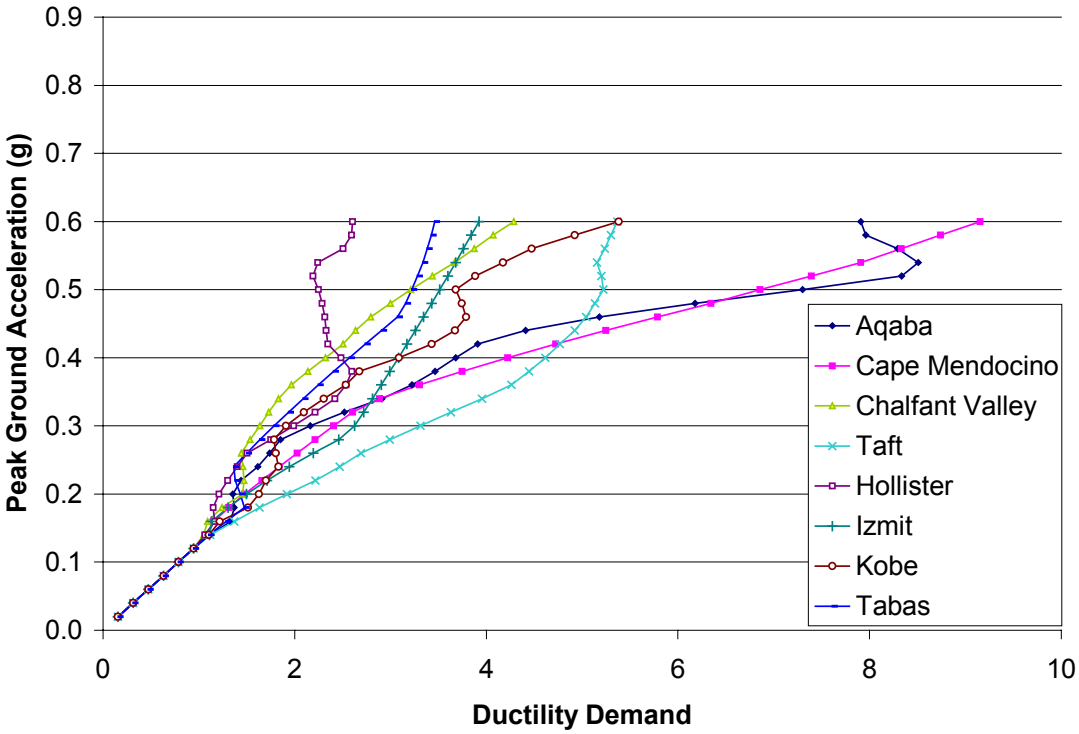

Figure 7.11b – IDA Ductility Demands for the Charleston 3 Story Model with a r_p value of -0.007 and a Yield Force Equal to 2.0C_s.

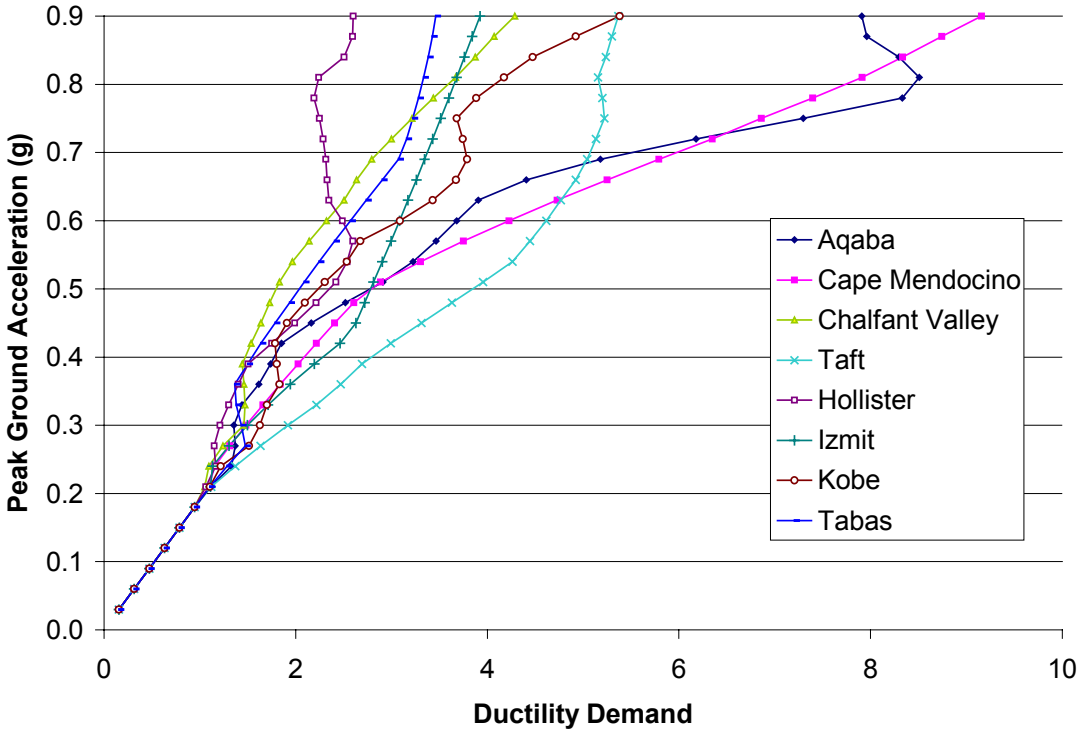

Figure 7.11c – IDA Ductility Demands for the Charleston 3 Story Model with a r_p value of -0.007 and a Yield Force Equal to $3.0C_s$.

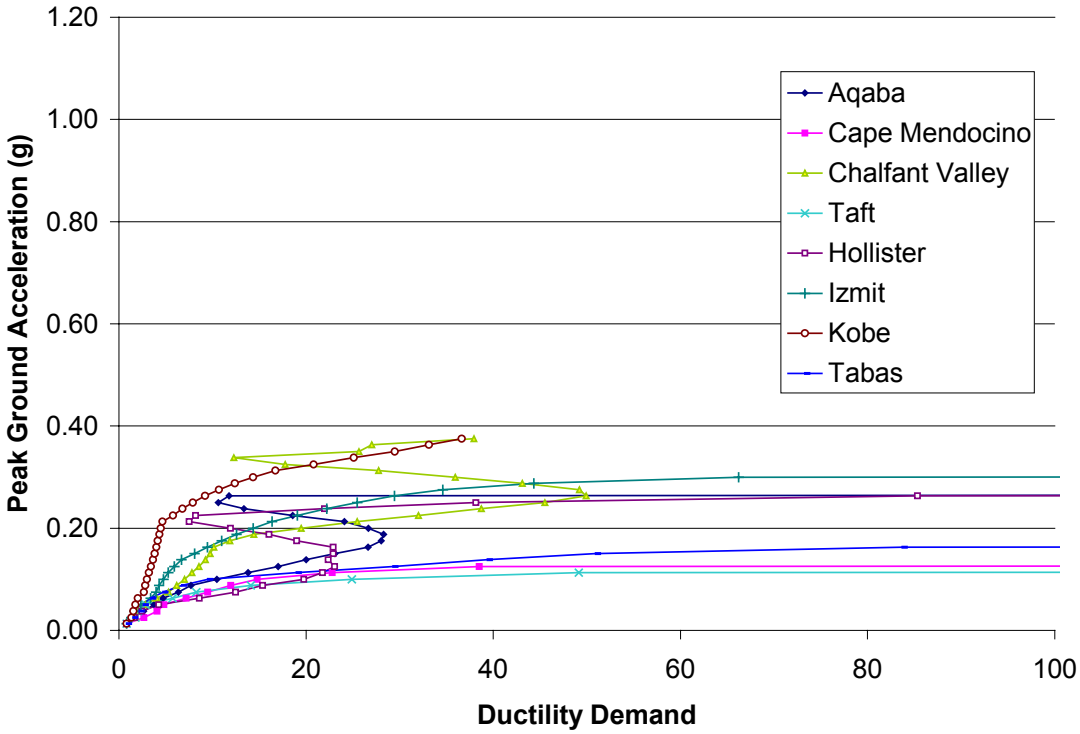

Figure 7.12a – IDA Ductility Demands for the New York City 3 Story Model with a r_p value of -0.023 and a Yield Force Equal to $1.0C_s$.

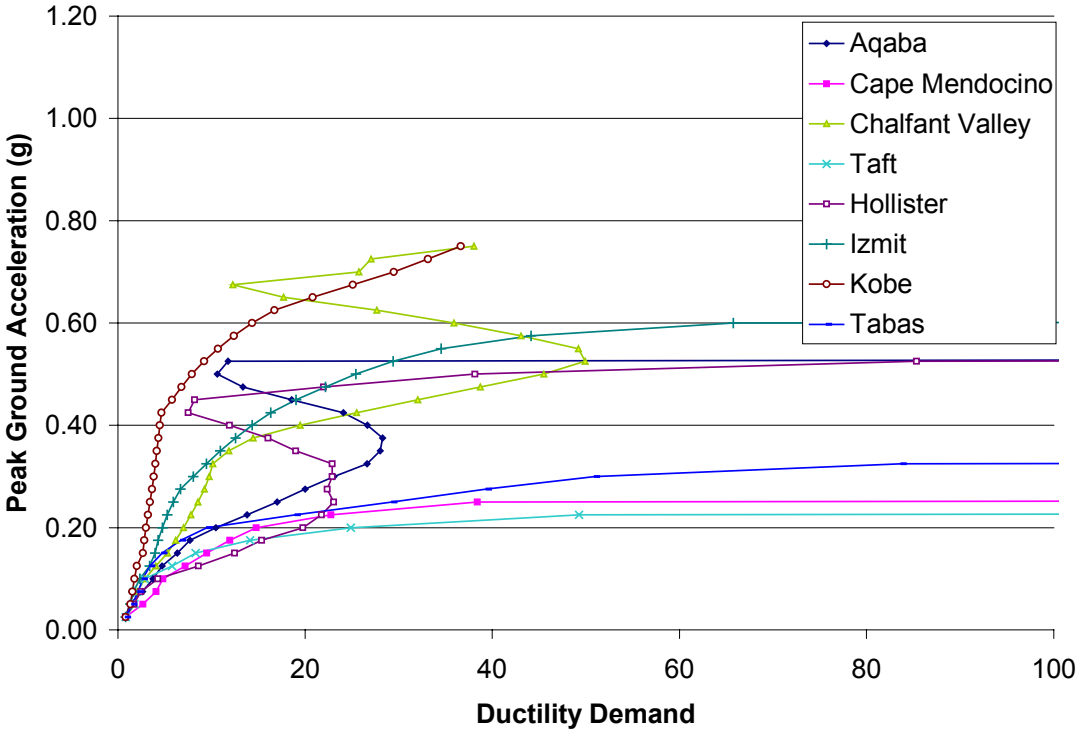

Figure 7.12b – IDA Ductility Demands for the New York City 3 Story Model with a r_p value of -0.023 and a Yield Force Equal to 2.0C_s.

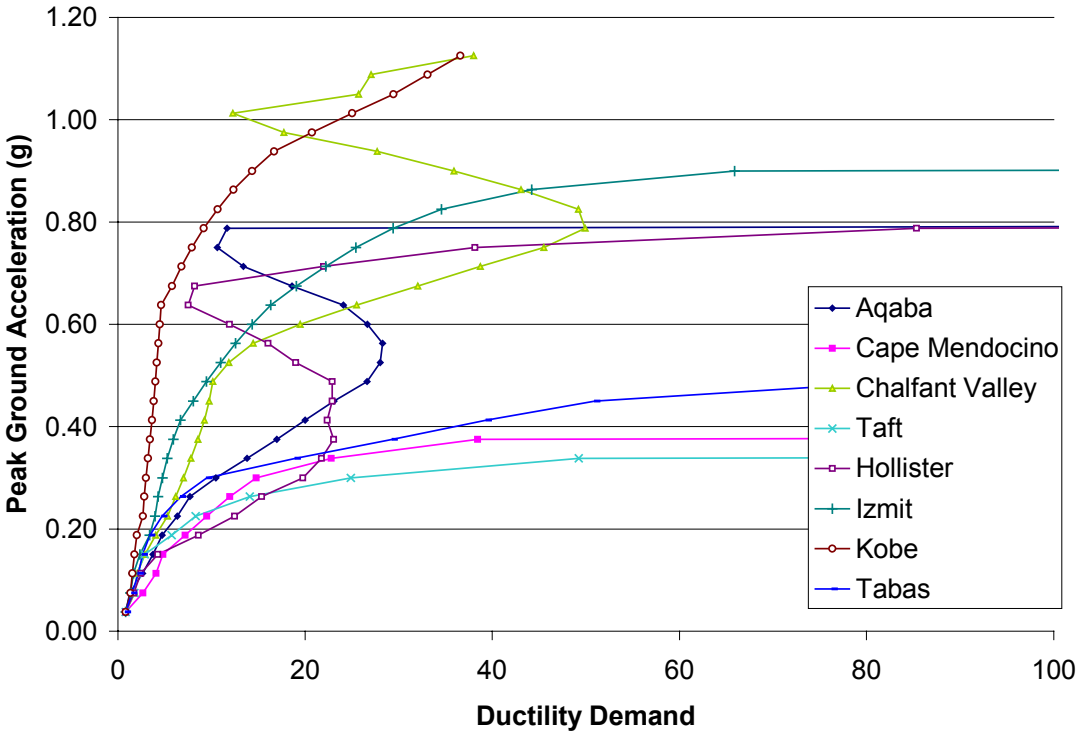

Figure 7.12c – IDA Ductility Demands for the New York City 3 Story Model with a r_p value of -0.023 and a Yield Force Equal to 3.0C_s.

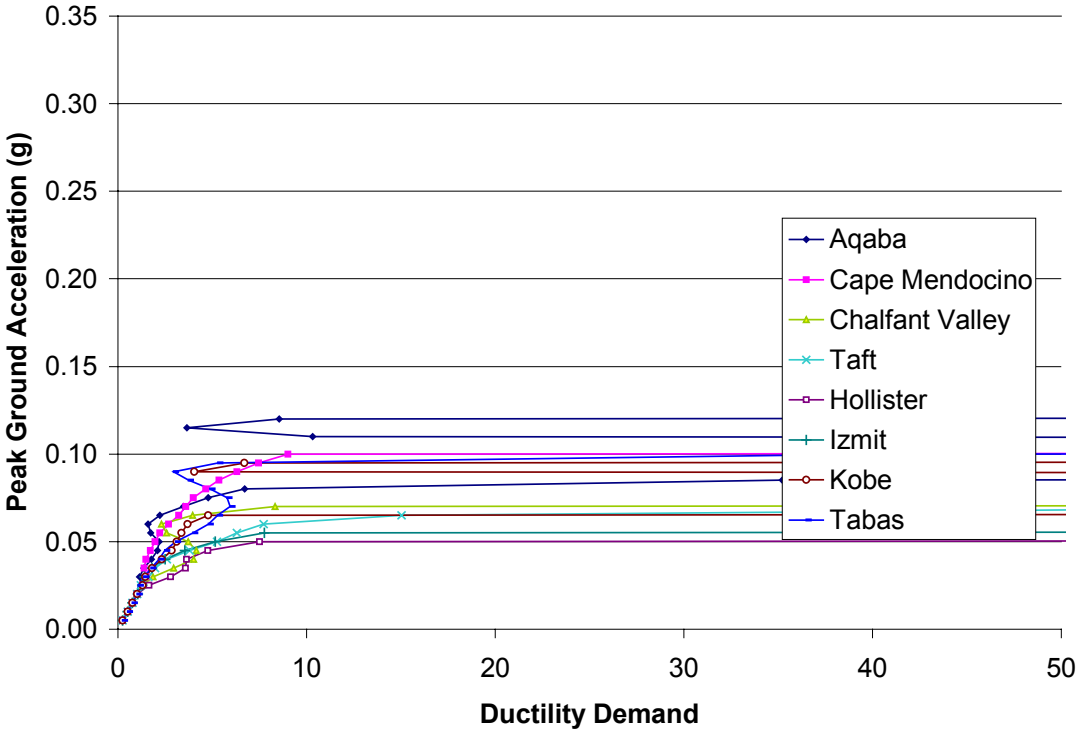

Figure 7.13a – IDA Ductility Demands for the Boston 5 Story Model with a r_p value of -0.103 and a Yield Force Equal to 1.0C_s.

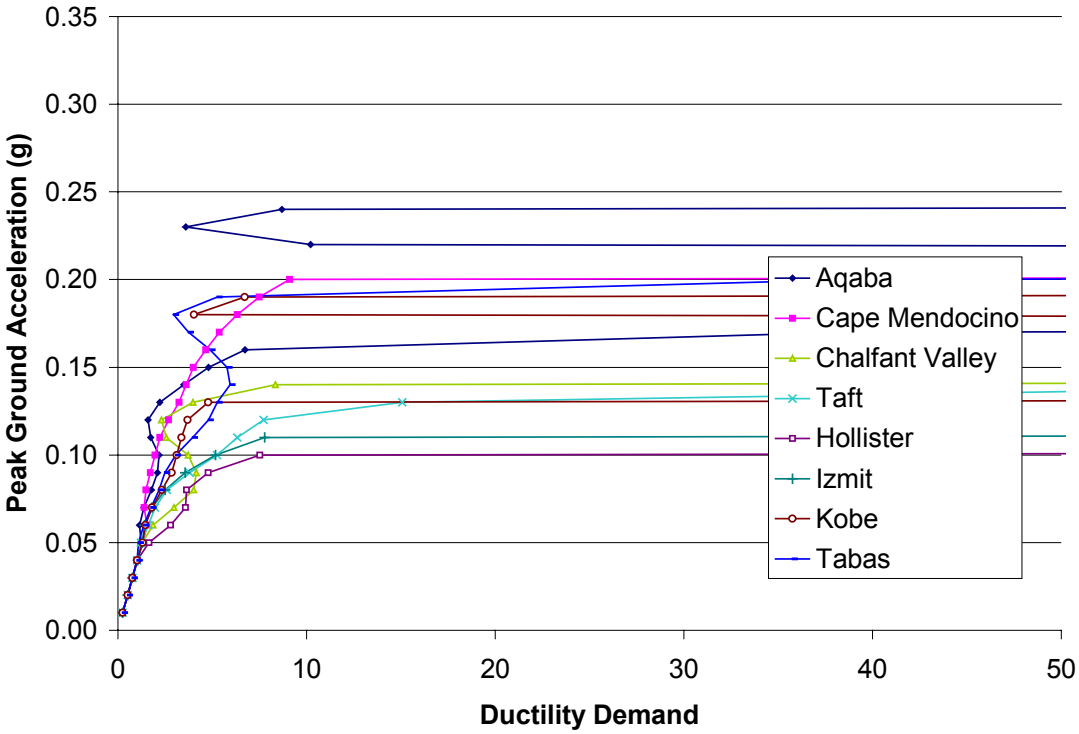

Figure 7.13b – IDA Ductility Demands for the Boston 5 Story Model with a r_p value of -0.103 and a Yield Force Equal to 2.0C_s.

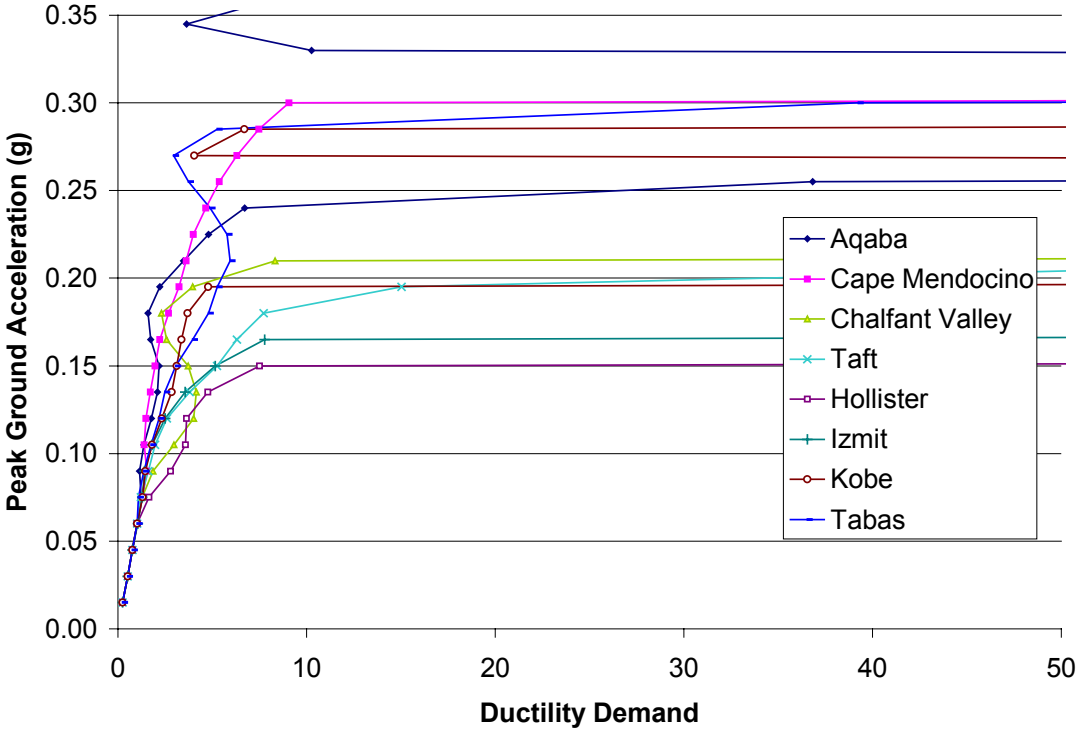

Figure 7.13c – IDA Ductility Demands for the Boston 5 Story Model with a r_p value of -0.103 and a Yield Force Equal to 3.0C_s.

From the results of Figures 7.10 through 7.13, it is clear that reducing the yield strength reduces the slope in the IDA curves. In fact, the shapes of the IDA curves for varying yield force are exactly the same for a particular model, but the are compressed down for decreasing yield strength. The lower the yield strength, the flatter the curves. Also, for those models that collapse, or have zero slope, the lower the yield strength, the lower the collapse intensity. Thus, it seems that any IDA analysis must properly include overstrength to be of any value.

Furthermore, as the r_p values decreased into the negative range, the curves "leaned over" quicker. For positive r_p values, the curves never leaned over; instead, they generally followed the equal displacement line. For very small negative r_p values, the models still generally followed the equal displacement line, but the dispersion increased. From the core and supplemental IDA analyses, it seems that dispersion is highest for small negative r_p values between 0.0 and about –0.03. Beyond r_p values of -0.03, the IDA curves all began to lean over at the same intensity, at which point strength primarily governed the collapse intensity.

7.3 - Summary

The purpose of the IDA study was to verify the results of the parameter study and to determine the collapse risks associated with WUS and CEUS structures. Two major aspects of the parameter study were verified by the IDA analysis. First, the IDA reinforced the correlation between the collapse intensities and the r_p values. The lower the r_p value, the lower the collapse intensity. Second, vertical accelerations were shown to affect the ductility demands in the IDA models at the intensity just before collapse. This is particularly important for IDA analysis, which is concerned with determining collapse points.

With regard to determining collapse points, there are two main ways that this is done in an IDA. The first involves using damage-based rules. In this study, four damage measures were used. Each one provided different results based on the type of response experienced by the structure. Each one also had different limits to signify collapse. Agreement between the various damage measures was not good. A specific damage measure may be useful for a particular type of structure, but used together there is a broad range of results.

The second method to determine collapse points is intensity-based. This method provided more consistent results among the various damage measures. However, there were still some discrepancies between the damage measures. It seems that more research could be done to understand the differences between the indices and in what situations they are most applicable.

A concerning issue about CEUS structures is that large stability ratios would cause large negative r_p values. This, coupled with uncertainty about overstrength, could prove disastrous for building. While this study indicated that most of the CEUS structures would not be in danger of collapse, that was assuming that there was an overstrength of 2.0. Furthermore, the designs were based on the 2/50 event. Many building designs have been based on the 10/50 event, which has been shown to be as much as six times less than the 2/50 event. Since the r_p values were large negative values, the collapse intensities were primarily controlled by strength. Thus, if the

overstrength were less than 2.0, the CEUS structure may very well be in serious trouble if the 2/50 event were to occur.

8.0 Conclusions and Recommendations

8.1 - Introduction

This study had two main objectives. The first was to identify structural and earthquake parameters that influenced collapse. The first objective was fulfilled in part through an extensive survey of literature dealing with collapse and seismic hazards. The remaining portion of the objective was achieved by conducting a rigorous parameter study of single-degree-of-freedom oscillators. The parameters were chosen based on the information obtained in the literature survey and reasonable design values from the NEHRP Provisions. Various structural and earthquake parameters were used.

The second objective was to determine if Central and Eastern United States (CEUS) buildings were more likely to collapse than Western United States (WUS) buildings if subjected to a severe but reasonable earthquake. The second objective was examined using incremental dynamic analysis (IDA). IDA provided a means to examine the performance of buildings subjected to several earthquakes over a range of intensities.

This chapter is a summary of the major findings from the literature survey, parameter study, and IDA. This chapter is also meant to be a guide for those who wish to continue with similar collapse related research.

8.2 - Summary of Conclusions

8.2.1 – Summary of Collapse and Related Literature Survey Findings

From the literature survey, it is clear that there is potential for significant earthquakes in the CEUS. Historically large earthquakes have occurred in the CEUS, although none in the last century. The CEUS geology further warrants the hazard. Furthermore, it is likely that CEUS structures are not properly designed to withstand the level of ground motion that could be expected.

Many structures in the CEUS would be classified as gravity load designed (GLD) structures. GLD structures are designed for lateral loads, but the gravity loads, by far,

dominate the design. Some characteristics of reinforce concrete (RC) GLD structures are as follows:

- Reinforcing splices near the joints
- Widely spaced column ties
- Discontinuous positive beam reinforcement
- Strong Column Weak Beam designs
- Poor confinement in the joints

GLD structures with these characteristics are likely to experience strength and stiffness degradation as well as have lower ductility capacities. Literature specifically addressing steel GLD structures could not be found; however, by design, such structures would also have lower ductilities and the potential for strength and stiffness degradation. For example, many of the structures in the CEUS would have pre-Northridge type steel connections, which are brittle and would likely crack for small ductility demands.

Based on the seismic hazards and the design practices for CEUS structures, it is possible that CEUS structures may be in danger of collapsing in the event of a significant but reasonable earthquake. While the concern is valid, collapse progression is somewhat difficult to quantify. To aid in the quantification of collapse progression, researchers have developed various damage measures. There are a wide variety of damage measures that one could use to track a structure's progression toward collapse. Some are arguably better than others at mirroring real damage accumulation, but damage accumulates differently for various materials and structural configurations. Consequently, the use of damage indices requires some knowledge of how damage will likely accumulate in a given structure.

Damage measures in conjunction with incremental dynamic analysis (IDA) allow one to examine the damage response of a structure over a range of intensities. IDA is very useful for determining stability limit points for analytical structural models.

One of the main factors influencing dynamic instability is P-Delta effects. Past researchers have studied P-Delta effects in many different contexts and have proposed many indicators of P-Delta sensitivity. It is generally accepted that the stability ratio is a good indicator of P-Delta sensitivity. Many researchers have studied it, and the NEHRP Provisions specify limits on it to ensure dynamic stability. Other researchers have argued

that residual displacements and earthquake duration are also factors that influence the probability that a structure may collapse.

From the literature, it would seem that vertical accelerations may or may not accentuate P-Delta effects. Some researchers found that vertical accelerations increased lateral displacements and some found that they did not make a difference. Based on the uncertainty, it seemed prudent to include vertical accelerations in this study.

8.2.2 – Summary of Parameter Study Findings

From the parameter study, it was found that all four structural parameters used to create the models influenced collapse. First, as the stability ratios increased, the number of collapses generally increased. Also, as the post-yield stiffness ratios decreased, the number of collapses generally increased. The number of collapses generally increased as the yield force decreased. The stiffness was influential in that it determined the periods of the structures and also was a factor in determining the yield displacements. The period of the structures dictated the displacement response, and yield displacement determined the subsequent ductility demand based on that displacement response.

Since all four of the parameters influenced collapse, a set of composite parameters proved to be better indicators of the collapse risk of a given structure. The two composite parameters used to determine collapse risk were r_p and ductility demand. The r_p values were determined according to equation 2.10 and were dependent on both post-yield stiffness ratio and stability ratio. The ductility demands were dependent on the yield force and stiffness. In actuality, modified forms of the r_p and ductility values proved to be fairly reliable indicators of collapse probability. The two r_p and ductility value derivatives used as indicators of collapse risk were the positive r_p ductility demand (μ_{+rp}), and the collapse r_p. It was found that for a series of models where only the r_p values were varied, the ductility demands were relatively constant when the r_p values were positive. This constant ductility value was called the positive r_p ductility demand (μ_{+rp}). It is important to note that the bilinear structures used in this study never collapsed when the r_p values were positive. Moreover, for the same series of models, displacements of the structures would drastically increase to a point that would most certainly be considered

collapsed, at a given negative r_p value. This was called the collapse r_p. Plotting the collapse r_p versus μ_{+rp} revealed a trend that was independent of earthquake record or intensity.

Vertical accelerations typically did not significantly influence lateral displacements until just before a structure was about to collapse. For example, if a structure had a negative r_p value, then there would be a corresponding μ_{+rp} that would likely cause collapse. As the response of a structure with a negative r_p approached the μ_{+rp} corresponding with collapse at that r_p, the vertical accelerations would likely affect the displacement response. From this study, it seems that the vertical accelerations could likely change the maximum lateral displacements by approximately 10 percent if the structure's ductility demand were close to $\mu_{+rp,}$ and the r_p value were close to the collapse r_p. The 10 percent increase is approximate, however. There were many structures that were never influenced by vertical accelerations and several where the vertical accelerations changed lateral displacements by up to 60 percent. It is important to note that the intensity of the vertical accelerations influenced the change in lateral displacements for those structures affected by them. As the vertical intensity increased, the change in lateral displacements generally increased.

Finally, residual displacements generally increased for decreasing r_p values. The residual displacements did not typically start accumulating until the r_p values dropped below about 0.15. As the r_p values became negative, the residual displacements quickly approached the maximum displacements.

8.2.3 – Summary of Incremental Dynamic Analysis Findings

The trends in the IDA reinforced the results from the parameter study. As with the parameter study, for example, the r_p values significantly affected the response of the structures. Specifically, as the r_p values decreased into the negative range, the amount of dispersion in the IDA results increased. The dispersion was smallest for positive r_p values and greatest for negative r_p values between 0.0 and about –0.05. This was a sort of transition range between structures that would never collapse (positive r_p) and structures that would collapse if subjected to any earthquake and at a relatively low intensity

(negative r_p less than about –0.1). Collapse in the context just described is an intensity-based rule, stipulating that a structure is collapsed when small increases in the intensity result in very large increases in the ductility demand. Similar results were obtained in the parameter study in that structures with lower negative r_p values collapsed at lower μ_{+rp} values.

The damage measures (DM) used in the IDA produced a wide variety of responses. The ductility demand and roof drift ratio DM's basically showed the same results, but due to varying limit states also varied from structure to structure. The Park and Ang damage index and the Kumar and Usami damage index provided a wide range of results as well. Due to the high amount of variability in the DM's used in this study, it seems that damage-based collapse rules are not universally applicable. Intensity-based collapse rules, on the other hand, are more universal because they are less dependent on the DM.

The parameter study results were further reinforced in that the vertical accelerations influenced the lateral displacements most at the point just before collapse. Those structures that tended to collapse had negative r_p values. Thus, the responses of structures with negative r_p values are much more likely to be influenced by vertical accelerations in an IDA than positive r_p structures. Since one of the main uses of IDA is to determine the collapse limit state of a structure and since vertical accelerations influence the response of a structure near its collapse point, it seems reasonable that the most accurate collapse limit state determinations would include vertical accelerations.

8.3 - Implications for CEUS and WUS Structures

There are several implications for CEUS and WUS structures based on the results of the parameter study and IDA study. The implications are related to strength demands and capacities and realistic structural periods.

8.3.1 – Strength Determination Issues

When designing a structure according to the NEHRP Provisions, the strength demands are determined based on a conservative approximation of the structural period. In most situations, the actual period determined from an analytical model will be longer than the approximate period used to calculate the design strength. The approximate period formulas will generally calculate shorter periods than those of a subsequent analytical model because the approximate period formulas account for the stiffness provided by non-structural elements, which is not typically accounted for in analytical models. Seismic force demands decrease with increasing period as evidenced by equation 2.10 in Chapter 2. Since the actual structural period will most likely be longer than the approximate structural period and the seismic force demands go down for increasing period, it follows that most structures would have higher strengths than would be necessary from a demand standpoint. Furthermore, if a structure had a shorter period than the approximate period, that is, were stiffer, then the seismic force demands may exceed the strength capacity assuming that the periods are not in the constant acceleration portion of the design spectrum. In a situation where the actual period is less than the approximate period, the design strength probably should be determined based on the actual period rather than the approximate period. This is not stated in the NEHRP Provisions, however.

8.3.2 – Concerning Characteristics of CEUS Structures

When creating the models for the IDA, it was determined that CEUS structures would have higher stability ratios than WUS structures based on the weights of the buildings and lateral stiffness requirements. It was shown that the higher stability ratios resulted in relatively large negative r_p values, which in turn caused the IDA curves to "lean over" at lower intensities and often suddenly. Since many of the CEUS models had large negative r_p values, they tended to collapse suddenly. The WUS structures, on the other hand, did not have such large negative r_p values and consequently "leaned over" more gradually. The sudden CEUS collapses made strength a very important structural

parameter, because the survival of the structure depended on it. Therefore, it seems like it would be a very worthwhile endeavor to accurately determine the actual strength of the CEUS structures. It is true that most structures have overstrengths of about 2 or 3, but that is not necessarily guaranteed. Due to the "seismic margin" prescribed by the NEHRP Provisions, all structures should have an overstrength of at least 1.5.

8.4 - Recommendations for Future Research

There are many ways that this research could be extended. In this section, two major extensions are presented. A list of several other ideas for further research on collapse is also presented.

8.4.1 – Multi-Degree-of-Freedom Models Including Vertical Accelerations

One way that this research should be extended is to investigate multi-degree-of-freedom (MDOF) systems. While the SDOF models used in this thesis were useful for determining general trends, MDOF models will be required to more fully study the effects of vertical accelerations on the various floors and joints of a structure. Past research has shown that vertical period and member flexibility can significantly influence the lateral response of structures. The SDOF models examined in this thesis had vertical periods, but the model vertical periods were essentially zero because all of the members were rigid. For structures with realistic member sizes and realistic vertical periods, it is very possible that the seismic demands would be amplified. Bozorgnia and Mahin (1998) chronicled the responses of twelve instrumented structures during the Northridge earthquake and noted that the vertical accelerations measured in the upper floors of the buildings were between about 1.5 and 2.7 times higher than in the lower stories. Also, Anderson and Bertero (1973) noted that the ductility requirements in critical regions of MDOF structures were influenced by vertical accelerations. They argued that this was particularly true in the upper stories of buildings because the lateral force requirements were comparatively lower than the gravity load requirements. Then, Hart et al. (1995)

examined the influence of vertical accelerations on special moment frames. The researchers found that column axial forces could be increased by as much as the original dead loads. Also, beam moments increased significantly, sometimes by an amount equal to the moments caused by the horizontal component of the ground motion.

By moving the SDOF study of this thesis to MDOF models, there is a significant jump in modeling complexity. Other researchers have noted this complexity. Ju, Liu, and Wu (2000), specifically studied the response of 3D frames subjected to vertical accelerations. They noted that distribution of the mass in the beams caused significant variability in the results. The researchers argued that having the mass associated with a given tributary area concentrated at one node in the center of the beam overly estimates the effects of vertical accelerations. They advocate using at least two nodes at the third points of beams with the mass distributed accordingly to accurately assess the vertical response of structures. Then, Hart et. al. (1995) studied the effects of mass location and distribution on the lateral response caused by vertical accelerations as noted a great deal of variability in the results. All this is said to reinforce the point that the transition to MDOF systems should be carried out carefully.

There are other factors that will complicate the analyses, but may show vertical accelerations to be more significant than in this study. For example, soft story problems may be accentuated by vertical accelerations. In a study by Bernal (1992a, 1992b), five of the six buildings he analyzed failed by a story mechanism, as opposed to a global mechanism. The story mechanism controlled collapse in the majority of these buildings because, in general, it takes much less energy to fail a story than an entire building. Also, modeling the axial-flexural interaction of the columns may worsen the effects of vertical accelerations in MDOF systems.

8.4.2 – Degrading Strength and Stiffness

The analyses conducted in this study should also be extended to include degrading structural parameters. OpenSees has degrading material models and some initial studies were conducted using them, but the results were inconclusive. More examination of the degrading models in OpenSees is required. For those interested in extending the work of

this study to degrading models, the information gleaned from the preliminary studies follows.

There are two different degrading material models in OpenSees, the *Hysteretic* and *BoucWen* materials. Each of these materials has parameters that will cause stiffness and strength degradation. However, the documentation on how these materials work and the significance of each parameter is nonexistent. In fact, it is not even commonly know that the *BoucWen* material is available in OpenSees.

There is, however, some literature available that provides clues as to how the *Hysteretic* and *BoucWen* materials work. Heine (2001), for example, studied degrading hysteric joints as they relate to wood and used the Bouc and Wen hysteretic formulation for his work. Heine provides a fairly detailed account of the parameters used in the Bouc and Wen formulation and some information on how the parameters affect structural response. Then, Zhang et al. (2002) studied the basic shapes of hysteresis loops for various structures and the effects of various parameters on the hysteresis loops. This study also describes the Bouc and Wen hysteresis formulation and the parameters associated with it.

There are even some studies where researchers have used the OpenSees degrading models. Haukaas (2003), for example, implemented sensitivity analysis capabilities in OpenSees and examined a variety of element formulations and material models for parameter sensitivity and reliability. In Haukaas' dissertation, he describes the parameters used in the actual *BoucWen* OpenSees material. In a dissertation by Elwood (2002), the *Hysteretic* material in OpenSees was used to model the hysteresis of reinforced concrete columns. Elwood also developed a limit state material model for modeling failures in reinforced concrete columns. In the appendices of Elwood's dissertation, he describes his formulation of the limit state material and provides some information on how the *Hysteretic* material works.

Even with the aforementioned literature, using the *Hysteretic* and *BoucWen* material models was not straightforward. Initially in this study, some preliminary models employing the degrading material models were created and analyzed using OpenSees, but a firm grasp of the effects of the various parameters was never obtained. For example, it seems that when including degradation in an analysis employing the *Hysteretic* material,

pinching of the hysteresis loops will always occur. It did not seem possible to have a simple bilinear force deformation relationship that would degrade in strength and stiffness. Consequently, the *Hysteretic* material was abandoned in this study because the main focus was on bilinear models.

The *BoucWen* material model, on the other hand, was closer to a bilinear formulation and included strength and stiffness degradation. The following TCL line of script shows the input format of the OpenSees BoucWen material:

```
uniaxialMaterial BoucWen 1   0.5 2520.0  6   6. 6.  665.0  0. 0. 0.
```

Ten parameters are required to define the BoucWen material. The parameters are as follows:

BoucWen Tag α K_0 n β γ A_0 D_{A0} D_μ D_ξ

where

Tag is used by OpenSees to identify the material

α controls the influence of the linear and hysteretic terms in the formulation

β, γ, and n control the shape of the hysteresis loop,

K_0 and A_0 influence the stiffness and strength of the material

D_{A0}, D_μ, and D_ξ cause degradation.

The problem with the above formulation is that the parameters used to define the BoucWen material do not correlate to real physical quantities. For example, the parameters that define the elastic modulus of the material do not correlate to units like psi or ksi. In fact, there are two parameters, A_0 and K_0, that define the elastic modulus of the *BoucWen* Material. Both parameters influence the strength and stiffness of the material simultaneously.

Since the parameters did not correlate to any real physical quantities, they were determined iteratively using a trial and error method until the stiffness and strength of each model was within an acceptable range. For the preliminary degrading models, it

was desired to have a set of models with a yield force of 34.5 kips, which was approximately equal to 9 percent of the structure's weight (386.1 kips). Also, the set was to include the seven stiffnesses used in the parameter study (see table 4.8 in chapter 4). For the *BoucWen* material, the following parameters were held constant: $\alpha = 0.5$ and $n = \beta = \gamma = 6.0$. To satisfy the strength and stiffness requirements given the constant parameters, A_0 and K_0 were varied. The A_0 and K_0 parameters were calibrated in the "cart" models using an oscillatory imposed displacement. Table 8.1 shows the A_0 and K_0 values required to achieve the desired strength and stiffness values.

Table 8.1 – Required A_0 and K_0 Values to Achieve a Given Lateral Strength and Stiffness using the *BoucWen* Material in OpenSees.

Building Stories	Real K (kips/in)	A0	Ko
3	79.41	665	2520
4	48.44	360	2790
5	33.03	230	3015
6	24.16	160	3180
7	18.56	115	3350
8	14.77	85	3560
9	12.07	66	3730

After creating table 8.1, there was a general trend between the A_0 and K_0 values. The equations to determine the general range of A_0 and K_0 to achieve a yield force of 34.5 kips and the desired stiffness are given by equations 8.1 and 8.2:

$$K_0 = \left(\frac{3 \times 10^{18}}{K_{real}} \right)^{0.2051} \quad \textbf{(8.1)}$$

$$A_0 = \left(\frac{K_{real}}{0.384} \right)^{1.22} \quad \textbf{(8.2)}$$

Equations 8.1 and 8.2 do not yield A_0 and K_0 values that will exactly produce a yield force of 34.5 kips and a prescribed stiffness, but they get close. It would be very useful to further determine connections between the parameters in the *BoucWen* model

and realistic structural parameters so that the *BoucWen* material could be implemented easier into realistic structures. The resulting shapes of the hysteretic curves produced from subjecting models with the *BoucWen* material having the parameters of Table 8.1 to the oscillatory imposed displacements described earlier are shown in Figure 8.1.

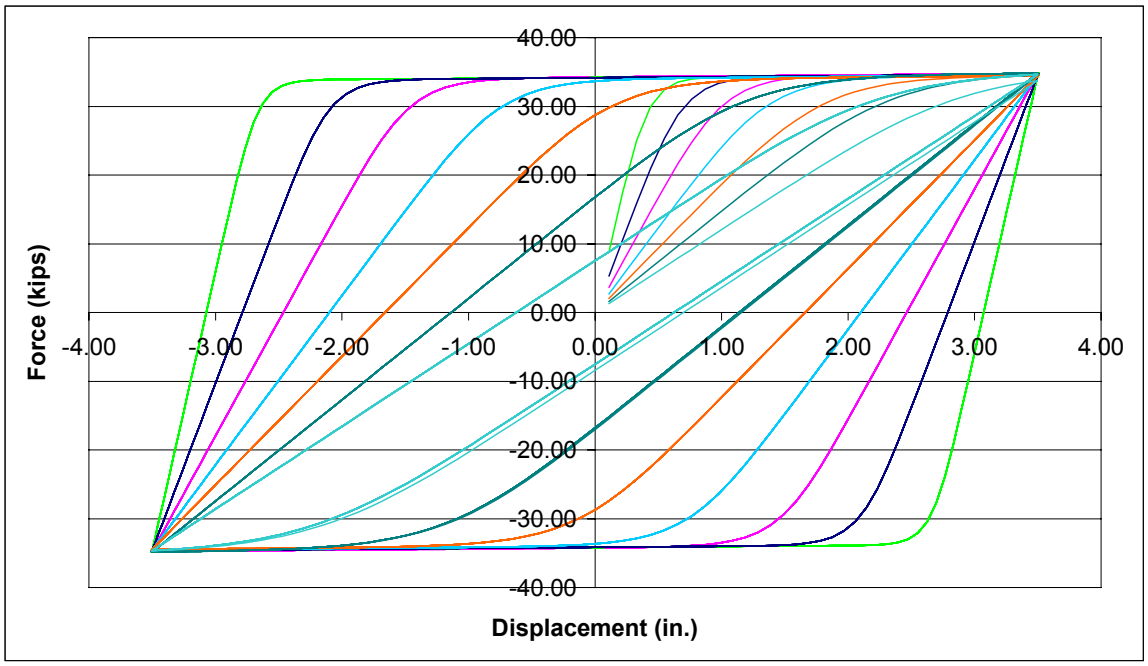

Figure 8.1 - Hysteretic Curves of Parameter Study Models Using the BoucWen Material

After calibrating the stiffnesses and strengths, the degradation parameters were explored. As with the strength and stiffness parameters, the degradation parameters did not seem to have any physical significance. After some experimentation, it was determined that D_{μ} caused strength degradation, D_{ξ} caused stiffness degradation, and D_{A0} caused both strength and stiffness degradation. For all of the degradation parameters, the values had to be quite small or else the hysteretic shape would be unreasonably distorted. The results of the degradation experimentation are shown in Figures 8.2, 8.3, and 8.4.

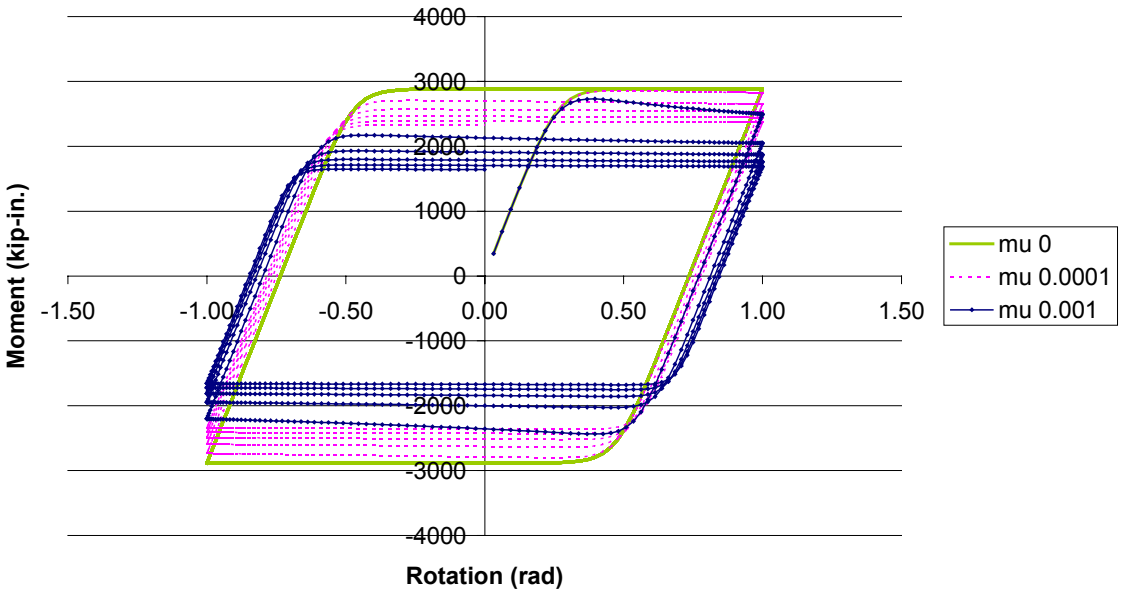

Figure 8.2 – Variation of D_{μ} in the Bouc Wen Material.

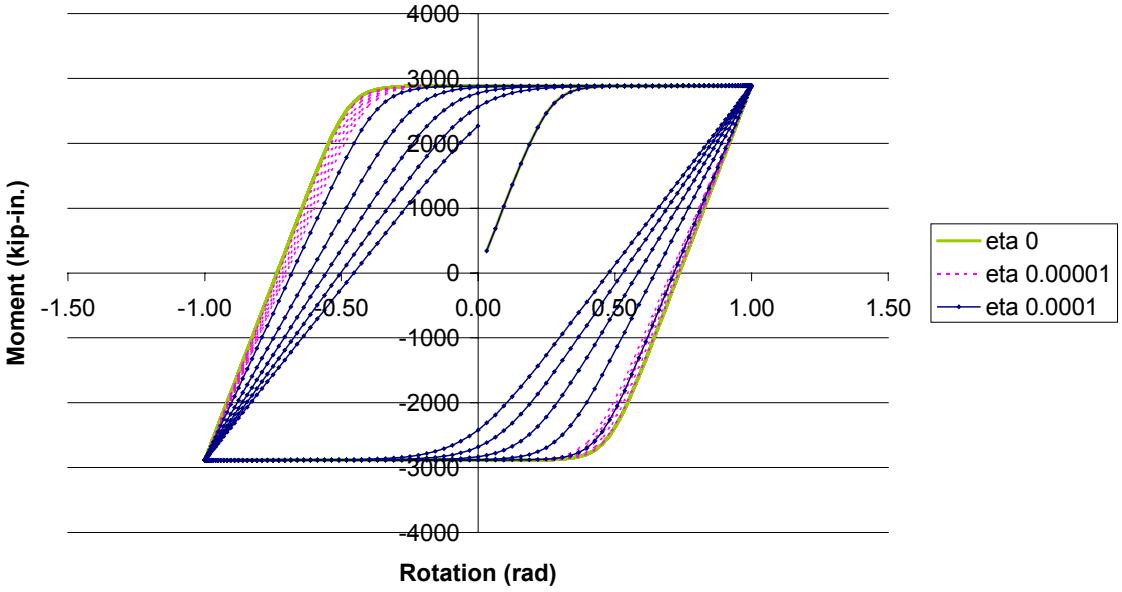

Figure 8.3 – Variation of D_{ξ} in the Bouc Wen Material.

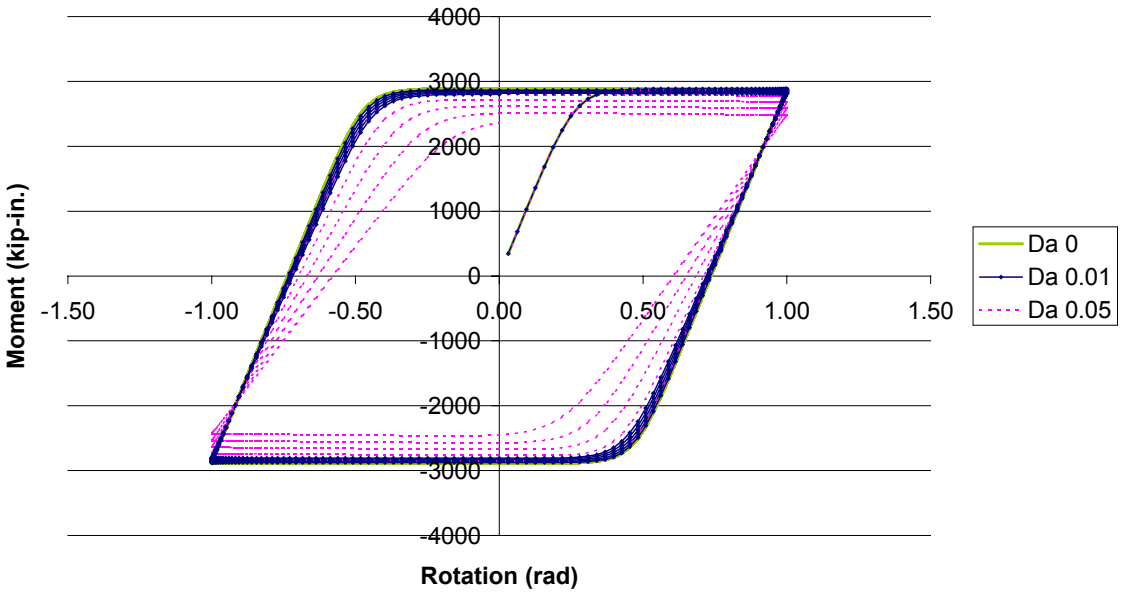

Figure 8.4 – Variation of D_{A0} in the Bouc Wen Material.

Figures 8.2, 8.3, and 8.4 show the effects of the degradation parameters. When the degradation parameters were used in the actual models, the same types of degradation did not occur. In fact it did not seem that much degradation was happening at all. The response histories were affected, but it was not clear why. In order to use the *BoucWen* material in the context of the research done in this thesis, more study of the material model will have to be done.

8.4.3 – Other Possible Extensions of This Research

1) Take inventory of the structural characteristics of CEUS buildings to help verify the validity of the current design codes. Also, determine realistic periods of the structures.
2) Determine better ways to characterize the ductility demand that corresponds to the collapse r_p values. It would be ideal if the elastic demands could be correlated with the collapse r_p because the elastic demands are easily determined from a displacement response spectrum. They do not require any nonlinear analyses. The μ_{+rp} value, on the other hand, requires several nonlinear analyses to be conducted on a structure with varied positive r_p values.

3) Conduct another parameter study where only a few stability ratios are used, but a much broader range of post-yield stiffness ratios would be used. Thus, a range of r_p values between about –0.25 and 0.25 would be created only by the variation of the post-yield stiffness ratio. In this way, the effects of the stability ratio on the periods of the models would be removed, but a range of r_p values would still be examined.
4) It would be useful to have more experimental data on dynamic P-Delta effects. A small scale study was conducted by Vian and Bruneau (2001), but further experimental research is necessary in this area.
5) It might be useful to conduct another parameter study using trilinear models this time.
6) Determine sets of horizontal and vertical acceleration components that would be representative of the intensity progression from near field earthquakes to far field earthquakes. Then, create a series of models of various heights and subject them to the sets of near field and far field ground motions. Such a study would provide insight into the realistic range where vertical accelerations are the most influential in a response history.
7) Repeat the study suggested in number six above, but use IDA. The ratio of vertical intensity to horizontal intensity should obey reasonable attenuation relationships.
8) It seems that the vertical acceleration component could be treated as another type of stability ratio. It could prove useful to try to develop this idea further. For example, the vertical acceleration stability ratio would be higher for near field structures and lower for far field structures.
9) It would be useful to study the effects of the horizontal and vertical ground motion phasing on the response of the structures. It would particularly be interesting to use IDA to do this.
10) Moving from SDOF models to MDOF models will significantly increase computing time. Consequently, the use of a supercomputer and parallel processing would be an interesting research avenue to pursue.
11) It would be useful to conduct IDA analyses for various site conditions, to get an idea of the effects of soil on the various parameters examined in this study.

References

Abrahamson, N. A., and Litehiser, J. J. (1989), "Attenuation of Vertical Peak Acceleration," *Bulletin of the Seismological Society of America*, Vol. 79, No. 3, pp. 549-567.

Amirbekian, R. V., and Bolt, B. A. (1998), "Spectral Comparison of Vertical and Horizontal Seismic Strong Ground Motions in Alluvial Basins," *Earthquake Spectra*, Vol. 14, No. 4, pp. 573-595.

Anderson, J. C. and Bertero, V. V. (1973), "Effects of Gravity Loads and Vertical Ground Acceleration on the Seismic Response of Multistory Frames," *5th World Conference on Earthquake Engineering, Rome, Proceedings*, pp. 2914-2923.

Araki, Y. and Hjelmstad, K. D. (2000), "Criteria for assessing dynamic collapse of elastoplastic structural systems" *Earthquake Engineering and Structural. Dynamics,* Vol. 29, No. 8, pp. 1177-1198

Ariaratnam, S. T. and Leung, K. C. K. (1990), "Parametric Effect of Vertical Ground Accelerations on the Earthquake Response of Elastic Structures," *Canadian Journal of Civil Engineering*, Vol. 17, pp. 209-217.

ASCE (2002), ASCE Standard: Minimum Design Loads for Buildings and Other Structures, ASCE 7-02, American Society of Civil Engineers, Reston, VA 2002.

Balendra, T., Tan, K. and Kong, S. (1999), "Vulnerability of reinforced concrete frames in low seismic region, when designed according to BS 8110," Earthquake Engineering and Structural Dynamics, Vol. 28, No. 11, pp.1361-1381.

Banon, H. Biggs, J. M., and Irvine, H. M. (1981), "Seismic Damage in Reinforced Concrete Frames," *ASCE, Journal of the Structural Division*, Vol. 107, No. ST9, pp. 1713-1729.

Banon, H. and Veneziano, D. (1982), "Seismic Safety of Reinforced Concrete Members and Structures," *Earthquake Engineering and Structural Dynamics*, Vol. 10, pp. 179-193.

Beavers, J. E. (2002) "A Review of Seismic Hazard Description in US Design Codes and Procedures," *Progress in Structural Engineering and Materials*, Vol. 4, No. 1, pp. 46-63.

Belazougui, M. (1989), "The October 1980 El-Asnam, Algeria earthquake and its building structures effects," *Bulletin of the International Institute of Seismology and Earthquake Engineering*, Vol. 23, pp. 1-17.

Beres, A., Pessiki, S. P., White, Richard N., and Gergely, Peter (1996), "Implications of Experiments on the Seismic Behavior of Gravity Load Designed RC Beam-to-Column Connections," *Earthquake Spectra*, Vol. 12, No. 2, pp. 185-198.

Bernal, D. (1987). "Amplification factors for nonlinear dynamic P-delta effects in earthquake analysis", *Earthquake Engineering and Structural Dynamics*, Vol. 15, No 5, pp. 635-651.

Bernal, D. (1992a), "Instability of buildings subjected to earthquakes", *Journal of Structural Engineering*, Vol. 118, No.8, pp.2239-2260.

Bernal, D. (1992b), "Dynamic Instability in Buildings Subjected to Earthquakes," *Report No. CE-92-14, Northeastern University, Boston, MA*.

Bernal, D. (1998), "Instability of buildings during seismic response", *Engineering Structures*, Vol. 20, No. 4-6, pp. 496-502.

Bozorgnia, Y., Mansour N., and Campbell, K. W. (1995), "Characteristics of Free-Field Vertical Ground Motion during the Northridge Earthquake," *Earthquake Spectra*, Vol. 11, No. 4, pp. 515-525.

Bozorgnia, Y., Mahin, S. A., and Brady, A. G. (1998), "Vertical Response of Twelve Structures Recorded During the Northridge Earthquake," *Earthquake Spectra*, Vol. 14, No. 3, pp. 411-432.

British Standards Institute (1985), "BS8110: Structural Use of Concrete, Parts 1, 2, and 3."

Challa, V. R., and Hall, J. F. (1994), "Earthquake Collapse Analysis of Steel Frames," *Earthquake Engineering and Structural Dynamics*, Vol 23, No. 11, pp. 1199-1218

Charney, F. A., and Harris, J. R. (1988), "BSSC/NEHRP P-Delta Issue: Comments for Review by Members of Technical Subcommittee 2," *Unpublished paper available from Charney*.

Chopra, A. K., Goel, R. K., and Chintanapakdee, C. (2003), "Statistics of Single-Degree-of-Freedom Estimate of Displacement for Pushover Analysis of Buildings," *Journal of Structural Engineering*, Vol. 129, No. 4, pp. 459-469.

Como, M., De Stefano, M., and Ramasco, R. (2003), "Effects of Column Axial Force – Bending Moment Interaction on Inelastic Seismic Response of Steel Frames," *Earthquake Engineering and Structural Dynamics*, Vol. 32, No. 12, pp. 1833-1852.

Computers and Structures Inc. (2002), *SAP 2000 Analysis Reference Manual.*

Cosenza, E., Manfredi, G., and Ramasco, R. (1993), "The Use of Damage Functionals in Earthquake Engineering: A Comparison Between Different Methods," *Earthquake Engineering and Structural Dynamics*, Vol. 22, pp. 855-868.

Cosenza, E., and Manfredi, G. (2000), "Damage indices and damage measures," *Progress in Structural Engineering and Materials*, Vol. 2, No. 1, pp. 50-59.

El-Attar, A. G., White, R. N., and Gergely, P. (1997), "Behavior of Gravity Load Design Reinforced Concrete Buildings Subjected to Earthquakes," *ACI Structural Journal*, Vol. 94, No. 2, pp. 133-145.

Elwood, K. J. (2002), "Shake Table Tests and Analytical Studies on the Gravity Load Collapse of Reinforced Concrete Frames," *Ph.D. Dissertation, Civil and Environmental Engineering, University of California, Berkeley, 2002*.

Fajfar, P. (1992). "Equivalent Ductility Factors, Taking into Account Low-Cycle Fatigue." *Earthquake Engineering and Structural Dynamics,* 21, pp. 837-848.

Federal Emergency Management Agency (2000a), *FEMA-350: Recommended Seismic Design Criteria for New Steel Moment Frame Buildings.*

Federal Emergency Management Agnecy (2000b), *NEHRP Recommended Provisions for Seismic Regualtions for New Buildings and Other Structures.*

Frankel, A., Mueller, C., Barnhard, T., Perkins, D., Leyendecker, B.V., Dickman, N., Hanson, S., and Hopper, M. (1996), National Seismic-Hazard Maps: Documentation June 1996, Open-File Report 96-532," *United States Geological Survey, Denver, Colorado.*

Ghosh, S. K., and Corley, W. G. (1986) , "Behavior of Reinforced Concrete Framing Systems," *The Mexico Earthquakes – 1985: Factors Involved and Lessons Learned, Proceedings, Mexico City, Mexico, September 19-21*, pp. 328-349.

Gupta, A., and Krawinkler, H. (1999), "Seismic Demands for Performance Evaluation of Steel Moment Resisting Frame Structures (SAC Task 5.4.3), *The John A. Blume Earthquake Engineering Center, Dept. of Civil and Environmental Engineering, Stanford University, Report No. 132, June*.

Gupta, A., and Krawinkler, H. (2000a), "Dynamic P-Delta Effects for Flexible Inelastic Steel Structures," *Journal of Structural Engineering*, Vol. 126, No. 1, pp. 145-154.

Gupta, A., and Krawinkler, H. (2000b), "Behavior of Ductile SMRF's at Various Seismic Hazard Levels," *Journal of Structural Engineering*, Vol. 126, No. 1, pp. 98-107.

Hanson, R. (1986), "Performance of Steel Structures," *The Mexico Earthquakes – 1985: Factors Involved and Lessons Learned, Proceedings, Mexico City, Mexico, September 19-21,* pp. 350-363.

Hart, G. C., et al. (1995), "Influence of Vertical Ground Motion on Special Moment-Resisting Frames," *SAC Technical Report 95-05*, pp. 3:1-52.

Haukaas, T. (2003), "Finite Element Reliability and Sensitivity Methods for Performance-Based Engineering," *Ph. D. Dissertation, Civil and Environmental Engineering, University of California, Berkeley, 2003*.

Heine, Christian P. (2001), "Simulated Response of Degrading Hysteretic Joints with Slack Behavior," *Ph. D. Dissertation, Department of Wood Science and Forest Products, Virginia Polytechnic Institute and State University, 2001.*

Higazy, E. M., Elnashai, M., Amr, S., and Agbabian, M. S. (1996), "Behavior of Beam-Column Connections Under Axial Column Tension," *ASCE Journal of Structural Engineering,* Vol. 122, No. 5, pp. 501-511.

Hjelmstad, K. D., and Williamson, E. B. (1998), "Dynamic Stability of Structural Systems Subjected to Base Excitation," *Engineering Structures*, Vol. 20, No. 4-6, pp. 425-432.

Hwang, H., Lin, H. M., Huijie, and Huo, J. (1997), "Seismic Performance Evaluation of Fire Stations in Shelby County, Tennessee," *Earthquake Spectra,* Vol. 13, No. 4, pp. 759-772.

Iyengar, R. N., and Shinozuka, M. (1972), "Effect of Self-Weight and Vertical Acceleration on the Behavior of Tall Structures During Earthquake," *Earthquake Engineering and Structural Dynamics*, Vol. 1, pp. 69-78.

Jennings, P. C., and Husid, R. (1968), "Collapse of Yielding Structures Under Earthquakes," Journal of Engineering Mechanics, Vol. 94, No. 5, pp. 1045-1065.

Kawashima, K., MacRae, G. A., Hoshikuma, Jyun-ichi et al. (1998), "Residual Displacement Response Spectrum" *Journal of Structural Engineering*, Vol. 124, No. 5, pp. 523-530.

Krawinkler, H. (1983), "Cumulative Damage in Steel Structures Subjected to Earthquake Ground Motions," *Computers and Structures*, Vol. 16, No. 1-4, pp. 531-541.

Krawinkler, H. (1987), "Performance Assessment of Steel Components," *Earthquake Spectra*, Vol. 3, No. 1, pp. 27-41.

Krawinkler, H., and Seneviratna, G. D. P. K. (1998), "Pros and cons of a pushover analysis of seismic performance evaluation," *Engineering Structures* Vol. 20, No. 4-6 , pp. 452-464.

Kumar, S. and Usami, T. (1996), "An evolutionary-degrading hysteretic model for thin-walled steel structures," *Engineering Structures,* Vol. 18, No. 7, pp. 504-514.

Kunnath, S. K., Hoffman, G., Reinhorn, A. M. and Mander, J. B. (1995),, "Gravity-Load-Designed Reinforced Concrete Buildings—Part I: Seismic Evaluation of Existing Construction," *ACI Structural Journal*, Vol. 92, No. 3, pp. 343-354.

Kunnath, S. K., Hoffman, G., Reinhorn, A M. and Mander, J. B. (1995), "Gravity-Load-Designed Reinforced Concrete Buildings—Part II: Evaluation of Detailing Enhancements," *ACI Structural Journal*, Vol. 92, No. 4, pp. 470-478.

Lee, H. and Woo, S. (2002), "Seismic performance of a 3-story RC frame in a low-seismicity region," *Engineering Structures*, Vol. 24, No. 6, pp. 719-734.

Leyendecker, E. V., Hunt, J. R. , Frankel, A. D., and Rukstales, K. S. (2000), "Development of Maximum Considered Earthquake Ground Motion Maps," *Earthquake Spectra,* Vol. 16, No. 1, pp. 21-40.

Lin, Y. K., and Shih, T. (1980), "Column Response to Horizontal-Vertical Earthquakes," *Journal of the Engineering Mechanics Division*, *ASCE,* Vol. 106, No. EM6, pp. 1099-1109.

Lybas, J.M., and Sozen, M.A. (1977), "Effect of Beam Strength and Stiffness on Dynamic Behavior of Reinforced Concrete Coupled Walls," *Department of Civil Engineering, University of Illinois at Urbana-Champaign, Ill., July.*

MacRae, G. A., Priestley, M. J. N., and Tao, J. (1993), "P-Delta Design in Seismic Regions," *Report No. SSRP – 93/05*, *Department of Applied Mechanics and Engineering Sciences, University of San Diego, La Jolla, California, June 1993*.

MacRae, G. A. (1994), "P-delta Effects on Single-Degree-of-Freedom Structures in Earthquakes", *Earthquake Spectra*, Vol. 10, No. 3, pp. 539-568.

MacRae, G. A., and Kawashima, K. (1997), "Post Earthquake Residual Displacement of Bilinear Oscillators," *Earthquake Engineering and Structural Dynamics*, Vol. 26, No. 7, pp. 701-716.

Maison, B. F., and Kasai, K. (1997), "Analysis of Northridge damaged thirteen-story WSMF building," *Earthquake Spectra*, Vol. 13, No. 3, pp. 451-473.

Mehanny, S. S. F., and Deierlein, G. G. (2001), "Seismic Damage and Collapse Assesment of Composite Moment Frames" *Journal of Structural Engineering*, Vol. 127, No. 9, pp. 1045-1053.

Meli, R. (1986), "Evaluation of Performance of Concrete Buildings Damaged by the September 19, 1985 Mexico Earthquake," *The Mexico Earthquakes – 1985: Factors Involved and Lessons Learned Proceedings, Mexico City, Mexico, September 19-21*, pp. 308-327.

Murty, C. V. R., Durgesh C. R., Bajpai, K. K., and Jain, S. K. (2003), "Effectiveness of Reinforcement Details in Exterior Reinforced Concrete Beam-Column Joints for Earthquake Resistance," *ACI Structural Journal*, Vol. 100, No. 2, pp. 149-156.

Mwafy, A. M., and Elnashai, A. S. (2001), "Static pushover versus dynamic collapse analysis of RC buildings", *Engineering Structures,* Vol. 23, No. 5, pp. 407-424.

Osteraas, J., and Krawinkler, H. (1989), "The Mexico Earthquake of September 19, 1985 – Behavior of Steel Buildings," *Earthquake Spectra* Vol. 5, No.1, pp. 51-88.

Park, Y., and Ang, A. H.-S. (1985), "Mechanistic Seismic Damage Model for Reinforced Concrete," *ASCE Journal of Structural Engineering*, Vol. 111, No. 4, pp. 722-739.

Quek, S.-T., Bian, C., Lu, X., Lu, W., and Xiong, H. (2002), "Tests on low-ductility RC frames under high- and low-frequency excitations," *Earthquake Engineering and Structural Dynamics*, Vol. 31, No. 2, pp. 459-474.

Repetto, P. A. I., and Seed, H. B. (1980), "Influence of site characteristics on building damage during the October 3, 1974 Lima earthquake," *UCB/EERC-80/41, Berkeley: Earthquake Engineering Research Center, University of California, September.*

Saadeghvaziri, M. A. (1988), "Inelastic Response of R/C Bridges Under Horizontal and Vertical Earthquake Motions," *Ph. D. Dissertation, University of Illinois at Urbana-Champaign*, 1988

Saadeghvaziri, M. A., and Foutch, D. A. (1991), "Dynamic Behavior of R/C Highway Bridges Under the Combined Effect of Vertical and Horizontal Earthquake Motions," *Earthquake Engineering and Structural Dynamics*, Vol. 20, pp. 535-549.

Saadi, M., and Sozen, M. (1981), "Simple Nonlinear Seismic Analysis of R/C Structures," *Journal of the Structural Division, ASCE,* Vol. 107, No. ST5, pp. 937-951.

Senerviratana, G. D. P. K., and Krawinkler, H. (1997), "Evaluation of Inelastic MDOF Effects for Seismic Design," *John A. Blume Earthquake Engineering Center, Dept. of Civil Engineering, Stanford University, Report No. 120, June.*

Shibata, A., and Sozen, M. A. (1976), "Substitute-Structure Method for Seismic Design in R/C," *Journal of the Structural Division, ASCE,* Vol. 102, No. ST1, pp. 1-18.

Shih, T.-Y., and Lin, Y. K. (1982), "Vertical Seismic Load Effect on Hysteretic Columns," *Journal of the Engineering Mechanics Division, ASCE*, Vol. 108, No. EM2, pp. 242-254.

Shooshtari, A., and Saatcioglu, M. (1999). "Significance of P-delta effects on seismic response of R/C structures," *Proceedings of the 8th Canadian Conference on Earthquake Engineering*, Vancouver, Canada, June 13-16, pp. 311-316.

Soliman, M. M., et al. (1993), "Implications of damage to Nasser School Building in Cairo earthquake of 12th October, 1992," *EGYQUAKE 1: Proceedings, First Egyptian Conference on Earthquake Engineering, 6-9 December 1993*, *Hurghada, Egypt, Egyptian Society for Earthquake Engineering, Faculty of Engineering, Cairo Univ., Giza, Egypt*, pp. 231-240.

Takizawa, H., and Jennings, P. C. (1980), "Collapse of A Model for Ductile Reinforced Concrete Frames Under Extreme Earthquake Motions," *Earthquake Engineering and Structural Dynamics*, Vol. 8, pp. 117-144.

Vamvatsikos, D. and Cornell, A.C. (2002a), "Incremental dynamic analysis", *Earthquake Engineering and Structural Dynamics*, Vol. 31, No. 3, pp. 491-514.

Vamvatsikos, D., and Cornell C.A. (2002b), "Direct Estimation of the Seismic Demand and Capacity of MDOF systems through Incremental Dynamic Analysis of an SDOF Approximation," *Proceedings of Eurodyn 2002, Munich, September.*

Vamvatsikos, D. (2002c), "Seismic Performance, Capacity and Reliability of Structures as Seen Through Incremental Dynamic Analysis," *Dissertation Submitted to the Department of Civil and Environmental Engineering, Stanford University, In Partial Fulfillment of the Requirements for the Degree of Doctor of Philosophy.*

Vian, D., and Bruneau, M. (2001), "Experimental investigation of P-delta effects to collapse during earthquakes," *MCEER-01-0001, Multidisciplinary Center for Earthquake Engineering Research, Buffalo, New York.*

Williamson, E. B., and Hjelmstad, K. D. (2001), "Nonlinear Dynamics of a Harmonically-Excited Inelastic Inverted Pendulum," *Journal of Engineering Mechanics*, Vol. 127, No. 1, pp. 52-57.

Williamson, E.B., and Rungamornrat, J. (2002), "Numerical Analysis of Dynamic Stability Under Random Excitation," *Engineering Structures*, Vol. 24, No. 4, pp. 479-490.

Williamson, E. B. (2003), "Evaluation of Damage and P-Delta Effects for Systems Under Earthquake Excitation," *Journal of Structural Engineering*, Vol. 129, No. 8, pp. 1036-1046

Zhang, H., Foliente, G. C., Yang, Y., and Ma, F. (2002), "Parameter Identification of Inelastic Structures Under Dynamic Loads," *Earthquake Engineering and Structural Dynamics*, Vol. 31, pp. 1113-1130.